Aus dem Physiologischen Institut der Ludwig-Maximilians-Universität München

Lehrstuhl Zelluläre Physiologie

Vorstand: Prof. Dr. Claudia Veigel

Expression, purification and characterization of human myosin 9a

Dissertation

zum Erwerb des Doktorgrades der Humanbiologie

an der Medizinischen Fakultät

der Ludwig-Maximilians-Universität München

vorgelegt von

Ewa Warchoł

aus Tomaszów Mazowiecki, Polen

2016

Mit Genehmigung der Medizinischen Fakultät

der Universität München

Berichtstatter:	Prof. Dr. Claudia Veigel
Mitbereichstatter:	Prof. Dr. André Werner Brändli
	Prof. Dr. Franz Urlich Hartl
Mitbetreuung durch den promovierten Mitarbeiter:	Dr. Christopher Batters
Dekan:	Prof. Dr. med. dent. Reinhard Hickel

Tag der mündlichen Prüfung: 09.02.2016

Abbreviations:

aa	Amino acid
ADP	Adenosine diphosphate
AM	Actomyosin
ATP	Adenosine triphosphate
CaM	Calmodulin
CFP	Cyan Fluorescent Protein
CM loop	Cardiomyopathy loop
CSF	Cerebrospinal fluid
DC	Dendritic Cell
Dd	*Dictyostelium discoideum*
DNA	Deoxyribonucleic acid
DLS	Dynamic Light Scattering
DTT	Dithiothreitol
ECL	Enhanced Chemiluminescence
EDTA	Ethylenediaminetetraacetic acid
EGTA	Ethylene glycol tetraacetic acid
ELC	Essential Light Chain
F-actin	Filamentous actin
FBS	Fetal Bovine Serum
FPLC	Fast Protein Liquid Chromatography
G-actin	Globular actin
GAP	GTPase Activating Protein
GFP	Green Fluorescent Protein
GTP	Guanosine Triphosphate
HBE	Human Bronchial Epithelium
HF	High Fidelity
HMM	Heavy Meromyosin
HRP	Horseradish Peroxidase
Hs	*Homo sapiens*
IEX	Ion Exchange Chromatography
IMAC	Immobilized Metal Affinity Chromatography
IPTG	Isopropyl β-D-1-thiogalactoyranoside
kDa	Kilo Dalton
kbp	Kilo base pairs
LDH	Lactic dehydrogenase
LMM	Light Meromyosin
MCS	Multiple Cloning Site
Mhc	Myosin heavy chain
MMD	Minimal Motor Domain

MOPS	3-(N-mopholino)propanesulfonic acid
MW	Molecular Weight
NADH	Nicotinamide adenine dinucleotide
nt	Nucleotide
PBD	PDZ-binding domain
PBS	Phosphate Buffered Saline
PCR	Polymerase Chain Reaction
PEP	Phosphoenolpyruvate
PK	Pyruvate kinase
RLC	Regulatory Light Chain
R_s	Stokes radius
RFP	Red Fluorescent Protein
S1	myosin subfragment 1
S.D.	Standard Deviation
SD	Subdomain
SDS-PAGE	Sodium Dodecyl Sulfate Polyacrylamide Gel Electrophoresis
SEC	Size Exclusion Chromatography
SF	*Spodoptera furgiperda*
SFM	Serum Free Medium
TBE	Tris/Borate/EDTA
TBS	Tris Buffered Saline
TEA	Triethanolamine
TRITC	Tetramethylrhodamine
WT	Wild Type

List of Figures

List of Tables

Table of contents:

Abstract

Myosins form a large family of actin-based motor proteins that are involved in different forms of cellular motility. Those include muscle contraction, intracellular transport, endo- and exocytosis and cell division and locomotion. Certain myosin isoforms are also involved in hearing and vision processes. So far, very little is known about the myosin class 9. Myosin 9 has been proposed to be involved in cell differentiation and morphology. Mammals express two class 9 myosins; myosin 9a is expressed in brain and its loss results in the formation of hydrocephalus, while myosin 9b appears to be involved in the directional movement of dendritic cells. On the structural level, myosin 9 contains a RhoGAP domain in its tail region, indicating it could link its mechanical activity along actin filaments to intracellular protein G signaling.

So far, only myosin 9b orthologs have been investigated. Here, I used the baculovirus/insect cell system to express recombinant human myosin 9a constructs, optimized the purification procedure and examined the function of myosin 9a motor *in vitro*. Designed constructs contained the motor and neck domains of myosin 9a, fused to different N- and C-terminal tags to facilitate purification. I addressed the ATPase activity of myosin 9a (particularly the Minimal Motor Domain construct) in the absence and presence of F-actin by means of an NADH enzyme-linked assay. The mechanical activity of myosin 9a was addressed by means of the gliding filament assay. The velocity of actin gliding over the lawn of surface-bound myosin 9a molecules was largely independent from the motor density on the surface of a flow cell.

In summary, this work presents the first successful purification of recombinant human myosin 9a motor constructs and describes basic mechanochemical properties of human myosin 9a motor. The results presented in this work provide framework for further investigation of myosin 9a properties, including investigation of the regulatory role of the tail domain of myosin 9a.

Zusammenfassung

Myosine bilden eine grosse Familie von Aktin-basierten Motorproteinen die an einer Vielzahl von Formen zellulärer Motilität beteiligt sind. Dies reicht von der Muskelkontraktion, intrazellulärem Membrantransport, Endo- und Exozytose, Zellteilung, Zellfortbewegung bis hin zu Prozessen beim Hör- und Sehvorgang. Über Myosine der Klasse 9 ist bisher sehr wenig bekannt. Myosin-9 soll an der Ausdifferenzierung von Zellen und an der Ausbildung der Zellmorphologie beteiligt sein. Der Verlust des im Säugergehirn exprimierten Myosin-9a führt zur Bildung eines Hydrocephalus, während Myosin-9b an der gerichteten Fortbewegung von dendritischen Zellen beteiligt zu sein scheint. Eine strukturelle Besonderheit von Myosin-9 ist eine RhoGAP-Domäne in der Schwanzregion. Dies eröffnet die interessante Möglichkeit, dass Myosine der Klasse 9 ihre mechanische Aktivität entlang von Aktin-Filamenten an intrazelluläres G-Protein Signalling koppeln können.

In der Literatur wurden bisher Myosine der Klasse 9b untersucht. In der vorliegenden Arbeit habe ich ein Baculovirus-Insektenzell-System verwendet, um rekombinante Myosin-9a Konstrukte zu exprimieren und exprimiertes Myosin-9a erstmals in vitro funktionell zu charakterisieren. Es gelang, eine Reihe verschiedener Konstrukte bestehend aus der Motordomäne sowie der Calmodulin-bindenden Nackendomäne, als GFP-Fusionsprotein, sowie mit verschiedenen N-und C-terminalen Tags erfolgreich zu exprimieren, aufzureinigen und zu lagern. Die ATPase Aktivität der exprimierten Myosin-9a Konstrukte (insbesondere das Konstrukts minimale Motordomäne) wurde mit Hilfe von NADH-enzyme-linked assays charakterisiert und die Myosin-typische Aktivierung der ATPase durch Aktin bestimmt. Die Untersuchung der mechanischen Aktivität des Motorproteins Myosin-9a erfolgte mit Hilfe von sogenannten Gleit-Filament assays. Die gemessene Gleitgeschwindigkeit der Aktin-Filamente, die über einen Rasen von Oberflächen-gebundenen Myosin-9 Motorproteinen fortbewegt wurden, war weitgehend unabhängig von der Motorprotein-Dichte auf der Oberfläche. Sie waren jedoch stark von der Art der Anheftung der Myosin-Motoren an die Oberfläche abhängig.

Zusammenfassend konnte ich erstmals Konstrukte des Motorproteins Myosin-9a erfolgreich exprimieren, aufreinigen und funktionell hinsichtlich ATPase und mechanischer

Aktivität hin untersuchen. Basierend auf den Ergebnissen dieser Arbeit sollen in Zukunft Myosin-9a Konstrukte einschliesslich der regulatorischen Schwanzregion hergestellt und in vitro charakterisiert werden.

CHAPTER 1: INTRODUCTION

1.1. Cytoskeletal motors actively navigate and organize complex cellular environments.

The eukaryotic cell is a sophisticated factory composed of dense protein and membrane networks that divide it into multiple compartments and organelles, each of which is responsible for different tasks; for example, maintenance and replication of DNA in the nucleus, energy production in mitochondria, sorting of vesicles by the Golgi apparatus or matrix attachment by cellular protrusions during cell locomotion. All that is governed by concerted action of cellular workhorses - proteins that have evolved different structures and functions as adaptations to a specific cellular compartment.

A single budding yeast cell contains on the order of up to 50 million different protein molecules (Ghaemmanghami et al., 2003) within 50μm^3 cell volume (Woldringh et al., 1993). A single protein would diffuse from one end to the other of a single yeast cell on the subsecond timescale (Moran et al., 2010). However, when one considers human cells, the necessity of efficient means of transportation becomes more apparent. A HeLa cell has a diameter of ~20μm and a volume of up to 5,000μm^3; it would take 5 - 20s for a protein to diffuse the full diameter of a single HeLa cell. Neurons are extremely long, with their axons extending up to 1m! It would take up to several hours for a protein to diffuse that distance, yet nervous signals are transported on a timescale of milliseconds.

Subsecond reaction timescales of individual cells are essential for the development and maintenance of multicellular organisms. Therefore, an efficient organization of cellular space has to be maintained. Mechanisms ensuring proper localization of cellular machineries in a spatiotemporal manner are necessary.

Eukaryotic cells have evolved multiple mechanisms to ensure an efficient organization of the cell; spatiotemporal regulation of protein activity by signaling pathways, electrochemical gradients across membranes, dynamic cytoskeletal structures contributing to cell polarity and migration, and molecular cargo transporters that deliver molecular parts to specific compartments.

Motor proteins associated with the cytoskeleton (kinesins, dyneins and myosins) function as anchors, tension generators and transporters, and, apart from cargo trafficking, are involved in spatial and temporal regulation of the cytoskeletal architecture. All motors utilize ATP as their energy source to perform above-mentioned functions. Kinesins and myosins share the highest structural similarity; in these motors the filament-binding site is localized opposite to the ATP site within a globular head. Dynein is composed of multiple units and its structure differs significantly from that of myosin and kinesin (Mallik and Gross, 2004).

Dyneins and kinesins utilize microtubules as their cellular tracks, whereas myosins bind to actin. Both microtubules and actin are highly dynamic polymers and hydrolyze GTP and ATP, respectively, to polymerize. Because one end of the polymer grows faster than the other, both microtubules and actin filaments exhibit polarity. In the cell most actin filaments point towards the cell membrane with their fast growing end. Due to the polarity of the motor binding site on actin and tubulin, the associated molecular motors move directionally along their filament tracks. Most myosins move towards the fast-growing end of actin filaments. This ensures their translocation towards the cell membrane; a single well-established reverse-directed motor, myosin 6, is employed in endocytosis and transports vesicles from the cell membrane to the cell center (Mallik and Gross, 2004).

Why have so many different types and isoforms of the cytoskeleton-associated molecular motors evolved? All couple ATP hydrolysis to binding and dissociation from their respective cytoskeletal tracks, enabling them to tether to filaments and to move along them. Each isoform exhibits specific adaptations of its ATPase cycle to perform its mechanical function (Vale, 1999). How that mechanochemical coupling is translated into a particular function in the context of the whole cell is of particular interest.

1.2. Structure of a muscle fibre and discovery of myosin. The sliding filament theory.

The name ‘myosin’ was given by Kühne (1864) to a protein extracted at high salt from muscle. The protein formed threads in water, therefore clearly was not globular. In 1939, Engelhardt and Lyubimova showed for the first time that those extracts exhibit an ATPase activity. This was followed by a demonstration that threads shorten in the presence of ATP. Simultaneously, time-dependent high salt treatment resulted in the separation of low- and high-viscosity fractions from the muscle. The high viscosity of the latter fraction, containing actin and myosin, was reduced upon addition of ATP in a high salt buffer. This was caused by the dissociation of the actomyosin complex; in a low salt buffer contraction was initiated by addition of ATP. The conclusive proof that the actomyosin interaction in the presence of ATP seen in extracts is the basic mechanism for muscle contraction was obtained with glycerol-extracted psoas muscle fibres. Upon addition of MgATP, fibres started contracting and generated tension comparable to that of living muscle (Szent-Györgyi, 2004).

Vertebrate muscles are composed of individual muscle fibers (or myofibers), each containing multiple nuclei and surrounded by the sarcolemma. Individual muscle fibers are composed of myofibrillar protein bundles. The contracting unit of striated skeletal muscle is the sarcomere (Figure 1.1). Actin and myosin are the main components of the contractile machine within the sarcomere, forming linear interdigitating arrays. Each sarcomere is 2 - 3μm long, extending between two Z-lines. Myosin forms 1.6μm long thick filaments in the A-band, whereas actin forms 1μm long thin filaments, extending from the Z-line to the H-zone. The H-zone is characterized by an empty space between the ends of thin filaments in the middle of the sarcomere. The I-band is the fraction of the thin filament in direct proximity to the Z-line with no overlapping thick filaments (Szent-Györgyi, 2004).

Electron micrographs of sarcomeres (Figure 1.1) revealed details about the structure of the thick filament (Huxely, 1957). Muscle myosin forms bipolar filaments by means of rod association of individual molecules. The globular heads point out from both ends of the thick filament, facing in opposite directions. The central region of the filament is not decorated with myosin heads and is formed only by myosin rods associated with one

another at low ionic strength. Globular myosin heads protruding from opposite ends of the filament connect to actin, forming crossbridges (Szent-Györgyi, 2004).

Proteolytic digestion of isolated thick filaments provided an insight into the role of individual myosin domains, formation of the filaments, and their mechanical properties (Figure 1.1). A single muscle myosin molecule is a hexamer composed of two heavy chains and two pairs of associated light chains. The globular N-terminal head with the regulatory and essential light chains is termed S1 (subfragment-1). It functions as an isolated crossbridge as it is able to bind actin and hydrolyze ATP. Two S1's are joined together by a short region of the rod and together they form a heavy meromyosin (HMM) molecule. The isolated region of the rod in HMM is called S2. The remaining portion of the rod, responsible for association of myosin molecules into filaments at physiological ionic strength is called light meromyosin (LMM). The whole rod region is mostly α-helical, enabling dimerization of individual myosin heavy chains (Szent-Gyȍrgyi, 2004).

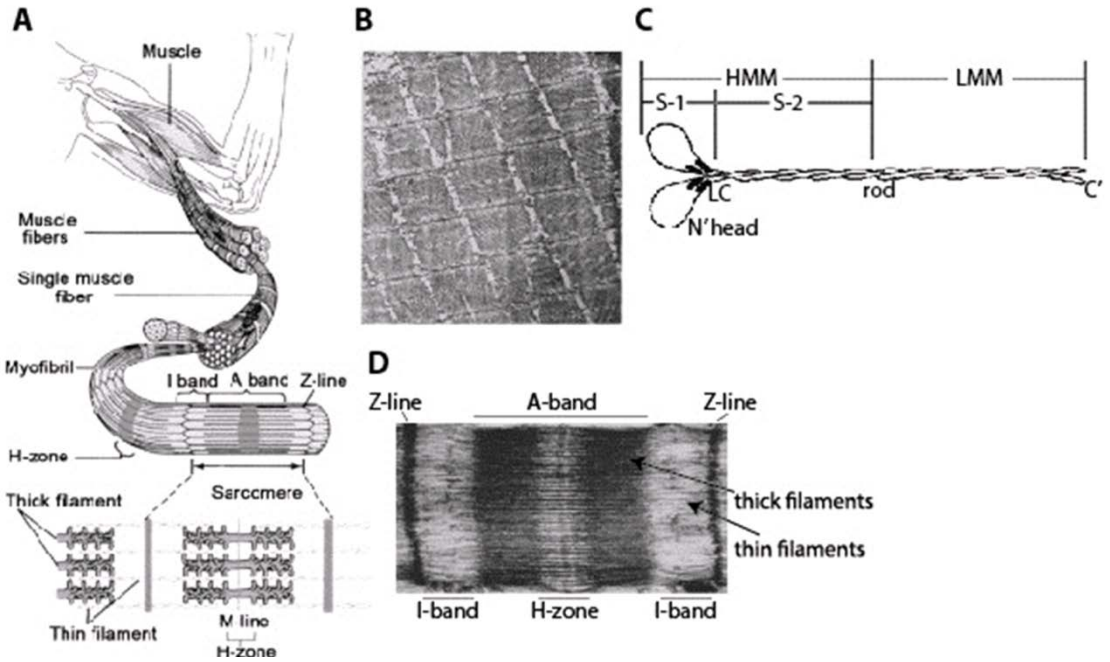

Figure 1.1. Organization of skeletal muscle and structure of a muscle myosin. **A:** a schematic depiction of the organization of human skeletal muscle; muscle fibers are multinucleated muscle cells surrounded by the sarcolemma. They are composed of myofibrils which are bundles of protein filaments organized in repeating units - sarcomeres. Sarcomeres are contractile units of muscles and are composed of interdigitating thick and thin filaments - myosin and actin, respectively. **B:** an electron micrograph of a section through a single muscle fiber. Regularly organized sarcomeres are easily distinguishable. Magnification 25,000. **C:** an electron micrograph of a sarcomere; Z-lines represent sarcomere borders. The length of thick filaments is represented by the A-band with myosin heads interacting with actin filaments in dark regions. The I-band is where thin filaments do not overlap with thick filaments. The H-zone is devoid of actin filaments with only rods of thick filaments present. Magnification 50,000. **D:** a schematic depiction of proteolytic fragments of a muscle myosin. The N-terminal globular head is associated with a pair of light chains (LC) and together they form S1 (subfragment-1) which binds actin and hydrolyzes ATP. Two heads of individual heavy chains are dimerized by a short rod region called S2 (subfragment-2). S1 and S2 together form a heavy meromyosin (HMM) molecule comprising two heads, two pairs of light chains and a region of coiled-coil. The remaining part of the rod, responsible for association of myosin into filaments at physiological ionic strength is called light meromyosin (LMM). Figures adapted from Huxley, 1957, Szent-Györgyi, 2004 and Batters et al., 2014.

In 1954 two groups (A.F. Huxley and R. Niedergerke, and H.E. Huxley and J. Hanson) proposed models to explain how the skeletal muscle contracts. These models remain valid in many aspects until today. By means of high resolution microscopy and using two independent experimental systems (intact frog muscle and isolated glycerinated myofibrils), it was revealed that during muscle contraction the length of the A-band encompassing thick filaments of myosin in the sarcomere does not change. Instead, shortening of the H-zone and I-band was observed. That led to the conclusion that transient interactions between myosin heads on the thick filament and actin in the thin filament must cause translocation of the latter towards the center of the sarcomere (Szent-Györgyi, 2004). That model is known as the sliding filament theory.

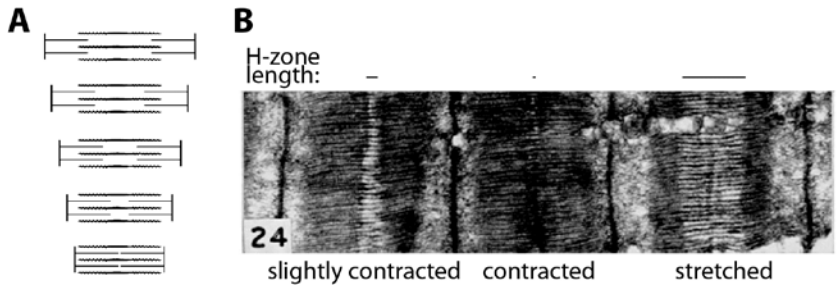

Figure 1.2. The sliding filament theory. **A:** a schematic depiction of interdigitating thick and thin filaments within the sarcomere, sliding past one another in the presence of MgATP. The sarcomere on the top is relaxed, while the sarcomere at the bottom is fully contracted. During the course of contraction, the length of thick and thin filaments remains constant, but the degree to which they overlap increases. This results in shortening of the H-zone and I-band and brings Z-lines closer together leading to shortening of the whole sarcomere. **B:** electron micrographs of sarcomeres contracted to different extents. In a stretched sarcomere, the degree of overlap between thin and thick filaments is the lowest and I-bands and H-zones are clearly visible. At full contraction, the ends of actin filaments in the center of the sarcomere are brought so close towards one another that the H-zone cannot be distinguished anymore. In a slightly contracted sarcomere, I-bands and the H-zone are still seen but are much shorter than in a stretched sarcomere. Bars represent the length of the H-zone in each sarcomere. Magnification 35,000. Figures adapted from Huxley, 1957 and Szent-Györgyi, 2004.

1.3. The myosin superfamily.

Myosins are molecular motors that utilize chemical energy from ATP hydrolysis and convert it into mechanical work coupled to force generation and movement along actin filaments (Howard, 1997). The myosin heavy chain comprises three conserved domains: an N-terminal head domain that is the catalytic core of the molecule; a neck region consisting of one or more IQ motifs that bind light chains of the calmodulin family; a C-terminal tail domain that specifies the function of a myosin (Sellers, 2000).

Myosins are evolutionarily conserved and present in all eukaryotic cells from protists to mammals. It has been suggested that all have evolved from one common ancestor myosin consisting of the catalytic head and neck regions. This might explain high sequence and structural similarities within these regions of known myosin heavy chains

studied to date, as opposed to their highly diverse tail structures (Thompson and Langford, 2002). Therefore, the classification of myosins is usually based on the highly conserved head sequences. The most recent genomic analysis of 2,269 myosin sequences from 328 eukaryotic species grouped myosins into 35 classes and 149 orphan myosins that could not be assigned to any of the groups (Figure 1.3), (Odronitz and Kollmar, 2007). According to this classification, the conventional myosin class 2 (Mhc in Figure 1.3) and unconventional myosin 1 comprise the biggest groups. There are at least 40 myosin genes in the human genome (Foth et al., 2006) encoding myosin heavy chains from at least 12 different classes (Berg et al., 2001).

The identification of skeletal muscle myosin was followed by the purification of two myosins (myosin 1 and myosin 2) from *Acanthamoeba castellani* (Pollard and Korn, 1973a and b). Myosin 2 from *Acanthamoeba* revealed structural similarity to the muscle myosin in that it formed filaments at physiological ionic strength (Pollard et al., 1978). Therefore, those myosins were grouped into myosin class 2 and termed conventional myosins (Sellers, 2000). Since then, conventional myosin 2 isoforms have been identified in smooth and cardiac muscles as well as non-muscle cells (Berg et al., 2001). All other myosin classes are called unconventional myosins.

The plethora of myosin isoforms and their wide distribution among eukaryotic organisms suggests they can perform a variety of cellular functions and that they are important for sustaining life. The functional and structural adaptation of conventional myosin to power muscle contraction was described above; conventional non-muscle myosin was shown to be involved in the constriction of the cytokinetic furrow during cell division (Glotzer, 2005) and in the formation of stress fibers (Hotulainen and Lappalainen, 2006). The unconventional myosins have been implicated in cell motility and polarity, vesicle transport, immune response, wound healing, signaling and actin reorganization (Cheney and Mooseker, 1995; Sellers, 2000).

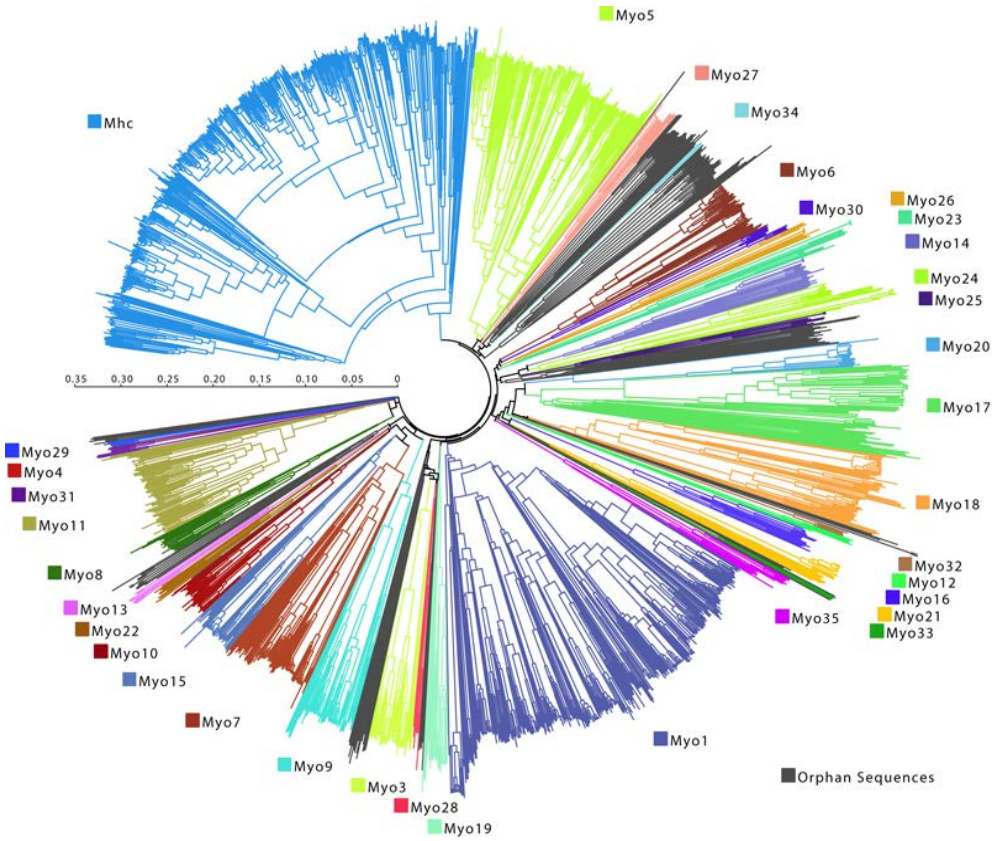

Figure 1.3. The phylogenetic tree of the myosin superfamily. The tree shows the classification of myosin motor domains into 35 classes and 149 orphan myosins. The classification was based on a multiple alignment of 1,984 myosin head sequences. The scale bar corresponds to the number of amino acids within a sequence. Individual groups are color-coded. Figure adapted from Odronitz and Kollmar, 2007.

1.4. Atomic structure of myosin S1.

Fast chicken skeletal muscle myosin S1, the first myosin to be crystallized, revealed many important features of the myosin structural organization (Rayment et al, 1993a). The globular N-terminal head is divided into two distinct parts by a large cleft (50kDa cleft) across the short axis of the head. The actin-binding site is formed by several elements of the cleft (pointing towards the actin filament), whereas the nucleotide-binding pocket is localized at the other end of the cleft. It is separated from the actin-binding site by 4 – 6nm. Therefore, it was proposed that the 50kDa cleft provides a communication route between the actin and the nucleotide sites. Such communication could be achieved by reciprocal

closing of the actin- and nucleotide-binding pockets at both ends of the cleft (Rayment et al., 1993b).

Historically, the myosin head can be divided into 25K, 50K and 20K subdomains, obtained by the proteolytic cleavage of surface exposed loop 1 (near the nucleotide pocket) and loop 2 (part of the actin interaction site), respectively, and corresponding to their respective molecular weights (Rayment et al, 1993a; Sweeney and Houdusse, 2010). Currently, more exact terms are used to describe structural rearrangements associated with individual domains: N-terminal (or 25K) subdomain, upper and lower 50K subdomain (U50K and L50K, respectively) and the converter. The converter functions as a hinge for the light chain binding domain (Sweeney and Houdusse 2010).

The globular myosin head is composed of α-helices surrounding the 7-stranded central β-sheet formed mainly by the N-terminal and U50K fragments and localized near the nucleotide-binding site, on the border between subdomains. Structural rearrangements of individual subdomains during the ATPase cycle of myosin are facilitated by sequential distortion of the β-sheet. Therefore, it has been termed the transducer (Sweeney and Houdusse, 2010).

Figure 1.4 shows the tertiary structure of nucleotide-free chicken myosin 5 with a truncated lever arm. The C-terminal part of S1 forms an extended α-helix (Fig. 1.4. light brown) anchored at the converter domain (Fig. 1.4. light blue) of the globular head and is stabilized by bound light chains. It is referred to as the lever arm throughout the text.

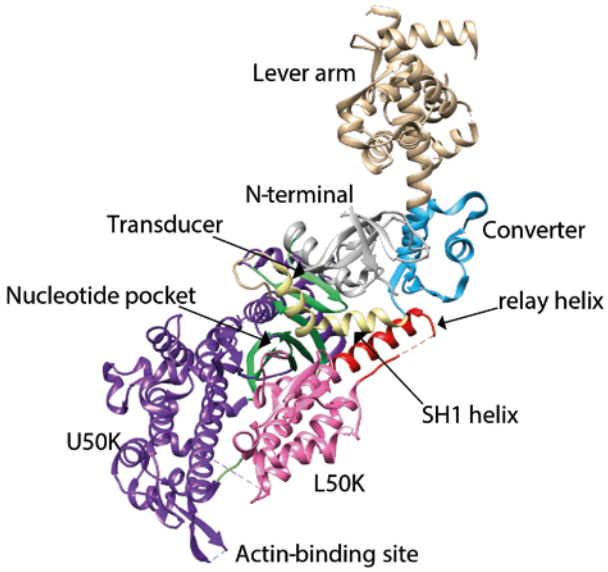

Figure 1.4. The tertiary structure of myosin S1. The figure shows nucleotide-free myosin 5 S1 (PDB #1oe9) including the head domain and a single IQ motif within the neck region, with a single light chain wrapped around it (light brown). Individual domains are color-coded as indicated. The N-terminal region (light gray) is located near the C-terminal lever arm (light brown). The majority of the globular head is divided into upper and lower 50K domains (U50K – purple and L50K – pink) by a 50kDa cleft with the actin-binding site and the nucleotide pocket at opposite ends. Multiple α-helices surround the central β-sheet transducer (green). A number of structural elements involved in the mechanochemical transduction are indicated: the SH1 helix – yellow, the relay helix – red and the converter – light blue. U50K and L50K of myosin 5 are connected by a ~5aa-long strut (light green, next to the actin binding site; Coureux et al., 2004). The primary actin interaction site of myosins, loop 2, could not be resolved and is shown as a dashed line between U50K and L50K. Borders of each domain where established by literature search and colors were adjusted with UCSF Chimera (Pettersen et al., 2004).

The structural organization of the active site of myosin is conserved across the family of NTPases, including G-proteins and microtubule-dependent motors, such as kinesins (Smith and Rayment, 1996). The nucleotide-binding pocket is formed by P-loop flanked by switch 1 and switch 2 regions (Figure 1.5). NTPases are characterized by a P-loop sequence of GXXXXGK(T/S) with myosins containing a conserved sequence GESG(A/S)GKT. In most myosins, switch 1 has a conserved sequence of NXNSSRFG, whereas switch 2 is characterized by the DIXGFE sequence, where X can by any amino

acid (Smith and Rayment, 1996; Saski and Sutoh, 1998; Sellers, 2000). Multiple interactions between the active site elements are pivotal for stabilization of specific conformations of the nucleotide binding pocket associated with the presence or absence of a nucleotide. (Trivedi et al., 2012; Coureux et al., 2003).

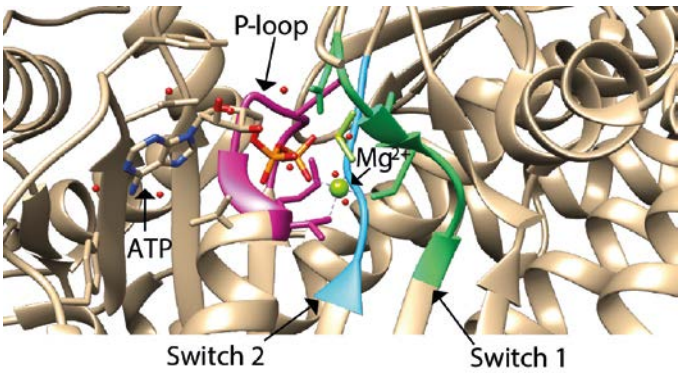

Figure 1.5. The nucleotide-binding site of myosin. The figure is based on the myosin 5 structure with an ATP analogue bound in the active site (PDB # 1w7j). ATP and a magnesium ion are indicated. Small red spheres are solvent molecules. Individual elements of the active site: P-loop, switch 1 and switch 2 are color-coded pink, green and blue, respectively.

1.5. Actin structure.

Vertebrates express three isoforms of actin: α-actin, present in skeletal, cardiac and smooth muscles, and β- and γ-actin, present in both muscle and non-muscle cells (Dominguez and Holmes, 2011). In cells, actin exists in a dynamic equilibrium between globular, monomeric G-actin and polymerized, fibrous F-actin. A single G-actin molecule is composed of two major domains, divided into two subdomains each (Kabsch et al., 1990). For the rest of the chapter the term ‘subdomains’ will be referred to as ‘domains’, in agreement with the literature (Oda et al., 2009; Fujii et al., 2010; Dominguez and Holmes, 2011).

G-actin is an ATPase with the nucleotide-binding pocket enclosed by all four domains of the monomer. MgATP binds to domains 3 and 4, whereas domains 1 and 2 form a hydrophobic groove for binding protein partners, including neighbouring actin monomers in the filament (Oda et al., 2009; Dominguez and Holmes, 2011). The crystal structure of a single G-actin molecule with bound ATP and a cryo-EM reconstruction of an actin filament (F-actin) are presented in Figure 1.6. As shown by the X-ray diffraction of aligned actin fibers (Oda et al., 2009) and cryoelectron microscopy (Fujii et al., 2010), actin filaments are composed of two F-actin protofilaments, wrapped around each other to form a right-handed helix with a helical repeat every 36nm (Trinick et al., 1986).

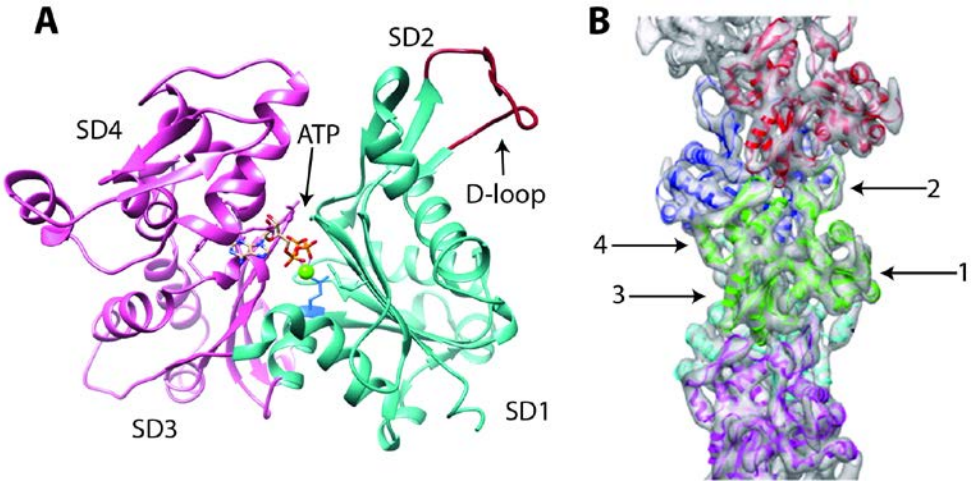

Figure 1.6. The structural organization of G- and F-actin. **A:** a crystal structure of a G-actin molecule with bound nucleotide. Two major domains are colored sea green and pink. ATP is coordinated by Ca^{2+} (green sphere). D-loop (involved in interactions with several binding partners and adjacent actin molecules) is depicted in dark red and Gln137, essential for ATP hydrolysis, is shown in blue. D-loop is ordered in this structure as it is adapted from the DNase I:actin complex structure (Kabsch et al., 1985; PDB #1atn). Individual (sub)domains (SD) are indicated. Note the deep cleft forming the nucleotide binding pocket. The structure was modified with UCSF Chimera. **B:** an atomic model of F-actin fitted into a cryo-EM density map with individual monomeric actin molecules embedded in the filament colored. Domains 1 - 4 in the green subunit are indicated. Figure adapted from Galkin et al., 2010.

1.6. The actin binding site of myosin and models of actomyosin interface.

Myosin binds actin either weakly or strongly depending on the presence or absence of ATP. Transition from the weak to strong interaction is essential for force generation and movement. The initial collision complex involving weak, mainly electrostatic interactions, is thought to isomerize to a strong (rigor) complex which involves major subdomain rearrangements accompanied by conformational changes in the active site and the release of hydrolysis products. Strong binding is thought to be achieved upon closure of the 50kDa cleft, rotation of the U50K subdomain towards the actin helix and increase in the contact area between actin and myosin (Lorenz and Holmes, 2010; Behrmann et al., 2012). Cleft closure seems to involve a conformational change in the strut that would bring the upper and lower subdomains in close proximity, allowing their interaction. Apart from the strut, multiple residues on the inner surface of the U50K and L50K might participate in maintaining closed cleft in the absence of a nucleotide. Sequence differences between different myosins might contribute to the extent of cleft closure and suggest structural adaptations to a biochemical function (Coureux et al., 2004).

When incubated with F-actin in the absence of the nucleotide, myosin S1 molecules bind the filament in the strong (rigor) conformation, producing 'decorated actin' (Figure 1.7) with all myosin heads binding in the same direction (Moore et al., 1970).

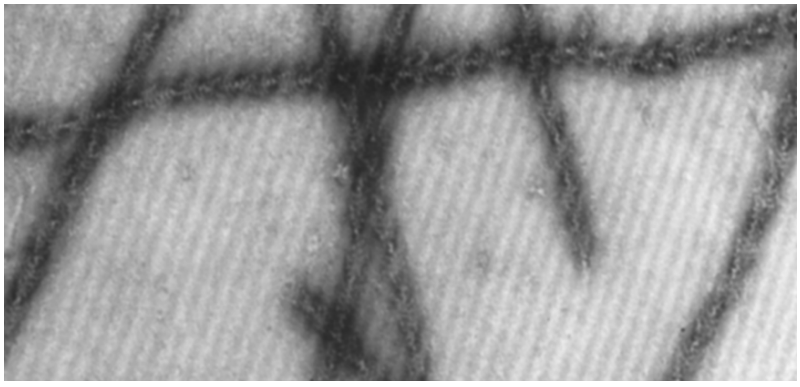

Figure 1.7. 'Decorated actin'. Myosin S1 molecules were incubated with F-actin and negatively stained images were acquired by EM. Magnification 180,000x. Figure adapted from Moore et al., 1970).

The crystal structure of nucleotide-free myosin 5 (Coureux et al., 2003) exhibits closed 50kDa cleft. Indeed, fitting of the crystal structure onto cryo-electron density maps of myosin 2-decorated F-actin revealed no major rearrangements of the tertiary structure of myosin 5 were necessary to achieve a good fit (Holmes et al., 2003; Holmes et al., 2004). Therefore, the nucleotide-free myosin 5 crystal structure provides a good explanation for how the rigor binding can occur. Even though other myosins in the apo (nucleotide-free) form exhibit open or only partially closed 50kDa cleft in detached states, cryo-EM maps of their complexes with actin suggest the cleft closes upon formation of the rigor state (Volkmann et al., 2000; Volkmann et al., 2003).

Fitting of the crystal structures of different myosin isoforms in different nucleotide states to cryo-EM maps of actomyosin complexes reveals that myosin surface loops that are disordered in crystal structures of detached myosins become ordered and clearly visible in cryo-EM densities. This suggests surface loops become stabilized and participate in interactions with actin filament (Volkmann et al., 2000; Volkmann et al., 2003; Lorenz and Holmes, 2010).

Multiple regions and surface loops near the apex of the myosin 50kDa cleft, as well as actin side chains, are thought to participate in the contact formation between actin and myosin (Lorenz and Holmes, 2010). Due to the lack of a co-crystal structure of myosin complexed with actin, the most detailed description of the myosin elements participating in direct interactions with actin in the rigor state comes from the subnanometer resolution (7.7Å) cryo-EM reconstructions of F-actin decorated with *Dictyostelium* MyoE in the presence of tropomyosin (Behrmann et al., 2012) (Figure 1.8). The initial contact area is formed by regions of the L50K subdomain of the myosin head and loop 2 between the U50K and L50K fragments, and is speculated to be mainly non-stereospecific in nature. Secondary contacts between actin and myosin are developed by surface loops of the U50K domain and include bond formation with actin side chains as well as stabilizing interactions with other myosin loops on the actin binding interface of myosin (Lorenz and Holmes, 2010, Gyimesi et al., 2008). Secondary contacts seem to be mainly hydrophobic. The U50K subdomain forms contacts with actin only in the rigor complex, whereas the L50K subdomain mediates both weak and strong interactions (Várkuti et al., 2012). In rigor,

myosin interacts with two actin monomers in the same F-actin strand, forming a contact surface of ~1800 Å (Lorenz and Holmes, 2010; Behrmann et al., 2012).

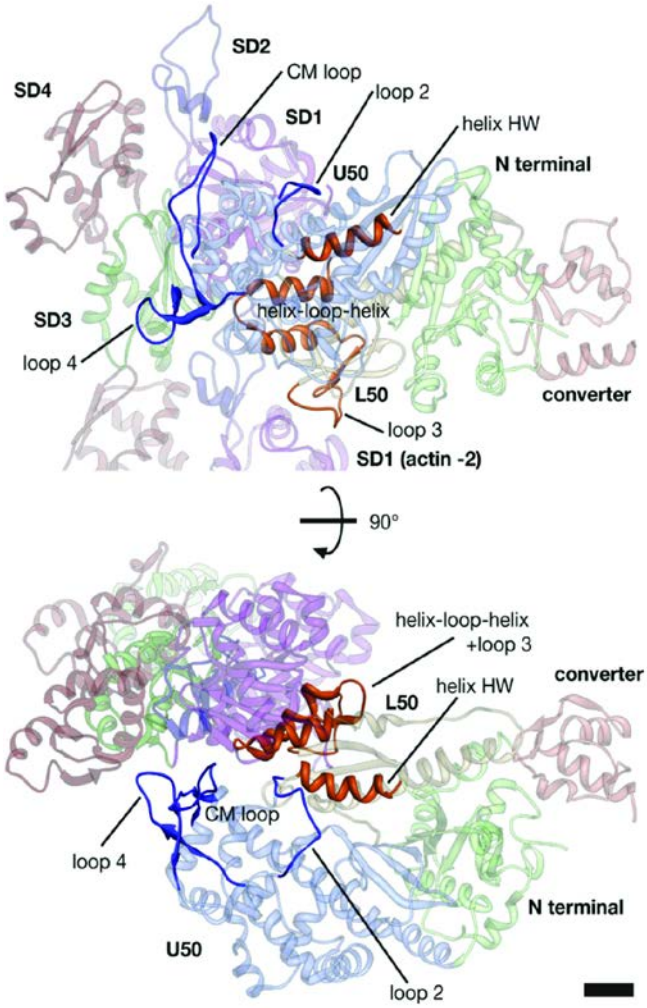

Figure 1.8. The actomyosin interface. The side and top views of the actomyosin contact surface of *Dictyostelium* MyoE. Regions on the myosin head involved in the interaction are highlighted and labeled: loop 2 (547-561aa), helix HW (563-577aa), loop 3 (422-501aa), loop 4 (278-298aa), CM loop (322-342aa) and helix-loop-helix motif (445-481aa). Regions highlighted in orange and blue are part of the L50K and U50K domains of myosin, respectively. Residue numbering corresponds to *Dictyostelium discoideum* MyoE. Scale bar 1nm. Figure adapted from Behrmann et al., 2012.

Models of the actomyosin surface are based on the fitting of myosin S1 crystal structures onto electron density maps of electron micrographs of myosin-decorated F-actin.

Since there is no crystal structure of any actomyosin complex available to date, one must keep in mind that EM reconstructions usually involve adjustments of the tertiary structure of the motor domain in solution to fit the electron density maps and thus serve only as models of an actomyosin interaction. Thus, docking of crystal structures onto density maps has to be accompanied by biochemical studies and single molecule mechanical experiments to unravel the molecular basis of weak-to-strong transition necessary for understanding the basis of force production by myosins (Veigel and Schmidt, 2011).

1.7. The structural basis of the relationship between the actin- and nucleotide-binding sites.

The mechanism of the mechanochemical coupling in myosins arises from structural rearrangements of individual subdomains of the myosin head associated with different nucleotide states. According to current models, introduction of ATP induces conformational changes of the active site elements that are communicated to the actin-binding site through the 50kDa cleft. Via this communication route, binding of ATP and formation of the rigor complex of myosin on actin are mutually exclusive; i.e., binding and hydrolysis of ATP require closing of the active site pocket which causes weakening of the affinity for actin and eventually dissociation of the actomyosin complex, whereas binding to actin induces conformational changes that result in the opening of the nucleotide-binding site and acceleration of product release. The central element in the reciprocal coordination of structural changes at the nucleotide- and actin-binding interface is the transducer. Coupled distortion of the β-strands links conformational changes of the active site to movement of subdomains. On the other hand, position of the lever arm appears to be directly coupled to the position of switch 2 during hydrolysis of ATP and to be communicated from the active site via relay loop and converter (Coureux et al, 2004; Holmes et al, 2004).

In the rigor state, the lever arm is in the ‘down’ position and all subdomains are tightly coupled. The U50K subdomain is moved towards an actin filament by means of the transducer distortion, resulting in closing of the 50kDa cleft on actin. This is associated with exclusion of water molecules from the cleft and involves formation of specific interactions between the L50K and U50K subdomains. Rotation of the U50K subdomain

towards the actin surface enables formation of secondary actin-binding interface essential for the achievement of the rigor state. Low nucleotide affinity in the rigor conformation stems from the specific active site conformation, whereby individual elements interact with one another in a way that hinders coordination of MgATP (Coureux et al., 2003; Coureux et al., 2004).

Upon binding of ATP (post-rigor), untwisting of the transducer occurs. It is associated with change in the position of switch 1 which enables coordination of Mg^{2+} and β- and γ-phosphates, as well as U50K moving away from actin surface, opening of the actin-binding cleft and dissociation of the actomyosin complex. This also causes closing of switch 2 on the γ-phosphate, necessary for ATP hydrolysis to occur and transition into the pre-powerstroke (transition) state. This is associated with the rotation of the L50K subdomain that applies strain on the relay helix (Holmes et al, 2004). To accommodate that strain, the relay forms a kink that results in a ~60^{o} rotation of the converter domain. This situates the lever arm in the up or 'primed' position. The transition state is regarded as the beginning of the powerstroke or a force-generating cycle of myosin.

It was proposed that after ATP hydrolysis myosin binds to actin in a step-wise manner, where each step is associated with an increase in the affinity for actin and a decrease in the affinity for the nucleotide in the myosin active site. The initial weak interactions are followed by a conformational change in the transducer (Geeves and Holmes, 2005). This introduces an intramolecular strain that could be released through straightening of the relay loop (Holmes et al, 2004). At this point, the converter domain would rotate back and the lever arm would undergo a swing to its rigor-like position, a phenomenon called a power stroke. This might be concomitant with the γ-phosphate release probably through a 'back door' mechanism (Yount et al, 1995). Simultaneously, distortion of the transducer would result in the movement of the U50K domain and closure of the actin cleft, separation of switch 1 and P-loop and destabilization of the myosin-nucleotide complex. Described model provides an explanation for how can actin act as a nucleotide exchange factor of myosin; upon strong binding to actin, a conformational rearrangement of the active site elements could disrupt high affinity coordination of Mg^{2+} (necessary for

maintenance of cleaved γ- phosphate) and nucleotide (Coureux et al, 2003).

1.8. The kinetic cycle of a myosin crossbridge.

The overall mechanism of the actomyosin ATPase cycle is conserved within the myosin superfamily. That is, the order of the kinetic pathway as well as kinetic intermediates are the same for all myosin motors. Yet, rates and equilibrium constants of individual steps within the cycle differ between isoforms and represent adaptations of different superfamily members to perform diverse mechanical and physiological functions. Thus, revealing the transition rates and population lifetimes of particular steps in the pathway is important for understanding biochemical adaptations of individual myosin isoforms to perform specific physiological tasks (De La Cruz and Ostap, 2004; Geeves et al., 2005; De La Cruz and Ostap, 2009).

The basis of the current view on the biochemical cycle of the myosin cross bridge is provided by initial measurements of (Lymn & Taylor, 1971) performed with rabbit muscle HMM. The Lymn and Taylor cycle explains how enzymatic events related to ATP binding and hydrolysis correspond to mechanical steps of the cross bridge. The kinetic cycle of Lymn and Taylor consists of 4 steps: i) a rapid dissociation of the actomyosin complex following ATP binding, ii) hydrolysis of ATP to ADP.Pi on free myosin in solution, iii) interaction of actin with the myosin-ADP.Pi complex, iv) product release from actomyosin. That data complements the mechanical cross bridge cycle where the dissociation of myosin from actin is followed by structural changes in myosin associated with the transition to the pre-power stroke conformation, subsequent recombination of myosin and actin and product release concomitant with the power stroke. The kinetic cycle of the mechanical cross-bridge is presented in Figure 1.9.

Furthermore, Lymn and Taylor's measurements show that i) the rate constant of ATP hydrolysis by HMM alone and actin-HMM complex is similar, ii) ATP binding causes a rapid dissociation of the actomyosin complex with the rate constant at least 10x faster than ATP hydrolysis and iii) actin accelerates product release as compared to the rate of HMM alone (Lymn and Taylor,1971).

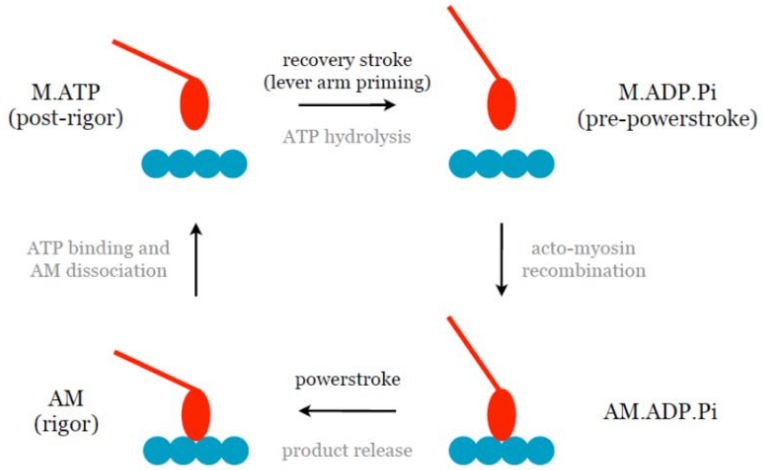

Figure 1.9. Lymn and Taylor kinetic pathway of the mechanical crossbridge. The rigor actomyosin complex (AM) dissociates upon ATP binding (M.ATP). Free myosin hydrolyzes ATP to ADP.Pi (M.ADP.Pi) concomitant with the rotation of the lever arm to the UP position (recovery stroke). The pre-power stroke state (M.ADP.Pi) recombines with actin (AM.ADP.Pi) and myosin undergoes a power stroke associated with product release resulting in formation of the rigor (AM complex). M - myosin, AM - actomyosin.

The Lymn and Taylor cycle implies a direct coupling between individual kinetic and mechanical steps of myosin on actin. Additionally, an indirect coupling model (3G model) proposed by Geeves et al. (1984) suggests that each step in the kinetic cycle (namely actomyosin complex formation, ATP binding and the release of hydrolysis products) is associated with at least two-step mechanical event. This model implies that force generation by crossbridges in the sarcomere occurs as a result of changes in the affinities between actin and myosin in a nucleotide-dependent manner. When binding to actin, myosin initially forms a weak collision complex with the thin filament, followed by an isomerization to a strong-binding complex. This change in the affinity between the two steps does not have to be accompanied by a large structural change of myosin S1, and can only constitute of small changes in the actomyosin interface. This is in contrast to the direct coupling model that suggests that force generation is the direct result of the conformational change in the myosin. After the rigor complex formation, an initial collision complex of actomyosin with ATP is formed, followed by an isomerization step associated with rapid dissociation of myosin from actin. The release of hydrolysis products from myosin occurs in a detached

state. If the isomerization to the strong actin-binding complex causes a structural change which results in force generation on actin, then product release would be associated with a reversal of that change (Bagshaw et al., 1974). The 3G model implies that such structural change would occur in a detached state of myosin, thus causing no negative force-generating event on actin (Geeves et al., 1984). The most widely accepted scheme of the actomyosin ATPase cycle is presented below:

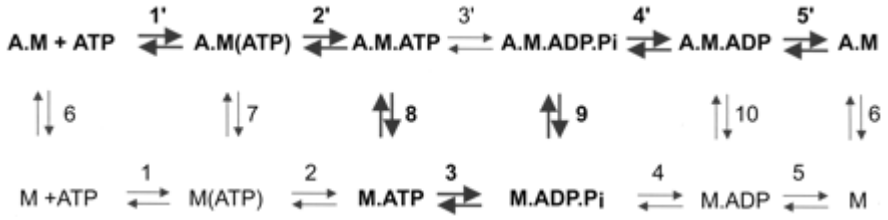

Figure 1.10. Model of the kinetic cycle of myosin S1. The top row represents actin-associated states and bottom row – actin-detached states. The major ATPase pathaway is highlighted in bold. Figure adapted from Liu et al., 2005.

1.9. The mechanism of the myosin ATPase activation by actin.

It has been proposed that actin and nucleotide binding are reciprocal, namely that binding of ATP to myosin causes dissociation of the actomyosin complex, whereas a recombination with actin accelerates product release (Conibear et al., 2003). Therefore, the recombination of myosin with actin following ATP hydrolysis and the transition from weak to strong actin binding is thought to be the basis for the activation of the intrinsic myosin ATPase by actin and results in the generation of force and motion on an actin filament.

The acceleration of the γ-phosphate release after hydrolysis is the first step of the isomerization to the strong actin-binding state. In order to achieve strong binding, the U50K domain would need to rotate towards the actin filament and L50K domain. Since switch 1 is structurally a part of the U50K domain, rotation of the latter would remove switch 1 from the active site. This would result in the opening of the nucleotide-binding pocket and destruction of bonds with the hydrolyzed nucleotide resulting in product release (Conibear et al., 2003; Holmes et al., 2003; Onishi et al., 2006).

By contributing ionic or hydrophobic interactions, which affect weak and strong actomyosin binding, different regions on the myosin surface influence the maximal ATPase rate (V_{max}) and apparent dissociation constant of myosin from actin in the presence of ATP (K_m). The overall charge of the primary actin interaction site of myosin, loop 2, modulates actin affinity (Bobkov et al., 1996; Murphy and Spudich, 2000; Joel et al., 2001). The lysine cluster at the end of loop 2 (which contains 2-4 lysine residues, depending on the myosin isoform) seems important for the transition from the weak to strong actin binding. This was demonstrated by the inhibition of the sliding velocity and the maximal ATPase activation by actin in mutants lacking the C-terminal lysines cluster in loop 2 (Joel et al., 2001). Furthermore, the cardiomyopathy (CM) loop of the U50K domain, which creates secondary stereospecific contacts with actin in the strong binding state, contains a cluster of hydrophobic residues with solvent-exposed side chains for actin interaction (Sasaki et al., 1999, Onishi et al., 2006). In agreement with its function in strong actin binding, necessary for product release, mutations in the CM loop led to the decreased actin-activated ATPase (Sasaki et al., 1999; Onishi et al., 2006). Furthermore, a conserved Arg right upstream of the CM loop corresponding to Arg397 in *Dictyostelium discoideum* myosin 2 is also essential for actin-activated ATPase (Sasaki et al., 1999). In human β-cardiac myosin, mutation of that residue to Gln causes familial hypertrophic myopathy (Geisterfer et al., 1990). It was proposed that residue is involved in the stabilization of a specific loop 2 conformation (Lorenz and Holmes, 2010). Therefore such severe phenotype caused by a single mutation is related to decreased actin affinity in mutants with substituted Arg at this position (Sweeney et al., 1994; Fujita et al., 1997). Also within the CM loop, a TEDS site (corresponding to Asp403 in *D. discoideum* myo2), containing one of the indicated residues, has been characterized (Kollmar et al., 2002). Myosins with Asp or Glu at this position are constitutively active, whereas Thr or Ser provides means of regulating the intrinsic ATPase activity by phosphorylation (Sasaki et al., 1999, Kollmar et al., 2002). Loop 3 of the L50K domain of myosin also contains a cluster of hydrophobic residues which contribute to strong actin binding and thus are necessary for actin-activated ATPase and accelerated γ-phosphate release from the nucleotide pocket (Kojima et al., 2001, Onishi et al., 2006).

Finally, a recently characterized activation loop located in the relay helix has been suggested to improve the efficiency of successful power strokes, i.e. performed in actin-attached, rather than actin-detached, state (Várkuti et al., 2012). That loop consists of a few amino acids with a conserved positive charge (usually Lys or Arg) at a position corresponding to Arg520 in *Dictyostelium discoideum* myosin 2. Following ATP binding, switch 2 closes on the nucleotide, leading to a change in the conformation of the lever arm into an UP position concomitant with ATP hydrolysis and transition into the beginning of the power stroke state. By means of the interaction of the activation loop with actin, that specific conformation of the lever arm is stabilized, therefore directing the catabolic fluxes towards successful force generation on actin and directly coupling hydrolysis product release to force production. Such mechanism might be essential for robust muscle contraction (Várkuti et al., 2012).

1.10. Generation of force and movement by a single crossbridge.

The sliding filament theory described in section 1.1. explains the mechanism behind the shortening of sarcomeres and muscle contraction. Myosin molecules (crossbridges) in thick filaments cyclically interact with actin in interdigitating thin filaments driving sliding of the two past each other. A few models have been proposed regarding the interaction and performance of individual crossbridges in the muscle sarcomere.

1.10.1. The thermal ratchet model (AF Huxley's 1957 model).

Binding of myosin to actin is dependent on the position of myosin in relation to the available binding site on actin. The myosin motor contains a flexible element that becomes extended as it undergoes thermal fluctuations in search for the next binding site. Extension of that element introduces strain into the motor domain. Binding of myosin to actin can occur only when strain is introduced into the spring element of the molecule, thus facilitating binding of extended molecules that would drive contraction, as opposed to molecules with a contracted elastic element. Strain produces force on actin filament and

drives contractile motion. Shortening of the elastic element during an actin-attached state results in strain relief. This is followed by the release of myosin from actin.

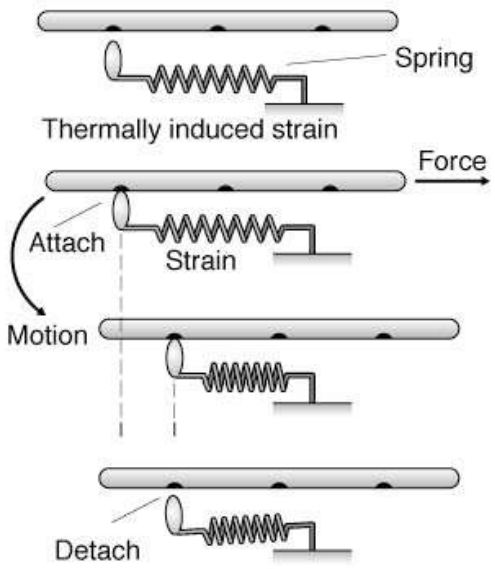

Figure 1.11. The thermal ratchet model based on Huxley, 1957. The myosin molecule contains an elastic spring element that undergoes thermal fluctuations along the filament lattice. In the presence of strain myosin attaches to actin, applying force and driving motion. Motor detaches from actin under strain release. Figure adapted from Howard, 2009.

Given a moderate rate of attachment, dependent on the relative position of myosin and actin, the rate of detachment of myosin from actin is low during force production and high at the end of it. During an isometric muscle contraction, the detachment rate of myosin crossbridges is slow. However, during active muscle shortening, the detachment rate will increase due to continuous change in the position of available binding sites on actin. This accounts for increased cycle rates and energy consumption during contraction. Furthermore, myosin will interact with any given actin binding site only for a limited period of time with the interaction time decreasing with the increasing shortening velocity. Therefore, the number of crossbridges bound to actin will decrease with higher shortening velocity, eventually leading to a decrease in muscle tension. At high shortening velocities, a number of crosbridges will exhibit a negative displacement on actin, causing a drag force. The number of positively (exerting force in the direction of movement) and negatively (exerting

drag) displaced crossbridges will reach an equilibrium at the maximum unloaded shortening velocity, resulting in the net force of muscle contraction equal 0.

1.10.2. The power stroke model (AF Huxley and Simmons 1971 model).

In the power stroke model, the strain in the myosin motor domain that results in force generation and motion along the actin filament lattice comes from a relatively large conformational change in the motor domain (Figure 1.12) (Howard, 2009). Such conformational change would occur as myosin rebinds actin following ATP hydrolysis, and would involve a rowing-like motion, the power stroke, that would bring about the displacement of the thin filament relative to the myosin crossbridge in the thick filament. The power stroke would occur concomitantly with ATP hydrolysis products release.

That model, also referred to as a swinging crossbridge model, did not provide a clear explanation as to what part of the molecule is the subject of the conformational change that leads to force generation and results in muscle contraction. The first crystal structure of myosin S1 (Rayment et al., 1993a) led the authors to hypothesize that the globular myosin head might bind actin in a relatively fixed orientation, allowing the C-terminal extended α-helical neck to rotate around the anchor point, behaving like a lever. In that sense large changes in the position of the neck would be the result of small changes in the motor domain. The rotation of the neck domain was proposed to be the basis of force generation and movement (Rayment et al., 1993b). This model is now known as the swinging lever arm model.

Following the hypothesis that the lever arm multiplies small conformational changes in the myosin motor domain into large scale mechanical steps on actin, an *in vitro* motility assay for quantitative measurements of myosin movement was developed to test the predictions. The first quantification of myosin movement rates along actin was made by using *Nitella* cells that contain well-organized, polarized actin cables. Application of skeletal myosin HMM covalently linked to fluorescent beads onto exposed actin cables in the presence of ATP resulted in robust and directional movement over long distances. It required ATP and enzymatically-active myosin molecules, confirming that the observed

motility was the result of the mechanochemical coupling in myosin molecules. The rate of movement was determined from the change in the position of fluorescent beads along an actin path during the timecourse of the experiment (Sheetz and Spudich, 1983). An improved version of the assay, that is routinely used nowadays, involved fully reconstituted actin-myosin system composed of isolated components (Kron and Spudich, 1986). Myosin molecules are fixed to a glass surface of an experimental chamber and covered with fluorescent phalloidin-stabilized actin filaments. Filaments move over long distances over the myosin-coated surface in the presence of ATP. The most important features of that assay include reproducibility and ease of preparation and enable testing different buffer conditions and myosin isoforms (Kron and Spudich, 1986; Harada et al., 1987). The velocity was not dependent on the species origin of actin (Kron and Spudich, 1986).

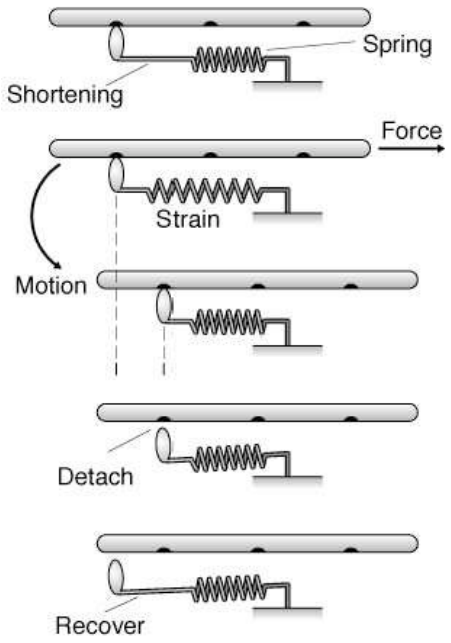

Figure 1.12. The power stroke model based on Huxley and Simmons, 1971. The myosin motor domain contains a spring-like element that undergoes a conformational change following binding to actin. This conformational change in the motor domain introduces strain into the molecule and causes generation of force on an actin filament. Strain relief occurs as the elastic element in the motor domain returns to its original position and is concomitant with actin displacement. This is followed by detachment of myosin from actin and recovery. Figure adapted from Howard, 2009.

1.10.3. Single molecule mechanics with optical tweezers.

The development of the *in vitro* motility assays enabled the investigation of mechanical properties of molecular motors working as an ensamble. However, similar to the situation in muscle, individual motor molecules deposited on the surface of the flow chamber do not have their kinetic cycles synchronized. That means that in any given population of motors in the direct viccinity of the filament, only a certain fraction will interact with the filament and produce force at any given timepoint. Furthermore, it still was unknown how a single motor would move on the filament. Would it exhibit periods of activity interspersed with unproductive periods? Or would it move in uniformly distributed discrete steps? How many ATP molecules are hydrolyzed per single step of myosin on the filament? Therefore, in order to reveal the action of individual motors in the muscle, one has to study them under conditions ensuring interaction of only a single motor with actin at a time.

This has been achieved by employing an optical trapping setting. First experiments with cytoskeletal motors in the optical trap were performed with kinesin (Svoboda et al., 1993). Individual kinesin molecules were attached to silica beads and deposited on microtubules attached to the coverslip surface. The bead was held in the laser trap and its position was detected throughout the experiment. In the presence of ATP kinesin exhibited robust movement along the microtubule lattice, causing displacement of the bead from the centre of the trap. Per single encounter with microtubule, kinesin would take multiple steps before detaching. Each step caused the bead displacement of 8nm, suggesting it spans a distance of one dimer in a protofilament. By changing the laser power, the load imposed on the bead could be adjusted. Individual step sizes were independent from the load applied, showing that kinesin can sustain low pN-range forces when travelling along microtubule. Furthermore, decreasing the ATP concentration caused slower velocity of kinesin on microtubule, without affecting the step size. This confirms the hypothesis that a single step happens per one ATP hydrolysis cycle (Svoboda et al., 1993).

A firm filament attachment to the coverslip surface might hinder unobstructed movement of the motor that follows a helical, instead of a linear, path along the filament. Thus, the assay geometry was improved to allow the filament to be unconstrained during

the experiment. An actin filament was suspended between two polystyrene beads trapped by laser above the coverslip surface. Myosin was deposited on silica beads firmy attached to the coverslip. Low myosin densities were used to ensure that observed interaction events include a single crossbridge. By bringing the actin filament in the proximity of the myosin-coated platform bead, the interaction was initiated. The position and Brownian motion of one of the beads was monitored. Upon the actomyosin interaction, the Brownian noise decreased due to an increase in the stiffness of the system. The displacement and force produced by myosin on actin was related to the change in the position of one of the beads in a trap (Finer et al., 1994). The schematic depiction of that assay geometry is shown in Fig. 1.13.

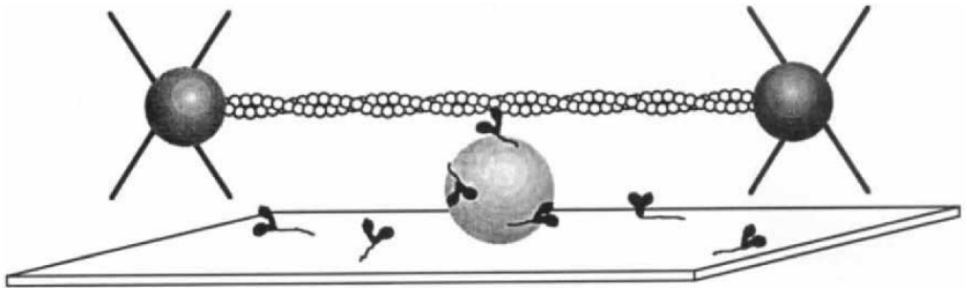

Figure 1.13. A three-bead optical trapping assay corresponding to Finer et al., 1994. Polystyrene beads (black) were trapped in a two-beam optical trapping laser. Actin filament ends were attached to solution-suspended beads coated with inactivated myosin molecules. Silica beads (gray) were attached to the coverslip surface and coated with myosin motors. The actin filament was brought close to the myosin platform, allowing an interaction between the motor and the filament.

The assay was used to directly measure the displacement and force produced by single-headed muscle myosin S1 molecules (Molloy et al., 1995). The attachment lifetime of individual actomyosin complexes was dependent on ATP at low ATP concentrations. This indicates that a single attachment is terminated by a new ATP molecule binding to myosin, and thus a single ATPase cycle is coupled to an individual step of myosin on actin. Furthermore, comparison of S1 and HMM molecules revealed that the displacement and forces produced were similar for both constructs. This suggests that in a dimeric muscle myosin 2 the heads are independent from each other and that a single crossbridge is enough

to generate force and movement in muscle (Molloy et al., 1995). This is in agreement with the lack of coordination of chemomechanical cycles of individual myosins in thick filaments in sarcomeres.

1.10.4. Load-dependence of muscle contraction.

In order to maintain efficient energy use, the shortening velocity of the sarcomere is high at low loads enabling rapid tension generation and muscle contraction. However, when high load is applied, at extended contraction duration, the shortening velocity is slower (Huxley and Simmons, 1971). From the molecular point of view this means that the muscle metabolism, and ultimately the kinetics of individual corssbridges, is strain-dependent.

Analysis of single interaction events of smooth muscle myosin S1 with actin revealed that the overall attachment lifetimes are dependent on the amplitude and direction of an applied load (Veigel et al., 2003). Similar to other myosin isoforms described below, smooth muscle S1 produced a working stroke in two phases contributing to different extents to the overall stroke. It was proposed the two conformational changes between two phases are associated with subsequent Pi and ADP release. Thus, the lifetimes of the first and second phase correspond to the amount of time spent in the ADP-bound and nucleotide-free forms, respectively. This is in agreement with the structural data that shows different conformations of the smooth muscle myosin lever in the presence and absence of ADP (Whittaker et al., 1995; Gopllub et al., 1996). In contrast to the first phase, the duration of the second phase was ATP concentration-dependent, suggesting the working stroke is terminated when new ATP molecule binds to myosin. The duration of the first phase was extended when the load applied in the direction of movement was increased. This suggests that the force-generating biochemical state of myosin (ADP-bound) might be dependent on the applied strain and thus control the interaction lifetime of crossbridges with the thin filament in muscle (Veigel et al., 2003). Indeed, in an unloaded muscle undergoing the maximal shortening velocity of contraction only 1% of all heads interact with actin and that number might increase up to 80% under an isometric force (Bagshaw et al., 1993). Therefore, the amount of myosin heads attached to thin filaments at a given time point acts as a mechanism to oppose an external load.

1.11. The lever arm hypothesis.

The power stroke model described above has been gradually updated to a swinging lever arm model, whereby the bulk part of myosin (i.e. the globular head) binds actin in a relatively fixed geometry and only the C-terminal part of S1 (i.e. the neck region) changes its orientation relative to actin. It was proposed that the small conformational changes in the active site of the motor are amplified into large swinging motion of the neck region. Because of that, the neck region is referred to as the lever arm (Holmes, 1995).

In order to visualize the change in the conformation of the neck region, actin was decorated with myosin S1 in the presence and absence of ADP, and imaged by cryoelectron microscopy. Initial experiments with skeletal muscle myosin S1 did not show any difference in the position of the lever arm. Experiments performed with brush border myosin 1 (BBM1) S1 and smooth muscle myosin S1 showed that the neck region changes its angle relative to actin upon ADP release. Based on image analysis, it was suggested that the end of the lever arm of BBMI and smooth muscle S1 would swing by ~7.2nm and ~3.2nm, respectively. That difference between the two myosins was attributed to a different amount of light chains bound to their lever arms (3 for BBM1 and 2 for smooth muscle myosin). Since the power stroke is the force-generating step in the myosin ATPase, it would only make sense if it occurred when myosin is strongly attached to actin. Thus, the electron micorscopy data provided direct evidence that ADP release acts at least as a part of the power stroke, which occurs during strongly-bound states of myosin on actin. Furthermore, it was concluded that the neck region converts small molecular changes at the active site into a large mechanical change, resulting in movement. Because of this, the light chain binding domain was termed the lever arm (Jontes et al., 1995; Whittaker et al., 1995). It was further confirmed that such angular change in the position of the neck domain occurs in a contracting muscle. By fluorescently labeling of regulatory light chains in isolated skeletal muscle fibers, tilting of the neck regions of myosin heads was observed by fluorescence polarization. This way individual power strokes of myosins within the thick filament of the sarcomere were observed (Irving et al., 1995).

Finally, the rotation of the neck region between the nucleotide-free state (that adopts a conformation of a rigor form of myosin) and the transition state (ADP.Pi state, thought to

represent the beginning of the power stroke) was shown in the crystal structure of *Dictyostelium* myosin 2 with bound ADP.Vanadate (a transition state analog) (Smith and Rayment, 1996). When compared to the nucleotide-free structure of chicken skeletal S1 (Rayment et al., 1993a), the lever arm swung by ~12nm in the transition state *Dictyostelium* myosin 2 structure (Figure 1.14). It is possible such conformational change could occur in an actin-bound state.

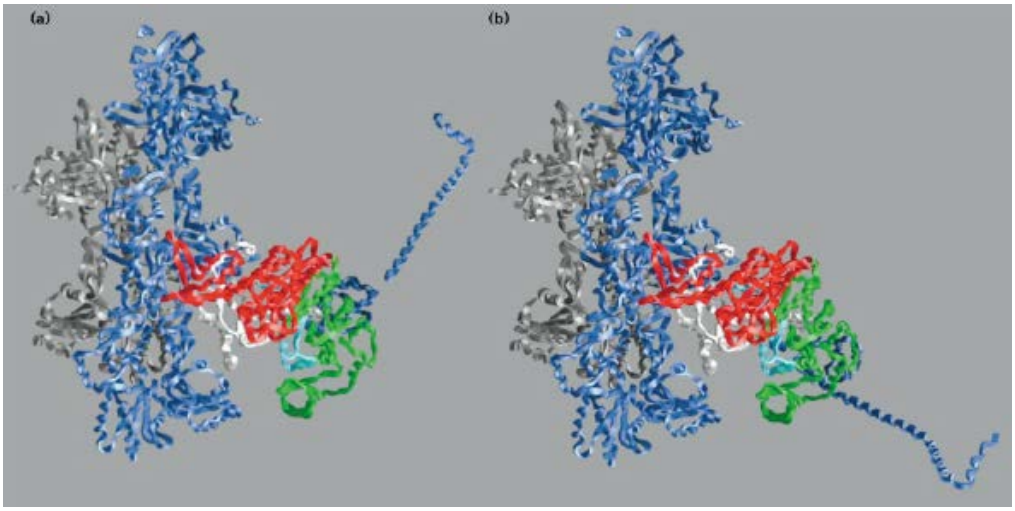

Figure 1.14. Structures of actin-bound myosin in the transition and rigor states. Reconstructions of the actomyosin complex in the transition (left) and rigor (right) states based on *Dictyostelium* myosin 2 with ADP.Vanadate and nucleotide-free chicken skeletal S1, respectively. The structures represent the beginning (left) and end (right) of the power stroke. The position of the lever arm in the *Dictyostelium* structure was restored from chicken skeletal S1 coordinates based on the position of the converter in that structure.

If the lever arm undergoes a dynamic large conformational change in association with the ATPase cycle, then the velocity of myosin should be proportional to the amplitude of the rotation of the lever, and therefore to the lever arm length. In combination with protein engineering strategies and recombinant protein expression, the *in vitro* gliding filament assay was used to prove the sliding velocity of myosin is linearly-dependent on the length of the neck domain (Figure 1.15; Uyeda et al., 1996). The lever arm of *Dictyostelium* myosin 2 was gradually shortened by a single light chain-binding site at a time or was extended by one additional motif. The sliding velocity was directly proportional to the

length of the neck domain with a y-intercept corresponding to the position of the fulcrum point in the motor domain, which serves as a pivot point over which the swinging of the lever occurs (an SH1-SH2 helix). A construct containing only the first IQ motif exhibited half the velocity of actin movement of the wild type, whereas one with an additional IQ motif added downstream of the wild type lever arm translocated actin 0.25 times faster than the wild type (Uyeda et al., 2002). In line with that, chimeric myosin constructs containing α-actinin repeats in place of IQ motifs functioned as artificial lever arms, resulting in faster sliding velocities in myosins containing more repeats (Anson et al., 1996; Ruff et al., 2001; Warshaw et al.,2000).

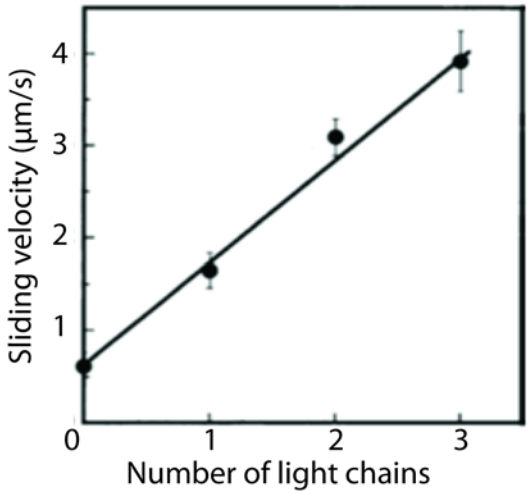

Figure 1.15. The sliding velocity of myosin is linearly dependent on the length of its lever arm. *Dictyostelium* myosin 2 containing 0, 1, 2 (wild type) or 3 light-chain binding motifs in the neck region translocated actin filaments in the *in vitro* motility assay with the sliding velocity proportional to the length of the lever of the construct used. The y intercept corresponds to the position of the fulcrum in the motor domain over which rotation of the lever arm occurs. Figure adapted from Uyeda et al., 1996.

1.12. The mechanochemical coupling in myosin motors.

How does the conformational change of the lever arm occur? How is force produced by myosin bound to actin? How is it coupled to steps in the myosin ATPase cycle? Which stage of the hydrolysis product release process is associated with force generation? Does

movement and force production occur simultaneously with actin binding after ATP hydrolysis?

A three-bead optical trapping assay was used to directly observe and measure isolated mechanical events of single-headed myosin 1 isoforms on actin (Veigel et al., 1999). Slower kinetics of myosin 1 (longer actomyosin interactions and slower hydrolysis products release, as compared to fast skeletal muscle myosin; Jontes et al., 1997) enabled better spatiotemporal resolution of the experiment. Individual actomyosin interactions were analyzed following ensemble averaging that involved synchronization of the beginning and end points of single displacements and reduction of the background noise. Both myosin isoforms underwent a two-phase working stroke on actin. The first phase was larger than the second phase and occured with a slight delay following actin binding. The second phase was linearly dependent on ATP concentration, suggesting the event is terminated with a new ATP molecule binding to the motor domain. Therefore, the force-generating power stroke occurs in two phases probably related to sequential hydrolysis products release, and is associated with the hydrolysis of a single ATP molecule (Veigel et al., 1999).

Finally, an improvement in the spatiotemporal resolution of optical tweezers enabled a direct observation and measurement of the power stroke of the fast rat non-muscle myosin 2B (Capitanio et al., 2006). The power stroke of myosin 2B occurred in two phases, proposed to correspond to Pi release and ADP release, respectively. Again, the first phase was larger than the second phase and occurred rapidly after binding actin. The detachment rate of myosin 2B from actin was dependent on the rate of ATP binding, indicating that ADP release occurs faster than ATP binding. This has been suggested to be the basis for the robust shortening velocity of conventional myosins in muscles (Capitanio et al., 2006).

A unidirectional two-phase power stroke which occurs with a delay after actin binding was also exhibited by recombinant single-headed myosin 5 S1 and intact dimeric myosin 5 (Veigel et al., 2002), myosin 6 (Lister et al., 2004) and myosin 10 (Takagi et al., 2014). Similar to (Veigel et al., 1999), the displacement produced in the first phase is larger than that produced in the second phase. It was proposed that the first phase of the working stroke is related to Pi release, wherease the second phase is associated with ADP release

and leads to the formation of a rigor state. The lifetime of the second phase is ATP-dependent, with a higher rate constant at higher ATP concentration (Veigel et al., 2002; Lister et al., 2004). The dependence of the rate constant of the second phase on ATP concentration is in agreement with solution kinetic experiments which show that ADP release is a rate-limiting step for both myosin 5 and myosin 6 (De La Cruz et al., 1999; De La Cruz et al., 2001).

The dependence of the stroke amplitude on the length of the lever arm was directly presented by using the combination of recombinant protein techniques and optical trapping assays. Single- and double-headed mutant myosin 2 and myosin 5 isoforms engineered to encompass a different number of the light-chain binding motifs in their neck regions (Ruff et al., 2001; Purcell et al., 2002), or with artificial neck domains composed of α-actinin repeats (Ruff et al., 2001) were used to measure the size of the power stroke (termed step size) in three-bead laser trap assays. Step sizes were obtained from the change in the mean displacement of the bead in one of the traps during binding of myosin to actin. The stroke size was directly correlated to the length of the myosin lever arm of both dimeric and monomeric myosins, regardless of whether it contained IQ motifs or α-actinin repeats. Kinetic properties of monomeric constructs were not affected by the length or composition of the lever arm.

The data described above suggests that all myosin isoforms share common mechanism of force production. The bound myosin state exists in two mechanical conformations associated with subsequent events in the ATPase cycle. The swinging of the lever arm is associated with nucleotide release. The amplitude of the stroke depends on the length of the lever arm and attachment lifetimes and detachment rates of myosin from actin represent differences in rate constants of the kinetic cycle of a given myosin isoform.

1.13. Processivity and duty ratio.

Processivity is defined as the ability of a molecular motor to take multiple steps upon its encounter with the cytoskeletal track. That means that processive myosins will undergo multiple ATPase cycles when associated with the filament and move longer

distances than a single step driven by a single ATPase cycle. In contrast, non-processive myosin motors perform only a single step on the filament before detaching from it (De La Cruz et al., 1999; Mehta et al., 1999, Higuchi and Endow, 2002). Processivity of a myosin motor can be easily assessed by *in vitro* motility assays, where the density of motors on the surface is gradually decreased until only a single motor interacts with a single actin filament; processive myosin will support translocation of the filament even at such low densities, whereas at least two non-processive motors are necessary for sliding of actin filaments, therefore releasing actin at lower densities (De La Cruz et al., 1999).

Duty ratio defines the fraction of the total ATPase cycle that myosin spends strongly bound to actin. Duty ratio and processivity are closely related, in that processive motors exhibit high duty ratios, i.e. spend most of their ATPase cycle in a strongly-bound actin state, whereas non-processive myosins are low duty ratio motors. Duty ratio is governed by the rate-limiting step of the ATPase cycle; for low duty ratio motors, Pi release, and therefore the entrance to the strong actin binding state, is the slowest step of the kinetic cycle, whereas high duty ratio myosins spend most of their cycle with ADP bound in the nucleotide-binding pocket (De La Cruz et al., 1999).

Duty ratio and processivity are important features governing an intrinsic physiological function of different myosin motors. Skeletal muscle myosin 2 is a non-processive motor and exhibits low duty ratio (Figure 1.16A), namely it spends most of its catalytic cycle in a weak actin-binding form. This ensures short-lived interactions with actin, consisting of a single power stroke per single encounter with the filament (Uyeda et al., 1991; De La Cruz and Ostap, 2004). Yet, the structural organization of thick filaments results in efficient muscle contraction. Despite working as an ensemble, there is no synchronization of the kinetic cycles of the heads in the thick filament and all heads are at different stages of the ATPase cycle at any given time point. By performing only a single power stroke upon interaction with actin in thin filaments of the sarcomere, individual myosin heads do not cause the drag on other myosin heads associated with actin. Those rapid interactions enable individual heads to perform as much work as possible, resulting in an efficient pulling of the filaments towards the center of the sarcomere and robust

contraction by means of many myosin heads asynchronously undergoing power strokes on the thin filament (Bagshaw et al., 1993).

On the other hand, mammalian myosin 5a is a processive, high duty ratio motor (Figure 1.16B) involved in the transportation of cellular cargo along actin (Reck-Petterson et al., 2000; Vale, 2003). Myosin 5a exhibits high affinity for ADP and spends most of its ATPase cycle with ADP present in the nucleotide-binding pocket (De La Cruz et al., 1999). How the occupancy of the strongly-bound actin state through the majority of its catalytic cycle contributes to the motility of myosin 5 will be discussed below.

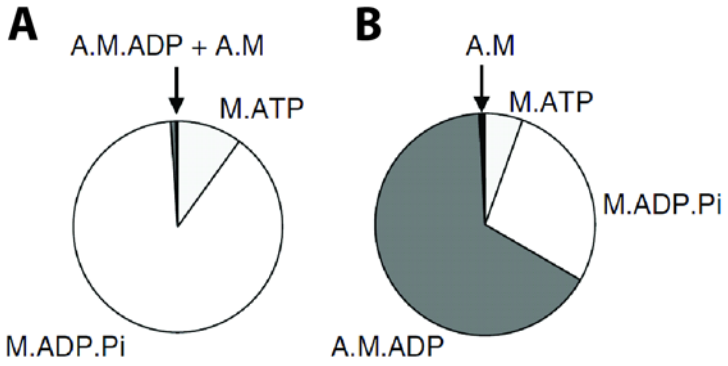

Figure 1.16. Full ATPase cycle of skeletal muscle myosin 2 (**A**) and mammalian single-headed myosin 5 (**B**) presented as a pie chart. The overall ATPase cycle (360^{o}) is divided into sectors corresponding to the time of the cycle each myosin spends in a given state. Skeletal myosin 2 and single-headed myosin 5 stay strongly attached to actin for 1% and 67% of the total cycle time, respectively. Figure adapted from De La Cruz et al., 1999.

1.14. The hand-over-hand mechanism of processivity of dimeric molecular motors.

Processive dimeric molecular motors, such as kinesin 1, myosin 5 and myosin 6 (myosin 6 is a conditional dimer), move on their respective cytoskeletal tracks for hundreds to thousands of nanometers, taking multiple steps per one diffusional encounter before they detach from the filament (Toprak et al., 2009; Mehta et al., 1999; Rock et al., 2001). Thanks to the ability to move long distances in crowded intracellular environments, those motors are efficient cargo transporters (Hammer and Sellers, 2012; Ross et al., 2008). How

is the processivity achieved? What is the molecular mechanism of the processive movement of cytoskeletal motors? What is the kinetic and mechanical tuning of processive molecular motors and how is it different from non-processive molecular motors?

The most widely accepted model for processive motility is the hand-over-hand model. In that model, starting from a point when both heads of a motor are bound to the filament – one in front of the other, the two heads of a dimeric processive molecular motor switch positions of the leading head. When the first leading head is strongly attached to the filament, the second head can bind ATP, release the filament and search for the next binding site in the direction of movement. Once that head rebinds to the filament, it becomes the new leading head. The motor undergoes multiple such cycles with two heads binding to successive binding sites in an alternating manner, resulting in multiple steps on the filament and long-range transport (Yildiz and Selvin, 2005).

The first evidence for the processivity within the myosin superfamily comes from studies on a tissue-purified myosin 5 motor (Mehta et al., 1999). Similar to conventional myosin, myosin 5 is composed of two heavy chains dimerized by a coiled-coil in the tail region (Cheney et al., 1993). Processivity implies that an individual molecular motor is enough to drive the translocation of the filament (Howard et al., 1989). By applying the *in vitro* motility assay, authors investigated the landing rate, velocity and the distance of actin filament gliding over the surface coated with the decreasing amount of the motor, to the point where only a single motor molecule is predicted to interact with a single filament. The landing rate exhibited the first-power dependence on the surface density of myosin 5, the fraction of filaments moving longer distances than their length increased by 1 with the increasing motor density, and the velocity of actin filament movement was independent from the density of the motor on the surface of the flow cell (Mehta et al., 1999). Thus, myosin 5 exhibits properties expected for a processive motor. An optical trapping assay was used to directly prove that a single myosin 5 molecule can undergo multiple steps on actin before dissociation. The detected bead underwent several position changes, associated with steps of myosin on actin, separated by dwell periods, resulting in a staircase-like signal of the position of the bead before it returned to its mean position upon the dissociation of

myosin from actin (Figure 1.17). The change in the bead position between dwell periods, equal to the step size of myosin 5, was ~36nm (Mehta et al., 1999).

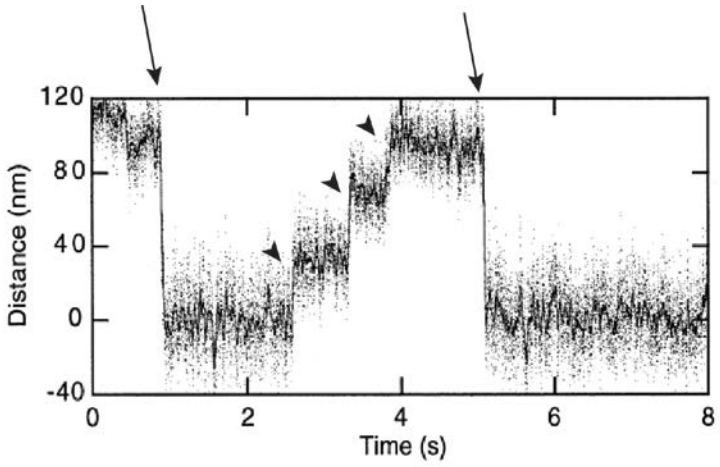

Figure 1.17. Processive runs of myosin 5 on actin. A three-bead optical trapping assay was used as described above. Individual interactions of myosin 5 with actin were observed by detecting the position of one of the trapped beads over time. Upon a single encounter with actin, myosin 5 underwent several steps (arrowheads) before detaching (arrows) and returning to its mean position (noise on the level corresponding to 0nm displacement). Figure adapted from Mehta et al., 1999.

After the direct demonstration of the processivity of myosin 5, the evidence for the hand-over-hand movement along actin came from one nanometer-resolution fluorescent studies (Yildiz et al., 2003). The centre of mass of a dimeric myosin 5 molecule moves ~37nm during each mechanical step. In a molecule moving in a hand-over-hand manner this means that while exchanging its position as the lead head, the binding sites for each individual head are ~72nm apart. Myosin 5 molecules were fluorescently labeled on the neck domain by exchanging light chains for fluorescent calmodulin. The reaction was carried out under conditions that ensured only a single calmodulin light chain was exchanged, resulting in myosin 5 molecules labeled with a single fluorescent dye at different positions within the neck domain. Myosin 5 molecules moving in the presence of ATP on surface-immobilized actin filaments were observed and three populations of steps of 74, 52 or 23nm were measured. Since the neck of myosin 5 contains 6 IQ motifs for the light chain binding, the three step size populations might arise from the different location of

the fluorescent calmodulin on the neck. Assuming that the distance between the dye and the centre of mass of myosin 5 (in the plane parallel to the filament) equals x, and that the centre of mass takes ~37nm steps, then each measured step size is equal to 37±2x nm. Thus, for the observed ~74nm steps the dye was attached next to the head domain, and for 23nm steps – next to the centre of mass (Yildiz et al., 2003). A schematic drawing of the hand-over-hand motility of myosin 5 is depicted in Figure 1.18.

Such processive motility imposes one important constraint on the mechanochemical activity of the two heads in a double-headed motor: at least one head has to remain in an actin-bound form during movement, as simultaneous ATP binding to both heads would result in the whole molecule diffusing away from the filament before completion of the run. This implies that in a processive motor both heads regulate each other's ATPase cycles to ensure spatiotemporal coordination of their mechanical performance. Transient kinetic analysis of recombinant single-headed myosin S1 revealed that the rate-limiting step of the ATPase cycle of myosin 5 is ADP release (De La Cruz et al., 1999). Single molecule optical trapping experiments confirmed that at saturating ATP concentrations and low load ADP release is the rate-limiting step of the catalytic cycle, with all other steps within the cycle occurring at much faster rates (Rief et al., 2000). This suggests tight mechanochemical coupling, whereby both the catalytic and mechanical cycles are regulated by the same rate-limiting step. Furthermore, the rate of ADP release from myosin 5 S1 is load-dependent (Veigel et al., 2005). Closer analysis of individual interactions of myosin 5 S1 with actin revealed that the lifetimes of ADP-bound myosin decreased when an external load was applied in the direction of movement and increased when the load was applied in the opposite direction. It was proposed that in a native molecule each head imposes load on the second head as the cycle progresses. That load would introduce an intramolecular strain and result in the coordination of ADP release rates of each head. When both heads are bound to actin, the lead head would experience a negative load (opposite to the direction of movement) and the trail head would experience a positive load (in the direction of movement). As a result, the ADP release from the lead head would be slowed down and accelerated in the trail head. Faster ADP release from the trail head would enable it to rapidly bind and hydrolyse a new ATP molecule. The lead head would still remain in the ADP-bound state and progress through its power stroke, throwing the detached trail head

forward. As the trail head becomes the new lead head, it rebinds to actin and imposes a positive load on the new trail head. The new trail head could then release ADP and undergo a new catalytic cycle. The ability of two heads in processive molecular motors to coordinate their ATPase cycles has been termed the gaited gate and suggested to be a mechanism responsible for increasing the processivity of a molecular motor (Veigel et al., 2002; Veigel et al., 2005).

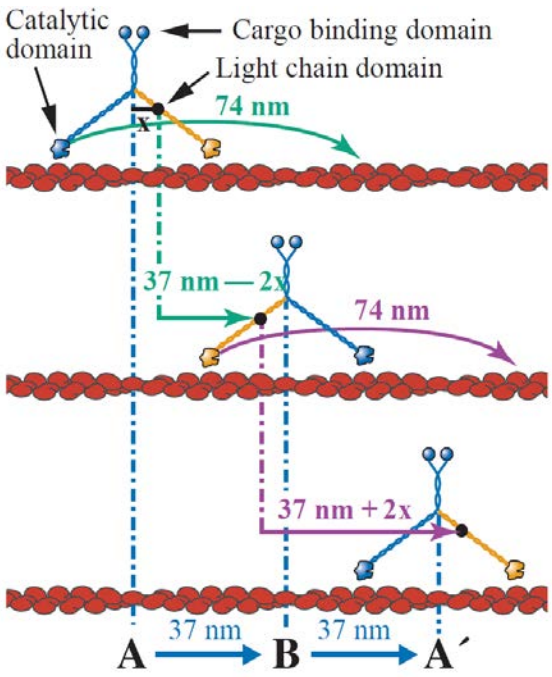

Figure 1.18. A hand-over-hand model of motility of myosin 5. During the processive hand-over-hand movement myosin 5 takes multiple steps, with the centre of mass moving ~37nm (blue dashed lines) and both heads switching positions of the lead head. This implies that two consecutive binding sites for each head are ~74nm apart. By attaching a single fluorescent dye on the neck of myosin 5, a hand-over-hand motility was directly demonstrated. As the first leading head (orange, top) undergoes a power stroke, but remains attached to the same actin monomer, the dye on the neck (black dot) will move 37-2x nm (green dashed line), where x is the distance between the centre of mass and the position of the dye. Simultaneously, the first trail head (blue, top) will bind to its next binding site, 74nm away in the direction of movement, and become the new lead head (blue, middle). The new trail head (orange, middle) will now swing 74nm to its next binding site. With the concomitant power stroke of the lead head, the centre of mass will change its position, and the dye will appear to be displaced by 37+2x nm (purple dashed line).

1.15. Myosin 9.

Firstly characterized in rat, members of the myosin class 9 are widely distributed in invertebrates (with the exception of *Drosophila*), which contain a single myosin 9 gene, and vertebrates which express two myosin 9 isoforms (Bement et al., 1994; Reinhard et al., 1995, Liao et al., 2010). Myr 5 and myr 7 from rat (the 5th and 7th unconventional myosins from rat) are human orthologs of myosin 9b and myosin 9a, respectively (Chieregatti et al., 1998; Abouhamed et al., 2009). Myo9b is mainly expressed in various immune cells, including dendritic cells and macrophages (McMichael et al., 2014; Xu et al., 2014), and intestinal epithelium (Bement et al., 1994), whereas myo9a is found in the ependymal epithelium of the brain ventrical system (Abouhamed et al., 2009).

Myosin 9 members are implicated in the differentiation and morphology of cells. Myo9a-deficient mice develop hydrocephalus (Abouhamed et al., 2009), whereas knockout of myo9b results in impaired directed migration of dendritic cells (DCs) both *in vitro* and *in vivo* and abolishes T cell activation by DCs, suggesting myo9b plays an important role in the development of primary immune response (Xu et al., 2014). Closer analysis revealed that epithelial cells lacking myosin 9 are irregularly shaped and display reduced maturation (Abouhamed et al., 2009, McMichael, 2014). Cell boundaries in the ependymal epithelium of brain ventrices of myo9a-/- mice lost linearity (Figure 1.19), suggesting they experienced an unequal tension along the plane of the epithelial sheet. This was caused by lower levels of occludin localization in tight junctions, resulting in an impaired cell-cell contact formation. Additionally, a great reduction in the number of multiciliated cells was observed, explaining improper flow of the cerebrospinal fluid (CSF) in brain ventrices resulting in hydrocephalus (Abouhamed et al., 2009). In line with disrupted cell-cell junctions, myosin 9 knockdown in 16HBE cell line (human bronchial epithelium) abolished collective cell migration in cell culture (Omelchenko and Hall, 2012).

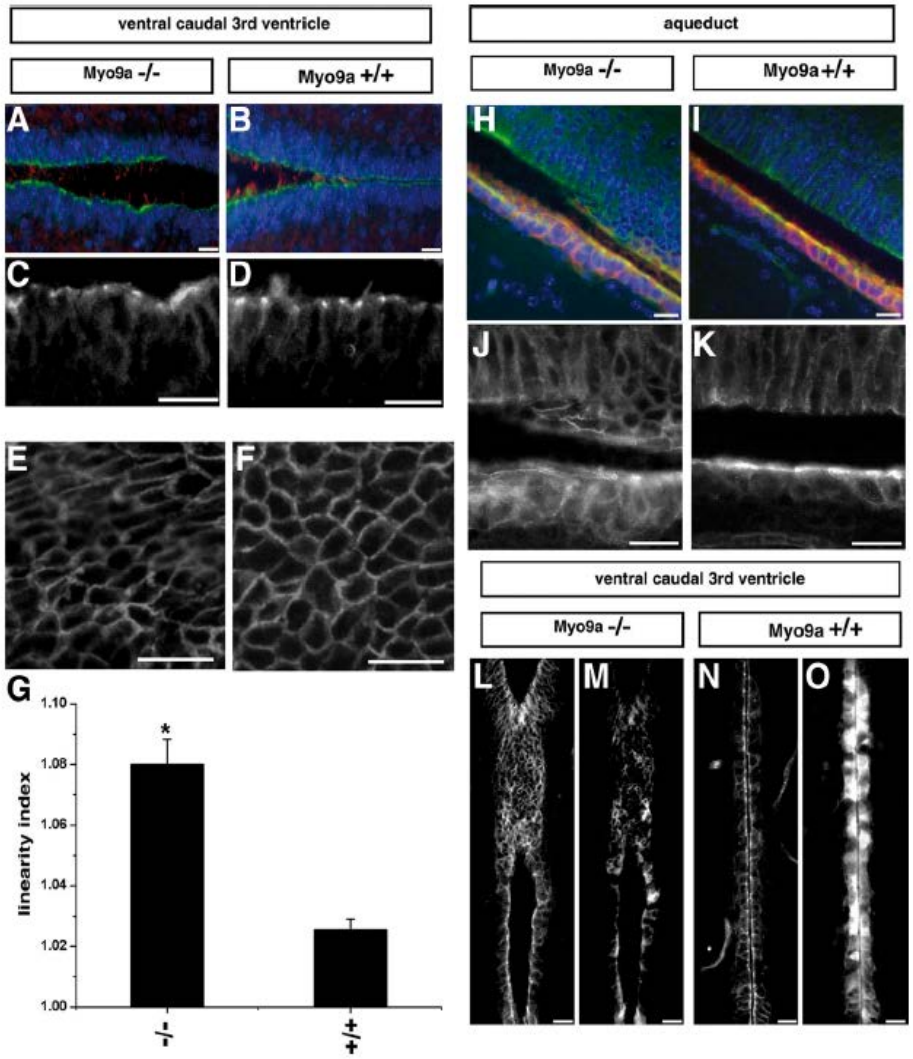

Figure 1.19. Changes in the ependymal cell shape and epithelium distortion upon loss of myosin 9a in the ventral caudal 3rd ventricle and the aqueduct of the ventrical system of the mouse brain. Coronal sections of P0.5 myo9a-/- **(A)** and WT **(B)** mice were immunostained with anti-E-cadherin (green; adherens junctions marker) and anti-acetylated tubulin (red; cilia marker) and DAPI (DNA marker). In myo9a-/- the ependymal epithelial layer is distorted and the number of multiciliated cells isreduced, as compared to WT mice. **C and D** is a close-up view of A and B, respectively, stained for E-cadherin, showing distortion of the ependymal cell layer. P3.5 myo9a-/- **(E)** and WT **(F)** mice sagittal sections stained for β-catenin (adherens junction marker) showing irregular cell shape in the ependymal cell layer in myo9a-/- mice as compared to WT. **G:** linearity index of ependymal epithelium of myo9a-deficient (-/-) and WT (+/+) mice. The linearity index is defined as the ratio of the junctional length to the distance between vertices and is significantly increased in myo9a-/- mice. Sagittal sections of aqueducts from the P3.5 myo9a-/- **(H)** and WT **(I)** mice were immunostained for β-catenin (green) and S-100 (red;

marker of mature ependymal cells) showing distortion and stenosis of the ependymal layer in the aqueduct of myo9a-/- mice. **J and K:** a close-up view of the selected area from H and I, respectively, stained for β-catenin. **L – O:** coronal sections of the ventral caudal 3rd ventricle of myo9a-/- and WT (myo9a+/+) mice showing disruption of cellular junctions in myo9a-deficient mice. Figure adapted from Abouhamed et al., 2009.

On the structural level, myosin 9 members exhibit several unique features; a large (100-150 aa) N-terminal extension upstream of the motor domain adopts a Ras-binding fold but lacks conserved residues necessary for Ras binding and therefore its function remains unknown (Kalhammer et al., 1997); loop 2 insert of ~150aa with a putative calmodulin binding site that might regulate motor properties by means of interacting with actin (Bähler, 2000; Liao et al., 2010); a RhoGAP domain in the tail that inhibits Rho-signalling by stimulating GTP hydrolysis by Rho GTPases both *in vitro* and *in vivo* (Müller et al., 1997; Chieregatti et al., 1998; Post et al., 1998, Omelchenko and Hall, 2012).

The presence of the RhoGAP domain in the tail of myosin 9 members poses an intriguing hypothesis that myosin 9 functions as a motorized signaling molecule in the cell, coupling its mechanical and signalling properties to spatiotemporally regulate Rho GTPases (Bähler, 2000; van den Boom, 2007). Rho GTPases are known effectors of the cytoskeletal architecture, including formation of stress fibers and focal adhesions (Narumiya, 1996; Ridley, 1996; Hall, 1998). Indeed, disruption of cell-cell contacts during collective cell migration was assigned to abolished formation of actin fingers - stress fiber-like actin protrusions that overlap with a neighbouring cell in the first phase of contact formation. That phenotype was caused by an inhibition of Rho signalling by overexpression of myosin 9a in 16HBE culture (Omelchenko and Hall, 2012; Omelchenko, 2012).

Evidence for the mechanical activity of myosin 9 *in vitro*, indicating it could spatiotemporally deliver RhoGAP domain to the sites of high Rho signalling, comes from biochemical studies of recombinant nematode myosin 9 (Liu et al., 2010), and native and recombinant human and rat myosin 9b constructs (Post et al., 1998; Inoue et al., 2002; Nalavadi et al.; 2005; Nishikawa et al., 2006). There is no data available on the mechanical or kinetic properties of myosin 9a orthologs. Available data suggests myosin 9 is a single-headed processive motor (Inoue et al., 2002; Post et al., 2002; Liao et al., 2010; Elfrink et

al., 2014). It is intriguing given that the processivity of a single-headed myosin motor cannot be explained by a hand-over-hand mechanism widely accepted for well-characterized processive motors like myosin 5 or myosin 6 (Yildiz et al., 2003; Yildiz et al., 2004a). It has been suggested that class 9-specific loop 2 insert might tether myosin 9 head to actin while enabling enough flexibility for a diffusive search of the next binding site. Loop 2 insert is well suited for such function given that loop 2 is the primary actin interaction site of myosin and the long insert behaves like an ectopic spring (Inoue et al., 2002; Struchholz et al., 2009; Elfrink et al., 2014). During myosin 9 motility, loop 2 insert would tether the head to the actin filament, allowing for dissociation of the head upon ATP binding and preventing releasing the filament. Following binding of the head to the subsequent actin site, the insert would release the filament and go back to its original position near the actin-binding cleft of myosin head (Figure 1.20; Nishikawa et al., 2006).

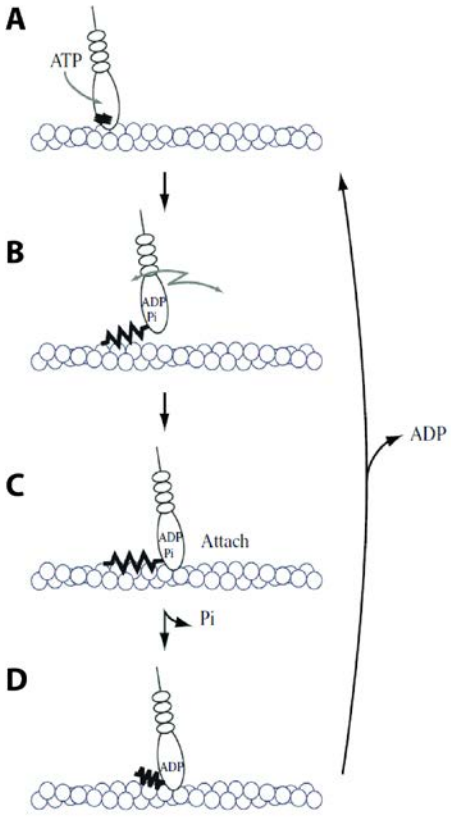

Figure 1.20. An inchworm-like model of processive motility of myosin 9 along actin. ATP binds to the active site of myosin bound to actin in rigor (**A**). That causes release of the head from the filament; simultaneously, the head is tetherted to the filament by a flexible loop-2 insert preventing full detachment of the myosin (**B**). ATP is hydrolyzed and the head diffuses along the filament lattice and attaches to the next actin-binding site (**C**). Following ATP hydrolysis and recombination of myosin with actin, γ-phosphate is released from the nucleotide-binding pocket, the head isomerizes to strong actin binding, loop-2 insert releases the filament and returns to its original position (**D**).

1.16. Significance and project objectives.

As opposed to conventional myosins which work in large assemblies to generate contraction, and dimeric myosins that pick up cargo and distribute it to specific cellular compartments, myosin 9 has been suggested to function as a monomeric processive motor involved in signaling events controlling cell morphology. It was proposed that myosin 9 contains a built-in cargo in the form of a RhoGAP domain, and transports it to the sites of action by means of its enzymatic activity (Bähler, 2000). At destination sites, the RhoGAP

domain of myosin 9 could be involved in downregulation of RhoGTPases, known effectors of the cytoskeletal architecture (Abouhamed et al., 2009; Hall, 1998). This poses a strict requirement on the spatiotemporal control of the intracellular localization of myosin 9 which could be regulated by its mechanochemical properties. Therefore, it is of interest how myosin 9 members couple their motor and signaling activities to efficiently regulate signaling pathways.

At present, there is no evidence that myosin 9a isoform is a mechanically and enzymatically active motor. Despite the sequence similarity with other myosin 9 isoforms which have been shown to display motor properties both *in vitro* and *in vivo* (Liao et al., 2010; van den Boom, 2007; Nalavadi et al., 2005; Post et al., 2002; Post et al., 1998), low tissue expression levels of myosin 9a as well as difficulties in obtaining a recombinant protein have hindered investigations of that particular member of the myosin superfamily. Before one tries to understand the relationship between the mechanochemical and signaling properties of myosin 9a, it is essential to examine if this myosin functions as a catalytically active mechanical motor.

The specific goals of the project include:

- a heterologous expression and purification of a recombinant active myosin 9a
- an investigation of its native structure
- an examination of its actin-binding properties
- an investigation of its catalytic activity
- an investigation of its mechanical activity

CHAPTER 2: MATERIALS AND METHODS

2.1. Buffer and media recipes

Western blot buffer

Ingredient	Final concentration	Mass or volume/1L
Trizma®Base	25mM	3.03g
Glycine	192mM	14g
Methanol	20%	200ml (shortly before the run)

ACEX buffer

Ingredient	Final concentration	Mass or volume/2.5L
Tris-HCl pH 8.0	2mM	2.5ml (2M stock)
ATP	0.2mM	5ml (0.1M stock)
$CaCl_2$	0.2mM	0.5ml (1M stock)
DTT	1mM	2.5ml (1M stock)

Myosin Lysis Buffer

Ingredient	Final concentration	Mass or volume/1L
KH_2PO_4 pH 6.8	90mM	90ml (1M stock)
K_2HPO_4	60mM	60ml (1M stock)
KCl	300mM	100ml (3Mstock)
DTT	1mM	1ml (1M stock)
Protease inhibitors		1 tablet/100ml

HisLow

Ingredient	Final concentration	Mass or volume/1L
Tris-HCl pH 7.5	50mM	50ml (1M stock)
Imidazole	40mM	2.7g
NaCl	500mM	200ml (2.5Mstock)
DTT	1mM	1ml (1M stock)

HisHigh

Ingredient	Final concentration	Mass or volume/1L
Tris-HCl pH 7.5	50mM	50ml (1M stock)
Imidazole	400mM	27.2g
NaCl	500mM	200ml (2.5Mstock)
DTT	1mM	1ml (1M stock)

Myosin Extraction Buffer (2x concentrated)

Ingredient	Final concentration	Mass or volume/1L
MOPS pH 7.2-7.4	20mM	4.2g
NaCl	1M	58.44g or 400ml (2.5M stock)
$MgCl_2$	10mM	10ml (1M stock)
EGTA	2mM	4ml (0.5M stock)
NaN_3 (for storage)	3mM	0.195g

For preparation of 1x Myosin Extraction Buffer add:

Ingredient	Final concentration	Mass or volume/0.2L
ATP	3mM	6ml (0.1M stock)
DTT	1mM	200µl
Protease inhibitors		1 tablet

Recheck pH

Myosin HMM buffer (2x concentrated)

Ingredient	Final concentration	Mass or volume/1L
MOPS pH 7.2-7.4	20mM	4.2g
EGTA	0.2mM	0.4ml (0.5M stock)
NaN_3 (for storage of concentrated stock)	3mM	0.195g

For preparation of 1x HMM add:

Ingredient	Final concentration	Mass or volume/50ml
NaCl	100/250/500mM	2ml/5ml/10ml (2.5M stock)
DTT	1mM	50µl

Recheck pH

Motility buffer (5x concentrated MB)

Ingredient	Final concentration	Mass or volume/50ml
MOPS pH 7.2-7.4	50mM	0.52g
KCl	125mM	2.1ml (3M stock)
EGTA	5mM	0.5ml (0.5M stock)
$MgCl_2$	5mM	0.25ml (1M stock)

For preparation of 1x MB add:

Ingredient	Final concentration
DTT	10mM
BSA (for MB-BSA)	1mg/ml
ATP (for MB +)	1mM
CaM (for MB +)	2µM

General Actin buffer (10x concentrated)

Ingredient	Final concentration	Mass or volume/50ml
Tris-HCl pH 8.0	50mM	2.5ml (1M stock)
$CaCl_2$	2mM	0.1ml (1M stock)

10x Polymerization Salts

Ingredient	Final concentration	Mass or volume/10ml
KCl	500mM	1.7ml (3M stock)
$MgCl_2$	20mM	0.2ml (1M stock)

For polymerization of small volumes of actin mix:

Ingredient	Final concentration
10x General Actin Buffer	1x
10x Polymerization Salts	1x
ATP	1mM
DTT	1mM

Actin polymerization buffer

Ingredient	Final concentration	Mass or volume/1L
MOPS pH 7.2	25mM	5.23g
$MgCl_2$	2mM	2ml (1M stock)
DTT	1mM	1ml (1M stock)
EGTA	1mM	2ml (0.5M stock)
KCl	50mM	16.7ml (3M stock)
NaN_3	3mM	0.195g

Gel filtration buffer

Ingredient	Final concentration	Mass or volume/1L
MOPS pH 7.2-7.4	10mM	2.1g
NaCl	150mM/500mM	60ml/200ml (2.5M stock)
EGTA/$CaCl_2$	0.1mM/0.2mM	0.2ml/0.2ml (0.5M/1M stocks)
DTT	1mM	1ml (1M stock)

ATPase buffer

Ingredient	Final concentration	Mass or volume/0.5L
MOPS pH 7.2-7.4	10mM	1.05g
KCl	50mM	4.2ml (3M stock)
EGTA	0.1mM	0.2ml (0.5M stock)
$MgCl_2$	1mM	0.5ml (1M stock)
DTT	1mM	0.5ml (1M stock)
CaM	5µM	

TG buffer (5x concentrated)

Ingredient	Final concentration (1x)	Mass or volume/5L
Trizma®Base pH 8.3	25mM	469.2g
Glycine	250mM	75.7g
SDS	0.1%	250ml (10% stock)

PBS (10x concentrated)

Ingredient	Final concentration	Mass or volume/1L
NaCl	1.3 7M	80.06g
KCl	27mM	2.01g
Na_2HPO_4 pH 7.2	100mM	14.2g
KH_2PO_4	18mM	2.45g

2x YT medium

Ingredient	Mass or volume/5L
Tris-HCl pH 7.0	~30ml
Tryptone	80g
Yeast extract	50g
NaCl	25g

LB medium

Ingredient	Mass or volume/1L
Tryptone	10g
Yeast extract	5g
NaCl	10g

Adjust pH to 7.0

B2B medium

B2B medium agar plates consist of 500ml LB medium supplemented with:

Ingredient	Final concentration	Mass or volume/0.5L
X-Gal	50µg/ml	1.25ml (20mg/ml stock)
IPTG	40µg/ml	84µl (1M stock)
Gentamycin	7µg/ml	70µl (50mg/ml stock)
Kanamycin	50µg/ml	1ml (25mg/ml stock)
Tetracyclin	10µg/ml	0.5ml (10mg/ml stock)
Agar	1.5%	7.5g

B2B liquid medium has the same recipe, except that there is no IPTG, X-Gal or Agar.

2.2. Oligonucleotides

All oligonucleotides have been purchased from Sigma-Aldrich or Eurofins MWG Operon following manufacturer's recommendations.

Name	Sequence (5' – 3')
GFPfwd	AGGATCCATGGTGAGCAAGGGCG
GFPrev	AAAAGCGGCCGCGGACTTGTACAGCTCGTCC
9aFLpFBNAfwd	AGGATCCATGAATATAAATGATGGAGG
9aFLpFBNArev	AAAAGCGGCCGCGACCATAAATTCATTATTTCC
9afwd	AAAAGCGGCCGCAATGAATATAAATGATGGAGG
MMD9afwd	AGGATCCATGGATGATTTATGTAG TTTACCTGATTTG
1019rev	TTCTAGATTACACCTCTTGGTGAAGCAGATC
1162rev	ATCTAGATTATTTTAAAGCTTTAAATCTTTGTCTTGC
1019revFLAG	TTCTAGACTACTTGTCATCGTCATCCTTGTAATCCACCTCTTGGTGAAGCAGATC
1162revFLAG	TTCTAGACTACTTGTCATCGTCATCCTTGTAATCTGATTTTAAAGCTTTAAATCTTTG

MMD9arev	AAAAGCGGCCGCCACCTCTTGGTGAAGCAGATCTTG
MMD9a-S1rev	AAAAGCGGCCGCTTTTAAAGCTTTAAATCTTTGTC
AviTag-fwd	P-GGCCGCAGGTGGCGGTCTGAACGACATCTTCGAGGCTCAGAAA ATCGAATGGCACGAAGC
AviTag-rev	P-GGCCGCTTCGTGCCATTCGATTTTCTGAGCCTCGAAGATGTCGT TCAGACCGCCACCTGC
EXTfwd	AAGGATCCATGAATATAAATGATGGAGG
EXTrev	AAAAGCGGCCGCTTAATCAAAGTCTTTCTGTTGAGGC
LOOP2fwd	AAAGTCGACATGGCTGGAAAAGTAAAATATGGG
LOOP2rev	AAAAAGCTTTCAAGCATTAGAGCGAATGCATTTTAC
RFPfwd	TTTTTTGGATCCATGGCCTCCTCCGAGGACG
RFPrev	TTTTTTGGATCCGGCGCCGGTGGAGTGGCG
CC1fwd	AGGATCCATGAGCCAGAGTGGTGTGGACTTGCAGG
CC1rev	AAAGTCGACGCTCTACTCTTTGCTTTGACTGATAGGAAG
CC2fwd	AGGATCCATGCCAGGTCCATCGTCTCCTGTTGTAG
CC2rev	AAAGTCGACGCTCTGAGCTATCAGCAGTCCCAATGG
pUC-M13F	CCCAGTCACGACGTTGTAAAACG
pUC-M13R	AGCGGATAACAATTTCACACAGG

Constructs were sequenced at NHLBI core facility or by GATC Biotech and sequences were analyzed by SerialCloner 2.1 or MacVector.

2.3. Experimental procedures

2.3.1. Sequence analysis

Initial domain analysis of myosin 9a was performed with SMART (Simple Modular Architecture Research Tool) algorithm and was enriched by manual analysis and literature searches. The calmodulin-binding site search was performed using Calmodulin Target Database as a reference for CaM target sequences. Sequence alignments were performed using COBALT (Constraint-based Multiple Alignment Tool) software. Analysis of the sequence for the presence of putative coiled-coil domains was performed with Paircoil2 (McDonnell et al., 2006).

2.3.2. DNA amplification, restriction, ligation and transformation to *E. coli* DH5α

A gene encoding full length human myosin 9a was chemically synthesized by GenScript (Piscataway, NJ, USA). The gene was cloned between XbaI and BamHI sites in the pUC57 vector and was used as a template for generation of all myosin 9a constructs used in this work.

GFP-9a-Head and GFP-9a-S1 were generated by amplification of the first 1019 or 1162 aa of myosin 9a, respectively, using 9afwd and 1019rev or 1162rev and introduced between NotI and XbaI restriction sites into pFastBac HT®B (Invitrogen). GFP was linked N-terminally to the motor domain by amplification with GFPfwd and GFPrev and ligation into BamHI and NotI sites. Both GFP and myosin 9a fragments were introduced in frame with the N-terminal 6x His-tag present in the vector. To add a FLAG-tag, primers were designed that contained a sequence complement to the last ~20 bases of the myosin 9a construct, followed by the sequence encoding the FLAG tag (DYKDDDK) upstream of the stop codon and XbaI site. Those were used together with an appropriate forward primer in PCR to ass the C-terminal FLAG-tag. PCR products flanked with BamHI and XbaI sites were ligated into pFastBac HT®B.

The Minimal Motor Domain constructs were amplified with MMD9afwd and MMD9arev and MMD9a-S1rev and introduced between BamHI and NotI sites in frame with a C-terminal FLAG-tag in customized pFBNA vector (kind gift of Dr. Attila Nagy, NHLBI, NIH). Introduction of an Avi-tag between the end of myosin 9a sequence and the FLAG-tag was achieved by digestion of 9aMMD and 9aMMD-S1 with NotI and ligation with chemically synthesized Avi-tag oligonucleotides carrying free phosphate groups at the 3’ end.

The full length human myosin 9a gene was amplified with 9aFLpFBNAfwd and 9aFLpFBNArev primers and introduced between BamHI and NotI sites into the pFBNA vector in frame with the C-terminal FLAG tag.

The putative coiled-coil fragments from myosin 9a tail were amplified with the indicated primers and introduced into the pET28a vector (Novagen). These were introduced

in frame with a C-terminal CFP in a customized pET28a vector. All constructs contain an N-terminal His-tag.

PCR amplifications were carried out in Mastercycler Personal (Eppendorf) or C1000 Touch™ Thermal Cycler (Bio-Rad). 50µl reactions were carried out using the Phusion® High-Fidelity PCR Kit (ThermoScientific) and included 10 µl 5x HF Buffer, 1 µl 10 mM dNTPs, 2.5 µl 10 µM both primers, 0.5 µl Phusion Hot Start DNA Polymerase and 50-100 ng DNA template. Reactions were programmed as follows:

1. 98^0C 1min
2. 98^0C 20sec
3. 70^0C 15sec
4. Ramp to 61^0C, 0.5^0C/sec
5. 72^0C 1-3min
6. 72^0C 5min
7. 4^0C ∞

Steps 2-5 were repeated 30x. Duration of the elongation step (5.) was adjusted accordingly to the size of an amplified fragment following manufacturer's specifications (30 sec/kbp). PCR products were analyzed by DNA electrophoresis to confirm the amplification of a DNA fragment of expected size and purified by the QIAquick PCR purification kit (QIAGEN) or the PureLink® PCR purification kit (Invitrogen) following manufacturer's guidelines.

DNA restriction was performed using the appropriate enzymes purchased from NewEngland BioLabs and according to specifications. In general, 40 µl reactions included 1x NEBuffer, 1x BSA (if required), 30 µl DNA, 2 µl of each enzyme (or 1 µl each enzyme/1 µg DNA) and were incubated for 3-4 h at 37^0C. The whole volume was mixed with 10 µl DNA loading dye and 10 µl SYBR Green (ThermoScientific) and digested products were separated by DNA electrophoresis. Digested constructs were purified by cutting them out of agarose gels and purifying them following instructions in the PureLink® Gel Extraction kit (Invitrogen) or the QIAquick Gel Extraction kit (QIAGEN).

Concentrations of gel-extracted DNA constructs were measured on BioPhotometer plus (Eppendorf) and ligations were performed using a 3:1 ratio of insert to vector in 10µl reactions including 2 µl Rapid Ligation buffer and 1 µl T4 DNA polymerase from the Rapid Ligation Kit (ThermoScientific).

Whole ligation reaction volumes were used to transform 100 µl *E.coli* DH5α cells, following a standard heat-shock protocol (2 min on ice; 30 sec in 42^0C; 5 min on ice). 200 µl of LB media was added to transformed cells and samples transformed with pET28 plasmids (carrying the kanamycin resistance gene) were shaken for 1 h 37^0C, 200 rpm. 150 µl or 70 µl of cell suspensions were plated on LB agar plates containing either 50 µg/ml ampicillin (for pFBNA and pFastBac plasmids) or 25 µg/ml kanamycin (for pET plasmids). Following an overnight incubation at 37^0C, single colonies were inoculated into 3 ml of liquid LB media containing the appropriate antibiotic. After overnight growth at 200 rpm, 37^0C, plasmid DNA was purified with the PureLink® Quick Plasmid Miniprep kit (Invitrogen) or the QIAprep Spin Miniprep kit (QIAGEN).

Isolated plasmids were subject to restriction analysis to confirm successful ligation into vectors. In 10 µl reactions supplemented with NEBuffer, 5 µl of purified DNA was cut with 0.5 µl of the appropriate enzymes for 1 h at 37^0C. DNA electrophoresis was performed to confirm the presence of the desired insert in the vector. Those samples that contained products of expected sizes were subject to sequencing to confirm the correct generation of the desired constructs.

2.3.3. Transformation and expression of proteins in *E.coli* BL21 cells

1 µl of plasmid containing myosin 9a tail fragments with the C-terminal CFP or a plasmid containing *Xenopus* calmodulin (CaM) incorporated in frame with the N-terminal His-tag, were used to transform 50 µl chemically competent One Shot® BL21 (DE3) *E. coli* cells (Invitrogen) following a standard heat-shock protocol. Cells were treated as described above for DH5α cells and single colonies from overnight agar plates were used to inoculate liquid starter cultures in 2x YT supplemented with 25 µg/ml kanamycin. 500 ml of media supplemented with kanamycin was inoculated with 50 ml of overnight starter

cultures. Cells were grown to OD_{600} = 0.6 and expression was induced with 1 mM IPTG for 5 h at 37^0C. Cell pellets were collected by 10 min centrifugation at 4000 rpm, 4^0C in the JLA-10.500 rotor (Beckman Coulter). Cell pellets from 1 L cultures were resuspended in 40 ml of the His-Low buffer with 1mM DTT and protease inhibitors cocktail and stored at -80^0C until use.

2.3.4. His-tag affinity purification of bacterially-expressed proteins

Pellets from 1L cultures were thawed in a water bath at 25^0C. Following sonication on ice for 5 min with 1 sec on/off bursts at 50% power (Bandelin HD 2070 sonicator) the soluble fraction was recovered by centrifugation at 20000 rpm, 4^0C, 20 min in the JA25.50 rotor (Beckman Coulter) and loaded automatically on the 5 ml His-Trap FF column (GE Healthcare) equilibrated with the His-low buffer on ÄKTA Purifier FPLC (GE Healthcare). The column was thoroughly washed with His-low until the A_{280} reached the baseline. The protein was eluted with His-high in a step-wise manner (Batters et al., 2012). Flow rates and pressure limits were set according to specifications to 1 ml/min and 0.5 MPa, respectively. Eluate fractions corresponding to peaks in the A_{280} signal were analyzed by SDS-PAGE. Pure fractions were pooled together and concentrated if necessary. Proteins were extensively dialyzed into 1x PBS + 1 mM DTT overnight, snap-frozen in liquid N_2 and stored at -80^0C until use. Figure 2.1 shows a representative SDS-PAGE gel from the purification of CaM.

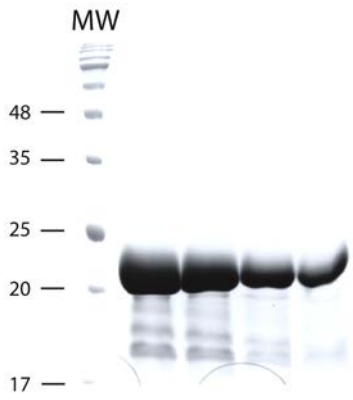

Figure 2.1. A representative SDS-PAGE gel of exogenous calmodulin purified from BL21 *E.coli* cells by means of His-tag affinity chromatography. MW – molecular weight. Expected MW of exogenous CaM: ~21 kDa. Lanes correspond to subsequent elution fractions.

2.3.5. Generation of recombinant bacmids

1 µl of pFastBac or pFBNA plasmids with incorporated myosin 9a fragments were used to transform 10 µl competent MAX Efficiency® DH10Bac™ *E.coli* cells (Invitrogen); cells were kept on ice for 30 min, followed by 45 sec at 42^0C and incubation on ice for 2 min. Cells were rescued in 90 µl S.O.C. media. Following a 4 h incubation at 200 rpm, 37^0C, 100 µl of 1:10 and 1:100 cell dilutions were plated on B2B agar plates, containing tetracyclin, kanamycin, gentamycin, X-gal and IPTG as specified above. Plates were incubated at 37^0C for 48 h and white colonies were picked to inoculate 3 ml of B2B media supplemented with the antibiotics. Simultaneously, the same colonies were restreaked on B2B plates and incubated for 48 h at 37^0C to confirm the formation of white colonies.

Cells were grown in liquid B2B media overnight at 200 rpm, 37^0C and collected by centrifugation at 4000 rpm, 10 min. DNA was extracted with the PureLink® HiPure plasmid miniprep kit (Invitrogen) following manufacturer's guidelines. Alternatively, bacmids were purified by an isopropanol extraction; after the resuspension of cells, lysis and neutralization with commonly available DNA miniprep kit buffers, ~800 µl supernatant was rescued by centrifugation, mixed with an equal volume of isopropanol and incubated for 20 min at -20^0C. DNA was pelleted by centrifugation in a tabletop centrifuge at max. speed, 20 min, 4^0C and after removal of the supernatant, washed with 0.5 ml of 70%

ethanol. DNA was recentrifuged and air-dried. Bacmids were resuspended in 40 µl of endonuclease-free water and stored in -20^{0}C until use. Since freeze-thaw cycles might hinder transfection efficiency, it is better to aliquot bacmid DNA before freezing.

Isopropanol extraction yields ~1000x higher DNA concentrations, yet cell transfections with DNA prepared in that way were not always successful. I attribute this to the fact that the isopropanol extraction results in the purification of both bacmid and chromosomal DNA and thus during transfection there might not be enough bacmid DNA to generate the virus. Bacmid extraction with a commercial miniprep kit yielded extremely low concentrations (~1 ng/µl), yet all transfections performed with those samples resulted in the successful generation of viruses.

Finally, the presence of desired constructs in isolated bacmids was confirmed by PCR with pUC-M13F and pUC-M13R primers following previously described specifications, with 4 min extension time.

2.3.6. Generation and amplification of a recombinant baculovirus

SF9 or SF21 cells were maintained in Grace's medium (Invitrogen) supplemented with 10% FBS (heat-inactivated), 1% Pluronic® F-68 (Invitrogen) and 1µg/ml normocin (Invivogen), or in SF900 II Serum Free Medium (Invitrogen) as suspension cultures at 27^{0}C, 140 rpm.

Viruses were generated and amplified according to manufacturer's guidelines. 0.6 x 10^6 cells were plated per well in 2 ml of medium in 6-well plates. After 15 min at RT, if kept in a serum-containing medium, media in wells was exchanged to Unsupplemented Grace's medium (Invitrogen). 100 µl of unsupplemented medium with 8 µl of Cellfectin® II reagent (Invitrogen) and 100 µl of unsupplemented medium with 12 µl of bacmid (prepared in separate tubes) were combined and incubated for 30 min at RT. The mix was added dropwise to the cell-containing wells and after 5-7 h incubation, the media was exchanged to remove free Cellfectin reagent and DNA and plates were incubated at 27^{0}C for ~1 week. Viruses were collected by centrifugation at 8000 rpm, 15 min. This was the P0 virus stock.

The virus titer was increased by subsequent virus amplification in increasing culture volumes to P3. $1.2*10^6$ cells/ml in 25 ml or 250 ml were infected with 250 µl or 2.5 ml of the preceding virus stock, respectively, and grown for 72 h, 140 rpm, 27^0C. After 72 h, cell viability should be as low as 30-50% as calculated for 1:1 cell suspention:Trypan Blue (Bio-Rad) mix in the TC20™ Automated Cell Counter (Bio-Rad). Viruses were collected by centrifugation at 8000 rpm, 15 min, 4^0C and stored long-term at 4^0C.

2.3.7. Expression and purification of myosin 9a motors from insect cells

500 ml cultures of SF9 or SF21 cells at $1.2*10^6$ cells/ml were co-infected with 15 ml of a myosin 9a baculovirus (P3 stock) and 10 or 15 ml of CaM baculovirus (P4 stock), for constructs without and with the lever arm, respectively. Proteins were expressed for 48 h at 27^0C, 140 rpm and pellets collected by centrifugation at 8000 rpm, 15 min, 4^0C were frozen and stored at -80^0C until use.

Protein was purified based on a modified procedure from Wang et al., 2000. Pellets from 1000 ml cultures were resuspended in 80 ml of the Myosin Extraction Buffer and sonicated for 5 min with 1 sec on/off bursts at 40% power (Bandelin HD 2070 sonicator). Cell slurry was rotated in the presence of ATP for 1 h, 4^0C to facilitate dissociation of myosin 9a from actin. Cell debris was removed by centrifugation at 20000 rpm, 20 min, 4^0C in the JA25.50 rotor (Beckman Coulter). The supernatant was combined with 0.9 ml of the Anti-FLAG M2 Affinity Gel (#A2220, Sigma Aldrich) prepared following manufacturer's instructions and nutated for 45-60 min at 4^0C. Resin with bound protein was rescued by centrifugation at 1600 x g, 6 min, 4^0C, resuspended in 10 ml of the Myosin Extraction Buffer and poured into a disposable 10 ml Poly-Prep® Chromatography column (Bio-Rad). Following settling of the resin, it was washed twice with 10 ml of the Myosin Extraction Buffer and twice with 10 ml of 100 mM NaCl Myosin HMM buffer. Protein was eluted with 4 ml of 0.1 mg/ml FLAG® peptide (#F3290, Sigma Aldrich) in 100 mM NaCl HMM buffer and immediately loaded on 0.2-0.3 ml of the Q Sepharose Fast Flow (#17-0510-10, GE Healthcare), equilibrated with 100 mM NaCl HMM buffer. Protein was eluted in 0.4 ml fractions of 250 mM and 500 mM NaCl HMM buffer. Protein yield, purity and

coelution of calmodulin light chain were confirmed by SDS-PAGE. Proteins were dialyzed overnight into 100 mM NaCl HMM or used directly after elution.

Before experiments, proteins were centrifuged at 160000 x g, 20 min, 4^0C, in the TLA-120 rotor (Beckman Coulter) to remove aggregates (Liao et al., 2010). Concentration was measured following the Christian-Warburg method that corrects protein concentration for the amount of the nucleic acid present in the sample. Absorbance at 260 nm and 280 nm was collected by Biophotometer plus (Eppendorf). Protein was used fresh within 2 days.

2.3.8. Dynamic Light Scattering

0.1 mg/ml myosin 9a in filtered 100 mM NaCl HMM buffer was used to measure the time-dependent stability of the preparations. Intensity of refracted light was used to obtain hydrodynamic radii of molecular species present in the samples using the Zetasizer µV (Malvern) with automatically adjusted settings. Measurements were performed 3x for each time point with each measurement lasting 1 min.

2.3.9. Stoichiometry of calmodulin binding to myosin 9a heavy chain and the effect of Ca^{2+} on CaM binding by myosin 9a

Xenopus calmodulin was expressed in *E.coli* BL21 cells and purified to homogeneity by His-tag affinity purification. Increasing amounts of CaM (0.05 – 1 µM) as well as known amounts of 9aMMD or 9aMMD-S1 (~0.5 µM) were separated by SDS-PAGE and gels were silver-stained (ThermoScientific). The staining intensity of the calmodulin standards was quantified by analysis of the gels in Image Lab (Bio-Rad) and plotted against calmodulin concentration generating a calibration curve. The amount of calmodulin in each myosin sample was also quantified by band densitometry and fitted to the calibration curve, giving the amount of CaM light chain in each myosin sample. The molar ratio of CaM to the myosin heavy chain was calculated providing the binding stoichiometry of calmodulin to myosin. Experiments were performed for three independent myosin preparations. The protocol was adapted from Köhler et al., 2005.

[Ca^{2+}]-dependent dissociation of calmodulin from 9aMMD was addressed by incubating equal amounts of myosin (~1 µM) preparation with increasing concentration of free $CaCl_2$ (0 – 1 mM free Ca^{2+}) for 30 min at RT (Trybus et al., 2007). 10 µM phalloidin-stabilized F-actin was added and the rigor complex was allowed to form for 20 min at RT. Samples containing myosin-actin mixtures as well as a negative control containing a mixture of exogenous calmodulin and actin were centrifuged at 80000 rpm, 20 min, 4^0C in the TLA.100 rotor (Beckman Coulter). Supernatants were combined with the SDS-loading dye and pellets were resuspended in equal volumes of 1x SDS-loading dye. Equal volumes of supernatant and pellets were separated by SDS-PAGE and stained with Commassie Blue. The intensity of CaM light chain in each pellet was assessed by band densitometry using ImageLab and normalized to CaM intensity in the absence of $CaCl_2$.

2.3.10. Steady-state ATPase assay

The actin-activated MgATPase activity of myosin 9a was assayed with an NADH-coupled assay at ~22^0C using Varian Cary 50 spectrometer (De La Cruz and Ostap, 2009). 1 mM PEP (#P7127, SigmaAldrich), 0.2 mM NADH (#N8129, SigmaAldrich), at least 18 U/ml lactate dehydrogenase and 12 U/ml puryvate kinase (#P0294, SigmaAldrich) in the ATPase buffer were mixed with 2 mM ATP and varying phalloidin-stabilized F-actin concentrations. Reactions were started by adding 0.1-0.2 mM myosin 9a and the decrease in the absorbance at 340 nm was followed for ~10 min. The MgATPase rate (1/s) at each actin concentration was calculated from the slope of A_{340}, final myosin concentration in the reaction and NADH extinction coefficient ε = 6220 $M^{-1}cm^{-1}$, according to equation 1:

$$Rate\ (1/s) = {}^{\Delta A340}/_{([myosin] * \varepsilon)}$$

The ATPase rate of F-actin alone was substracted from actomyosin rates. Modifications of the assay included increased salt concentration, supplementing the buffer with 2 µM exogenous calmodulin and/or 100 µM free Ca^{2+}. Measurements were repeated with 3 different myosin preparations for each actin concentration and data was fitted to the Michaelis-Menten equation:

$$V = V0 + (^{Vmax * [actin]}/_{Kactin + [actin]})$$

where V is the rate at a given actin concentration, V_0 is the basal ATPase activity in the absence of actin, V_{max} is the maximum actin-activated ATPase rate, K_{actin} is the actin concentration at which myosin exhibits half maximal ATPase activity (apparent K_m for actin) and [actin] is the actin concentration used. Values of V_{max} and K_{actin} were obtained by fitting the data in SigmaPlot 12.0.

2.3.11. Myosin 9a biotinylation

9aMMD-Avi and 9aMMD-S1-Avi were expressed and handled as described above. Pellets were thawed on ice, resuspended in the Myosin Extraction Buffer and sonicated. Proteins were biotinylated by supplementing the cell slurry with 2 mM ATP, 4 mM D-biotin (#B4501, SigmaAldrich) and 1 µM BirA ligase and rotated 1 h, 4^0C (Li and Sousa, 2012). Purification was performed as before and successful biotinylation was confirmed by western blot.

2.3.12. Gliding filament assay

Methods for the gliding filament assay were adapted from Rock et al., 2000 and Sellers, 2001.

1 µM G-actin in the General Actin Buffer was briefly sonicated in a water bath for 15 sec and polymerized by adding 2 mM ATP and 1x Polymerization Salts for 30 min at RT. Actin was fluorescently labelled with 1 µM TMR-phalloidin **(**#P1951, SigmaAldrich) for 30 min at RT or overnight at 4^0C. Actin stock prepared in this way is stable for weeks.

Two pieces of a double-sided Scotch tape, separated by ~2 mm, were attached to a glass slide. A 24x40 mm coverslip (BRAND) was attached on top, creating a flow cell with ~10 µl volume.

For a nonspecific protein immobilization on the surface, coverslips were covered with 2% nitrocellulose in amyl acetate and allowed to dry before attaching to a glass slide with a nitrocellulose-covered surface facing the flow cell area. 0.2 mg/ml (unless indicated otherwise) of myosin 9a in 1x MB- was introduced into the flow cell and incubated for 4 min. Unbound myosin was washed out with double 1x MB- wash and 1 mg/ml BSA in 1x MB-BSA was incubated in the flow cell for 4 min. 20 nM TMR-actin in 1x MB-BSA was allowed to attach to myosin for 3 min and unbound actin was removed by thorough washing. Motility was initiated by flushing in 1x MB+ (containing 2 mM ATP, 20 mM DTT, 0.02 mg/ml catalase, 0.1 mg/ml glucose oxidase, 3 mg/ml glucose). Where stated, the motility buffer was supplemented with exogenous calmodulin and/or $CaCl_2$.

To achieve robust translocation of actin filaments by myosin 9a, a specific surface immobilization of the motor was required. The coverslip surface was covered with 1mg/ml biotinylated-BSA for 4 min, followed by 4 min incubation with 1 mg/ml streptavidin (#S4762 SigmaAldrich) in 1x MB-. Unbound streptavidin was removed from the flow cell and biotinylated myosin 9a was incubated for 4 min, followed by adding 20nM TMR-actin as before. Motility was initiated by addition of ATP.

Frames were collected every 3 sec for 10 min in epifluorescence using Eclipse Ti microscope (Nikon), 60x 1.49 NA ApoTIRF objective (Nikon) and Andor CCD camera. Recordings were analyzed by GMimPro (Mashanov and Molloy, 2007) using 5-frame averaging and velocities were determined by tracking moving actin filaments for at least 7 consecutive frames. At least three independent myosin preparations were used to investigate the mechanical properties of myosin 9a.

2.3.13. Steady-state actin binding affinity of myosin 9a

0.8-1 µM 9aMMD in 30 µl of 100 mM NaCl HMM was incubated with increasing actin concentrations (0 – 15 µM) of phalloidin-stabilized F-actin in the presence and absence of 2 mM MgATP or MgADP (Nalavadi et al., 2005). To deplete the solution of the nucleotides, 1 U/ml apyrase and 5mM EDTA were supplemented. Samples were incubated ~30 min on ice and ultracentrifuged 80,000 rpm, 20 min, 4^0C in the TLA.100 rotor. The

supernatant was combined with 1x final SDS loading dye and pellets were resuspended in equal volume of 1x SDS loading dye. Equal volumes of supernatant and pellet were separated by SDS-PAGE and gel densitometry was used to determine fractions of bound myosin at each actin concentration.

In the presence of a nucleotide, myosin 9a would pellet itself in the absence of actin. To correct the amounts of myosin bound to actin in the presence of nucleotides for the amount of myosin pelleted in the absence of actin, equation 3 was used (Guzik-Lendrum, 2013):

$$Pcorr = {(Puncorr - Palone)}\Big/{(100 - Palone)}$$

where P_{corr} – amount of myosin bound to actin corrected for myosin pelleted in the absence of actin, P_{uncorr} – uncorrected fraction of bound myosin, P_{alone} – amount of myosin pelleted in the absence of actin.

The fraction of myosin bound at each actin concentration was plotted against actin concentration and fitted to a quadratic equation using SigmaPlot 12.0 providing values of dissociation constants (K_d) for F-actin in each nucleotide state.

All experiments were performed at least 3 times with different myosin preparations and final K_d values are presented as $K_d \pm$ S.D.

2.3.14. Native molecular weight calculations

100 µl of pure 9aMMD or a mix of protein standards was loaded on a Superdex 200 Increase GL 10/300 (GE Healthcare), equilibrated with the Gel Filtration buffer containing 150 or 500 mM salt and supplemented with 0.1 mM EGTA. Runs were controlled with an ÄKTA purifier system (GE Healthcare) with 0.5 ml/min flow rate and 3 MPa pressure limit. The absorbance at 280 nm was monitored and the identity of peak eluate fractions was analyzed by SDS-PAGE. The partition coefficient (K_{av}) was obtained from equation 4 (below) and related to the natural logarithm of Stokes radius ($\ln R_s$). The elution volume

(V_e) and the void volume (V_0) were obtained from the A_{280} trace, whereas the total column volume (V_c) was calculated from the equation for a volume of a cylinder, taking into account column dimensions provided by the manufacturer.

$$Kav = {(Ve - V0)}/{(Vc - V0)}$$

4-20% sucrose gradients were formed in an appropriate Gel Filtration Buffer by incubation of 4% sucrose solution on top of 20% sucrose solution in the Polyallomer Quick Seal centrifuge bottles (Beckman Coulter) at ~45^0 for 1-2 h at 4^{0}C. 100 µl of purified 9aMMD or a solution containing protein standards were layered on top of 6 ml gradients. Samples were centrifuged for 18 h at 38,000 rpm in the SW Ti 60 Beckman Coulter rotor. Following centrifugation, ~300 µl fractions were collected from the bottom of the tube by dripping and separated by SDS-PAGE.

Protein markers included 4 mg/ml BSA (NewEngland BioLabs), 5 mg/ml ovalbumin, 4 mg/ml RNase A and 3 mg/ml aldolase (GE Healthcare).

Native molecular weight was calculated according to equation 5 (below) with sedimentation coefficient ($s_{20,\omega}$) obtained from a calibration curve of protein markers separated on a sucrose density gradient, R_s obtained from the gel filtration, Avogadro's number N = 6.02 x 10^{23}, viscosity coefficient η = 1 x 10^{-2} g $s^{-1}cm^{-1}$, solution density ρ = 1 g cm^{-3} and partial specific volume υ = 0.72 cm^3g^{-1}.

$$MW = {S20,\omega * N * 6 * \pi * \eta * Rs}/{1 - \upsilon * \rho}$$

The method was adapted from Lister et al., 2004 and Batters et al., 2012 and references therein.

2.3.15. Actin preparation and polymerization

Acetone dried powder was prepared from rabbit skeletal muscle (Spudich and Watt, 1971). 6 g was stirred in 120 ml of ACEX for 30 min, 4^0C. The solution was filtered through 4 layers of prewet cheesecloth and the resulting pellet was stirred in an additional 80 ml of ACEX. Resulting supernatants were combined and spun at 20000 rpm in the JA 25.50 rotor for 15 min, 4^0C. The soluble fraction was transferred to a beaker and, whilst stirring, brought to a final concentration of 5 mM Tris-HCl, pH 8.0, 50 mM KCl, 2 mM $MgCl_2$ and 1 mM ATP and stirred for 2 h, 4^0C. To remove tropomyosin, the solution was adjusted to 800 mM KCl and pH 8.3-8.5 and centrifuged at 70000 rpm, 40 min, 4^0C in the Ti 70 rotor (Beckman Coulter). Pellets were softened in the ACEX buffer followed by homogenization on ice for 30 min. The resulting solution was dialyzed overnight in the remaining ACEX buffer. The following day, the solution was recentrifuged at 13000 rpm, 15 min, 4^0C and concentrated if necessary. Concentration was measured as in equation 6:

$$[A] = {A290 - A310}/{0.62}$$

where [A] is the actin concentration, A290 and A310 are absorbance values at 290 and 310 nm, respectively, and 0.62 is the extinction coefficient of actin. A representative SDS-PAGE gel from the purification of actin is shown in Figure 2.2.

Actin polymerization was performed by dialysis of larger G-actin volumes in Slyde-A-Lyzer 10 MWCO cassettes (Pierce) in 1 L of the Actin Polymerization buffer overnight at 4^0C. Following dialysis, F-actin was stabilized with equimolar phalloidin (#P2141, SigmaAldrich) dissolved in 100% ethanol or used fresh (without phalloidin-stabilization) within 1 week.

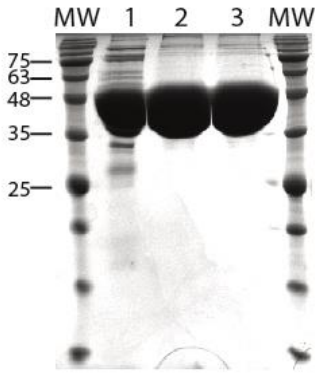

Figure 2.2. A representative SDS-PAGE gel from the purification of actin. MW – molecular weight. Expected MW of G-actin: ~42 kDa.Lanes 1-3 correspond to subsequent steps in the purification procedure.

2.3.16. Western blots

Proteins were separated by SDS-PAGE and transferred to a nitrocellulose membrane in the western blot buffer for 1 h, 100 V. Membranes were blocked for 30-60 min at RT, with 3% skimmed milk in PBS + 0.1% Tween-20, followed by incubation with the appropriate antibody for 1 h at RT or overnight at 4^{0}C. 1:10000 Streptavidin Poly-HRP or 1:2000 mouse monoclonal ANTI-FLAG® M2-Peroxidase (HRP) antibody dilutions in 3% skimmed milk were used. Membranes were washed with PBST 3 x 15 min at RT. The signal was developed for 2 min at RT, with Clarity Western ECL Substrate and collected using ChemiDoc XRS+.

2.3.17. Calculation of the ionic strength and free calcium concentration

Ionic strength was calculated from equation 7.

$$I = {}^{1}/_{2} \sum_{i=0}^{n} ci * zi^{2}$$

,where I – ionic strength, ci – molar concentration of ion i, zi – charge of ion i.

Free calcium concentration was calculated with Maxchelator.

CHAPTER 3: CLONING, EXPRESSION, PURIFICATION AND HYDRODYNAMIC PROPERTIES OF MYOSIN 9A

3.1. The primary structure of human myosin 9a

Human myosin 9a consists of 2548aa and a single heavy chain has the molecular weight of 292.7kDa. An initial domain analysis of human myosin 9a using the SMART algorithm (http://smart.embl-heidelberg.de) indicates the presence of a Ras-association domain followed by a myosin motor domain, a neck region with 5 IQ motifs and a tail domain with a RhoGAP domain and segmented coiled-coil regions. Closer look at the sequence, including sequence alignments and literature search, provided an additional insight into the structural organization of human myosin 9a: i) the Ras-association domain lacks conserved residues essential for mediating interactions with Ras and thus its function remains unknown (Kalhammer et al., 1997), ii) loop 2 is extended as compared to other

myosin classes and contains a putative CaM-binding motif, similar to other myosin 9 isoforms (Struchholz et al., 2009; Liao et al., 2010; Elfrink et al., 2014), iii) following the motor domain, the neck region contains 6 IQ motifs (as opposed to initial SMART analysis which indicated only 5 IQ motifs in the neck region), separated by 4-18 aa, iv) active site elements are conserved in sequence with other myosin family members, v) a PBD region is present at the C-terminal end of the myosin 9a tail and mediates interactions with PDZ-containing proteins (Handa et al., 2013), vi) PairCoil2 analysis (McDonnell et al., 2006) of the human myosin 9a sequence revealed two putative coiled-coil regions between 1500-1532 and 2314-2359aa of the tail. A schematic overview of myosin 9a is presented in Figure 3.1.

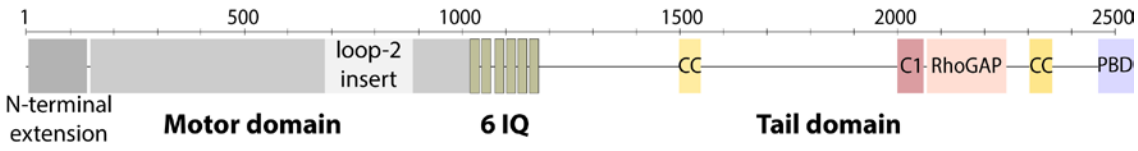

Figure 3.1. A schematic representation of the domain architecture of human myosin 9a based on available reports and sequence alignments. A motor domain, a neck region (6IQ) and a tail domain are indicated. Positions of an N-terminal extension (1-148 aa) and loop 2 insert (684-892 aa) are depicted. Note there is a total number of 7 putative calmodulin-binding sites: 1 in the loop 2 insert (not depicted) and 6 in the neck region. CC - coiled-coil, RhoGAP – Rho GTPase-activating protein, PBD: PDZ-binding domain, C1: protein-protein and protein-phospholipids interaction domain.

3.2. Description of primary sequence of developed human myosin 9a constructs

A schematic overview of myosin 9a genetic constructs developed for this study is presented in Figure 3.2. Genetic constructs encoding the motor domain for expression in the baculovirus/insect cell system are presented in Figure 3.2A. GFP-9a-S1 and GFP-9a-Head consist of the first 1162 and 1019aa of human myosin 9a, respectively. Those constructs encompass the full head, including the N-terminal extension, the loop 2 insert and an actin- and ATP-binding sites as well as the whole converter region. Additionally, GFP-9a-S1

includes the full neck region with 6 IQ motifs for light chain binding. An N-terminal GFP-tag was added to facilitate purification. The whole construct was introduced in frame with an N-terminal His-tag to facilitate affinity capture of the protein. As described below, IMAC affinity chromatography resulted in low protein yields and unsatisfactory purity. To further improve the homogeneity of my preparations, a FLAG-tag was fused to the C-terminus of the myosin fragments. Once the expression and purification of motor truncations was optimized, I attempted to express and purify the full length protein. However, further optimization is necessary to obtain recombinant full length myo9a.

The function of the N-terminal extension of myosin 9a is unknown and currently it is impossible to assess its impact on the functioning of the motor. In order to investigate the properties of the myosin 9a motor *per se*, I developed constructs truncated after the N-terminal extension, encompassing a minimal motor domain with the lever arm (9aMMD-S1; 149-1162aa) and without it (9aMMD; 149-1019aa). The minimal motor domain encompasses structural elements that enable a full catalytic activity. Based on sequence alignments with Dd myosin 2 whose minimal motor domain starts with E89 (personal communication with Dr. JR Sellers, NIH), the minimal motor of human myosin 9a begins with D149. 9aMMD and 9aMMD-S1 were cloned in frame with the C-terminal FLAG-tag to aid purification. Furthermore, to facilitate specific immobilization of the protein on the surface of a flow chamber for the *in vitro* gliding filament assay (described in Chapter 3), a biotin-binding site, an Avi-tag, was introduced between the C-terminus of a myosin 9a fragment and the FLAG-tag. All constructs were designed to maintain C-terminal tags in frame for proper translation. Alignment of the primary head and neck sequences of human myosin 9a and Dd myosin 2 heavy chains is presented in Figure 3.3 with the most conserved regions highlighted to facilitate reader's understanding of the functional elements present in individual myosin 9a motor constructs developed for this study.

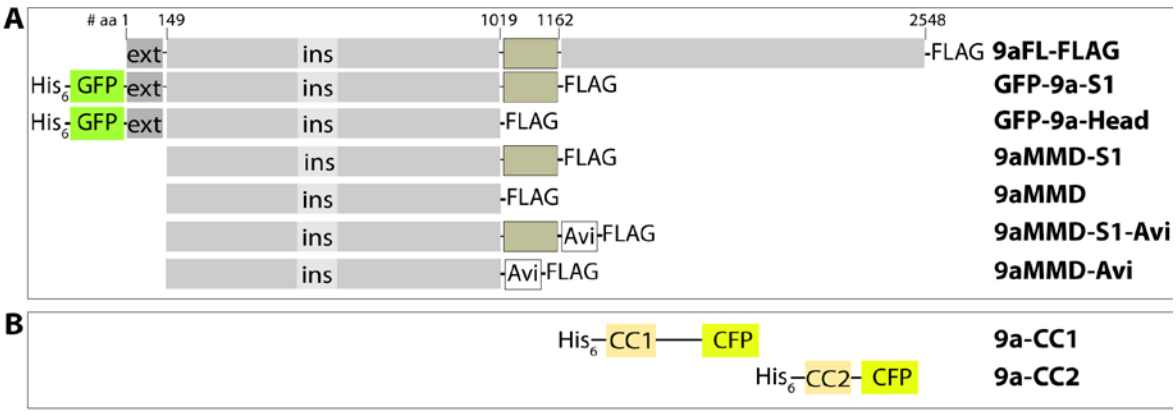

Figure 3.2. A summary of myosin 9a genetic constructs developed for this study. Domain organization and names of each construct are indicated. Numbers of strategic amino acids within human myosin 9a sequence are depicted. **A**: constructs designed for the expression in insect cells, **B**: constructs expressed in bacteria. Tags of each construct and their localization in relation to myosin 9a fragments are indicated. GFP and CFP: Green and Cyan Fluorescent Protein, MMD: Minimal Motor Domain, CC: coiled-coil, S1: Subfragment-1, ins: loop-2 insert, ext: N-terminal extension, N-terminal gray – motor domain, brown – neck domain, C-terminal gray – tail domain.

To study the propensity of myo9a to dimerize, smaller tail fragments encompassing the putative coiled-coil sequences were cloned with a C-terminal fluorescent tag and an N-terminal His-tag (Figure 3.2B) and expressed in the *E.coli* host.

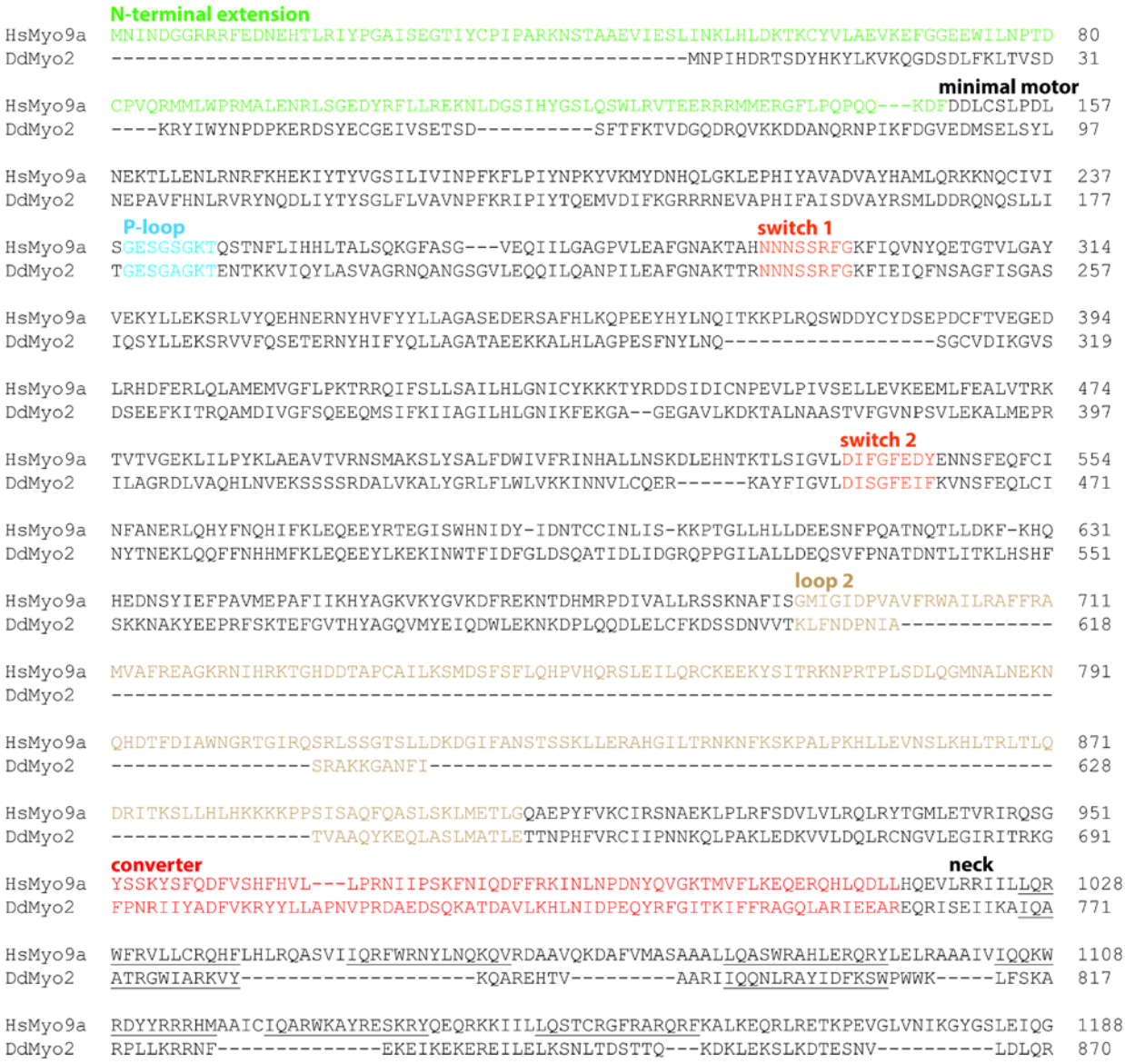

Figure 3.3. Alignment of the primary heavy chain sequences of the head and neck domains of human myosin 9a (HsMyo9a; UniProt: B2RTY4) and slime mold myosin 2 (DdMyo2; UniProt: P08799). Functional domains are highlighted and the beginning of the minimal motor domain and neck regions is indicated in black.

3.3. Generation of recombinant baculoviruses with a Bac-to-Bac system and initial purification trials

The tail domain of myosin is not essential for its activity. Therefore, initial attempts to purify myosin 9a focused on shorter constructs, GFP-9a-S1 and GFP-9a-Head with an N-terminal His_6-tag. That construct contains all structural elements necessary for a mechanochemical activity. It was established previously that a GFP fusion to a myosin (at either end of the protein) does not affect its activity (Wang et al., 2003). The GFP-tag served as a visual marker for protein expression, solubility and binding to the resin. A His-tag provides means for a cost-effective, quick and automated protein purification procedure by means of protein capture on a nickel column. The recombinant baculoviruses were generated with the Bac-to-Bac system (Life Technologies) as described below.

Cloning of GFP-9a-S1 and GFP-9a-Head was done in parallel and is presented in Figure 3.4. A chemically-synthesized gene encoding the full length human myosin 9a was used as a template for an amplification of the desired myosin 9a fragments. GFP was amplified using templates available in the lab. PCR products were cloned into the pFastBac™HTB vector, following procedures described in Chapter 2. The expression cassette contains the polyhedrin promoter for high levels of protein expression, an N-terminal His-tag followed by a protease cleavage site and a Multiple Cloning Site (MCS). Transposition sites (Tn7R and Tn7L) flank the expression cassette and are essential for a site-specific transposition of the gene of interest into a baculovirus shuttle vector (bacmid). A schematic drawing of the pFastBac vector with introduced myosin 9a constructs along with a PCR amplification of individual elements and the restriction analysis of manipulated vectors is presented in Figure 3.4.

The pFastBac plasmids with correctly introduced GFP-9a-Head and GFP-9a-S1 were used to transform *E.coli* DH10Bac cells. That strain contains a bacmid vector with an *att*Tn7 target site for a transposition of the gene of interest and a gene encoding a lacZ protein. A helper plasmid encodes proteins necessary for the transposition to occur. A successful transposition disrupts the *lacZ* gene, thus enabling a blue/white screening of colonies grown on plates supplemented with IPTG and X-gal. The bacmid DNA was isolated from white colonies (as those had the *lacZ* gene disrupted) and was subjected to

PCR to confirm a successful introduction of the gene of interest to the bacmid. Bacmid is large in size (~135kbp) and thus the PCR analysis was a method of choice at this stage. The PCR analysis was performed with a pair of primers annealing to the vector backbone, so that a resulting PCR product of ~2300bp + the size of the insert was expected to appear on the gel if the transposition occurred. GFP-9a-Head and GFP-9a-S1 have 3795 and 4224bp, respectively. PCR analysis revealed ~6100 and ~6525bp products (Figure 3.5C), confirming a successful introduction of genes into the bacmids.

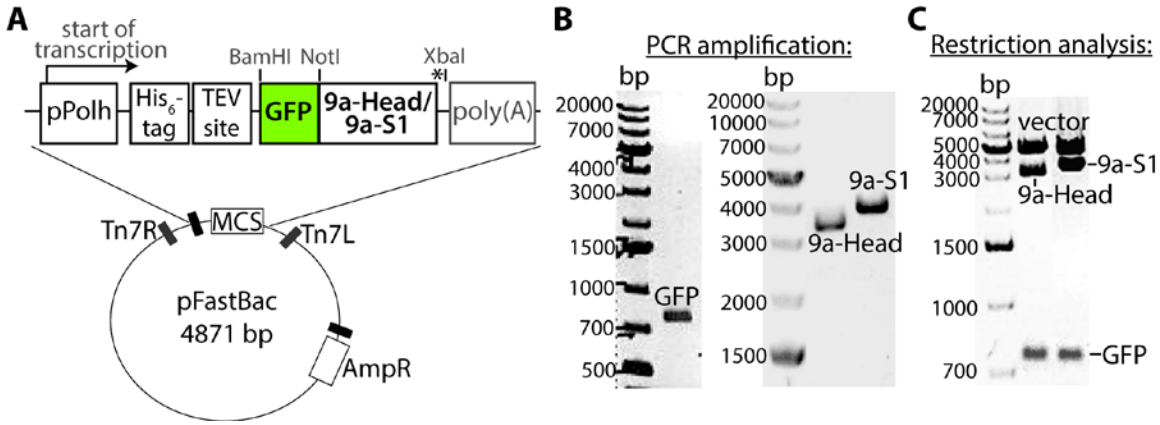

Figure 3.4. Cloning of GFP-9a-S1 and GFP-9a-Head. **A:** a schematic picture of the pFastBac™HTB vector with an ampicillin resistance gene (AmpR), transposition sites (Tn7) and a Multiple Cloning Site (MCS) depicted. A close-up view on the MCS presents an expression cassette containing a polyhedrin promoter (pPolh), a His_6-tag, a TEV protease site, a myo9a construct and a poly(A) signal. GFP and myo9a fragments were introduced between BamHI, NotI and XbaI sites within the MCS. (*) indicates the stop codon at the end of a myo9a fragment sequence. **B:** a gel electrophoresis of the PCR products confirmed successful amplification of GFP and myo9a fragments with expected sizes (GFP: 738bp, 9a-Head: 3057bp and 9a-S1: 3486bp). The pFastBac vector and PCR fragments were digested with indicated restriction enzymes. Following ligation and transformation to *E.coli* DH5α, plasmid DNA was purified. Ligation of GFP and myo9a fragments was done separately. **C:** a restriction analysis of the pFastBac plasmids. Following digestion of small amounts of extracted DNA with BamHI, NotI and XbaI, samples were analyzed by gel electrophoresis, revealing three products as expected: a vector backbone (~4.9kb), myosin 9a fragments (~3kb for 9a-Head and ~3.5kb for 9a-S1) and a GFP (738bp). Finally, plasmids were sequenced to confirm a correct reading frame.

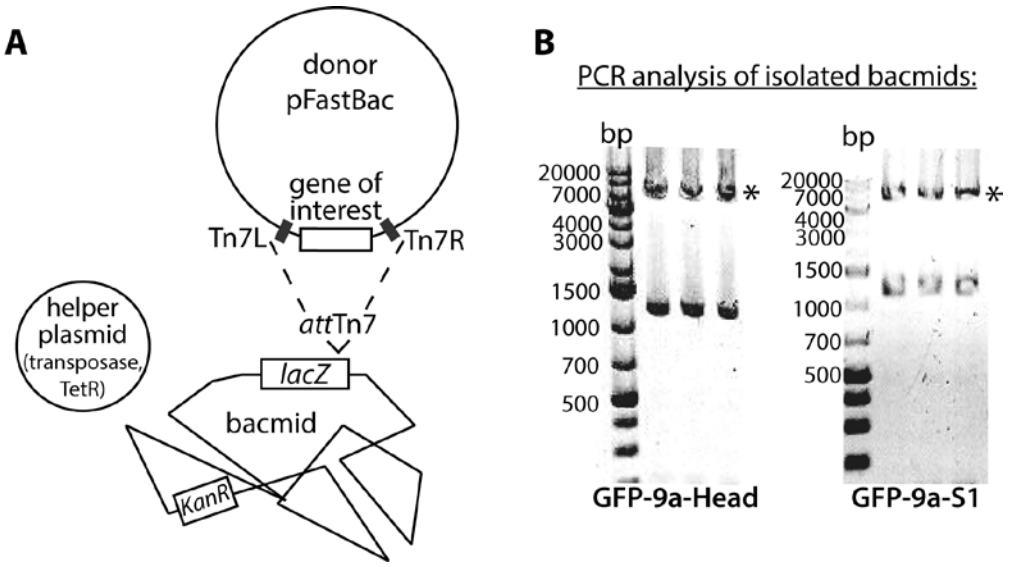

Figure 3.5. Generation of recombinant bacmids encoding GFP-9a-Head and GFP-9a-S1. **A:** a schematic drawing of a transposition of the gene of interest to a bacmid. *E.coli* DH10Bac cells were transformed with a donor pFastBac plasmid containing a gene of interest (in this case GFP-9a-Head or GFP-9a-S1) in the expression cassette flanked with transposition sites. The target bacmid vector contains an *att*Tn7 for a site-specific transposition from the donor plasmid. Recombination with the target bacmid occurs with a help of transposase encoded by the helper plasmid. Cells were plated on agar plates supplemented with kanamycin, tetracylin and gentamycin selection markers and IPTG and X-gal. Transposition disrupts the *lacZ* gene, resulting in an inhibition of X-gal cleavage and hinders the development of blue color during 48h plate growth. Bacmid DNA was subjected to a PCR analysis with primers flanking the transposition region. **B:** A representative DNA electrophoresis gel showing products of the bacmid PCR analysis. Successful transposition was confirmed by the presence of ~6.1kb and ~6.5kb bands for GFP-9a-Head and GFP-9a-S1 corresponding to the size of the donor plasmid and inserts. Bands of correct sizes on gels are indicated with asterisk. Note that due to a large size of the bacmid (~135kb), primers might anneal nonspecifically to other sequences within the bacmid, resulting in nonspecific PCR products represented by lower size bands on the gels.

Spodoptera frugiperda cells, SF9 or SF21 cells, were plated in 6-well plates and infected with recombinant bacmid DNA as described in the Methods section. P0 viruses were collected after ~10 days and scaled up to generate a high-titer stock. After amplification of the virus to a P3 stock, whole-cell lysates were analyzed by SDS-PAGE to assess protein expression (Figure 3.6A). As compared to a negative control (non-infected

cells), cells infected with GFP-9a-Head and GFP-9a-S1 baculoviruses express proteins of expected molecular weights (~165kDa for GFP-9a-S1 and ~130kDa for GFP-9a-Head).

P3 viruses were used to infect larger volume cultures. 500ml cultures were coinfected with equal volumes of GFP-9a-S1 or GFP-9a-Head and calmodulin (CaM) virus and protein was expressed for 72h at 27^0C, 140rpm. Pellets were resuspended in the Myosin Lysis Buffer (phosphate buffer) and sonicated to release the protein from cells. The soluble fraction was loaded on a 5ml HisTrap FF™ (GE Healthcare) column equilibrated with the His-low buffer on ÄKTA Purifier (GE Healthcare). Column was washed and protein was eluted with the His-high buffer using a step gradient protocol (Batters et al., 2012). GFP-9a-S1 and GFP-9a-Head bound and eluted from the column between 50-100 mM imidazole, but the protein yield wasn't satisfactory and many contaminants were present in the sample, rendering it unsuitable for subsequent biochemical analysis (Figure 3.6B-C).

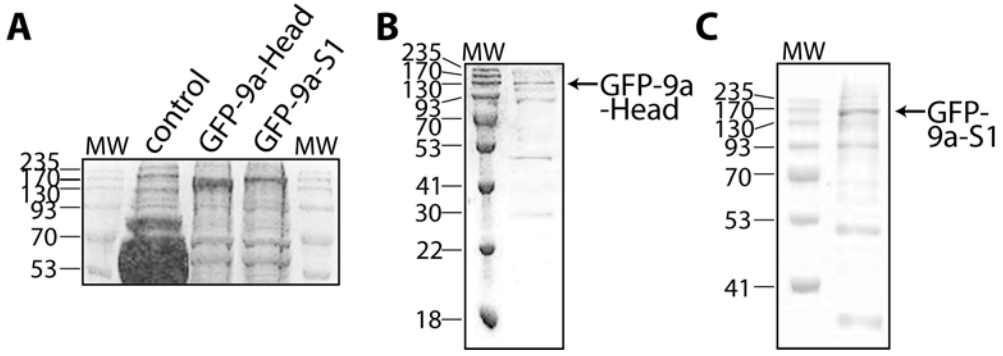

Figure 3.6. Expression and purification of GFP-9a-Head and GFP-9a-S1. **A:** protein expression was assessed by SDS-PAGE of cell pellets from the P3 virus stock. As compared to non-infected cells (control), cells infected with GFP-9a-Head and GFP-9a-S1 viruses expressed proteins of expected molecular weights (~130kDa and ~165kDa, respectively). 500ml SF21 cultures were coinfected with equal volumes of high-titer P3 stocks of recombinant myosin 9a and calmodulin baculoviruses and proteins were expressed for 72h at 27^0C, 140rpm. Cells were collected and following disruption of the cell membrane, the soluble fraction was loaded onto a His-trap affinity chromatography column using an automated FPLC system. The column was washed to remove nonspecifically bound proteins and myosin was eluted with an increasing imidazole concentration. Elution fractions were analyzed by SDS-PAGE. Protein bands with sizes corresponding to those of GFP-9a-Head (**B**) and GFP-9a-S1 (**C**) were found in the eluted samples, along with multiple contaminants. Low yield and purity rendered the protein unsuitable for subsequent biochemical analysis.

Judged by the visual inspection of cell pellets, high amounts of the protein remained in the insoluble fraction. That might indicate that myosin 9 aggregates during expression. In order to improve the amount of protein in the supernatant, I used Sarkosyl detergent to extract the myosin from cells. That detergent disrupts protein aggregates (Frankel et al., 1991). Following sonication as described above, cell debris was collected and resuspended in a Sarkosyl buffer (1% Sarkosyl, 20mM TriEthanolAmine). After 30min nutation, the soluble fraction was applied to a 5ml HisTrap FF™ column and processed as before with a step-wise dilution of Sarkosyl with each wash of the column. The Sarkosyl extraction significantly improved the protein yield in the supernatant and a highly pure myosin fraction was obtained by means of the IMAC purification (Figure 3.7). Nonetheless, the Sarkosyl-extracted myosin 9a was rendered inactive as tested by the *in vitro* motility assay and an ATPase assay.

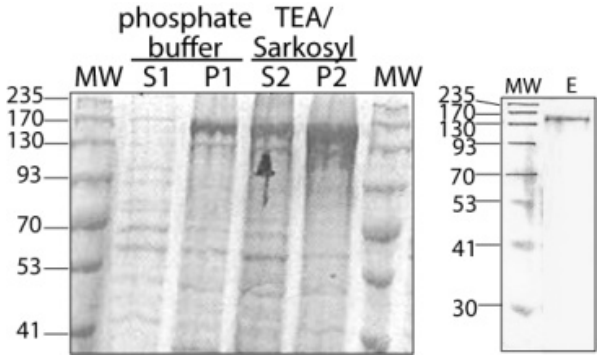

Figure 3.7. Extraction of GFP-9a-S1 by Sarkosyl yielded more protein in the soluble fraction and improved the purity of the protein after affinity chromatography. Left panel: an SDS-PAGE analysis of myosin 9a extraction by Sarkosyl showed an increase in the amount of GFP-9a-S1 in the soluble fraction. SF9 cells expressing GFP-9a-S1 were resuspended in a buffer with or without Sarkosyl. Proteins from insoluble (P) and soluble (S) fractions were separated on an SDS-PAGE gel followed by Commassie staining. Note the improvement in the amount of GFP-9a-S1 in the soluble fraction after the Sarkosyl extraction (S1) as compared to a buffer without Sarosyl (S1), as indicated by an arrow. Right panel: a His-tag affinity purification of GFP-9a-S1 after Sarkosyl extraction. Cell pellets were processed as described and the soluble protein fraction was loaded on a His-trap column. The column was washed and the protein was eluted with an increasing imidazole concentration, yielding highly pure GFP-9a-S1 sample. MW: molecular weight, S: Supernatant, P: Pellet, E: Eluate, TEA: Triethanolamine.

Taken together, the recombinant myosin 9a showed low solubility when expressed in the baculovirus/insect cell system under conditions described. The solubility was significantly improved by Sarkosyl extraction. The amount of soluble protein obtained with Sarkosyl improved the yield of pure GFP-9a-S1 protein fractions. Nevertheless, the protein did not hydrolyze ATP in an ATPase assay and did not translocate actin filaments in the *in vitro* motility assay. Thus, an alternative purification method had to be established.

3.4. Cloning of FLAG-tagged myosin 9a constructs. Optimization of expression and purification of myosin 9a.

A FLAG-tag was linked to the C-terminal end of myosin 9a motor constructs (Figure 3.8A), providing means of a highly specific capture of the protein from the supernatant (Lichty et al., 2005). GFP-9a-Head and GFP-9a-S1 constructs were used as templates for the addition of the C-terminal FLAG-tag. Reverse primers were designed that bypass the stop codon of myosin 9a-Head and -S1, hybridizing to 21 nucleotides upstream of the stop codon. Additionally, the primers contained a genetic sequence encoding the FLAG-tag (aa sequence: DYKDDDDK) in frame with an N-terminal His-tag, GFP and myosin 9a. A stop codon and an XbaI restriction site were added after the FLAG-tag sequence. GFP-9a-Head and GFP-9a-S1 with the C-terminal FLAG tag were generated by PCR with the GFPfwd primer and described myo9a reverse primers. Amplified fragments were treated as previously and introduced into a pFastBac vector. Bacmid was created and analyzed as before. A schematic drawing of the constructs developed at this stage is presented in Figure 3.8, along with appropriate DNA gels. From this point on, those constructs are simply referred to as GFP-9a-Head and GFP-9a-S1 within the text.

Non-fluorescent versions of those constructs in pFastBac were also developed (Figure 3.9) but have not been used in this study.

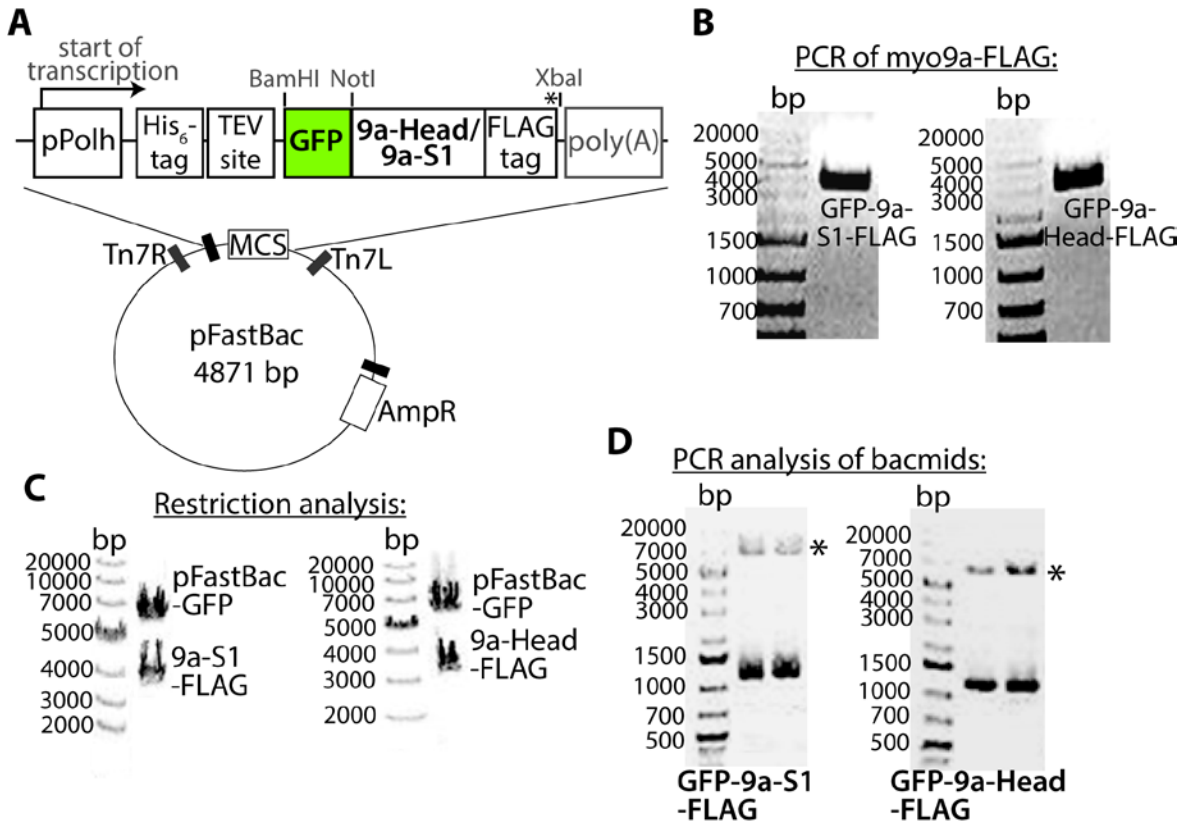

Figure 3.8. Cloning and bacmid generation of C-terminally FLAG-tagged GFP-9a-Head and GFP-9a-S1. A: a schematic picture of a pFastBac vector containing GFP-9a-Head/GFP-9a-S1 fused to a C-terminal FLAG tag. The expression cassette elements are the same as before. **B:** amplification of GFP-myo9a fragments with reverse primers adding a C-terminal FLAG-tag upstream of the stop codon yielded products of expected sizes (~3100bp for GFP-9a-Head and ~3500 for GFP-9a-S1). Cloning into the pFastBac vector was performed as previously described. **C:** recombinant plasmid DNA was isolated and subjected to the restriction analysis. Samples were digested with NotI and XbaI enzymes and analyzed by DNA electrophoresis revealing the presence of two fragments as expected: a pFastBac vector backbone with GFP (expected size ~5.5kb) and 9a-S1-FLAG (3510bp) or 9a-Head-FLAG (3081bp). Those samples were sequenced and used to produce recombinant bacmids. **D:** a PCR analysis of purified recombinant bacmids confirmed a successful transposition of the genes of interest from the donor pFastBac vector into the bacmid. The size of expected products were ~6.1kb and ~6.5kb (including the size of the donor vector and the insert) for GFP-9a-Head-FLAG and GFP-9a-S1-FLAG, respectively. Localization of the expected products on the gel is indicated with an asterisk.

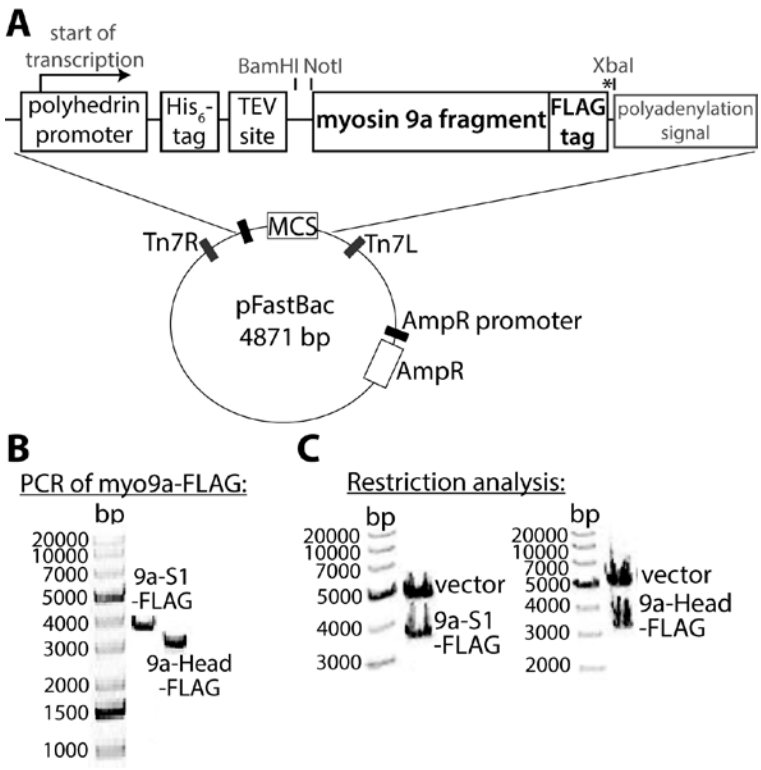

Figure 3.9. Cloning of non-fluorescent 9a-Head and 9a-S1 with a C-terminal FLAG tag. **A:** a scheme of the expression cassette for 9a-Head and 9a-S1 linked to the C-terminal FLAG-tag. **B:** a PCR amplification of 9a-S1-FLAG and 9a-Head-FLAG yielded products of expected sizes. A forward primer for myosin 9a and reverse primers described above were used to amplify the desired fragments. **C:** amplified myosin 9a fragments and the pFastBac vector were digested with NotI and XbaI and ligated. Plasmids were amplified in *E.coli* cells and correct recombinants were confirmed by the restriction analysis; plasmids were digested with NotI and XbaI and analyzed by DNA electrophoresis, revealing two products with sizes corresponding to the pFastBac vector backbone and myosin 9a inserts as indicated.

Time-dependent protein expression was assessed for GFP-9a-S1 in a 6-well format by seeding the cells at $6x10^5$ cells/well and infecting with a recombinant myosin 9a virus. Cells were harvested at 24, 48, 60 and 72h post-infection and whole-cell lysates were analyzed by SDS-PAGE (Figure 3.10A). Simultaneously, the solubility of GFP-9a-S1 was assessed in the following way: 25 ml cultures of $1x10^6$ cells/ml were coinfected with 5ml of the myosin 9a and calmodulin virus and shaken 140rpm, 27^0C for 60h. Cells were collected and sonicated in the Myosin Extraction Buffer in the presence of ATP to facilitate the dissociation of myosin from the host actin cytoskeleton. Following 30min nutation at 4^0C,

soluble and insoluble fractions were separated by SDS-PAGE, transferred to a nitrocellulose membrane and analyzed by a western blot with an anti-FLAG antibody to confirm the presence of myosin 9a in the soluble fraction (Figure 3.10B). Still, a lot of protein was found in the insoluble fraction. One possibility might be insufficient cell disruption during sonication, hindering the release of the protein to the supernatant. However, as assessed by fluorescence microscopy (Figure 3.10C), cells were fully lysed, indicating that poor recovery of myosin 9a in the soluble fraction might be due to improper folding or aggregation during expression.

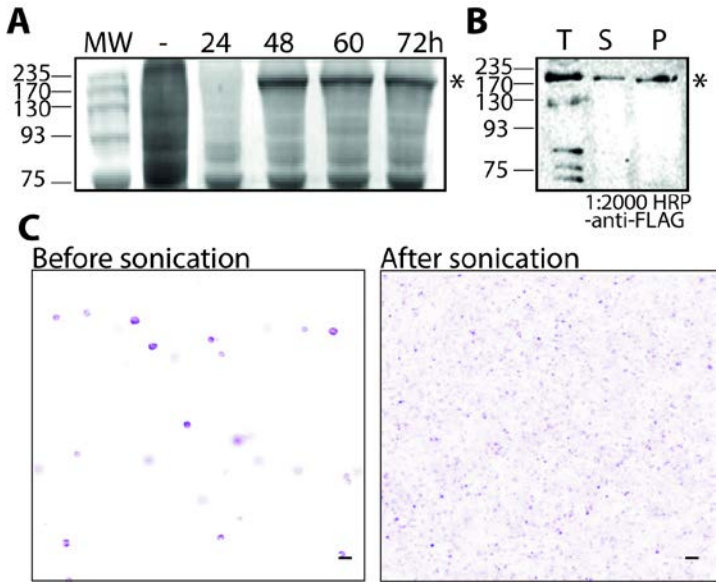

Figure 3.10. Time-dependent expression and solubility of myosin 9a, with GFP-9a-S1 as an example. **A:** SDS-PAGE analysis of whole cell lysates taken 24, 48, 60 and 72h post-infection with GFP-9a-S1 virus. The cell lysate of non-infected cells (-) was included as a negative control. The asterisk indicates the position of the protein band corresponding to the molecular weight of the GFP-9a-S1 heavy chain. Note the protein was expressed at 48h post-infection with no further increase in the protein yield afterwards. **B:** solubility of myosin 9a was confirmed by a western blot with an HRP-conjugated anti-FLAG antibody. Fractions of Total (T), Supernatant (S) and Pellet (P) were separated on an SDS-PAGE gel, transferred to a nitrocellulose membrane and blotted with the anti-FLAG antibody. The asterisk indicates the position of the GFP-9a-S1 protein band. **C:** fluorescent images of GFP-9a-S1-expressing SF21 cells before (left) and after (right) sonication. Note that before sonication cells are clearly visible in the image field whereas after sonication only the cell debris is present in the sample confirming effective cell disruption. Scale bar: 40µm.

The amount of coexpressed calmodulin can affect expression levels and solubility of myosin (Zhu et al., 1996). The best myosin:calmodulin ratio for the expression and preparation of active myosin 9a was assessed for GFP-9a-S1 as this construct contains 7 putative calmodulin binding sites (as opposed to a single putative CaM binding site in 9a-Head). Small-scale cell cultures (250ml) were coinfected with GFP-9a-S1 virus and varying amounts of CaM virus. As assessed previously, the protein was expressed after 48h and there was no further increase in protein yield after that time. Thus, after 48h expression, GFP-9a-S1 was purified by means of FLAG-tag affinity chromatography with ~0.3ml affinity resin. The molecular composition of the eluate fractions was assessed by SDS-PAGE, confirming the presence of bands corresponding to the GFP-9a-S1 heavy chain and CaM light chains in all conditions tested (Figure 3.11). The best yields were obtained for cultures coinfected with the equal volumes of myosin 9a and calmodulin viruses. Apart from the protein of interest, an additional band of ~100kDa was present in all samples. That co-product is very often present in the FLAG resin eluates and is suspected to be a host chaperone (personal communication with Dr Jr Sellers, NIH). However, since that contaminant contributed to more than 50% of the protein content of my samples, an additional purification step had to be employed to further improve the purity.

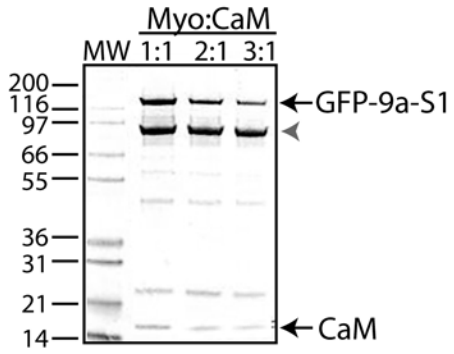

Figure 3.11. Small-scale expression and purification of GFP-9a-S1 co-expressed with varying amounts of calmodulin. 250ml insect cell cultures were coinfected with constant amount of GFP-9a-S1 virus and varying amounts of CaM virus and expressed for 48h at 27^0C, 140rpm followed by FLAG affinity chromatography as described in Materials and Methods. Eluate fractions from cultures with different myosin:CaM ratios were analyzed by SDS-PAGE. GFP-9a-S1 copurified with calmodulin from all culture conditions tested. However, cultures infected with the equal amounts of myosin and CaM viruses provided the highest yield of myosin 9a in the sample. A major contaminant at ~100kDa was present in all samples (indicated by a grey arrowhead). Protein bands corresponding to GFP-9a-S1 and calmodulin (CaM) are indicated.

Large-scale expression and purification of myosin 9a motor constructs using FLAG affinity chromatography yielded identical results, in that two main co-products were present in the sample (Figure 3.12). An attempt to rebind the protein to His-affinity resin proved unsuccessful. Thus, following FLAG purification, the eluted protein (in a buffer containing 100mM NaCl) was applied to ion exchange resin and eluted with an increasing ionic strength in a step-wise manner. This led to the separation of myosin 9a from major contaminants present in the sample, resulting in preparations reaching ~95% purity as estimated by a gel densitometry analysis. Furthermore, ion exchange chromatography has proven a successful means of concentrating the protein. The implementation of that two-step purification protocol (1^{st} step: FLAG affinity; 2^{nd} step: ion exchange chromatography) resulted in homogenous preparations of myosin 9a proteins (Figure 3.12 and see below). Eluate fraction of GFP-9a-Head from FLAG affinity resin did not contain any contaminants but subsequent application of the sample to ion exchange resin resulted in the concentration of the protein and separation of two fractions: with and without bound calmodulin. The latter one did not exhibit any activity in enzymatic assays and thus was omitted from

experiments. GFP-9a-S1 eluted from the ion exchange resin at 500mM NaCl and GFP-9a-Head at 250mM NaCl. Usually, from ~1 x 10^9 cells, up to 0.6mg of protein was obtained. GFP-9a-S1 and GFP-9a-Head exhibited enzymatic activity, as assessed by the steady-state ATPase and *in vitro* motility assays (see next chapters).

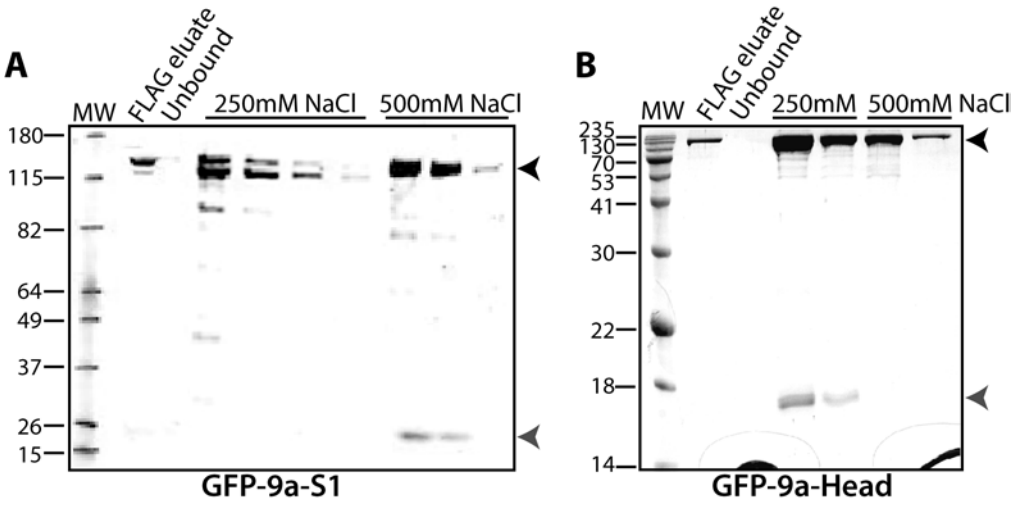

Figure 3.12. Implementation of ion exchange chromatography as the second step of the myosin 9a purification resulted in homogenous preparations of the protein. Representative SDS-PAGE gels showing individual purification steps of GFP-9a-S1 (**A**) and GFP-9a-Head (**B**). Myosin 9a constructs were purified by means of FLAG affinity chromatography as described above. Protein present in FLAG eluates was bound to ion exchange chromatography resin and eluted in fractions with 250mM and 500mM NaCl, as indicated. Full binding of FLAG eluate specimen to the ion exchange resin was confirmed by the lack of the protein in the 'Unbound' fraction, referring to an ion exchange flow through. The majority of GFP-9a-S1 eluted at 500mM NaCl, whereas GFP-9a-Head was present in two fractions: with bound calmodulin (eluting at 250mM NaCl) and without bound calmodulin (eluting at 500mM NaCl). Positions of the myosin heavy chain and calmodulin are indicated by black and grey arrowheads, respectively.

3.5. Expression of full length myosin 9a needs further optimization

Encouraged by the successful expression and purification of myosin 9a motor truncations described above, I attempted to express full length myosin 9a (9aFL-FLAG). Full myosin 9a sequence containing 2548aa was amplified by PCR and introduced into a

customized pFBNA vector containing a C-terminal FLAG-tag, followed by the production of recombinant bacmid (Figure 3.13).

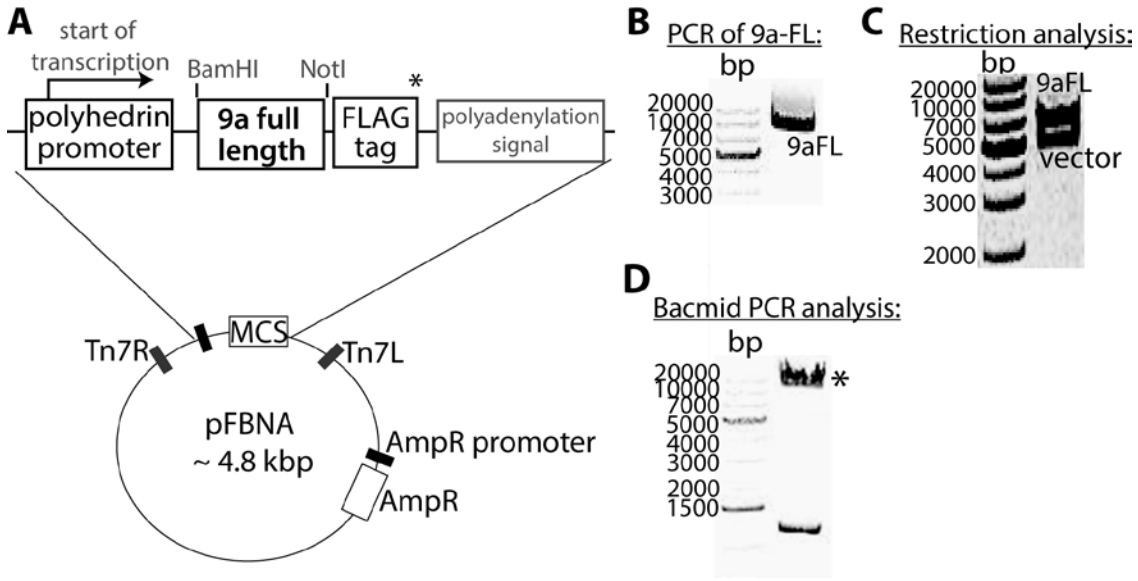

Figure 3.13. Cloning and recombinant bacmid production of 9aFL-FLAG. **A:** a schematic drawing of the structure of the pFBNA plasmid encoding 9aFL-FLAG. 9aFL was introduced between BamHI and NotI sites in frame with the C-terminal FLAG-tag under control of the polyhedrin promoter. An asterisk indicates a stop codon upstream of the FLAG-tag. **B:** Full length myosin 9a was amplified by PCR and analyzed by gel electrophoresis to confirm the correct size of the product (7641bp) and ligated into the pFBNA vector following previously described procedures. **C:** the restriction analysis of pFBNA after introduction of the 9aFL gene confirmed the presence of the insert, as analyzed by gel electrophoresis; following restriction with BamHI and NotI, two bands corresponding to the vector backbone (~4.8kbp) and the 9aFL fragment (~7.6kbp) appeared on the gel. **D:** gel electrophoresis of PCR products of bacmid amplification revealed a band of the size corresponding to ~10kbp (indicated by asterisk) as expected after successful transposition into the bacmid.

The recombinant baculovirus was developed and scaled to the P3 stock as before. Small scale SF9 culture was co-infected with equal volumes of 9aFL-FLAG and CaM baculoviruses. Cells were collected and the expression of the protein was analyzed by SDS-PAGE and a western blot. As shown in Figure 3.14, no protein band corresponding to full length myosin 9a (expected MW: ~293kDa) was resolved on an SDS-PAGE gel and there was no signal on the western blot. As a positive control for the western blot, GFP-9a-Head

with a FLAG-tag was ran on SDS-PAGE and transferred to a nitrocellulose membrane, alongside samples from myo9a FL expression. GFP-9a-Head gave a positive signal on the western blot, as opposed to samples infected with 9aFL virus. This suggests that the expression of full length myosin 9a needs further optimization.

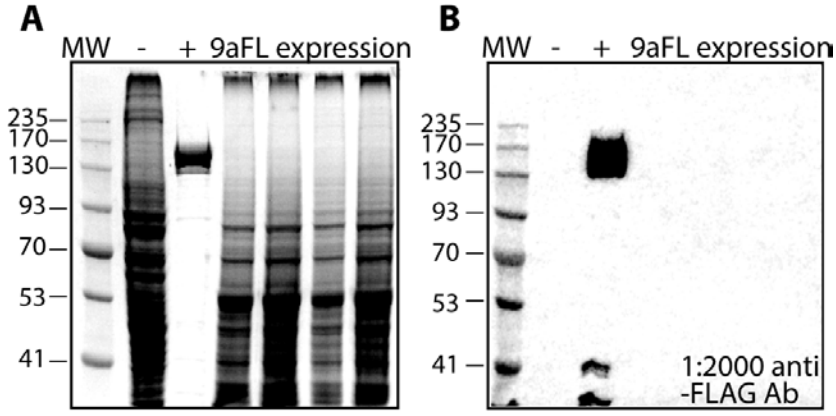

Figure 3.14. 9aFL-FLAG is not expressed in the baculovirus/insect cell system under conditions used. Small-scale SF9 cell cultures were coinfected with equal amounts of 9aFL and CaM viruses and protein was expressed for 48h at 27^0C, 140rpm. Samples of non-infected cells (-), FLAG-tagged GFP-9a-Head (+) and samples infected with 9aFL virus (9aFL expression) were separated on an SDS-PAGE gel (**A**) and transferred to a nitrocellulose membrane, followed by blotting with an anti-FLAG Antibody (**B**). No band corresponding to the 9aFL protein was resolved on SDS-PAGE and no signal was observed on a western blot in samples infected with the virus. A positive control for the western blot gave the positive signal, confirming that the lack of the signal in 9aFL samples is related to the lack of protein expression, instead of a faulty western blot.

3.6. Cloning and purification of Minimal Motor Domain constructs; confirmation of protein identity and stability

The N-terminal extension of myosin 9a has an unknown function. It was proposed that it adopts a Ras-binding fold (Bähler, 2000). However, close inspection of the sequence revealed it lacks conserved residues essential for binding of Ras (Kalhammer et al., 1997). Currently, there is no information on a possible function of protein domains that adopt the Ras-binding fold but are unable to bind Ras. It is therefore difficult to speculate on an impact of that domain on myosin 9a activity. Still, it is plausible that the N-terminal extension: i) does not affect the acitivity of myosin 9a, ii) is essential for an enzymatic

activity of myosin 9a, or iii) inhibits the activity of myosin 9a. In order to rule out or confirm any one of those scenarios, I designed and developed recombinant baculoviruses expressing myosin 9a constructs containing a minimal motor domain (a minimal part of the sequence essential for the biochemical performance), lacking the N-terminal extension.

I created Minimal Motor Domain constructs with (9aMMD-S1) and without (9aMMD) the lever arm, introduced them into the pFBNA vector with a C-terminal FLAG-tag, created recombinant bacmids and baculoviruses, expressed and purified those proteins as before. A schematic drawing of the expression cassette including those constructs and individual steps of the recombinant bacmid production as well as SDS-PAGE analysis of protein expression are shown in Figure 3.15.

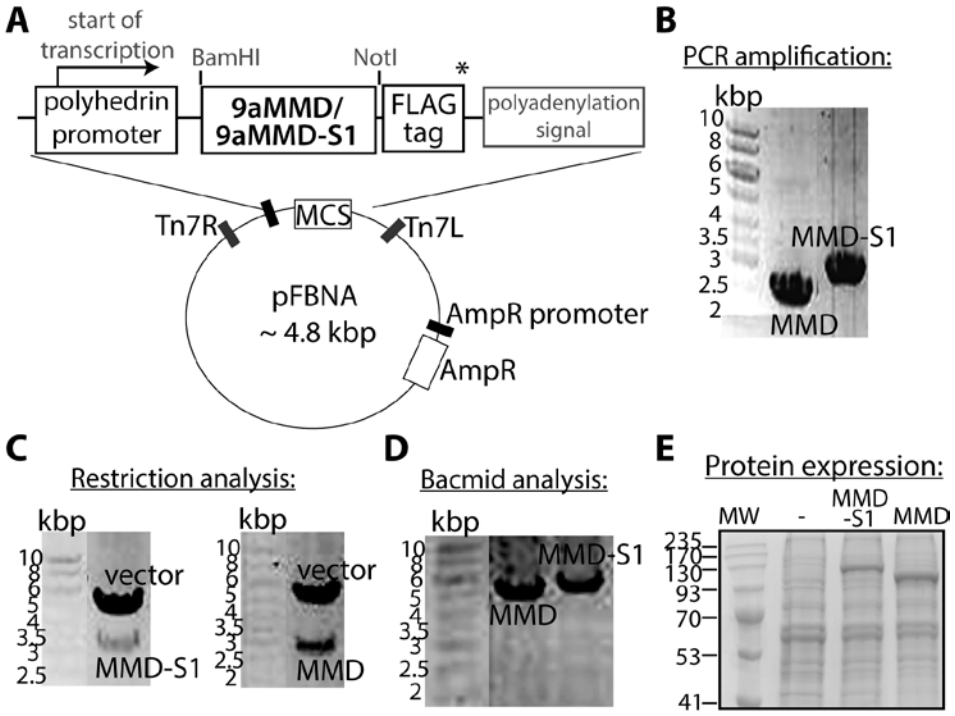

Figure 3.15. Cloning, production of recombinant bacmids and expression of 9aMMD and 9aMMD-S1. **A:** a schematic drawing of the expression cassette of the pFBNA vector with MMD constructs introduced between BamHI and NotI sites, in frame with the C-terminal FLAG-tag. An asterisk indicates a stop codon. **B:** gel electrophoresis of PCR products of MMD and MMD-S1 revealed the presence of expected products (2613bp for MMD and 3042bp for MMD-S1). **C:** the recombinant pFBNA plasmid was subjected to the restriction analysis with BamHI and NotI enzymes, revealing the presence of two bands on DNA gel corresponding to the vector backbone (~4.8kbp) and MMD-S1 and MMD

fragments, respectively. **D:** a PCR analysis of isolated recombinant bacmids confirmed successful transposition. **E:** protein expression was assessed from P3 virus pellets by the separation of whole-cell lysates on SDS-PAGE. As compared to non-infected cells (-), cells infected with MMD-S1 or MMD viruses expressed proteins with corresponding molecular weights (118.5kDa and 100kDa, respectively).

A purification protocol described for GFP-9a-Head and GFP-9a-S1 was successfully applied to the purification of 9aMMD constructs. A representative SDS-PAGE gel of 9aMMD and 9aMMD-S1 is shown in Figure 3.16A. As for previously described constructs, 9aMMD-S1 eluted at 500mM NaCl and 9aMMD at 250mM NaCl from IEX. Identity of the heavy chain was confirmed by an anti-FLAG western blot of final myosin preparations (Figure 3.16B). Based on previous reports the head of myosin 9 binds calmodulin and the binding site has been mapped to the N-terminus of the unique myosin 9 loop 2 insert (Liao et al., 2010). Sequence comparisons revealed the presence of that putative CaM-binding site in the loop 2 insert of human myosin 9a, too. Thus, both 9aMMD and 9aMMD-S1 were co-expressed with calmodulin. As shown in Figure 3.16A, 9aMMD copurified with ~17kDa protein that underwent a calcium-dependent shift in electrophoretic mobility (Figure 3.16C), as expected for an authentic calmodulin (Liao et al., 2010). Furthermore, similar to GFP-9a-Head, 9aMMD eluted from ion exchange both at 250mM and 500mM NaCl. As opposed to the 500mM NaCl fraction, the 250mM NaCl fraction coeluted with calmodulin. This has raised an intriguing possibility that myosin 9a exists in two states in the cell – with and without bound calmodulin. However, activity assays revealed that myosin 9a lacking calmodulin bound to the motor domain is rendered inactive.

Taken together, the minimal motor domain constructs can be readily expressed in the baculovirus/insect system and purified by means of FLAG-tag affinity chromatography followed by ion exchange. The latter step provides efficient means of separating two fractions of 9aMMD (with and without bound calmodulin) present in cells. Since only the fraction that contained bound calmodulin exhibited enzymatic activity, the developed purification protocol results in an efficient separation of active and inactive motors. These results suggest that calmodulin binding to myosin 9a head is essential for protein activity *in*

vitro. However, a possible regulation of myosin 9a activity in cells by means of calmodulin binding and dissociation from the head cannot be ruled out.

Various storage conditions of myosin 9a constructs were examined, including snap-freezing of myosin 9a in the presence of 20% sucrose or 50% glycerol and storage at -80^{0}C or in liquid N_2. However, this led to a loss of activity within few days. Thus, purified proteins were used fresh within two days following the purification.

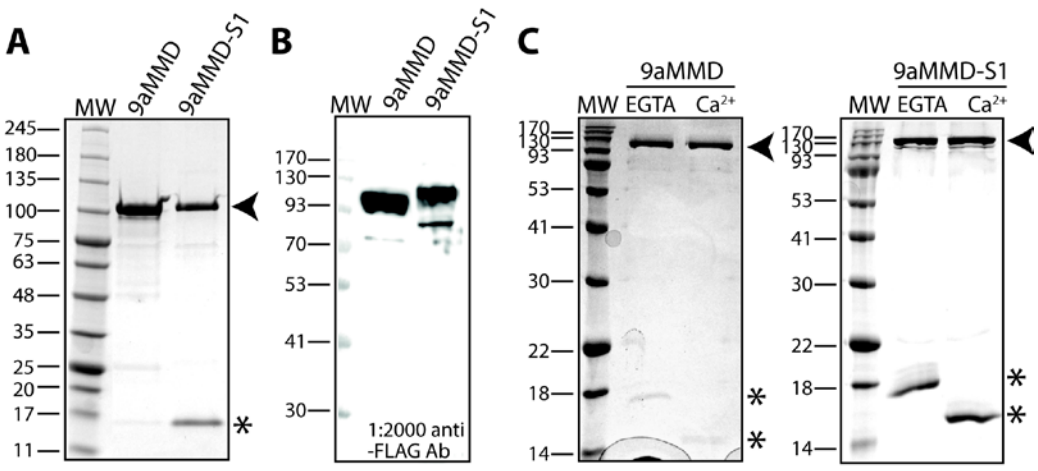

Figure 3.16. Purification of 9aMMD and 9aMMD-S1 by FLAG-tag affinity chromatography and IEX. Confirmation of protein identity. **A:** a representative SDS-PAGE gel of 9aMMD and 9aMMD-S1 purified with a previously described protocol, separated on a 4-20% Tris-Glycine gel. An arrowhead indicates myosin heavy chains of 9aMMD and 9aMMD-S1 and asterisk indicates calmodulin light chains copurified with each construct. Note the difference in the amount of calmodulin copurified with 9aMMD and 9aMMD-S1. **B:** an anti-FLAG western blot of 9aMMD and 9aMMD-S1. Myosin samples were separated on a 10% SDS-PAGE gel, transferred to a nitrocellulose membrane and blotted with an HRP-conjugated anti-FLAG antibody. Signal was developed with the ECL Western Blotting Substrate kit. **C:** a calmodulin mobility shift assay. 9aMMD and 9aMMD-S1 were incubated with 1mM EGTA or 5mM $CaCl_2$ for 15 min at RT and separated on a 15% SDS-PAGE gel. Arrowheads indicate myosin heavy chains and asterisk indicates calmodulin. Shift in the mobility of the light chain protein band in the presence of calcium confirmed its identity as calmodulin.

When analyzed by electron microscopy, both 9aMMD and 9aMMD-S1 existed as single molecules. No molecules with two heads or protein aggregates were observed,

suggesting that both 9aMMD and 9aMMD-S1 exist as monomers in a homogenous solution. There was no electron density corresponding to an extended neck domain observed in electron micrographs of 9aMMD-S1, suggesting it might be wrapped around the motor domain in a nucleotide-free state (Figure 3.17).

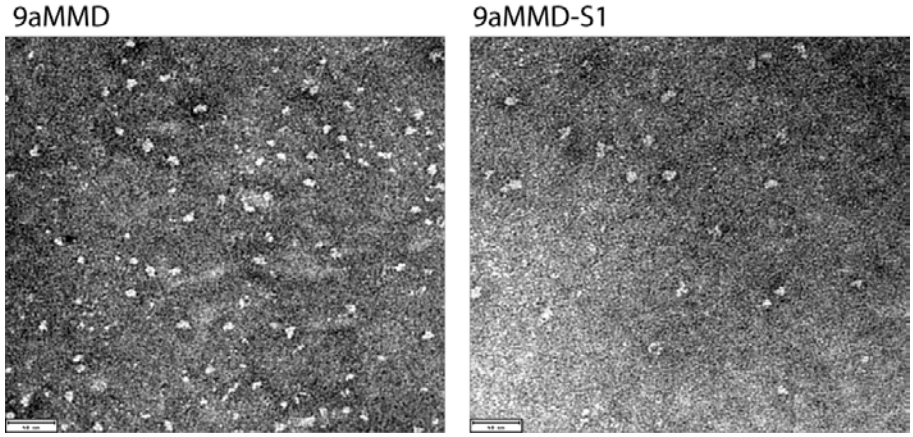

Figure 3.17. Negatively stained EM images of 9aMMD (left) and 9aMMD-S1 (right). Images show individual myosin molecules in solution. Neither 9aMMD, nor 9aMMD-S1 form higher-order structures and both constructs exist as monomers in solution. In case of 9aMMD-S1, no evident electron density corresponding to an extended neck region is visible, suggesting the light chain-binding domain might be wrapped on the motor domain. Scale bar 40nm.

Stability of 9aMMD and 9aMMD-S1 preparations over time was assessed by DLS (Dynamic Light Scattering; Shiba et al., 2010). Calmodulin binding to each construct made it challenging to assess the stability by the temperature-dependent unfolding since the dissociation of calmodulin from the heavy chain and calmodulin unfolding would contribute to the overall signal, making it impossible to determine the melting temperature of the myosin heavy chain. Assuming that drop in the myosin activity would be related to the protein degradation and/or aggregation, the intensity of molecular species present in the sample was measured at different time points over 48h (Figure 3.18). A high-speed centrifugation of protein eluates was used to remove nonspecific aggregates, ensuring homogeneity of the sample. Protein was diluted to 0.1mg/ml in a filtered elution buffer and the intensity of molecular species present in the sample was measured. Both 9aMMD and 9aMMD-S1 samples contained mainly a single component. The intensity of the peak in

each case was constant over the course of 48h (Figure 3.18), suggesting the protein sample did not change its composition over 2 days.

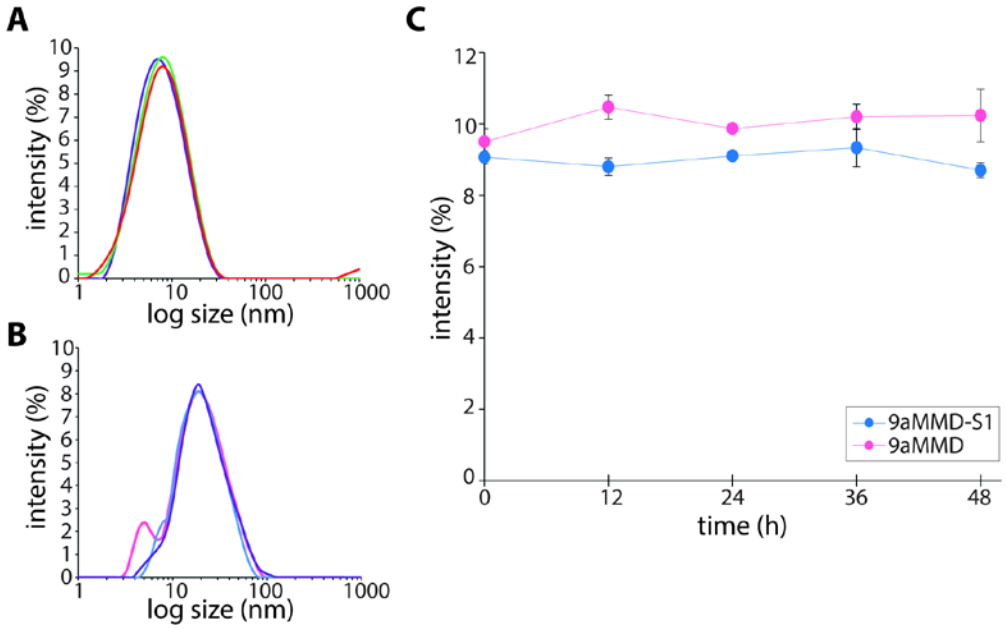

Figure 3.18. Stability of 9aMMD and 9aMMD-S1 over time measured by DLS. Intensity of 0.1 mg/ml protein sample was measured at different time points during 48 h. The intensity of the molecular species in the sample was traced over time revealing no change in the molecular composition of the sample. All measurements were performed in 3 repeats on each myosin preparation, with 3 independent preparations used for the data set. **A and B:** examples of DLS measurements of 9aMMD and 9aMMD-S1, respectively (note the shift in the size of the molecule from 8.1±0.2 nm for 9aMMD to 11±0.1 nm for 9aMMD-S1). **C:** an average intensity from each measurement over 48h from 3 independent preparations was plotted against time (▪9aMMD-S1, ▪9aMMD). Data points represent mean±S.D. (n=3).

3.7. Calmodulin stoichiometry

Human myosin 9a contains 7 putative CaM-binding sites. The actual number of bound light chain molecules per heavy chain was assessed by protein band densitometry (Figure 3.19). Bacterially-expressed calmodulin was used as a standard for the generation of the calibration curve. Increasing concentrations of CaM and known myosin concentrations (calculated based on their extinction coefficients and A_{280}) were separated on SDS-PAGE gels and calibration curve was obtained from the band intensity of CaM

standards after staining of the gels. The intensity of the CaM band in the well with known myosin concentration was interpolated to the trend line and the molar ratio of light chain:heavy chain (LC:HC) was calculated. 9aMMD-S1 (7 IQ motifs) bound 5.8 ± 1.4 CaM molecules per heavy chain and 9aMMD (1 IQ motif) - 1.1 ± 0.7 CaM molecule per heavy chain based on 3 independent measurements. That suggests that out of the 7 available CaM-target sites in 9aMMD-S1 only 6 IQ motifs were occupied by CaM light chains. The remaining IQ motif might bind a different light chain, not bind any light chain at all or had lost its light chain during purification. Given that 9aMMD copurified with a single CaM light chain per heavy chain, it is safe to assume that the previously mentioned IQ motif at the N-terminus of the loop 2 insert of myosin 9 is the binding site for that CaM. Therefore, only 5 IQ motifs within the neck region might be occupied by CaM light chains under conditions used.

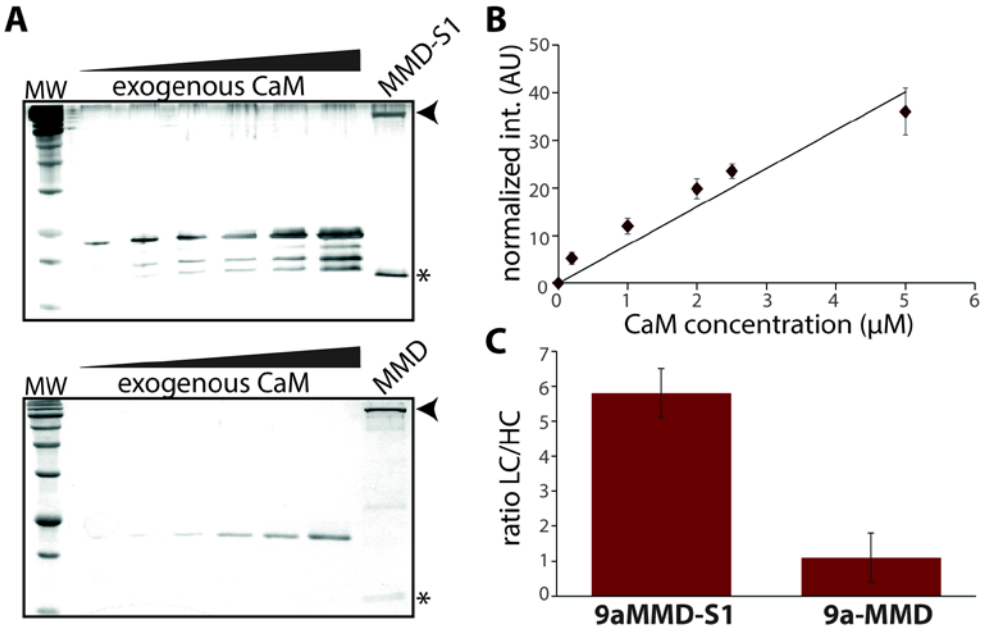

Figure 3.19. Stoichiometry of calmodulin binding to myosin 9a constructs. **A:** known cncentrations of free CaM and 9aMMD and 9aMMD-S1 samples were separated on SDS-PAGE gels and either silver-stained (MMD-S1) or Commassie-stained (MMD). Arrowheads indicate myosin 9a heavy chain positions and asterisk indicates CaM. **B:** band intensities at each CaM concentration were plotted against CaM concentration and the calibration curve was produced for interpolation of the CaM amount present in myosin samples. **C:** a molar ratio of the light chain to the heavy chain [LC]/[HC] was calculated revealing 5.8±1.4 CaM molecules bound to 9aMMD-S1 and 1.1±0.7 CaM molecules per

9aMMD heavy chain. Values given are mean ± S.D. from 3 independent myosin preparations.

3.8. Dimerization of myosin 9a

Paircoil2 analysis of human myosin 9a suggested that myosin 9a contains two putative coiled-coil domains in the tail domain (Figure 3.20). Coiled-coil domains are α-helical domains that form primary oligomerization units in proteins. They are characterized by the presence of heptad repeats of mainly apolar and hydrophobic residues (Burkhard et al., 2001). In order to test the propensity of the putative coiled-coil domains of myosin 9a for oligomerization, I cloned myosin 9a tail regions encompassing those fragments into a pET vector. Expression cassettes contained an N-terminal His-tag and a C-terminal CFP to facilitate purification. Proteins were expressed in *E.coli* BL21 cells and purified by His-tag affinity chromatography (Figure 3.21).

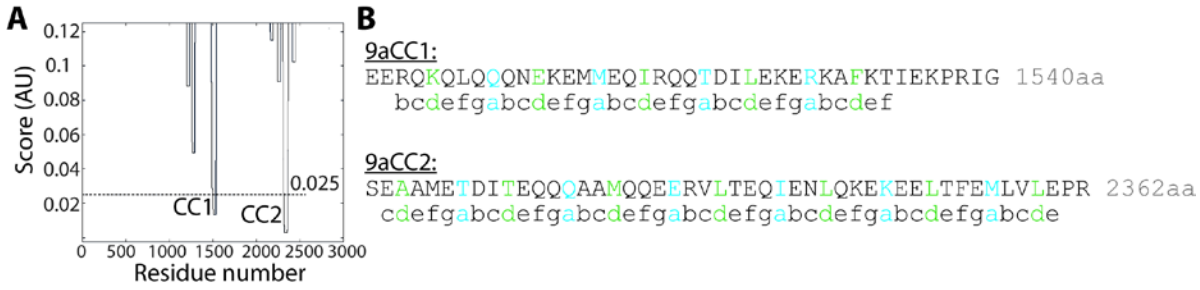

Figure 3.20. Paircoil2 analysis of human myosin 9a sequence reveals the presence of two putative coiled-coil domains in the tail. **A:** Paircoil2 analysis of the full length human myosin 9a sequence revealed the presence of two regions in the tail domain with high probability of dimer formation (0.025 probability cutoff – dashed line). **B:** sequences of the putative coiled-coil fragments are presented with individual residues assigned to particular positions within the heptad repeat of a coiled-coil with hydrophobic residues corresponding to a and d positions indicated.

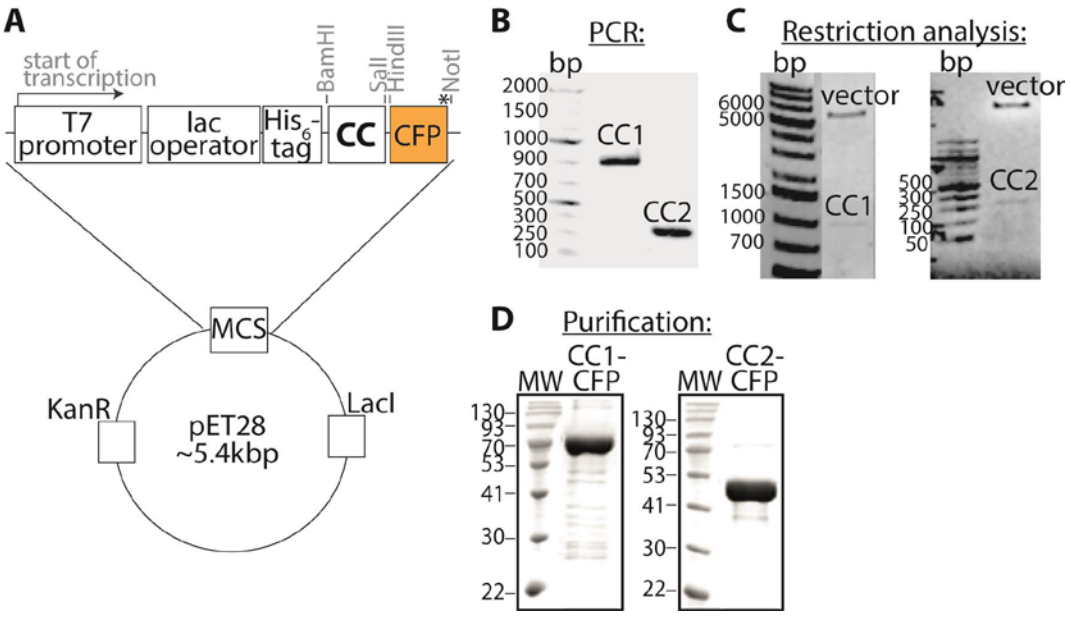

Figure 3.21. Cloning and purification of putative coiled-coil myo9a regions. **A:** a schematic drawing of an expression cassette of the pET28a+ vector with introduced myo9a tail fragment encompassing the putative coiled-coil domain (CC) upstream of CFP. An asterisk indicates a stop codon. **B:** amplification of tail fragments of myo9a encompassing the putative CC domains by PCR generated fragments of expected sizes (~900bp for CC1 and ~250bp for CC2). **C:** recombinant pET28 plasmids with the myo9a tail fragments were isolated and subjected to the restriction analysis with BamHI and SalI enzymes. Separation of the fragments on DNA gels revealed the presence of two bands in each case, corresponding to the vector backbone and tail fragments of myo9a encompassing CC1 and CC2. **D:** putative coiled-coil fragments were expressed in *E.coli* BL21 cells by means of an IPTG induction and purified by His-tag affinity chromatography.

The native molecular weight (MW) of a protein can be properly determined by Size Exclusion Chromatography (SEC) only for globular proteins. To correct for molecular shapes deviating from globular, the behavior of the molecule of interest in the gel filtration media is better related to its hydrodynamic radius (Stokes radius – R_s), rather than the MW. A sedimentation coefficient ($s_{20,\omega}$) is another hydrodynamic parameter that is a function of mass and shape of a protein. Combination of SEC and rate zonal centrifugation in linear sucrose gradients was used to determine the native molecular weight of myosin 9a constructs as described in Materials and Methods (Lister et al., 2004 and references therein). Calibration of the gel filtration column and sucrose gradient media was performed

with globular protein markers (GE Healthcare). Stokes radii and sedimentation coefficients of the protein markers were related to the separation of proteins in gel filtration and sucrose gradients, respectively (Figure 3.22).

The oligomerization state of the putative coiled-coil sequences from myo9a was studied by the combination of SEC and sucrose density gradients (Figure 3.23). Given that isolated protein domains might not represent the behavior of those domains in the context of the whole protein, different buffer conditions were tested. In case of isolated coiled-coil fragments, an increased salt concentration might lead to the stabilization of the helical structure, which in turn could facilitate coiled-coil formation *in vitro* (Mateja et al., 2006).

Indeed, when performed in lower and higher ionic strength buffers, CC1 exhibited shift into higher molecular weights both in SEC and the sucrose gradient (Figure 3.23A and B). In contrast, the molecular weight of CC2 did not change with an increase in the ionic strength of the buffer (Figure 3.23C and D). A native molecular weight of CC1 at lower ionic strength was slightly lower than that calculated from the aa sequence. That difference might be attributed to an experimental error. Nevertheless, at higher ionic strength that MW increased ~ 2-fold. Those results indicate that when appropriate conditions are maintained, or in the context of the whole protein, the putative coiled-coil 1 (CC-1) could form dimers (Figure 3.23F). In contrast, the calculated MW of CC2 corresponded well with what is expected for a monomer, regardless of the ionic strength of the buffer. This suggests CC2 might form a stable α-helical structure that does not dimerize in solution.

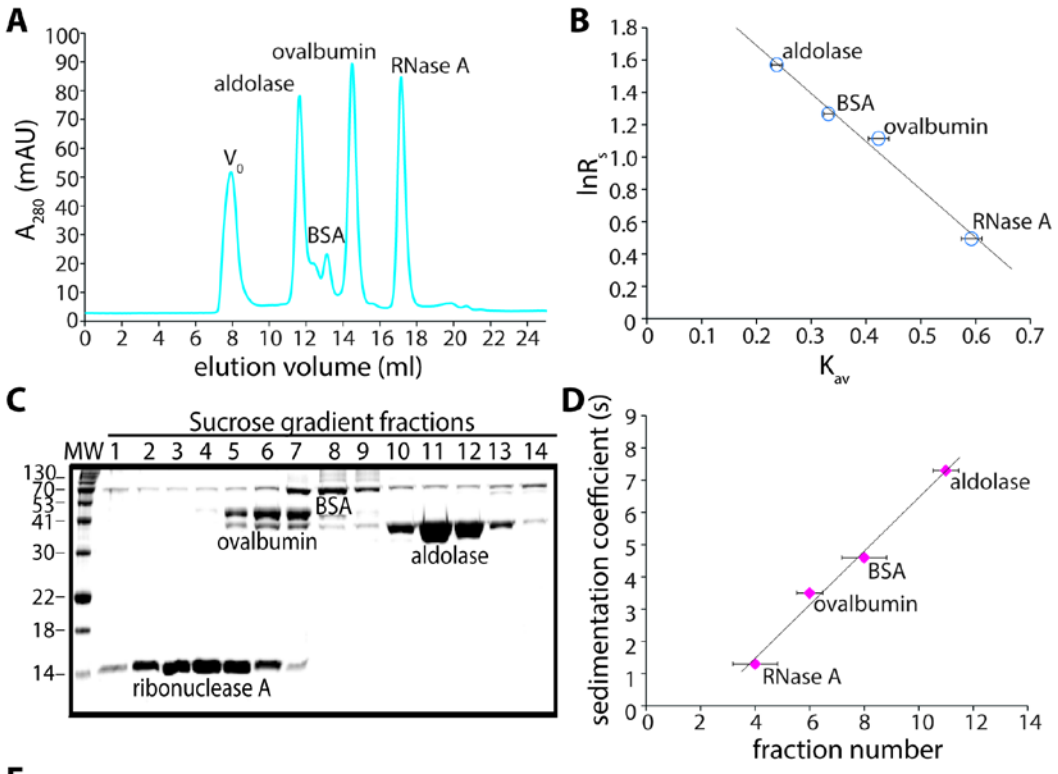

E

Protein standards	Stokes radius, R_s (nm)	Elution Vol. (ml)	Void Vol. V_0 (ml)	Partition coeff. K_{av}	lnR_s	sedimentation coefficient (s)	eluate fraction	MW from aa seq. (kDa)
RNase A	1.64	17.14	7.9	0.59	0.52	1.3	4	13.7
Ovalbumin	3.05	14.47	7.9	0.42	1.04	3.5	6	44
BSA	3.55	13.09	7.9	0.33	1.30	4.6	8	66
Aldolase	4.81	11.65	7.9	0.24	1.58	7.3	11	158

Figure 3.22. Calibration of SEC and sucrose density gradients. Globular protein markers with known hydrodynamic properties and molecular weights were separated on a Superdex gel filtration column and in 6-20% sucrose gradients. 100 µl of ~4mg/ml of aldolase, BSA, ovalbumin and Rnase A was used for calibration. **A:** a representative gel filtration trace of marker proteins separated on the Superdex 200 10/300 GL with individual peaks corresponding to the void volume (V_0), aldolase, BSA, ovalbumin and RNase A as indicated. **B:** a standard calibration curve was produced by plotting the natural logarithm of Stokes radii (lnR_s) of protein markers versus their partition coefficients (K_{av}). Data was collected from 3 independent runs of marker proteins and is presented as means±S.D. of K_{av}. **C:** a representative SDS-PAGE gel of protein markers separated in a linear 6-20% sucrose gradient. Note that aldolase is a homotetramer, composed of 36kDa subunits. **D:** a standard calibration curve of known sedimentation coefficients (s) of protein standards versus the elution fraction number. **E:** a table summarizing known and calculated parameters of protein markers.

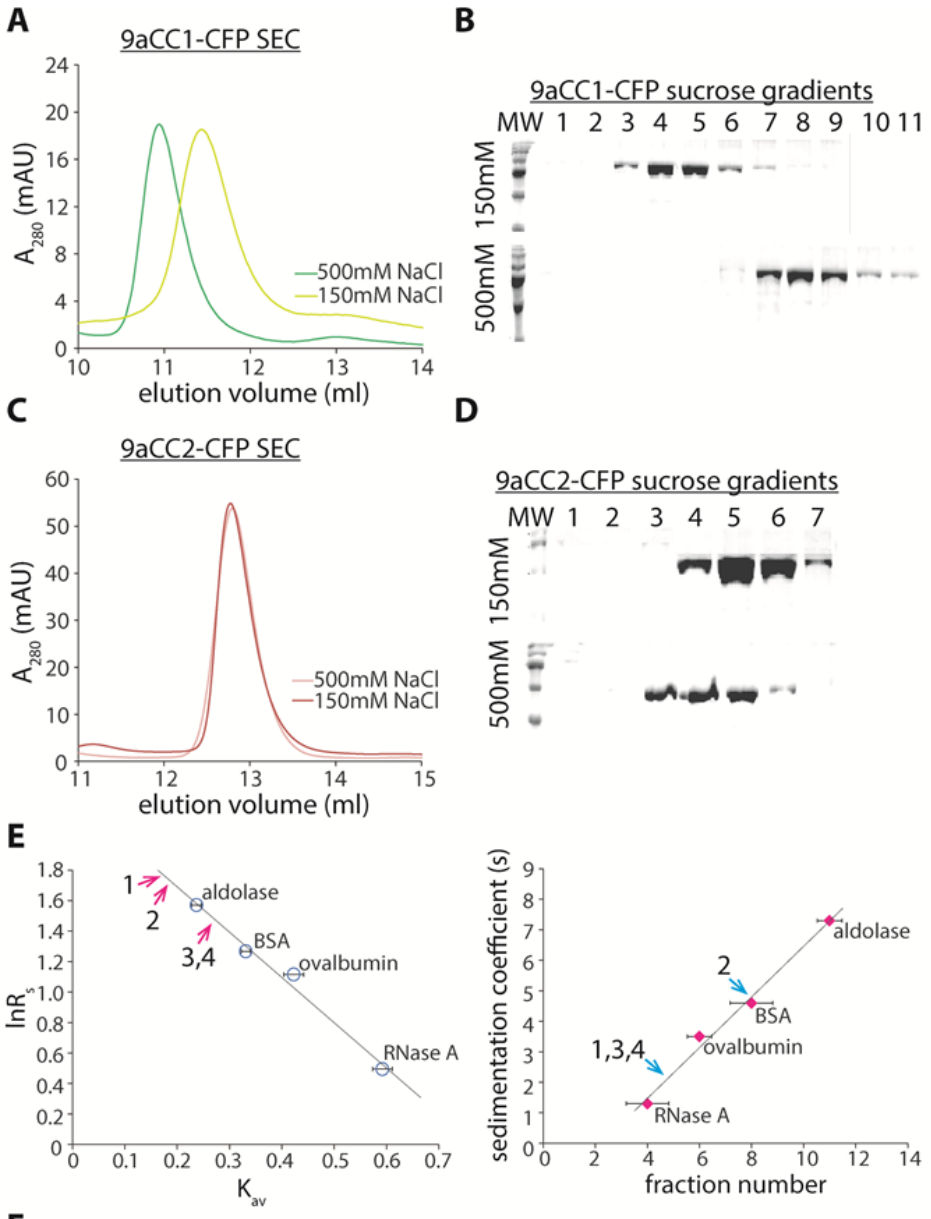

F

Protein	Stokes radius, R_s (nm)	Elution Vol. (ml)	Void Vol. V_0 (ml)	Partition coeff. K_{av}	lnR_s	sed. coeffi. (s)	eluate fraction	MW from aa seq. (kDa)	native MW (kDa)
1. 9aCC1/150	5.41	11.43	8.3	0.22	1.69	2.3	5	62.6	47.3
2. 9aCC1/500	5.88	10.96	8.3	0.18	1.77	4.8	8		107.9
3. 9aCC2/150	4.11	12.77	8.3	0.29	1.41	2.3	5	37.7	36.6
4. 9aCC2/500	4.08	12.81	8.2	0.30	1.41	2.3	5		36.3

Figure 3.23. Analysis of the oligomerization state of putative coiled-coil fragments of human myosin 9a. **A:** 100µl of 1mg/ml 9aCC1-CFP was separated on the Superdex 200 10/300 GL column in a buffer containing either 150mM (yellow) or 500mM (green) NaCl. **B:** 1mg/ml 9aCC1-CFP was separated in a linear 6-20% sucrose gradient prepared in a buffer containing either 150mM or 500mM NaCl. Eluate fractions were separated on SDS-

PAGE gels and are indicated. Note the shift of 9aCC1-CFP into a higher molecular weight at higher ionic strength. **C:** 100µl of 1mg/ml 9aCC2-CFP was separated on the Superdex 200 10/300 GL column in a buffer containing either 150mM (red) or 500mM (pink) NaCl. **D:** 1mg/ml 9aCC2-CFP was separated in a linear 6-20% sucrose gradient prepared in a buffer containing either 150mM or 500mM NaCl. Eluate fractions were separated on SDS-PAGE gels and are indicated. There was no shift in the molecular weight of 9aCC2-CFP between two buffers. **E:** an interpolation of CC1 and CC2 parameters obtained by SEC and sucrose gradients to the standard calibration curves. Numbers assigned to each arrow correspond to CC1 and CC2 at different ionic strengths, as described in (F). **F:** a table summarizing CC1 and CC2 hydrodynamic properties. Calculated native molecular weights of both fragments are highlighted. Note that for CC1 there was a ~2-fold increase in the molecular weight at higher ionic strength indicating that this putative coiled-coil sequence might dimerize. Furthermore, the calculated native molecular weight of CC1 at 150mM NaCl was somewhat lower than that expected from the aa sequence. That difference can be assigned to an experimental error and might suggest the protein shape deviates strongly from globular in solution. In contrast, the calculated native molecular weight of CC2 was not affected by the ionic strength of the buffer and was in a very good agreement with the expected MW obtained from aa sequence, indicating the protein adopts globular shape in solution and does not form dimers at conditions tested.

CHAPTER 4: INTERACTION OF MYOSIN 9A MINIMAL MOTOR DOMAIN WITH ACTIN AND STEADY-STATE ATPASE ACTIVITY OF HUMAN MYOSIN 9A

4.1. Human myosin 9a bundles actin

Previous reports suggest that the extended loop 2 insert of myosin class 9 members might act as an additional actin-binding site. This implies myosin 9 could crosslink actin filaments (Struchholz et al., 2009).

To test the possibility of actin crosslinking by myosin 9a, mixtures containing increasing 9aMMD:F-actin ratios were subjected to a low-speed centrifugation (15000 x g). At such low speed, single polymerized actin filaments remain in solution. On the other hand, the total native molecular weight of bundled actin filaments would be high enough to cause their sedimentation. Following the centrifugation, the equal amounts of supernatant and pellet were separated on SDS-PAGE gels (Figure 4.1). As expected, in the absence of 9aMMD in the solution most actin remained in the supernatant. However, the amount of actin in the pellet increased in the presence of increasing 9aMMD concentrations. Finally, at a critical 9aMMD concentration, essentially all actin was pelleted in the presence of high molar ratios of myosin 9a, as compared to a control sample that did not contain myosin 9a. An increase in the amount of pelleted actin at such low centrifugation speed is consistent with an increase in the molecular weight, which could be achieved via the crosslinking of actin filaments. These results suggest that myosin 9a bundles actin filaments, causing sedimentation of F-actin under conditions when most actin would remain in the solution. The minimal motor domain if enough to cause crosslinking of actin filaments.

In order to directly visualize bundling of actin filaments by myosin 9a, mixtures of actin and 9aMMD were applied to carbon grids, negatively stained and visualized by electron microscopy (in collaboration with Dr. Neil Billington, NHLBI, NIH and Dario Saczko-Brack, LMU). In the absence of ATP, 9aMMD crosslinked actin filaments, forming clearly visible ladder-like patterns (Figure 4.2A). Individual crosslinks were separated by 36nm, corresponding to the helical repeat of an actin filament (Walker et al., 2000; Egelman, 2010). Those actin structures were visible as soon as 5 minutes after an incubation of myosin with actin. Even at excess myosin in the sample and extended incubation times, no decoration of individual actin filaments by myosin 9a was observed. Also at shorter incubation times (up to 1min), no binding of myosin to actin was seen. Upon introduction of ATP to the sample, all myosin dissociated from filaments (Figure 4.2B). This is a direct evidence that human myosin 9a binds actin in an ATP-sensitive manner. This is also the first direct visualization of actin bundling by a myosin class 9 member.

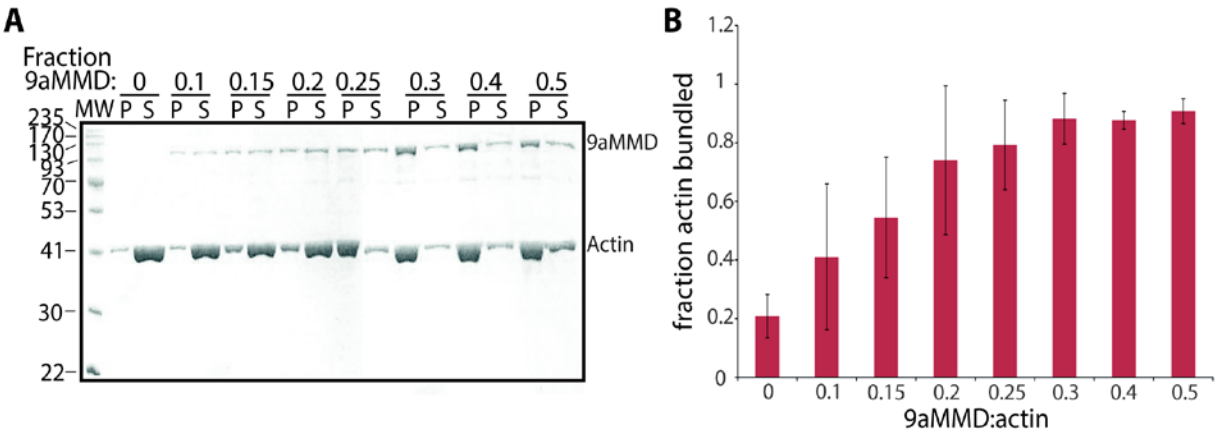

Figure 4.1. 9aMMD bundles F-actin. **A:** 2µM phalloidin-stabilized F-actin was incubated with increasing 9aMMD concentrations (0 - 1 µM) for 20min, RT, and centrifuged at 15000 x g. Equal amounts of supernatant and pellet were separated on an SDS-PAGE gel and band intensities were measured. **B:** quantification of the amount of actin present in the pellet at increasing 9aMMD concentrations. In the absence of 9aMMD, around 20% of all actin present in the sample was found in the pellet following the low speed centrifugation. With the increasing amount of 9aMMD, the amount of actin in the pellet increased, until a critical 9aMMD concentration was reached at which nearly all actin was found in the pellet. Experiments were performed with three independent myosin preparations (n = 3) and bars represent mean values ± S.D.

Results presented in this section indicate that human myosin 9a might act as a molecular motor that cross-links actin filaments in an ATP-dependent manner. An additional actin-binding site resulting in the formation of cross-links is localized within the minimal motor domain of human myosin 9a.

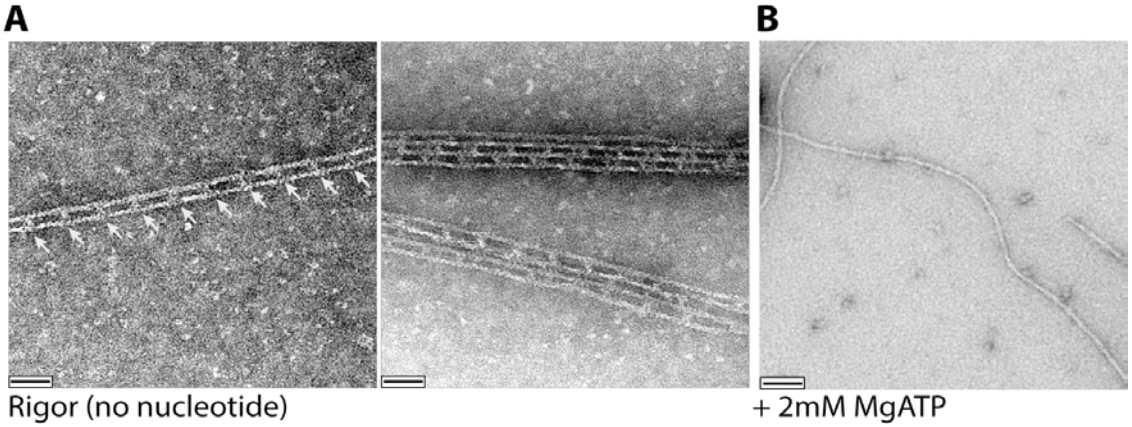

Figure 4.2. Negatively stained images of 9aMMD interacting with actin. **A:** 9aMMD crosslinked actin filaments in the absence of a nucleotide. Even at high myosin:actin ratios no decoration of single filaments was observed. 9aMMD molecules bound actin filaments in a very regular manner, with distances between individual crosslinks corresponding to the length of the helical actin repeat (36nm; white arrows). **B:** upon addition of ATP all myosin dissociated from actin filaments. Scale bars: 40nm.

4.2. Steady-state kinetics of human myosin 9a in the absence of calcium

The actomyosin ATPase cycle is conserved within the myosin superfamily in that ATP binding to myosin causes the dissociation of myosin from actin, followed by ATP hydrolysis by myosin, rebinding of myosin to actin and the release of hydrolysis products associated with strengthening of the actomyosin interaction (De La Cruz and Ostap, 2004). The basal rate of ATP hydrolysis by myosin is stimulated by actin, following the Michaelis-Menten steady-state kinetics. The ATPase rate at increasing [actin] can be measured by means of an NADH enzyme-linked assay (Figure 4.3).

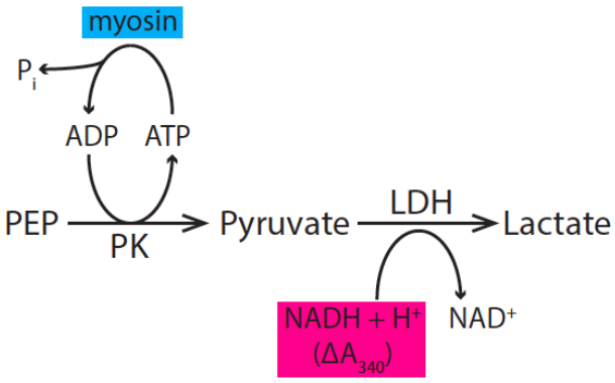

Figure 4.3. A schematic drawing of an NADH enzyme-linked assay reaction. NADH is oxidized to NAD^+ in a series of reactions coupled to ATP hydrolysis such that one molecule of oxidized NADH is equal to one molecule of ATP hydrolyzed by myosin. The assay is performed in the presence of an ATP regenerating system; pyruvate kinase (PK) converts phosphoenolpyruvate (PEP) to pyruvate in a reaction that uses ADP from the myosin ATPase cycle and regenerates it to ATP; subsequently, pyruvate is converted into lactate in a reaction catalyzed by lactate dehydrogenase (LDH) coupled to oxidation of NADH. NADH, but not NAD^+, absrobs light at 340nm and thus the ATPase rate of myosin can be obtained from the rate of the decrease in NADH absorbance (De La Cruz and Ostap, 2009). The myosin ATPase rate at increasing actin concentration follows the Michaelis-Menten kinetics. By fitting the data to the equation 4 (Materials and Methods), the maximal activation rate of myosin (V_{max}) at saturating [actin] and an actin concentration necessary for the half maximal myosin activation (K_m) can be determined. V_0 is the basal myosin ATPase rate in the absence of actin.

To ensure that none of the buffer components used for the assay interfered with myosin activity, I first performed control experiments with rabbit skeletal muscle myosin HMM in the ATPase buffer used for myosin 9a, containing 10mM MOPS pH 7.3, 50mM KCl, 0.1mM EGTA, 1mM $MgCl_2$ and 1mM DTT. It is well established that this protein behaves as a *bona fide* myosin with its basal ATPase rate stimulated ~100 times by actin and with K_m = 18μM (Millar and Geeves, 1983). In conditions used here and at 22^0C, the basal ATPase rate of rabbit skeletal HMM was stimulated ~100-fold from V_0=0.06 s^{-1} to V_{max}=7.5 s^{-1} and K_m = 15μM (Figure 4.4 and Table 4.1). This is in good agreement with previously reported values of K_m (Millar and Geeves, 1983) and V_{max} of 7.8 s^{-1} (Webb and Corrie, 2001). Thus, the buffer chosen for the assay was compatible with myosin activity.

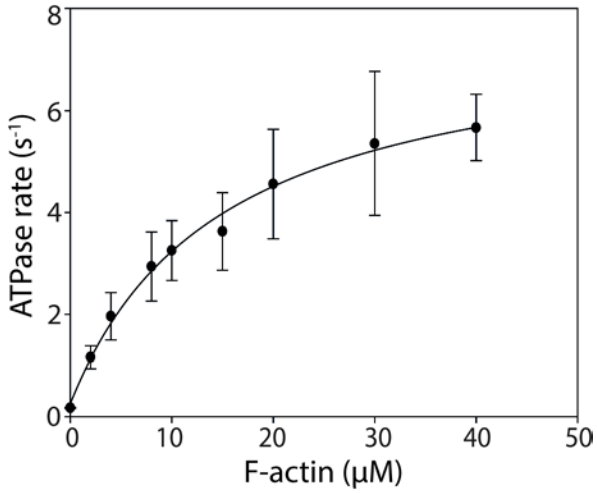

Figure 4.4. An actin-activated ATPase activity of rabbit skeletal muscle myosin HMM. The ATPase rate of 50nM myosin in the ATPase buffer supplemented with 2mM ATP, 0.2mM NADH and an ATP-regenerating system (1mM PEP, 18U/ml LDH, 12U/ml PK) was measured in the absence and presence of an increasing actin concentration (0 - 40μM F-actin, phalloidin-stabilized) by following the decrease in the NADH absorbance at 340nm over at least 10min time period at 22^0C. V_0 = 0.06 ± 0.05 s^{-1}, V_{max} = 7.5 ± 0.4 s^{-1} and K_m = 15 ± 3.2μM at 22^0C were obtained by fitting the data points to Michaelis-Menten kinetics. Data points represent an average from three independent measurements ± S.D. (n = 3).

Having confirmed the correct buffer composition, I measured the ATPase rates of GFP-9a-Head and GFP-9a-S1 at increasing [actin]. Previous reports on the actin-activated ATPase activity of myosin 9 orthologs state that low actin concentrations (up to 20μM) are enough to reach the maximum ATPase activation (Liao et al., 2010). Previously, *C. elegans* myo9 head revealed a10-fold activation by actin, whereas the head-neck construct showed only minor activation by actin in the absence of calcium. The head domain exhibited high basal ATPase rate (~0.5 s^{-1}) that decreased to 0.13 s^{-1} in the head-neck construct (Liao et al., 2010). Minor actin-activation (from 1.18 s^{-1} to 1.58 s^{-1}) was also reported for rat myo9b truncation encompassing the head and neck domains, whereas full length rat myo9b was activated 10-fold by actin. The basal ATPase rate of full length rat myo9b was also 10-fold lower than that of the head-neck construct, suggesting the tail domain of myosin 9 might stimulate the actin-activation of the ATPase rate (Struchholz et al., 2009). Based on the available reports, it is difficult to see any prominent pattern of an enzymatic activity within

the myosin class 9. Several features of the ATPase activity of human myosin 9a could be expected based on previous reports on other myosin 9 isoforms: i) a high basal ATPase rate, ii) an activation of the basal ATPase rate of the head domain by actin, iii) an inhibition of the actin-activation by the neck region, iv) the lack of activation of the ATPase rate by actin in the absence of the tail domain.

100 - 200nM GFP-9a-Head or GFP-9a-S1 was used to measure ATPase rates at increasing actin concentrations (0 - 20μM) as described above. The actin-dependence of the ATPase rate of GFP-9a-Head and GFP-9a-S1 is presented in Figure 4.5 (A and B, respectively). Both constructs showed similar, low basal ATPase rates ($0.17 \pm 0.014\ s^{-1}$ for GFP-9a-Head and $0.18 \pm 0.016\ s^{-1}$ for GFP-9a-S1) indicating that the neck region does not affect the catalytic activity of human myosin 9a. Furthermore, the basal ATPase rate of neither GFP-9a-Head nor GFP-9a-S1 was stimulated by actin. This is surprising given that all catalytically active myosins characterized so far display actin-activated ATPase activities. Nevertheless, this result shows that human myosin 9a is enzymatically active and able to hydrolyze ATP.

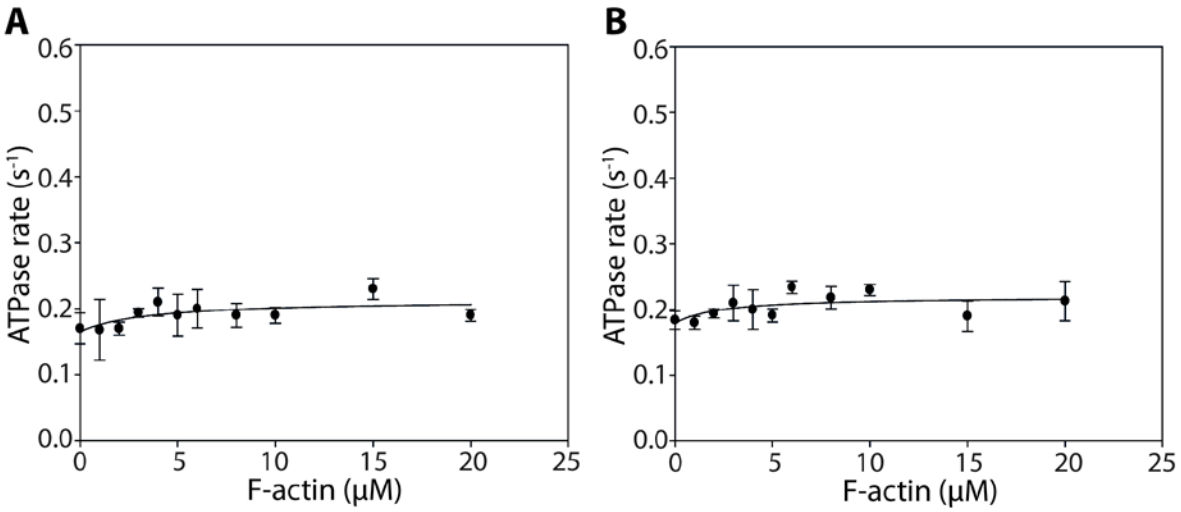

Figure 4.5. An actin-dependent ATPase rate of GFP-9a-Head **(A)** and GFP-9a-S1 **(B)**. 100 - 200nM myosin was used to measure the rate of ATP hydrolysis in the buffer supplemented with 2mM highly pure ATP and an ATP-regenerating system in the absence and presence of phalloidin-stabilized F-actin (0 - 20μM). Basal ATPase rates (V_0) were 0.17 ± 0.014 s^{-1} for GFP-9a-Head and 0.18 ± 0.016 s^{-1} for GFP-9a-S1 and no actin-activation was observed for either construct. Measurements were performed at 22^0C and NADH absorbance was followed at 340nm for at least 10min. Each data point represents an average from 3 independent measurements from separate myosin preparations ± S.D. (n = 3).

Even though not reported previously for other myosin 9 isoforms, it is interesting to speculate that the N-terminal extension of myosin 9 head could regulate the actin-activated ATPase activity of human myosin 9a. Therefore, I investigated the actin-dependent ATPase activity of minimal motor domain constructs, truncated after the ~150aa long N-terminal extension (Figure 4.6). 9aMMD and 9aMMD-S1 contain the minimal sequence of a myosin head domain required for its enzymatic and mechanical activity; 9aMMD-S1 additionally encompasses the neck region of the native myosin 9a sequence. Both constructs exhibited the same basal ATPase rate (V_0 = 0.12 ± 0.01 s^{-1} for 9aMMD and V_0 = 0.13 ± 0.02s^{-1} for 9aMMD-S1) that did not differ significantly from those obtained for constructs containing the N-terminal extension. Actin did not further stimulate the basal ATPase rate of minimal motor domain constructs. Therefore, the N-terminal extension of human myosin 9a does not influence its enzymatic properties. Since there was no difference in the actin-dependent

ATPase activity of all human myo9a constructs developed, following experiments focused on 9aMMD.

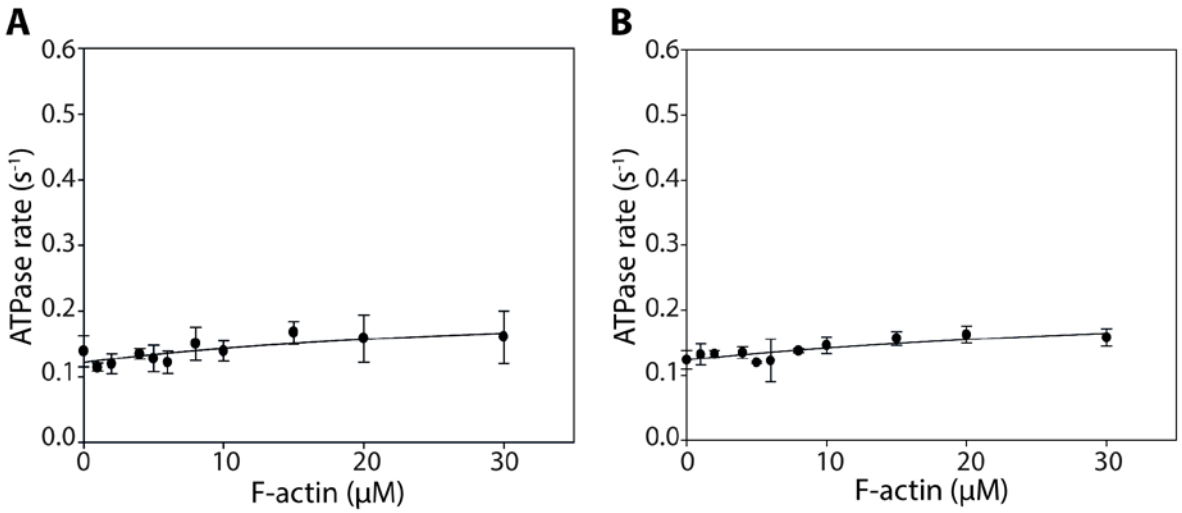

Figure 4.6. An actin-dependent ATPase rate of 9aMMD **(A)** and 9aMMD-S1 **(B)**. 100 - 200nM myosin was used to measure the rate of ATP hydrolysis in the buffer supplemented with 2mM highly pure ATP and an ATP-regenerating system in the absence and presence of phalloidin-stabilized F-actin (0 - 30μM). Basal ATPase rates (V_0) were 0.12 ± 0.01 s^{-1} for 9aMMD and 0.13 ± 0.02 s^{-1} for 9aMMD-S1 and no actin-activation was observed for either protein. Measurements were performed at 22^0C and NADH absorbance was followed at 340nm for at least 10min. Each data point represents an average of 3 independent measurements from separate myosin preparations ± S.D. (n = 3).

Previously, the actin-activated ATPase activity of *Acanthamoeba* myo1, a motor which also crosslinks actin filaments, was shown to be dependent on the myosin:actin ratio. It was proposed that the enzymatic activity of myo1 could only be observed at myosin concentrations that enabled cooperative actin binding (Albanesi et al., 1985). Therefore, I investigated the function of an actin-activated ATPase activity of 9aMMD on the myosin concentration (Figure 4.7). 235 - 70nM 9aMMD was used to measure the ATP hydrolysis rates in the absence and presence of F-actin stabilized with phalloidin (0 - 20μM). There was no effect of the 9aMMD concentration on the V_{max} and the rates at 20μM [actin] did

not differ from the basal rates at all myosin concentrations tested. Thus, the enzymatic activity of human myosin 9a does not depend on the myosin:actin ratio.

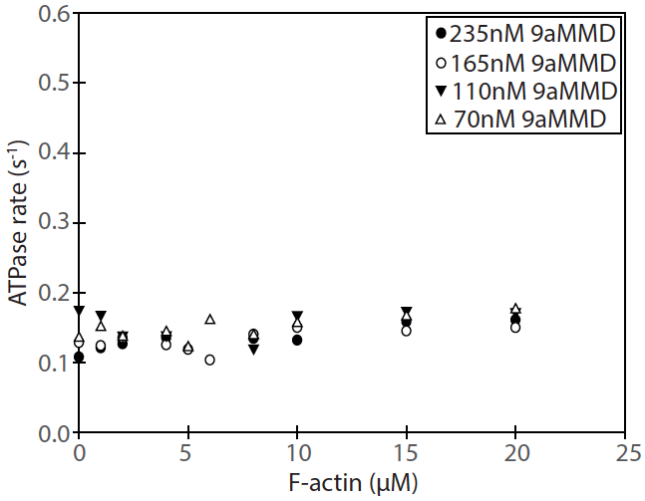

Figure 4.7. The dependence of the actin-activated ATPase rate of 9aMMD on myosin concentration. The rate of ATP hydrolysis of 235nM (black circles), 165nM (open circles), 110nM (black triangles) and 70nM (open traingles) 9aMMD was measured in the buffer supplemented with 2mM highly pure ATP and an ATP-regenerating system in the absence and presence of phalloidin-stabilized F-actin (0 - 20μM). Measurements were performed at 22^0C and NADH absorbance was followed at 340nm for at least 10min. No difference in the rate of ATP hydrolysis within the range of actin concentrations used was observed at any 9aMMD concentration.

It was shown previously that phalloidin affects protein-protein interactions between the phalloidin-stabilized actin and non-muscle myosin 2A and non-muscle myosin 2C. In both cases, the V_{max} of the actin-activated steady-state ATPase activity in the presence of phalloidin-stabilized F-actin was decreased 3-4-fold as compared to phalloidin-free F-actin (Diensthuber et al., 2011). The effect of phalloidin-decorated versus phalloidin-free F-actin on an actin-dependent ATPase activity of 9aMMD is shown in Figure 4.8. Phalloidin does not influence maximal ATPase activity of human myosin 9a.

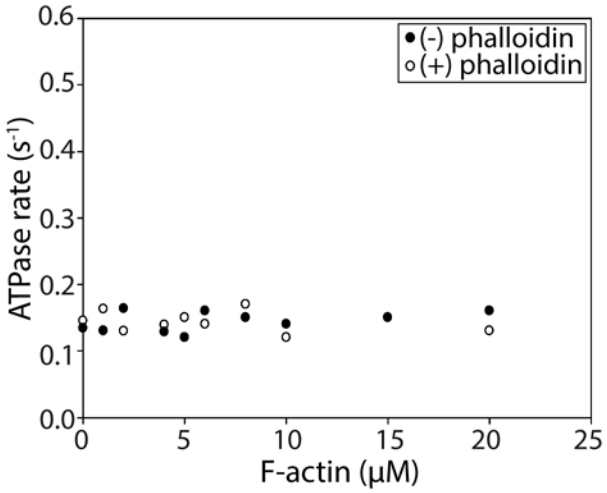

Figure 4.8. The effect of phalloidin stabilization of F-actin on the maximal ATPase activity of 9aMMD. The ATPase rate of 150nM 9aMMD was measured in the buffer supplemented with highly pure ATP and an ATP-regenerating system in the presence of 0 - 20μM phalloidin-stabilized F-actin (open circles) or phalloidin-free F-actin (black circles). Measurements were performed at 22^0C and NADH absorbance was followed at 340nm for at least 10min. There was no difference in the maximum steady-state ATPase activity (V_{max}) of 9aMMD in either sample. Therefore, phalloidin does not influence the ATPase activity of human myosin 9a.

It was shown before that ionic strength has a profound effect on the V_{max} of mouse brain myosin 5 S1 and HMM constructs (Wang et al., 2000). I tested the effect of the ionic strength of the buffer on the actin-dependent steady-state ATPase activity of human myosin 9a (Figure 4.9). Here as well, no change in the V_{max} was observed. Therefore, the lack of the stimulation of the basal ATPase rate of human myo9a by actin does not depend on the ionic strength.

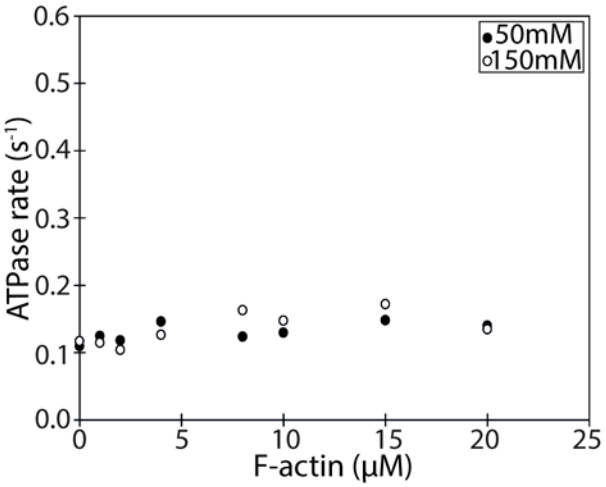

Figure 4.9. The dependence of the maximal ATPase activity of 9aMMD on the ionic strength of the buffer. The ATPase rate of 150nM 9aMMD was measured in a buffer supplemented with highly pure ATP and an ATP-regenerating system in the presence of 0 - 20μM phalloidin-stabilized F-actin. Buffers contained 50mM (black circles) or 150mM (open circles) KCl. Measurements were performed at 22^0C and NADH absorbance was followed at 340nm for at least 10min. There was no difference in the maximum steady-state ATPase activity (V_{max}) of 9aMMD in either sample. Therefore, the ionic strength of the buffer does not influence the maximum steady-state ATPase activity of human myo9a.

Finally, the maximal actin-activated steady-state ATPase activity of mouse brain myosin 5 S1 was increased in the presence of exogenous calmodulin supplemented in the buffer, probably reflecting extra calmodulin molecules saturating IQ motifs in the neck region of the myosin (Wang et al., 2000). On the other hand, the length and net charge of loop 2 (the primary actin interaction site of myosins) was shown to influence the ATPase rate of myosins, probably by regulating their interactions with actin (Bobkov et al., 1996). The loop 2 of myosin 9 is extended and was proposed to bind calmodulin (Liao et al., 2010). It is plausible the binding affinity of calmodulin to loop 2 of myosin 9 could affect its interaction with actin. Since an isomerization of the weak actin binding state after ATP hydrolysis to the strong actin binding state was proposed to be essential for the acceleration of the release of hydrolysis products (Holmes et al., 2003), it is plausible that a specific binding mode of calmodulin to myosin 9a loop 2 is necessary for the actin stimulation of ADP release.

First, I added extra calmodulin to ATPase reactions of 9aMMD at saturating [actin]. No change in the ATPase rate was observed even in the presence of 1mM exogenous CaM (Figure 4.10). Therefore, the lack of the actin stimulation of the basal ATPase rate of 9aMMD caused by the weak association of calmodulin in the absence of calcium with the motor domain can be excluded.

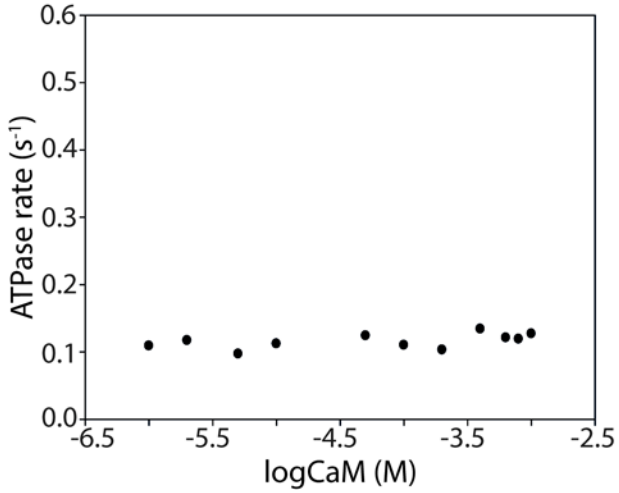

Figure 4.10. The dependence of the maximal actin-activated ATPase activity of 9aMMD on exogenous calmodulin. The ATPase rate of 300nM 9aMMD was measured in the buffer containing 2mM ATP, an ATP-regenerating system and 30μM phalloidin-stabilized F-actin. The buffer was supplemented with exogenous calmodulin (1μM - 1mM) and absorbance of NADH was followed at 340nm for at least 10min. Data was plotted as a function of the maximal ATPase rate (s^{-1}) on calmodulin concentration presented as logCaM in the presence of a saturating actin concentration. Supplementing the buffer with as much as 1mM exogenous calmodulin does not influence the V_{max} of human myosin 9a.

In summary, the minimal motor domain of human myosin 9a is enzymatically active, but its basal ATPase rate is not stimulated by actin. Neither the N-terminal extension nor the neck domain of human myo9a regulate an actin-dependent ATPase activity of human myosin 9a. It was shown previously that the basal ATPase activity of full length rat myo9b was activated 10-fold by actin (Nalavadi et al., 2005). Therefore, it would be interesting to examine the steady-state ATPase activity of the full length human myo9a to address the possible role of the tail domain in regulating the ATPase activity of the myosin in the presence of actin.

4.3. Steady-state kinetics of human myosin 9a in the presence of calcium

Binding of Ca^{2+} ions to calmodulin can regulate the affinity and association of CaM with its target binding site (Manceva et al., 2007; Bayley et al., 1996). It is interesting to speculate that Ca^{2+} binding to the CaM light chain in the head domain of human myosin 9a could affect its interactions with actin in the presence of a nucleotide and regulate its actin-activated ATPase activity. I assessed the effect of Ca^{2+} on the actin-activated ATPase activity of 9aMMD. 9aMMD was not actin-activated in the absence of Ca^{2+}; however, in the presence of 100μM free Ca^{2+} (pCa 4), the basal ATP hydrolysis rate was stimulated ~3-fold by actin (Figure 4.11) from $V_0 = 0.13 \pm 0.02\ s^{-1}$ to $V_{max} = 0.49 \pm 0.03\ s^{-1}$. Data was collected from 3 independent 9aMMD preparations and 100 - 200nM 9aMMD was used for measurements. F-actin concentration necessary to reach the half maximal activation was $K_m = 2 \pm 1.3$μM which indicates high actin affinity of 9aMMD in a weak actin binding state (in the presence of ATP or ADP.Pi). That data indicates that in the presence of Ca^{2+}, the actin- and nucleotide-binding sites of 9aMMD become coupled (they regulate each other in a reciprocal way).

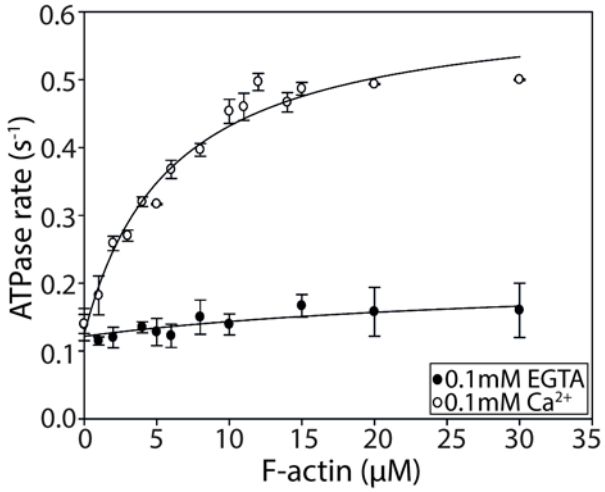

Figure 4.11. Ca^{2+} induces actin-activation of the steady-state ATPase activity of 9aMMD. The rate of ATP hydrolysis of human myosin 9a was measured in the presence of 100 - 200nM 9aMMD in a buffer supplemented with 2mM highly pure ATP, an ATP-regenerating system, 0 - 30μM phalloidin-stabilized F-actin and 0.1mM free Ca^{2+} (open circles). NADH absorbance was measured at 340nm for at least 10min at 22^0C and three independent 9aMMD preparations were used to collect the data. Data points were fitted to

Michaelis-Menten kinetics, with $V_0 = 0.13 \pm 0.02\ s^{-1}$, $V_{max} = 0.49 \pm 0.03\ s^{-1}$ and $K_m = 2 \pm 1.3\mu M$. Data points represent the mean value from three independent measurements ± S.D. (n = 3). Data obtained in the absence of Ca^{2+} (closed circles) was explained earlier in the text and is shown on the plot as a reference.

The ATPase activity of human myosin 9a at 22^0C in the absence and presence of phalloidin-stabilized F-actin is summarized in Table 4.1. For comparison, experimental data obtained for rabbit skeletal muscle myosin HMM is also included.

Table 4.1. The steady-state ATPase activity of human myosin 9a.

Parameter	**rabbit skeletal HMM**	**GFP-9a-Head/EGTA**	**GFP-9a-S1/EGTA**
V_0 (s^{-1})	0.06 ± 0.05	0.17 ± 0.014	0.18 ± 0.016
V_{max} (s^{-1})	7.5 ± 0.4	ND	ND
K_m (μM)	15 ± 3.2	ND	ND
Parameter	**9aMMD/EGTA**	**9aMMD/0.1mM Ca^{2+}**	**9aMMD-S1/EGTA**
V_0 (s^{-1})	0.12 ± 0.008	0.13 ± 0.02	0.13 ± 0.02
V_{max} (s^{-1})	ND	0.49 ± 0.03	ND
K_m (μM)	ND	2 ± 1.3	ND

Ca^{2+} could induce the actin-activation of the steady-state ATPase of 9aMMD by causing the dissociation of CaM from the motor domain. Such mechanism of the regulation of the ATPase activity of myosin has been proposed for several different myosin isoforms, whereby Ca^{2+}-induced dissociation of CaM from the neck domain activated the actin stimulation of the ATPase rate (Krementsov et al., 2004). I investigated the association of CaM with 9aMMD at increasing [Ca^{2+}] by incubating 0.8μM 9aMMD with 20μM phalloidin-stabilized F-actin for 20min at RT, followed by a high-speed centrifugation. Equal volumes of supernatant and pellet were separated on a 15% SDS-PAGE gel to assess the presence of CaM in either the supernatant or pellet (Figure 4.12). Variations in the amount of $CaCl_2$ present in the buffer included the lack of Ca^{2+} (EGTA) and presence of 10

- 1000μM free Ca^{2+}. Simultaneously, in order to exclude the possibility of CaM pelleting by itself or binding to actin on its own, a control containing 1μM exogenous CaM was mixed with 20μM actin and treated the same way. As indicated in Figure 4.12, CaM was present in pellet fractions containing 9aMMD at all $CaCl_2$ concentrations, even as high as 1mM. In a control that did not contain any myosin, CaM was found in the supernatant fraction, confirming that CaM did not pellet on its own and did not bind actin (right gel). Therefore, CaM present in pellet fractions (left gel) represents a myosin-bound CaM fraction. That data suggests that the actin-activation of the steady-state ATPase activity of 9aMMD in the presence of Ca^{2+} cannot be attributed to a simple dissociation event of CaM from myo9a head upon addition of $CaCl_2$.

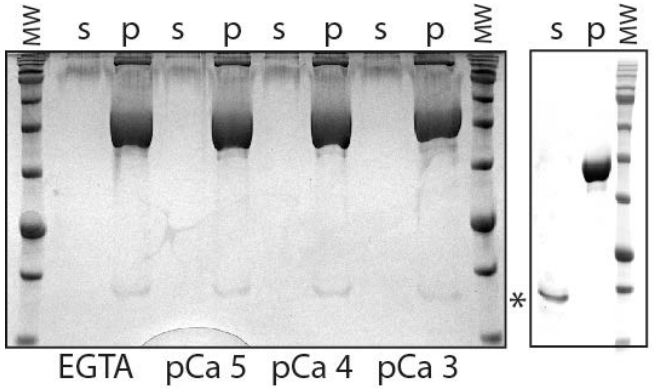

Figure 4.12. The effect of Ca^{2+} on binding of CaM to the head domain of human myosin 9a. 0.8μM 9aMMD was mixed with 20μM phalloidin-stabilized F-actin in the absence (EGTA) and presence of 10, 100 and 1000μM free Ca^{2+} (pCa 4 - 5) in the buffer containing 0.1mM EGTA and 100mM KCl. In a separate sample, 1μM exogenous CaM was mixed with 20μM phalloidin-stabilized F-actin in the same buffer in the absence of $CaCl_2$. Samples were incubated for 20min at RT, followed by 20min, 100000rpm, 4^0C centrifugation. Supernatant was collected and pellets were resuspended in the same volume of PBS. Equal volumes of supernatant and pellet were separated on a 15% SDS-PAGE gel and stained with Commassie-Blue to confirm the presence of CaM in either supernatant or pellet at increasing [Ca^{2+}]. The experiment was performed with three independent 9aMMD preparations and a representative SDS-PAGE gel is shown. As depicted on the left gel, CaM (indicated by asterisk) was always found in the pellet fractions with myosin, even at 1mM Ca^{2+} (pCa 3). A negative control containing only CaM and actin (right gel) was treated the same way and free CaM (asterisk) was found in the supernatant, confirming CaM did not pellet on its own or bind to actin. Therefore, all CaM found in samples containing myosin was 9aMMD-associated and Ca^{2+} did not induce dissociation of CaM from 9aMMD. M - myosin, A - actin, s - supernatant, p - pellet.

4.4. Interaction of human myosin 9a with actin in different nucleotide states

9aMMD is enzymatically active (it hydrolyzes ATP), but its basal ATPase rate was stimulated by actin only in the presence of Ca^{2+}. It raised a possibility that in the absence of Ca^{2+} 9aMMD would not bind actin in the presence of ATP, which would explain the lack of the actin-activated steady-state ATPase. Upon addition of Ca^{2+}, the head-bound CaM did not dissociate from loop 2, but instead Ca^{2+} could induce a conformational change in CaM molecule which in turn could regulate binding of myosin to actin in the presence of ATP by inducing a structural rearrangement of loop 2 of myo9a that would facilitate actin binding.

Binding of myosin 9a to actin in different nucleotide states was addressed by an actin spindown assay in the absence and presence of 2mM MgATP or 2mM MgADP (Figure 4.13A-C). 0.8 - 1μM 9aMMD was incubated with increasing amounts of phalloidin-stabilized F-actin (0 - 15μM) in the presence or absence of nucleotides. To investigate the rigor binding state, apyrase was used to fully deplete the solution from any nucleotides present. Samples were incubated in the buffer containing 100mM KCl and 0.1mM EGTA (unless otherwise stated; see below) for 30min on ice, followed by a high-speed centrifugation (20min, 100000rpm, 4^0C). Supernatant was collected and pellet was resuspended in an equal volume of PBS. Equal amounts of supernatant and pellet were separated on SDS-PAGE gels. Band density was measured and the amount of 9aMMD present in the pellet was plotted against F-actin concentration (Figure 4.13D). In the presence of the nucleotide some 9aMMD always pelleted on its own (in the absence of F-actin). In those cases the amount pelleted in the presence of actin was corrected by the amount that pelleted on its own. Data points were fitted to a quadratic equation and dissociation constants (K_d) in each nucleotide state were determined to be 425 ± 21.1nM in rigor (in the absence of the nucleotide), 810 ± 93nM in the presence of ATP and 590 ± 89nM in the presence of ADP. Taken together, 9aMMD binds actin with high affinity (nanomolar range) in all nucleotide states. The highest affinity exhibited in the absence of the nucleotide decreased 2-fold in the presence of ATP. The binding affinity in the ADP state was between the rigor and the ATP-state affinity. The binding of 9aMMD to actin in the absence of the nucleotide reached full saturation at higher actin concentrations (F_{max} = 100%), but only F_{max} = 62 ± 3.2% and F_{max} = 71 ± 2% of 9aMMD bound at saturating [F-

actin] in the presence of ATP and ADP, respectively. Therefore, human myosin 9a binds actin in a nucleotide-sensitive manner. Binding parameters are summarized in Table 4.2.

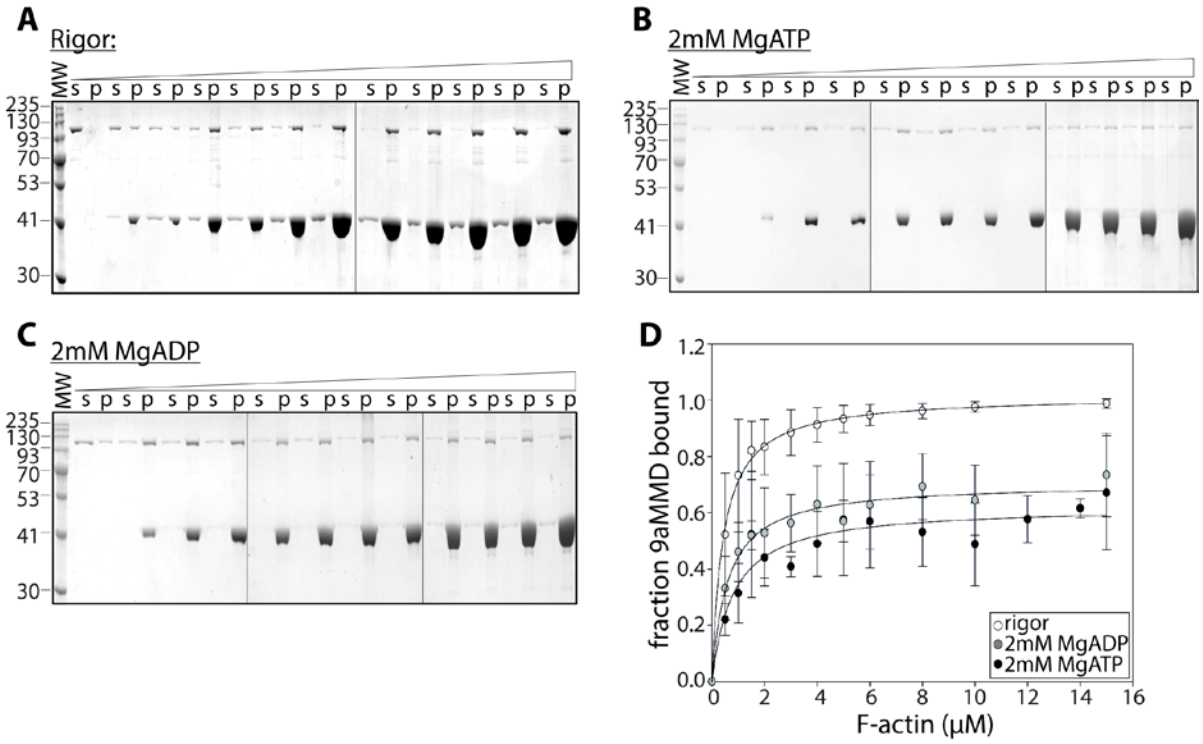

Figure 4.13. Binding of 9aMMD to actin in different nucleotide states. 0.8 - 1μM 9aMMD was incubated with increasing amounts of phalloidin-stabilized F-actin (0 - 15μM) in the absence **(A)** or presence of 2mM MgATP **(B)** or 2mM MgADP **(C)**. Samples were incubated for 20min on ice in the buffer containing 10mM MOPS, 0.1mM KCl, 1mM DTT, 0.1mM EGTA and 4mM $MgCl_2$. Following centrifugation 20min, 100000rpm, 4^0C, supernatants were collected and pellets were resuspended in an equal volume of PBS. The equal volumes of supernatant and pellet were separated on 10% SDS-PAGE gels and stained with Commassie-Blue. Band densities of 9aMMD in the supernatant (s) and pellet (p) were measured at each actin concentration and the fraction of 9aMMD bound was plotted against [F-actin] **(D)**. In the presence of nucleotides a fraction of 9aMMD pelleted by itself and the fraction bound to actin was corrected by the amount of 9aMMD pelleted on its own. Dissociation constants (K_d) were obtained by fitting the data to a hyperbola and obtained values were: K_d = 425 ± 21.1nM in rigor (open circles), K_d = 810 ± 93nM in the presence of ATP (black circles) and K_d = 590 ± 89nM in the presence of ADP (gray circles). 9aMMD binding saturated at 100% in the absence of a nucleotide (rigor) but in the presence of a nucleotide, binding of 9aMMD to actin plateaued at 62 ± 3.2% with ATP and 71 ± 2% with ADP. Data points were collected from three independent 9aMMD preparations and are represented as mean values ± S.D. (n = 3).

The apparent substoichiometric binding of 9aMMD in the presence (but not in the absence) of nucleotides could indicate that a fraction of 9aMMD in the sample is incapable of binding actin, for example because of protein aggregation or degradation. Alternatively, two states of 9aMMD could exist in a dynamic equilibrium: a binding-incompatible and binding-compatible state. To distinguish between those two possibilities 9aMMD was sedimented with 10μM F-actin following 20min incubation on ice in the presence of 2mM MgATP as described above. The unbound fraction of 9aMMD present in the supernatant after the 1st spin was re-mixed with 10 μM F-actin, incubated as before and re-sedimented in a high-speed spin. The equal volumes of supernatant and pellet from the 1st and 2nd spin were analyzed by SDS-PAGE to determine the amount of myosin that rebound to actin. In parallel, myosin from the 1st spin was subjected to the resedimentation in the absence of actin to compare the amount of 9aMMD pelleting by itself to that pelleted with actin in the 2nd spin (Figure 4.14). If the presence of a nucleotide renders the myosin permanently incompetent of binding actin there should be no difference in the amount of 9aMMD pelleted in the 2nd spin in samples with and without actin. In an alternative scenario, if myo9a exists in a dynamic equilibrium between a state that binds actin and a state that does not bind actin, a higher amount of myosin should bind to actin in the 2nd spin as compared to a sample resedimented without actin. Indeed, when 9aMMD present in the supernatant from the 1st spin (58% of the total 9aMMD amount) was resedimented in the absence of actin only 11% of 9aMMD pelleted by itself, but the amount of 9aMMD present in the pellet of the 2nd spin in the presence of actin was 58% (Figure 4.14B, blue bars). Therefore, actin binding by myosin 9a is not hindered in the presence of a nucleotide; instead, two states of myo9a exist in an equilibrium when the nucleotide is present - actin binding-competent and -incompetent. The rate of this equlibrium could regulate binding of human myo9a to actin in a weak actin-binding state.

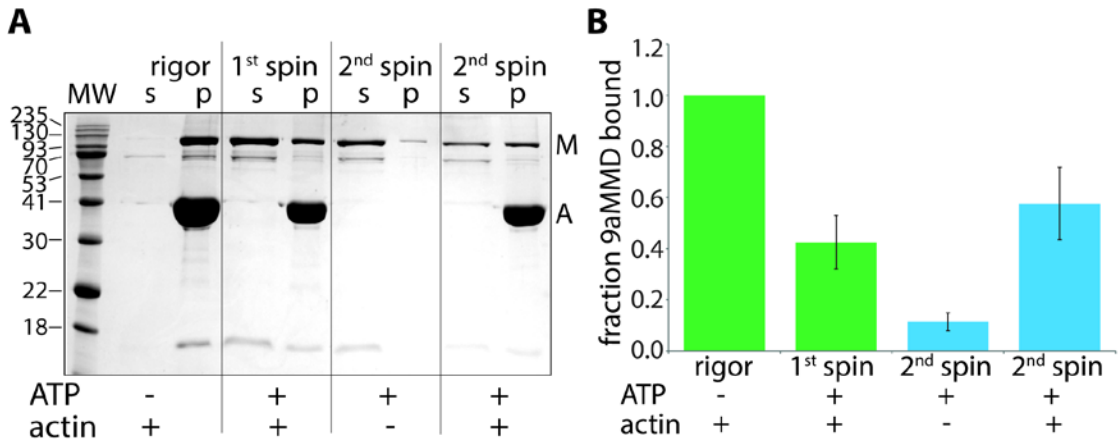

Figure 4.14. 9aMMD exists in two actin-binding states (binding-compatible and binding-incompatible) in the presence of ATP. 1.5μM 9aMMD was incubated with 10μM F-actin in the absence (rigor) and presence of 2mM MgATP for 20min on ice and centrifuged 20min, 100000rpm, 4^0C. A sample depleted of the nucleotide (rigor) was sedimented and separated on the gel to confirm full binding of 9aMMD to actin in the rigor state. In the presence of 2mM MgATP, a large fraction of 9aMMD was found in the supernatant. That fraction from two parallel spins, containing unbound 9aMMD fraction, was used in the 2nd spin without and with 'freshly' added 10μM F-actin, following 20min incubation on ice as before. **A:** a representative SDS-PAGE gel of 9aMMD rebinding to actin in the presence of ATP. Supernatant (s) and pellet (p) fractions show the amount of 9aMMD in each fraction in rigor and with ATP, from the 1st and 2nd spin. The presence or absence of ATP and actin are indicated below the gel. **B:** band densities were used to quantitate the amount of 9aMMD rebinding to actin as compared to the amount of 9aMMD pelleting by itself after recentrifugation. In rigor, all 9aMMD bound to actin. In the presence of ATP, only 42 ± 10% of total myosin amount bound to actin. From 58% of unbound 9aMMD fraction from the 1st spin, 11 ± 3.5% pelleted itself and 58 ± 14% was found in the pellet with actin following resedimentation (2nd spin). Therefore, 46% more of 9aMMD was found in the pellet in the presence than in the absence of actin, confirming that binding of 9aMMD to actin is not hindered in the presence of a nucleotide and that 9aMMD exists in a dynamic equilibrium between a binding-compatible and binding-incompatible state. M - myosin, A - actin. Data were collected from three independent myosin preparations and are presented as mean ± S.D. (n = 3).

Considering the profound effect of Ca^{2+} on the stimulation of the basal ATP hydrolysis rate of 9aMMD by actin, I investigated the effect of Ca^{2+} on binding of 9aMMD to F-actin in the presence of ATP. 9aMMD was cosedimented with 0 - 8μM F-actin as described previously in the presence or absence of 0.1mM Ca^{2+}. Samples were treated as previously and band density measurements were used to quantitate fractions of 9aMMD

bound to actin in the presence and absence of calcium (Figure 4.15). Calcium did not affect the dissociation constant or the maximal fraction of 9aMMD binding to high actin concentrations in the presence of ATP.

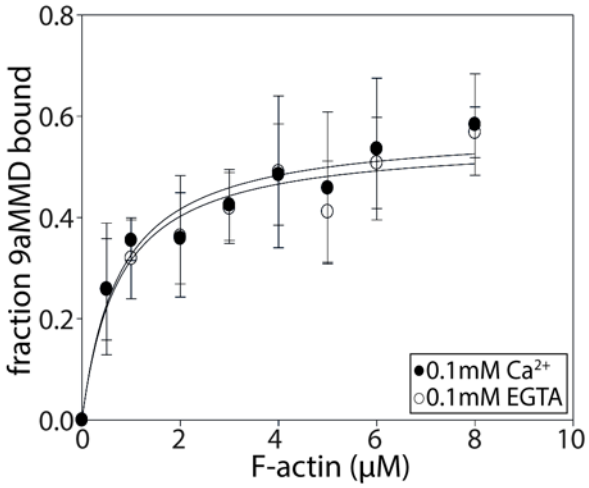

Figure 4.15. The effect of Ca^{2+} on actin binding by 9aMMD in the presence of 2mM MgATP. 0.8μM 9aMMD was mixed with increasing [F-actin] (0 - 8μM) in the presence (black circles) and absence (white circles) of 0.1mM free Ca^{2+}. Following 20min incubation on ice, samples were centrifuged 20min, 100000rpm, 4^0C and equal volumes of supernatant and pellet were analyzed by SDS-PAGE. Band density of 9aMMD fractions present in supernatant and pellet fractions were used to calculate the amount of 9aMMD bound, corrected for the amount of 9aMMD pelleting itself in the absence of actin. The amount of 9aMMD pelleted was plotted against [F-actin] and data was fitted to a hyperbolic equation, providing dissociation constants (K_d) and maximal fraction bound (F_{max}). Values are: K_d = 829 ± 67nM in the absence and K_d = 817 ± 74nM in the presence of 0.1mM Ca^{2+} with F_{max} = 59 ± 4 and F_{max} = 63 ± 2.1, respectively. Data points represent mean value from three independent 9aMMD preparations ± S.D. (n = 3).

Table 4.2. Actin-binding affinity of 9aMMD in different nucleotide states.

Parameter	Rigor	ATP/EGTA	ATP/Ca^{2+}	ADP
K_d (nM)	425 ± 21.1	810 ± 93	817 ± 74	590 ± 89
F_{max} (%)	101 ± 0.8	62 ± 3.2	63 ± 2.1	71 ± 2

CHAPTER 5: MECHANICAL PROPERTIES OF HUMAN MYOSIN 9

5.1. The *in vitro* gliding filament assay

The *in vitro* gliding filament assay (or motility assay) allows direct visualization of the mechanical activity of myosin. Using purified components, a system resembling that of the muscle sarcomere is reconstituted. The flow chamber is composed of a microscope glass slide, two parallel pieces of a double-sided tape and a coverslip, so that the total volume of the chamber is ~10µl. In the simplest version of the assay, the coverslip is coated with nitrocellulose; upon introduction of myosin to the chamber, the motor adheres nonspecifically to the surface. Unbound protein is washed out from the flow cell and free binding sites on the coverslip surface are blocked with BSA. Actin filaments stabilized with fluorecent-phalloidin (TRITC-actin) are introduced to the assay chamber and allowed to attach to the lawn of myosin motors on the surface. Introduction of ATP to the flow cell initiates enzymatic cycle of surface-attached myosins that interact with fluorescent actin filaments, resulting in translocation of actin filaments across the field of myosins on the surface. The assay was developed by Kron and Spudich, 1986. A schematic representation of the assay is presented in Figure 5.1.

A nonspecific attachment of myosin to nitrocellulose results in different geometries of molecules on the surface. This might render myosin motors incapable of undergoing a series of conformational changes necessary to propel a filament and thus hinder the motility. In order to attach myosins to the surface in a specific conformation, one can use an antibody raised against a C-terminal tag (i.e. GFP) or a C-terminal part of a myosin (i.e. tail). Such site-specific immobilization orients the myosin heads towards the volume of the

flow cell, enabling unrestrained progression through the mechanochemical cycle and effective power strokes resulting in translocation of actin filaments.

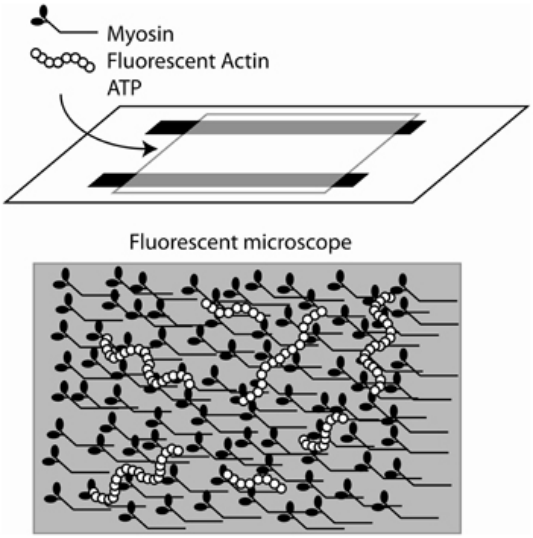

Figure 5.1. A schematic depiction of the *in vitro* motility assay. Flow chamber is constructed from a microscope glass slide, two pieces of a double-sided tape and a nitrocellulose-covered coverslip. Myosin is introduced into the chamber and adheres nonspecifically to the surface. Unbound protein is washed out and BSA is introduced to block free binding sites on the coverslip. Fluorescent actin filaments are introduced into the chamber and allowed to bind to the lawn of myosins. ATP is introduced to induce translocation of actin filaments. Image adapted from Batters et al., 2014.

Fast skeletal muscle myosin is a well established control of myosin function. I used a rabbit skeletal HMM fragment to assess the buffer compatibility with the assay. I applied 0.2mg/ml rabbit skeletal HMM to a flow cell constructed of a nitrocellulose-covered coverslip. Following blocking of free binding sites, TRITC-actin was introduced and motility was initiated by adding 2mM MgATP. Fluorophores on actin were excited in epi-fluorescence. Rabbit skeletal HMM robustly propelled actin filaments in the presence of ATP. GMimPro algorithm for the detection of single molecules (Mashanov and Molloy, 2007) was used to track individual filaments over time and a velocity distribution plot was obtained (Figure 5.2). Rabbit skeletal HMM actively translocated fluorescent actin filaments with a mean velocity of ~5.5μm/s at 22^0C, which corresponds well with previously reported values (Homsher et al., 2003, Sheetz et al., 1984).

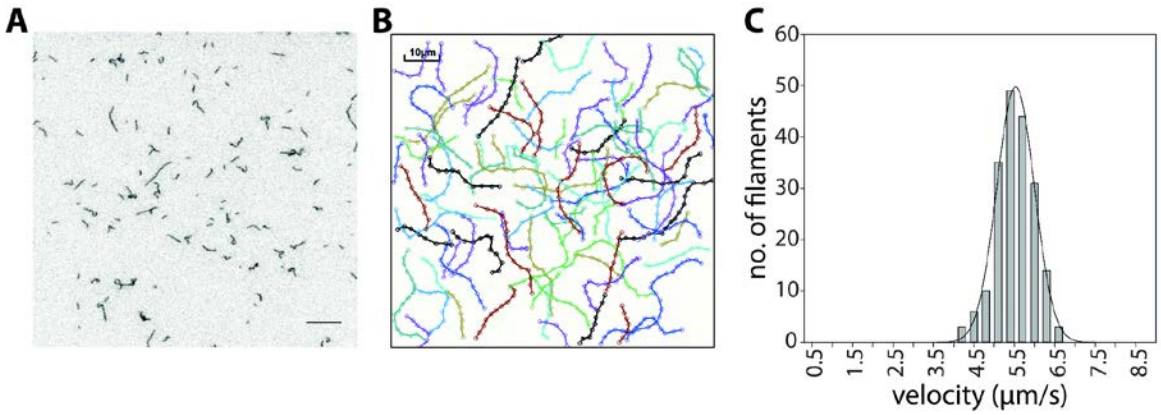

Figure 5.2. The *in vitro* gliding filament assay of rabbit fast skeletal muscle myosin HMM. **A:** 0.2mg/ml rabbit skeletal HMM was applied to a flow chamber and adhered to a nitrocellulose-covered coverslip. Actin was stabilized with TRITC-phalloidin and excited in epi-fluorescence using the Nikon Eclipse Ti microscope. An image represents fluorescent actin filaments (black) bound to myosin molecules on the surface of a coverslip. Scale bar: 10µm. **B:** motility was initiated by introducing 2mM MgATP and individual frames were acquired every 0.2s. A leading end of each filament gliding over a field of myosins was tracked using the GMimPro algorithm. An image represents tracks of individual filaments over time confirming active translocation of filaments by rabbit skeletal HMM. Scale bar: 10µm. **C:** a velocity distribution plot of rabbit skeletal HMM. 189 filaments were tracked over the time course of recorded videos. Mean velocity was ~5.5µm/s at 22^0C. Three separate flow cells were used to collect the data for this analysis.

5.2. Human myosin 9a nonspecifically attached to the surface binds actin in an ATP-sensitive manner but does not translocate filaments

Initial motility assays were performed with GFP-9a-S1 and GFP-9a-Head immobilized nonspecifically on nitrocellulose-covered coverslips. The interaction of rabbit skeletal HMM (as a control) and GFP-9a-S1 and GFP-9a-Head with actin at indicated motor concentrations in the presence of ATP is presented in figure 5.3 (lower panel). The collective pixel intensity from the first 50 (rabbit skeletal HMM) or 150 (myo9a) frames is presented as the Maximal Intensity Projection (Figure 5.3, lower panel). Both myo9a constructs bound actin in the absence of the nucleotide (Figure 5.3, 1^{st} frame). Upon introduction of ATP and at 0.2mg/ml motor concentration, no change in the position of actin filaments was observed (0.2mg/ml GFP-9a-Head). At 0.05mg/ml motor and in the presence of ATP (0.05mg/ml GFP-9a-Head and 0.05mg/ml GFP-9a-S1) actin filaments

started jittering and single dissociation and rebinding events of actin filaments were observed. However, no translocation of filaments occured. Supplementing the motility buffer with 2x molar excess of exogenous calmodulin or increasing the ionic strength of the buffer and warming the glass slide to ~30^0C did not improve the quality of the assay. This result suggests that at least a fraction of the motor on the surface is enzymatically active (as it released and rebound filaments). The coupling between the actin- and nucleotide-binding sites in GFP-9a-Head and GFP-9a-S1 is very poor, as showed by the lack of the actin-activated ATPase activity of those proteins. This might explain why those proteins were not able to translocate actin filaments, despite progressing through catalytic cycles on the surface of the coverslip. It is also plausible that a fraction of the motor on the surface is catalytically inactive or that a surface geometry of myosin enables binding of actin filaments but prohibits the mechanochemical cycle. By lowering the motor surface density, the number and spatial distribution of the active and inactive heads will change enabling active motors to undergo their catalytic cycles. This is consistent with the fact that at higher motor densities of GFP-9a-Head the filaments were rigidly attached to the surface and did not change their position, whereas lowering the motor density on the surface allowed dissociation and rebinding of the filaments.

In order to test whether the N-terminal extension regulates the mechanical activity of human myosin 9a, I repeated the motility assays with the minimal motor domain constructs – 9aMMD and 9aMMD-S1. Both constucts encompass the minimal sequence of the head domain of myosins essential for the enzymatic activity; 9aMMD-S1 additionally contains the full neck region with 6 IQ motifs.

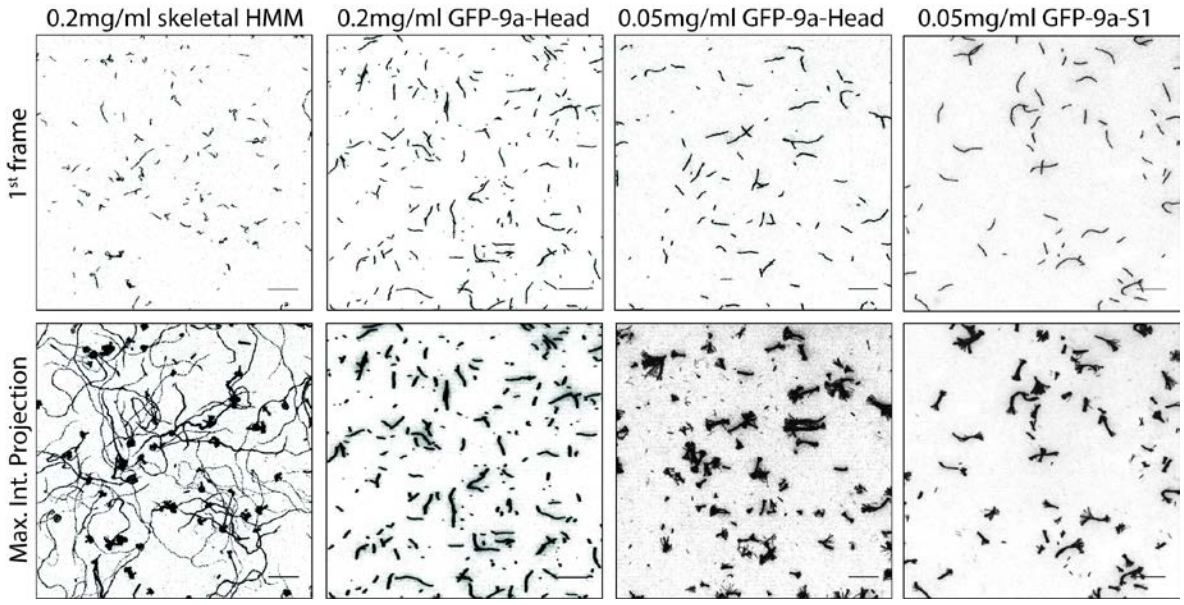

Figure 5.3. GFP-9a-Head and GFP-9a-S1 nonspecifically attached to the coverslip surface are enzymatically active but do not translocate actin filaments. 0.2mg/ml rabbit skeletal HMM, 0.2mg/ml GFP-9a-Head, 0.05mg/ml GFP-9a-Head and 0.05mg/ml GFP-9a-S1 were attached nonspecifically to a nitrocellulose-covered coverslip. TRITC-actin was bound to myosin on the surface and imaged in epi-fluorescence on the Nikon Eclipse Ti fluorescent microscope using 60x 4.2 NA oil objective (Nikon). '1st frame' shows actin filaments (black) attached to myosins on the surface of a flow chamber in the absence of ATP. 2mM MgATP was added to initiate the motility and frames were collected every 200ms in case of skeletal HMM and every 3min in case of myo9a. 'Max. Int. Projection' of the first 50 (skeletal HMM) or 150 (myo9a) frames represents the collective pixel intensity across indicated frames. Robust translocation of actin filaments is evident for rabbit skeletal HMM. At 0.2mg/ml myo9a no activity upon introduction of ATP was seen and filaments did not change their positions over time. When myo9a surface density was lowered to 0.05mg/ml, jittering of actin filaments over an attachment point and single dissociation /rebinding events were observed but no directional translocation of actin filaments took place. Data was collected from three independent myosin preparations and a representative image plane is shown. Scale bar: 10μm.

Based on previous results, whereby lower motor densities of GFP-9a-Head and GFP-9a-S1 supported mechanical activity, 0.05mg/ml of 9aMMD and 9aMMD-S1 were applied to flow cells constructed with nitrocellulose-covered coverslips (Figure 5.4). Both proteins bound actin (1st frame) and addition of ATP initiated actin filament jittering and rebinding (Max. Int. Projection). Still, no directional translocation of actin filaments was

observed. This suggests that the N-terminal extension of human myo9a is not necessary for motility and that minimal motor domain constructs are mechanically active but attached nonspecifically to the surface do not support the translocation of actin filaments. This might be due to specific motor geometries on the surface of the coverslip that do not support the mechanochemical activity. Alternatively, the lack of actin translocation can be explained by poor coupling between the actin- and nucleotide-binding sites in 9aMMD and 9aMMD-S1, as became evident in the ATPase assays.

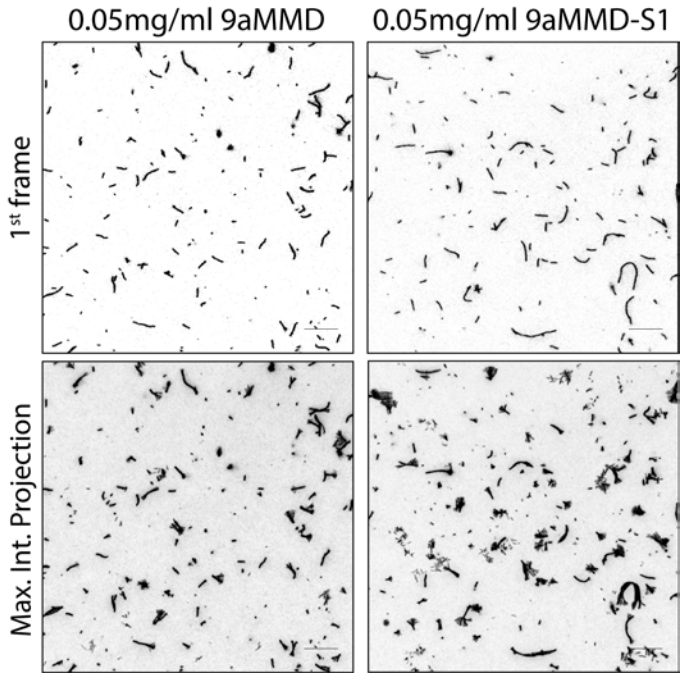

Figure 5.4. Mechanical properties of 9aMMD and 9aMMD-S1 nonspecifically attached to the coverslip surface in the absence of calcium. 0.05mg/ml 9aMMD or 9aMMD-S1 was applied to a flow cell constructed with a nitrocellulose-coated coverslip. TRITC-actin was introduced to the flow cell and imaged as before. Both constructs bound actin (1st frame; black). 2mM MgATP was introduced to initiate cycling of surface-attached myosins and frames were collected every 3min. The first 150 frames were used to obtain Max. Int. Projection representing the collective pixel intensity within indicated time period in a single field of view. No translocation of actin filaments was observed. Jittering of actin around an anchor point and single dissociation/rebinding events were observed. Data was collected from three independent myosin preparations and a representative image plane is shown. Scale bar: 10μm.

A possibility that human myosin 9a is motile only on a specific actin structure (i.e. bundled actin-filaments in filopodia or stress fibers or branched filaments in lamellipodia)

cannot be excluded. It has been previously proposed that myosin 10 preferentially moves on fascin-actin bundles, parallel actin filaments cross-linked by fascin into rigid bundles that filopodia are composed of (Ricca and Rock, 2010). Electron micrographs revealed that 9aMMD cross-links actin filaments, which might indicate it requires two parallel filaments for motility. In line with that, rat myo9a transiently expressed in 16HBE cells was found to co-localize with actin bundles at the cell periphery (Omelchenko, 2014). Stable fascin-actin bundles were generated by an overnight incubation of fascin with actin and were applied to flow cells to examine their translocation by 9aMMD (Figure 5.5). Fascin-actin bundles bind directly to a glass surface of a coverslip that was not blocked with BSA. Surprisingly, no fascin-actin bundles bound to 9aMMD immobilized on the surface. Even though a preference towards other specific actin architectures cannot be excluded, human myosin 9a does not bind fascin-actin bundles. It is possible that mechanical properties of filaments within the bundle (i.e. rigidity) disable tethering by myo9a. Alternatively, myo9a binding sites on actin are buried within the bundle causing the observed effect.

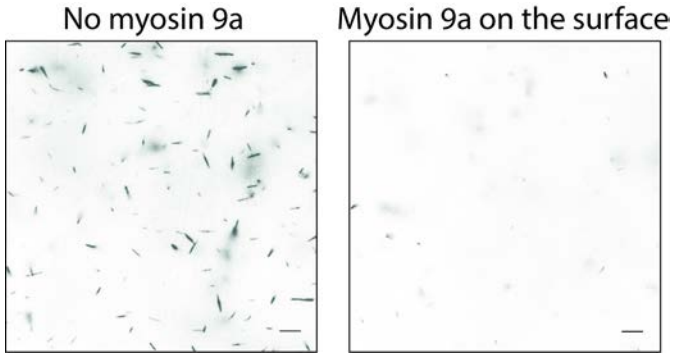

Figure 5.5. Human myosin 9a does not bind fascin-actin bundles. Facin-actin bundles were prepared by an overnight incubation of 3:8 molar ratio of fascin to phalloidin-stabilized F-actin at 4^0C. Bundles are lean, rigid rods (black) and bind directly to the glass surface of a coverslip (No myosin 9a). When 0.2mg/ml biotinylated 9aMMD was immobilized on the coverslip, no binding of bundles to the surface was observed (Myosin 9a on the surface).

As stated above, the lack of actin translocation might be a result of poor coupling between the actin- and nucleotide-binding sites in the absence of Ca^{2+}. However, adding

Ca^{2+} to the ATPase assays switch on that coupling in 9aMMD. Therefore, it is plausible that 9aMMD requires Ca^{2+} for the mechanical activity. I assessed the effect of Ca^{2+} on the motility of nonspecifically-immobilized 9aMMD by supplementing the motility buffer with 0.1mM Ca^{2+}. In agreement with the steady-state ATPase data, individual filaments were propelled in a smooth, directional fashion by myosin (Figure 5.6). The mean velocity of 9aMMD in the presence of 0.1mM Ca^{2+} was 9.6nm/s at 22^0C. That result suggests that calcium binding to CaM light chain associated with the head of 9aMMD might be necessary to induce coupling of the mechanochemical cycle of human myosin 9a.

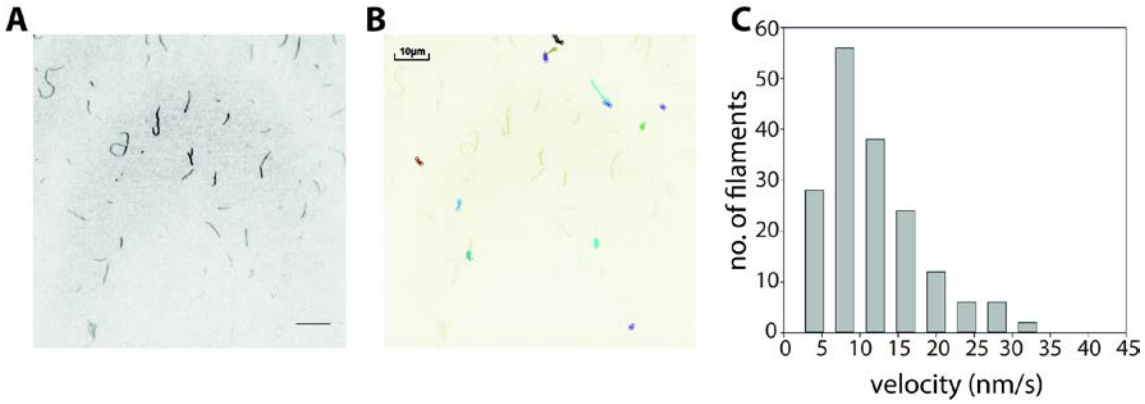

Figure. 5.6. Mechanical properties of 9aMMD nonspecifically attached to the coverslip surface in the presence of calcium. 0.05mg/ml 9aMMD was deposited in the flow cell. TRITC-actin was added and imaged in epi-fluorescence as before. 9aMMD bound actin **(A)** and propelled single filaments when 2mM MgATP was added in the presence of 0.1mM Ca^{2+}. Moving filaments were tracked in GMimPro **(B)** and the velocity distribution was obtained **(C)**. 162 actin filaments from three independent myosin preparations were used to measure the velocity and the mean velocity of 9aMMD in the presence of 0.1mM Ca^{2+} was 9.6nm/s at 22^0C. Scale bar: 10µm.

5.3. Cloning, purification and biotinylation of an Avi-tagged myosin 9a

Despite the fact that supplementing the motility buffer with 0.1mM Ca^{2+} initiated motility, actin transport was very poor with only a few filaments moving within the field of view for very short distances (Figure 5.7B). This suggests that multiple different

orientations of myosin on the surface might still contribute to an inefficient translocation of actin filaments by myosin 9a.

To immobilize myosin 9a in a specific conformation on the nitrocellulose surface, two additional constructs were developed: 9aMMD-Avi and 9aMMD-S1-Avi with the C-terminal Avi-tag. An Avi-tag (GLNDIFEAQKIEWHE) serves as a biotin-binding site, enabling biotinylation of myosin 9a constructs on the C-terminus. Oligos encoding an Avi-tag were chemically-synthesized and contained sticky ends with phosphate groups on the 5' end for ligation into an appropriate plasmid. pFBNA plasmids with 9aMMD and 9aMMD-S1 were digested with NotI and the Avi-tag was introduced in frame with the C-terminal FLAG-tag for the affinity chromatography (Figure 5.7A). The presence of 9aMMD and 9aMMD-S1 inserts in pFBNA after introduction of an Avi-tag was confirmed by restriction analysis (Figure 5.7B). Given the small size of the Avi-tag, its correct introduction into the plasmid was confirmed by sequencing. Recombinant bacmids were obtained as described previously and successful transposition was confirmed by PCR (Figure 5.7C).

Recombinant baculoviruses expressing 9aMMD-Avi and 9aMMD-S1-Avi were produced as before and protein was expressed and purified as before except that after the sonication of cells, BirA ligase, D-biotin (Sigma Aldrich) and additional ATP were added the the sample and the cell slurry was rotated for 1h at 4^0C. Soluble fraction was collected by centrifugation and purification followed as previously described. Protein biotinylation was confirmed by a western blot with an HRP-conjugated streptavidin (Figure 5.8).

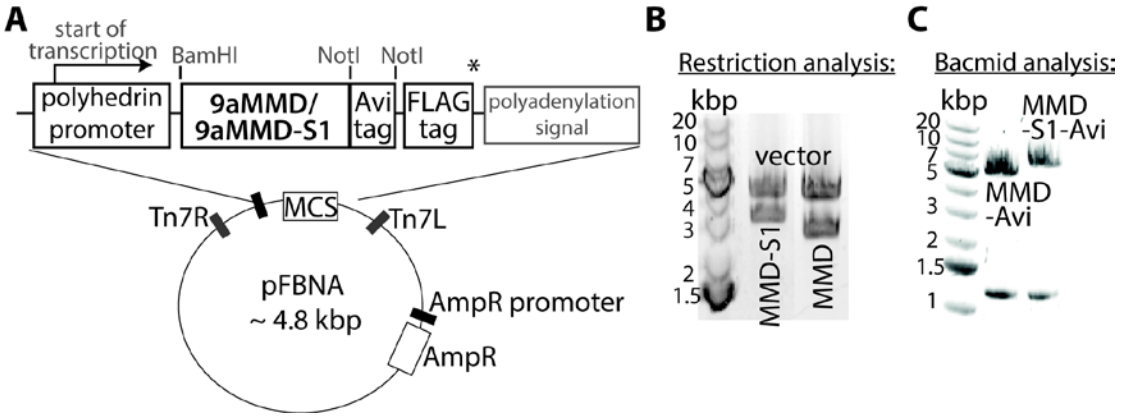

Figure 5.7. Cloning and bacmid generation of 9aMMD-Avi and 9aMMD-S1-Avi. **A:** a schematic drawing of the expression cassette of 9aMMD-Avi and 9aMMD-S1-Avi. Previously developed 9aMMD and 9aMMD-S1 constructs in the pFBNA vector were used as templates for fusion of the Avi-tag. Two antiparallel strands carrying DNA sequence encoding an Avi-tag (GLNDIFEAQKIEWHE) and containing sticky ends compatible with the NotI restriction site as well as a phosphate group attached to the 5' end of each strand were chemically synthesized (Sigma Aldrich). Equal amounts of each strand were mixed, incubated at 95^0C for 5min followed by slow cooling to allow hybridization of two strands. Myo9a plasmids were digested with NotI following general protocols and mixed with a 3-molar excess of Avi-tag oligos. DNA pieces were ligated by T4 DNA ligase following the manufacturer's protocol (Thermo Scientific) and transformed into *E.coli* DH5α cells using a heat-shock protocol. Plasmid DNA was isolated. The Avi-tag was introduced in frame with the N-terminal myo9a fragments and the C-terminal FLAG-tag. **B:** the presence of 9aMMD and 9aMMD-S1 regions was confirmed by restriction analysis with BamHI and NotI enzymes. Digestion products were analyzed on an 0.6-0.8% agarose gel revealing two bands in each sample: one corresponding to the vector backbone (expected size: ~4.8kbp) and one corresponding to either 9aMMD-S1 (expected size: ~3kbp) or 9aMMD (expected size: ~2.6kbp), as indicated on the gel presented. Correct introduction of the Avi-tag for each construct was confirmed by sequencing. **C:** *E.coli* DH10Bac cells were transformed with appropriate plasmids and recombinant bacmids were obtained as previously described. Successful transposition was confirmed by PCR. Products were analyzed by gel electrophoresis, revealing bands of expected sizes (~5.5kbp and ~6kbp for 9aMMD-Avi and 9aMMD-S1-Avi, respectively).

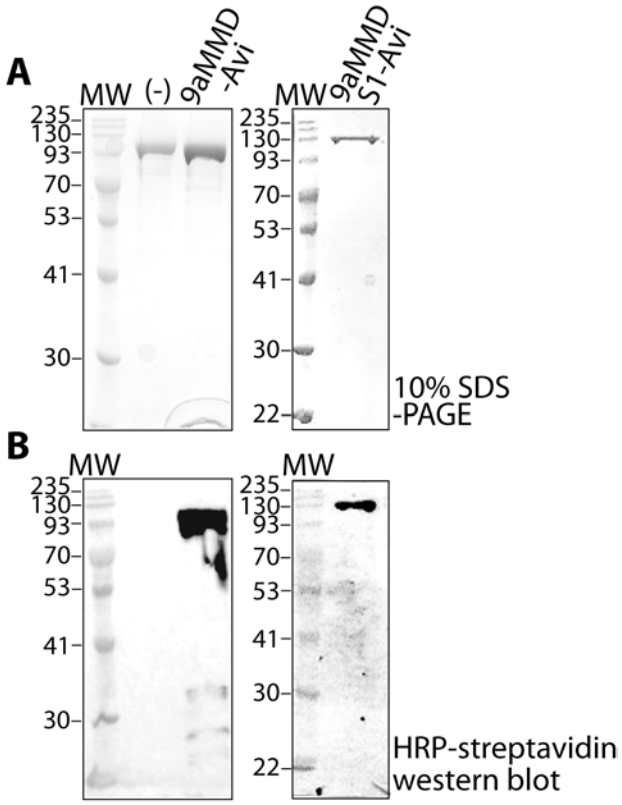

Figure 5.8. Purification and biotinylation of 9aMMD-Avi and 9aMMD-S1-Avi. **A:** a representative SDS-PAGE gel of purified 9aMMD-Avi and 9aMMD-S1-Avi. The purification protocol described before was used. Purified proteins correspond well with the expected molecular weights (~120kDa for 9aMMD and ~135kDa for 9aMMD-S1). **B:** samples presented in A were transferred to a nitrocellulose membrane and assayed for the presence of biotin by incubation with an HRP-conjugated streptavidin. The negative control (-) indicates 9aMMD-Avi preparation in the absence of BirA ligase. Adjacent lanes contained 9aMMD-Avi and 9aMMD-S1-Avi biotinylated in the presence of BirA ligase. Signal was developed with a commonly accessible ECL kit and confirmed successful biotinylation of 9aMMD-Avi and 9aMMD-S1-Avi.

5.4. Site-specifically immobilized 9aMMD actively transports actin

Biotinylated 9aMMD-Avi was used in the *in vitro* motility assay. Biotin-BSA was applied to the flow chamber, followed by an addition of streptavidin, 0.2mg/ml biotinylated 9aMMD and TRITC-actin. Actin filaments were excited in epi-fluorescence and frames were acquired every 3min for 10min at 60x optical zoom with 4.2NA Nikon objective and Nikon Eclipse Ti microscope. Motility buffer was supplemented with 2mM MgATP, 100mM KCl and 0.5% methylcellulose. 9aMMD specifically immobilized on the flow cell

surface actively translocated actin filaments (Figure 5.9) with all filaments within the image plane moving. The mean velocity obtained from 576 filaments was 34.7nm/s. This is the first direct evidence that human myosin 9a translocates actin filaments and therefore could function as a mechanically active molecular motor in a cell. The velocity is ~160 times lower than that of skeletal muscle myosin reported here (5.5μm/s).

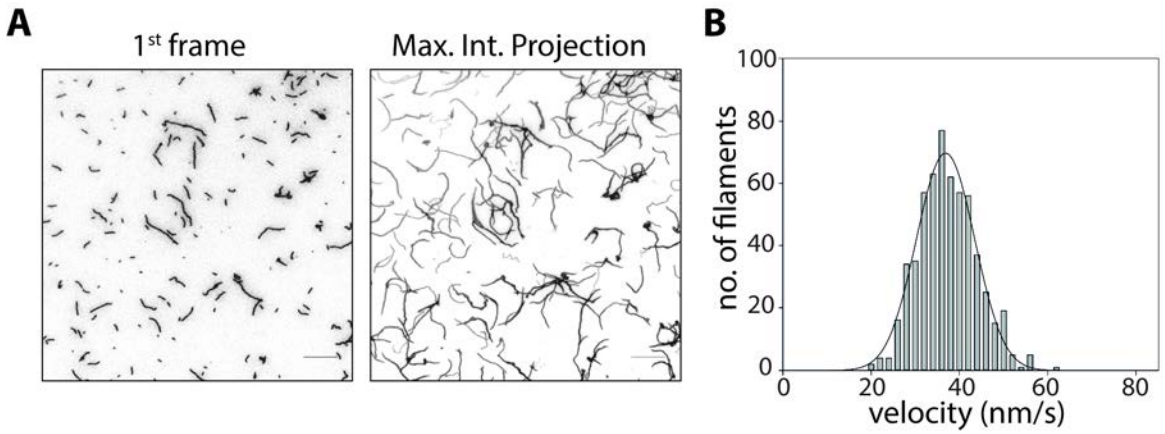

Figure 5.9. 9aMMD-Avi specifically attached to the coverslip surface actively translocates actin filaments. **A:** 0.2mg/ml 9aMMD-Avi was immobilized on the coverslip surface via a streptavidin-biotin linkage and TRITC-actin was introduced into the flow cell. Actin filaments (black) were excited in epi-fluorescence on the Nikon Eclipse Ti microscope revealing binding to surface-attached myosin motors (1st frame). Motility was initiated with 2mM MgATP in a motility buffer supplemented with 100mM KCl and 0.5% methylcellulose at 22^0C. Subsequent frames were acquired every 3min for 10min and the Maximum Intensity Projection (representing the collective pixel intensity from all frames) from a representative image plane is shown revealing active translocation of actin filaments. **B:** a velocity distribution plot of 9aMMD-Avi. 576 individual filaments from at least three independent myosin preparations were tracked and mean velocity was 34.7nm/s.

Methylcellulose is a viscosity agent that has the ability to compensate for the lack of weak actin binding by myosins (Joel et al., 2001). Previous reports on other myosin 9 isoforms all state that methylcellulose was necessary to maintain actin filaments close enough to the surface for the motility to occur (Liao et al., 2010, Elfrink et al., 2014). Therefore, initial *in vitro* motility assays with 9aMMD-Avi were supplemented with 0.5% methylcellulose. However, when assayed in the absence of methylcellulose, the motility was not affected (Figure 5.10); the average velocity in the absence of methylcellulose (no MetCel) was 34.6 ± 4.5nm/s and 37.4 ± 5.9nm/s in the presence of 0.5% methylcellulose

(0.5% MetCel) in the motility buffer supplemented with 2mM MgATP and 100mM KCl. Therefore, human myosin 9a interacts with actin in a weka actin-binding state and methylcellulose is not required for actin translocation by human myosin 9a. All following *in vitro* motility assays of myo9a were performed in the absence of methylcellulose in the motility buffer.

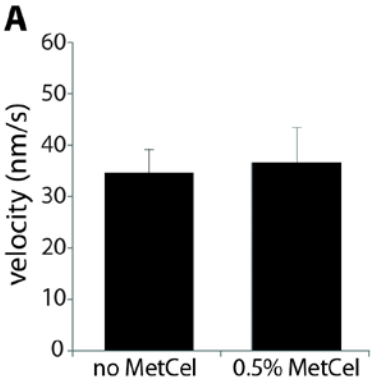

B

condition	velocity (nm/s)	S.D.	n
no MetCel	34.6	4.5	234
0.5% MetCel	37.4	5.9	576

Figure 5.10. Methylcellulose is not required for actin translocation by 9aMMD-Avi. 0.2mg/ml biotinylated 9aMMD-Avi was immobilized on a coverslip via the streptavidin-biotin linkage. Following binding of TRITC-actin, motility was initiated by flashing in a motility buffer supplemented with 2mM MgATP and 100mM KCl at 22^0C. Translocation of filaments was observed in the absence (no MetCel) or presence (0.5% MetCel) of 0.5% methylcellulose in the motility buffer. Frames were acquired every 3min for 10min total time using 60x zoom, 4.2NA objective (Nikon) and a CCD camera under the Nikon Ti Eclipse fluorescent microscope. Three independent flow cells were prepared for each condition and bars in **(A)** represent average velocity ± S.D. The table summarizing the average velocities at each condition is shown in **(B)**. The average velocity in the absence of methylcellulose was 34.6 ± 4.5nm/s and 37.4 ± 5.9nm/s in the presence of 0.5% methylcellulose. Average values were obtained from velocities of 234 and 576 filaments in the absence and presence of 0.5% methylcellulose, respectively.

The actin-activated ATPase activity of full length myosin 5 increased in the presence of Ca^{2+} (Wang et al., 2004; Lu et al., 2006), similarly to 9aMMD. Conversly, Ca^{2+} inhibited the motility of myosin 5. Motility was partially restored in the presence of CaM (Krementsov et al., 2004). Ca2+ caused dissociation of CaM from the neck domain of myosin 5, associated with a conformational change from a folded to an unfolded state compatible with binding actin, resulting in an increase in the maximal ATPase. However, the lever arm lost its rigidity upon CaM dissociation, causing inhibition of motility (Wang

et al., 2004; Krementsov et al., 2004). The putative CaM-binding site of 9aMMD is in the loop 2 region and its interactions with CaM could influence the dynamics of the actomyosin complex of myosin 9a. I tested the effect of Ca^{2+} and exogenous CaM on the maximal velocity of actin translocation by 9aMMD-Avi in the *in vitro* motility assay (Figure 5.11). Supplementing the motility buffer with 0.1mM Ca^{2+} or 10μM exogenous CaM (~5-fold molar excess of calmodulin to myosin) did not affect the speed of 9aMMD. Therefore, the interactions between CaM and loop 2 of hyman myosin 9a do not affect the dynamics of the actomyosin complex.

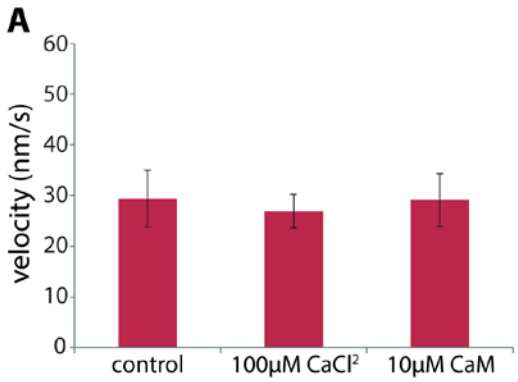

B

condition	velocity (nm/s)	S.D.	n
control	29.4	5.6	210
100μM $CaCl_2$	26.9	3.3	132
10μM CaM	29.1	5.2	300

Figure 5.11. The effect of $CaCl_2$ and exogenous calmodulin on the velocity of 9aMMD-Avi. 0.2mg/ml biotinylated 9aMMD-Avi was immobilized on a coverslip surface via the streptavidin-biotin linkage. TRITC-actin was bound and motility was initiated by introducing a motility buffer supplemented with 2mM MgATP in the absence (control) and presence of 0.1mM Ca^{2+} or 10μM exogenous CaM at 22^0C. Motility buffer contained 50mM KCl. Subsequent frames were collected as before. Three independent flow cells were used to collect data for each condition. Bars in **(A)** represent average velocities ± S.D at each condition. As summarized in **(B)**, average values were 29.4 ± 5.6 in the absence of additives (control), 26.9 ± 3.3 in the presence of 0.1mM Ca^{2+} and 29.1 ± 5.2 in the presence of ~5-fold molar excess of CaM from 210, 132 and 300 filaments, respectively.

The dependence of the motility of myosin on ionic strength is related to the affinity of myosin to actin in the presence of ATP (Wang et al., 2000). The effect of ionic strength on 9aMMD motility was addressed (Figure 5.12). At a constant motor density (0.2mg/ml), site-specifically immobilized 9aMMD-Avi bound and supported movement of fluorescent actin filaments over a great range of ionic strengths (25 - 500mM KCl) in the absence of methylcellulose. An average velocity increased nearly 4-fold in the range from 25 to

200mM KCl with the maximum sliding velocity of 65.6 ± 9.8nm/s, followed by the decrease in average velocities at higher [KCl] (Figure 5.12A). A decrease in the sliding velocity of 9aMMD was associated with the dissociation of filaments from the coverslip surface (Figure 5.12B). It was difficult to track filaments above 500mM KCl because of strong filament jittering over a relative anchor point and low sliding velocities. Figure 5.12C presents a table summarizing sliding velocities and fraction of filaments that remained bound as a function of [KCl] in a buffer supplemented with 2mM MgATP at constant 9aMMD surface densities (0.2mg/ml). 9aMMD bound and propelled actin filaments even at 500mM KCl in the absence of methylcellulose. This reflects high affinity of human myo9a for binding actin in the presence of ATP and at high ionic strength.

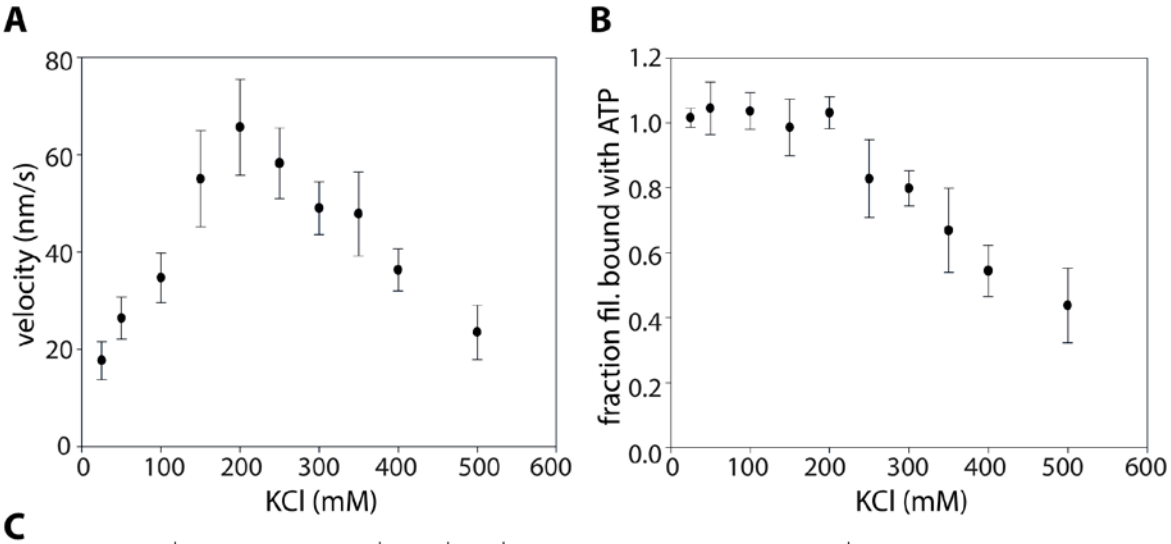

C

KCl (mM)	velocity (nm/s)	S.D.	n	fraction fil. bound with ATP	S.D.
25	17.7	3.9	49	1.02	0.03
50	26.4	4.3	175	1.04	0.08
100	34.7	5.1	162	1.04	0.06
150	55	9.9	147	0.99	0.09
200	65.6	9.8	87	1.03	0.05
250	58.2	7.3	121	0.83	0.12
300	49	5.4	166	0.80	0.05
350	47.8	8.6	45	0.67	0.13
400	36.3	4.3	101	0.54	0.08
500	23.5	5.6	36	0.44	0.11

Figure 5.12. The effect of increasing ionic strength on the sliding velocity and filament attachment to 9aMMD. 0.2mg/ml biotinylated 9aMMD-Avi was immobilized on a coverslip surface via the streptavidin-biotin linkage. TRITC-actin was bound and motility was initiated by introducing a motility buffer supplemented with 2mM MgATP and indicated [KCl]. Subsequent frames were collected as before. **A:** the dependence of the sliding velocity of actin by 9aMMD on the ionic strength. The average velocity increased nearly 4-fold in the range of [KCl] between 25 and 200mM, followed by a sharp decrease. **B:** the dependence of an actin filament binding by 9aMMD on the surface as a function of [KCl]. No dissociation of filaments from the myosin-coated surface took place up to 200mM KCl; at higher [KCl] filaments jittered and started dissociating, resulting in a linear decrease of the fraction of filaments bound at increasing [KCl]. Data points represent average values ± S.D. from at least three separate flow cells. **C:** a table summarizing mean sliding velocities of actin over the constant surface density of 9aMMD and fractions of filaments bound to the myosin-coated surface at increasing [KCl].

The steady-state ATP affinity of 9aMMD was also assayed in the *in vitro* motility assay by calculating the average sliding velocities of 9aMMD over a range of an increasing ATP concentration (Figure 5.13). The sliding velocity increased with an increasing [ATP] and data points were fitted to a quadratic equation. The half-maximal velocity was reached at K_{ATP} = 0.37 ± 0.085mM. The velocity was constant above 0.6mM ATP.

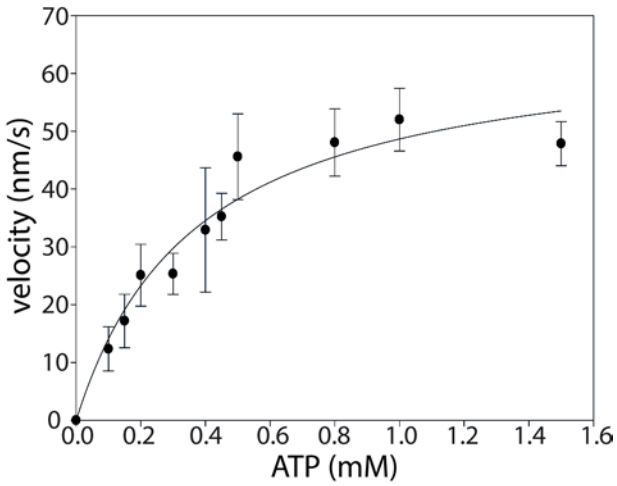

Figure 5.13. The dependence of 9aMMD velocity on ATP concentration. 0.2mg/ml biotinylated 9aMMD-Avi was immobilized on a coverslip surface via the streptavidin-biotin linkage. TRITC-actin was bound and motility was initiated by introducing a motility buffer supplemented with 100mM KCl and indicated Mg[ATP]. Subsequent frames were collected as before. Data points represent average values ± S.D. from at least three

independent flow cells for each [ATP]. Data was fitted to a quadratic equation and the half maximal velocity was reached at K_{ATP} = 0.37 ± 0.085mM.

5.5. The neck region of human myosin 9a acts as a lever arm

It was previously reported that the sliding velocity of the head and head-neck constructs of *C. elegans* myosin 9 was the same, suggesting that the neck domain of myosin 9 does not act as a lever arm (Liao et al., 2010).

I investigated the role of the neck domain in the regulation of the sliding velocity of human myosin 9a in the *in vitro* motility assay. Assays with the biotinylated 9aMMD-S1-Avi (encompassing the minimal motor domain and the neck domain of human myo9a) were set up as described above. Initial attempts did not result in translocation of actin filaments in the presence of ATP (Figure 5.14). Filaments jittered around an anchor point and individual dissociation/rebinding events were observed, but no active transportation of filaments took place.

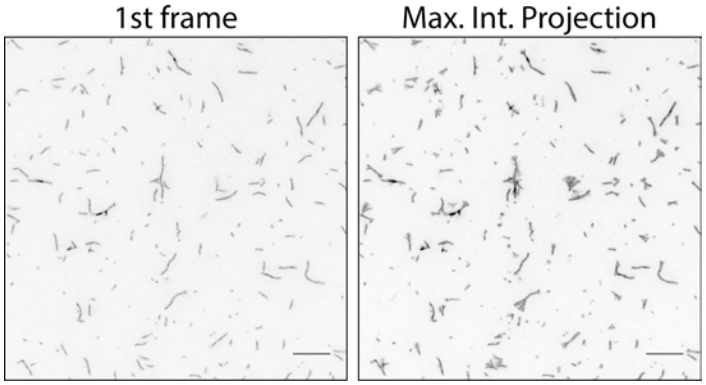

Figure 5.14. Sie-specifically immobilized 9aMMD-S1-Avi does not support actin sliding in the absence of exogenous calmodulin. 0.2mg/ml biotinylated 9aMMD-S1-Avi was immobilized specifically in the flow cell through attachment to a streptavidin-covered coverslip. Unbound motor was removed and free binding sites on the coverslip were blocked with BSA. Fluorescent actin filaments (black) were added to the chamber and imaged in epifluorescence as before. Motility buffer containing 2mM MgATP and 100mM KCl was introduced and frames were acquired every 3min for 10min. 9aMMD-S1-Avi bound actin filaments (1st frame; black). Upon addition of ATP no directional translocation of actin filaments was observed; instead, filament ends jittered and individual dissociation/rebinding events were observed (Max. Int. Projection). Scale bar: 10µm.

Given that 9aMMD actively translocated actin filaments, lack of actin transport by 9aMMD-S1 was surprising. 9aMMD-S1 contains six additional CaM-binding sites, as compared to 9aMMD. It is possible that one or more IQ motifs within the neck region of 9aMMD-S1 are not saturated with CaM. This could lead to a decrease in the rigidity of the lever arm and inhibition of power strokes. I attempted to optimize the assay by adding a 5-fold molar excess of exogenous calmodulin to the motility buffer. Indeed, supplementing the motility buffer with 10μM exogenous CaM was required for active translocation of actin filaments by site-specifically immobilized 9aMMD-S1-Avi (Figure 5.15). The mean sliding velocity of 9aMMD-S1 was 204.4nm/s (n = 232) - almost 6 times greater than that of 9aMMD (34.7nm/s). Therefore, the neck domain of human myosin 9a functions as a lever arm to increase the step size and sliding velocity of the myosin. Note that the filament traces in the Maximum Intensity Projection for 9aMMD-S1 appear longer than for 9aMMD. Since these were obtained from the same amount of frames for both constructs, it is apparent that 9aMMD-S1 slides actin filaments faster than 9aMMD.

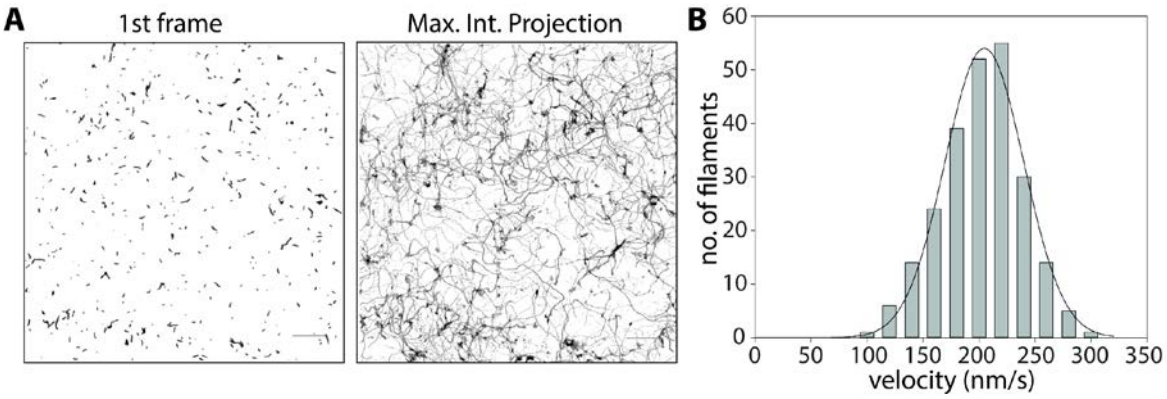

Figure 5.15. 9aMMD-S1 site-specifically immobilized on the coverslip surface actively translocates fluorescent actin filaments in the presence of the 5-fold molar excess of exogenous calmodulin. **A:** 0.2mg/ml biotinylated 9aMMD-S1-Avi was immobilized specifically in the flow cell through attachment to a streptavidin-covered coverslip. Unbound motor was removed and free binding sites were blocked with BSA. Fluorescent actin filaments (black) were added to the chamber and imaged in epifluorescence as before. Motility buffer containing 10μM exogenous calmodulin, 2mM MgATP and 100mM KCl was introduced and frames were acquired every 3min for 10min. 9aMMD-S1-Avi bound actin filaments (1st frame; black). Upon introduction of the motility buffer, directional translocation of actin filaments was observed and is presented as the Maximum Intensity Projection of the collective pixel intensity from all frames. Scale bar: 10μm. **B:** a velocity distribution plot of 9aMMD-S1-Avi. Mean velocity was 204.4nm/s. At least three separate

flow cells were prepared with 9aMMD-S1-Avi from each of the two independent purifications and mean velocity was obtained by tracking 232 filaments.

Given that the neck region of human myo9a binds calmodulin light chains, I addressed the effect of Ca^{2+} on the sliding velocity of 9aMMD-S1 in the presence of 10μM exogenous CaM in the motility buffer. Surprisingly, as little as 1μM Ca^{2+} fully inhibited the mechanical activity of 9aMMD-S1. Together with the fact that supplementing the motility buffer with the 5-fold molar excess of CaM was required for the translocation of actin by 9aMMD-S1 in the absence of Ca^{2+}, and that very low [Ca^{2+}] inhibited the motility, at least two possibilities could be considered. Firstly, the requirement for an exogenous calmodulin in the buffer might indicate that at least a single light chain molecule binds to the neck region with low affinity, causing compliance in the molecule and hindering actin translocation. In the presence of excess calmodulin, there would be enough light chain in the solution to compensate for a weak binding to an IQ motif, providing enough rigidity for the neck region for effective power strokes and robust translocation of actin. Secondly, Ca^{2+}-loaded CaM could bind an IQ motif (at least one) with a lower affinity, causing the dissociation of calmodulin from the IQ motif, once again introducing compliance in the neck region. In this situation, maintaining the rigid lever arm could be challenged even in the presence of exogenous CaM in the solution.

To assess the effect of Ca^{2+} on the association of CaM with 9aMMD-S1, an actin spin-down assay was used. ~1μM 9aMMD-S1 was mixed with 10μM phalloidin-stabilized F-actin in the absence and presence of an increasing Ca^{2+} concentration. Since as little as 1μM Ca^{2+} inhibited the motility of 9aMMD-S1, I used 1-10μM Ca^{2+} in the assay. Following 20min incubation in RT, samples were ultracentrifuged and equal volumes of supernatant and pellet were separated on a 4-20% SDS-PAGE gel (Figure 5.16). CaM present in the supernatant would represent the light chain fraction that dissociated from 9aMMD-S1, whereas that found in the pellet would represent the myosin-associated CaM fraction. Unexpectedly, a fraction of calmodulin dissociated from myosin in the absence of Ca^{2+} (EGTA); Ca^{2+} did not cause any further dissociation of CaM as there was no visible difference between the amount of CaM in the supernatant and pellet fractions at increasing [Ca^{2+}]. This means either that CaM binds to the neck region of human myosin 9a with such

very low affinity that shear forces acting on the sample during a high-speed centrifugation are enough to separate the light chain from the heavy chain or that the association of CaM with myosin in that particular construct is unstable. Such instability could result from the lack of myosin domains stabilizing the interaction between CaM and the heavy chain (for example, the N-terminal extension of myosin 9). Alternatively, the neck region of human myosin 9a might preferentially bind other types of light chains in a native intracellular environment. Currently, the effect of Ca^{2+} on the motility of 9aMMD-S1 cannot be investigated.

Nevertheless, the requirement for exogenous CaM in the motility buffer suggests weak association of calmodulin light chain with at least one IQ motif within the neck of human myosin 9a. Furthermore, addition of Ca^{2+} to the motility buffer weakens the association of CaM with the neck region to the point where it cannot be compensated for by the addition of extra light chain.

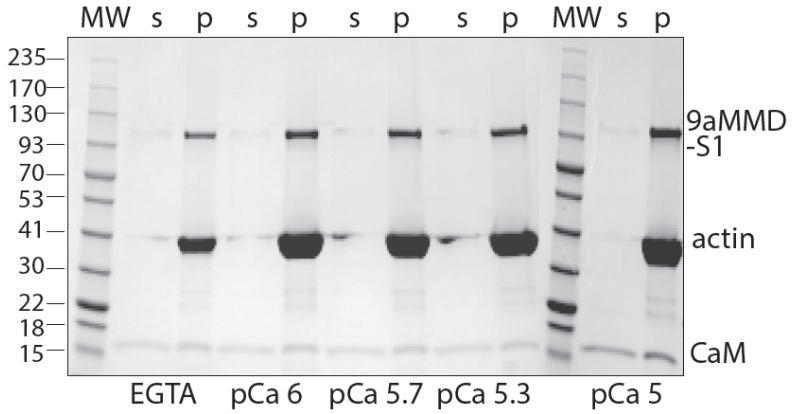

Figure 5.16. The effect of Ca^{2+} on the association of CaM with 9aMMD-S1. ~1μM 9aMMD-S1 was mixed with 10μM phalloidin-stabilized F-actin in the absence (EGTA) and presence of 1-10μM Ca^{2+}. Myosin was allowed to bind to actin for 20min at RT and supernatant and pellet were obtained at 100000rpm, 20min, 4^0C. Supernatant was collected and pellet was dissolved in equal volume of PBS. Equal volumes of supernatant and pellet were mixed with a loading dye and separated on a 4-20% Tris-glycine gel (Bio-Rad) to assess the association of CaM with 9aMMD-S1 heavy chain in the absence and presence of increasing [Ca^{2+}]. CaM fraction present in the supernatant represent light chain molecules

that dissociated from the heavy chain whereas CaM present in pellets remains associated with 9aMMD-S1 heavy chain. A representative SDS-PAGE gel from three independent runs is shown. [Ca^{2+}] is depicted in the form of pCa below the gel. Positions of 9aMMD-S1, actin and CaM on the gel are indicated. In the absence of Ca^{2+} (EGTA), a fraction of CaM was found in the supernatant suggesting that the binding of CaM to the neck region of human myosin 9a is so weak that shear forces acting in the tube during an ultracentrifugation are enough to separate it from the heavy chain. Alternatively, CaM binding might me stabilized by intramolecular interactions provided by the tail domain or the N-terminal extension. Further dissociation of CaM upon addition of low micromolar [Ca^{2+}] was not observed.

5.6. Processivity of human myosin 9a

Previously it was shown that rat myo9b and *C. elegans* myo9 are single-headed processive molecular motors. The processivity (the ability to undergo multiple steps on an actin filament before dissociation) of a monomeric motor is puzzling; it was suggested that the class 9-specific loop 2 insert is the determinant of processivity (Nishikawa et al., 2006, Liu et al., 2010, Elfrink et al., 2014).

As 9aMMD appeared more stable in the motility assays, I used this construct for the following experiments. In order to investigate the processivity of human myo9a, I first assayed the oligomerization state of 9aMMD in the solution. Hydrodynamic properties of 9aMMD (Stokes radius and sedimentation coefficient) were determined by the gel filtration and a centrifugation in a linear sucrose gradient (Figure 5.17). 9aMMD exists as a single conformer in the solution, as indicated by elution in a single peak from a gel filtration column and a single fraction from the sucrose density gradient (Figure 5.17A). The expected molecular weight of a monomeric 9aMMD is ~120kDa. The behavior of 9aMMD in the gel filtration media and the linear sucrose gradient suggests it has similar biophysical properties to that of aldolase, indicating it is a globular protein in solution (Figure 5.17B). The native molecular weight of 9aMMD calculated from the parameters obtained was 121.8 ± 0.4kDa from three independent experiments, which is in a very good agreement with the molecular weight expected for a monomeric 9aMMD with a single calmodulin bound. Therefore, 9aMMD is a globular protein and a monomer in solution.

To determine if 9aMMD is a single-headed processive molecular motor, the *in vitro* motility assay was performed at decreasing motor surface densities and the velocity of actin translocation was measured (Figure 5.18). For a processive myosin, as little as a single molecule is enough to propel actin; if 9aMMD is processive, no decrease in the velocity as a function of a decreasing motor density should take place (Howard et al., 1989). Flow chambers were prepared as before with varying motor concentrations. Knowing the molar concentration of 9aMMD-Avi applied to the flow cell and given that the total flow cell volume is ~10μl with the surface area of ~72μm^2, motor surface densities were calculated. All surface densities of 9aMMD assume that all molecules entered the flow cell, none was denatured and half adsorbed to each surface of the chamber. 9aMMD supported actin translocation even at very low surface densities (~$10^2/\mu m^2$). Actin translocation velocities did not change over the range of surface densities tested. At lower surface densities filaments exhibited nodal pivoting and finally free filament ends swiveled around a single attachment point. Filaments moved over a single contact point and when filament end reached the tethering point, it diffused away. These are characteristics of processive motility. Therefore, a single-headed 9aMMD moves processively on actin.

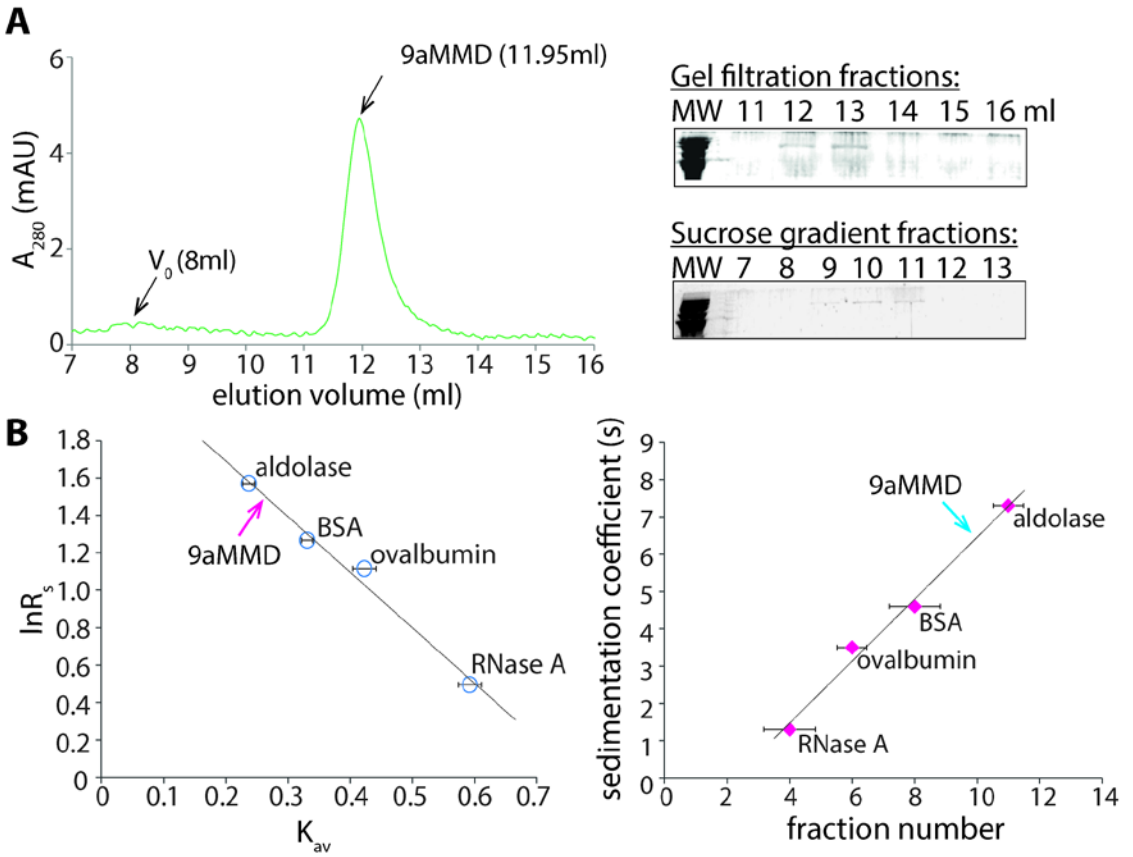

C

Protein	Stokes radius, R_s (nm)	Elution Vol. (ml)	Void Vol. V_0 (ml)	Partition coeff. K_{av}	lnR_s	sed. coeffi. (s)	eluate fraction	MW from aa seq. (kDa)	native MW (kDa)
9aMMD	4.65	11.95	8.0	0.25	1.54	6.5	10	119.1	121.8

Figure 5.17. 9aMMD is a monomer in solution. **A:** hydrodynamic properties of 9aMMD were assessed by gel filtration and sucrose gradient centrifugation. 100µl of 0.2mg/ml purified 9aMMD was separated on the Superdex 200 10/300 GL column (GE Healthcare) calibrated with protein markers as indicated in Figure 3.21. A representative UV trace is shown. 9aMMD eluted in a single peak at 11.95ml. The void volume of the column V_0 = 8ml. The identity of the peak was confirmed by SDS-PAGE. The partition coefficient (K_{av}) of 9aMMD was calculated from the elution and void volume as described in Materials and Methods. 100µl of 0.2mg/ml purified 9aMMD was layered on top of a 6-20% sucrose gradient and centrifuged 37000rpm, 18h, 4^0C. Fractions were collected and analyzed by SDS-PAGE. 9aMMD eluted as a single species in the 10^{th} fraction. **B:** lnR_s and sedimentation coefficient of 9aMMD were determined by an intrapolation of 9aMMD K_{av} and elution fraction obtained from gel filtration and sucrose gradients to standard curves. In both cases, 9aMMD elutes slightly faster than aldolase (158kDa), suggesting it is a monomer in solution. **C:** calculation of the native molecular weight of 9aMMD in solution gives 121.8 ± 0.4kDa (n = 3) which is in a very good agreement with the expected

molecular weight of 119.1kDa for a single heavy chain with one CaM molecule bound. Therefore, 9aMMD is a monomer in solution.

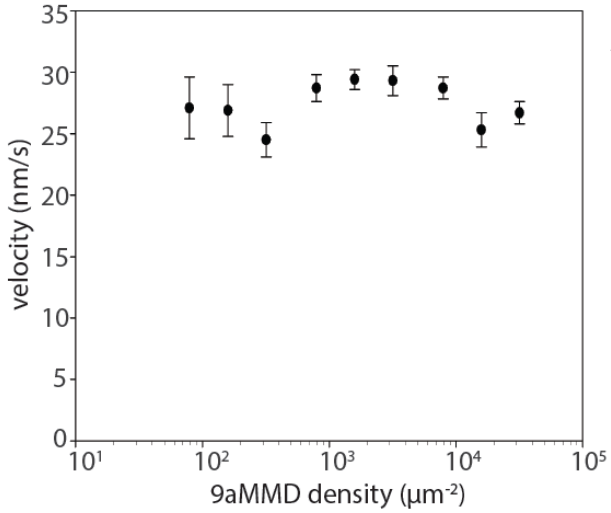

9aMMD density (μm^{-2})	velocity (nm/s)	S.D.	n
7.9 x 10^4	26.7	0.6	198
1.6 x 10^4	25.4	0.7	213
7.9 x 10^3	27.3	0.6	153
3.2 x 10^3	28.2	0.8	114
1.6 x 10^3	28.5	0.6	86
7.9 x 10^2	27.9	0.7	45
3.2 x 10^2	24.9	1.1	39
1.6 x 10^2	27.1	2.1	33
7.9 x 10^1	27.5	2.5	33

Figure 5.18. 9aMMD exhibits properties of a processive molecular motor. A plot shows 9aMMD velocity (nm/s) as a function of the surface motor density (μm^{-2}). The table summarizes velocities at decreasing motor densities. Indicated motor densities of biotinylated 9aMMD-Avi were deposited on a streptavidin-covered coverslip and motility was initiated and traced as before. Sliding velocities of actin filaments were quantified and data points represent average velocities ± S.D. Three independent flow cells were prepared for each myosin density. The number of filaments tracked for each motor density is indicated in the table.

CHAPTER 6: DISCUSSION

Based on the primary protein sequence similarity of the motor domains, the myosin superfamily is composed of 35 classes and 149 sequences that cannot be assigned to any of the classes (Odronitz and Kollmar, 2007). Myosins exhibit the same structural organization, in that they are composed of a globular N-terminal head that can progress through the mechanochemical cycle, a regulatory neck domain that serves to amplify the step size, and a C-terminal tail domain with highly divergent functional domains. However, considerable differences in rate constants of the enzymatic cycle steps, actin affinity and rates of motility exist even when one considers myosins assigned to a single class. Additionally, some myosins are processive, high duty ratio motors, whereas others undergo only one step on actin before dissociating. For example, human myosin 5c was suggested to spend most of its ATPase cycle in a weak actin-binding form and did not exhibit processive movement on actin (Watanabe et al., 2008), as opposed to highly processive myosin 5a which exhibits high duty ratio properties (De La Cruz, 1999; Moore et al., 2001). Taken together, myosin motors have their enzymatic properties tailored to suit their cellular tasks, specified by the versatile tail domains (De La Cruz and Ostap, 2004; Sellers, 1999).

Due to the presence of a RhoGAP domain in the tail, the physiological role of myosin 9 is highly unique within the superfamily. It was proposed before that myosin 9 regulates the architecture of actin filaments it moves along (Bähler, 2000). This poses an intriguing possibility that myosin 9 is a motorized signaling molecule. However, how myosin 9's mechanochemical performance is coupled to its signaling role is unknown. In order to tackle that problem, one first needs to characterize its *in vitro* biochemical properties. Here, I showed that a previously uncharacterized protein, human myosin 9a, exhibits features of a myosin: i) it binds actin, ii) it hydrolyzes ATP, iii) it undergos ATP-dependent motility.

6.1. Cloning, expression and purification of enzymatically active human myosin 9a

Previous attempts to obtain recombinant myosin 9a have not been successful, with many of them fruitless at the level of gene amplification (personal communication with Dr. N Billington, NIH and Dr. C Batters, LMU). Here, I cloned strategic protein fragments and produced recombinant baculoviruses for protein expression in the baculovirus/insect cell system. The main advantage of that expression system over a bacterial system is that it provides eukaryotic capabilities of the protein translation and post-translational modifications machinery (Busconi and Michel, 1995). It therefore is a system of choice for expression of myosin motors.

I successfully cloned human myosin 9a truncations and created recombinant bacmids with the Bac-to-Bac system (Invitrogen). Bacmids were generated in genetically engineered *E.coli* cells that support an efficient site-specific transposition of a gene of interest from the donor pFastBac plasmid into a shuttle bacmid vector. All bacmids generated with that system contained the appropriate myosin 9a fragments. SF9 cells transfected with bacmid DNA showed signs of virus production – increased cell diameter, inhibited cell growth and eventually cell lysis.

The sequence borders of the strategic regions of human myosin 9a were assigned based on sequence alignments with *Dictyostelium* myosin 2 (Figure 3.3). It is known that the minimal sequence requirement for an enzymatically active motor of Dictyostelium myosin 2 contains amino acid residues E89-I759 (personal communication with Dr. J Sellers, NHLBI, NIH; Kuhlman and Bagshaw, 1998; Woodward et al., 1995). Therefore, the minimal motor domain of human myosin 9a is expected to be composed of D149-H1016. Amino acid residues upstream of D149 were assigned to be the class-specific N-terminal extension. The neck region in *Dictyostelium* myosin 2 contains only 2 IQ motifs, and finishes at W808. Additional 3 putative light chain-binding sites, as compared to *Dictyostelium* myosin 2, extend the neck domain of human myosin 9a. Based on the localization of the IQ motifs following the motor domain of human myosin 9a, its neck domain finishes with F1152. The remaining sequence was assumed to form a C-terminal tail. Thus, individual human myosin 9a fragments were designed to encompass the strategic

residues; the first 1019 and 1162aa encompass the full head or head-neck regions of 9a-Head and 9a-S1, respectively. The minimal motor domain constructs start with D149 and finish with V1019 and E1162 for proteins without and with the neck domain. It has been established that the light chain-binding region of myosin is not required for the normal ATPase activity, but amplifies the motility rate (Kurzawa et al., 1997; Woodward et al., 1995; Kuhlman and Bagshaw, 1998; Waller et al., 1995). Therefore, it was expected that human myosin 9a constructs truncated at V1019 should exhibit normal ATPase properties of the intact molecule. The goal of adding the light chain-binding domain (constructs truncated at E1162) was to investigate its effect on the motility rate of myosin 9a.

Protein expression was assessed based on the presence of a protein band on SDS-PAGE gels corresponding to an appropriate molecular weight in cell lysates after virus amplification. This was followed by initial purification trails of GFP-9a-Head and GFP-9a-S1 by means of a His-tag affinity chromatography. The fluorescent tag provided means for quick analysis of protein solubility and binding to the resin. Protein yields obtained by the His-tag affinity purification were low, and many by-products were present in the eluates. Based on the visual inspection, lots of protein was in an insoluble form. In order to improve the solubility, 1% Sarkosyl was used to disrupt protein aggregates. Indeed, when purified on the HisTrap affinity chromatography after Sarkosyl extraction, I obtained highly pure fractions of human myosin 9a motor constructs. Unfortunately, the protein did not show any activity in the *in vitro* motility assay and did not hydrolyze ATP as assessed by the NADH-linked ATPase assay. Supposedly, the use of Sarkosyl resulted in the loss of the enzymatic activity by myosin 9a. Therefore, means of obtaining highly pure proteins under native conditions had to be established.

In order to achieve more specific capture of the protein on the resin, I added a C-terminal FLAG tag to non-fluorescent or GFP-tagged 9a-Head and 9a-S1 constructs. I chose to continue with the fluorescent variants at this stage to be able to quickly assess protein amount in the soluble fraction. Additionally, a GFP-tag served as a marker for assessing cell disruption by sonication. Beforehand, cells expressing GFP were clearly distinguished in the fluorescent microscope. Following the sonication, no intact cells were seen in the field of view. Simultaneously, the time-dependence of the total amount of

expressed protein was assessed by SDS-PAGE analysis of whole cell lysates 24, 48, 60 and 72h post-infection with myosin 9a virus. The maximum amount of protein expressed was achieved at the 48h time point, and no further increase in the yield was observed with time. Therefore, 48h expression time was chosen as the most optimal. The presence of the protein in the soluble fraction was directly proved by an anti-FLAG western blot. GFP-9a-S1 contains 7 putative CaM-binding sites (one in the class-specific loop 2 insert and 6 in the neck domain) and therefore its level of expression was suspected to be dependent on the amount of CaM present in cells. Indeed, when expressed with varying amounts of CaM virus, the yield of GFP-9a-S1 in the eluate varied greatly. Taken together, performing the analysis of time-dependent protein expression and CaM coexpression on the protein yield turned ut essential for establishing a successful expression protocol for obtaining highest yields of myosin 9a possible. Simultaneously, capture of the protein on the FLAG resin resulted in much more pure protein preps and yields compared to the His column. It is worth mentioning that the amount of the FLAG resin (1ml) used was 5 times lower than the volume of the His column (5ml) and could contribute to the purification results. Nevertheless, protein samples obtained from the FLAG-tag affinity purification contained 3 proteins as characterized by SDS-PAGE: ~160 kDa which matched the molecular weight expected for the heavy chain of GFP-9a-S1, ~18 kDa which matched the expected CaM MW and ~100 kDa which corresponded to an uncharacterized by-product of the FLAG affinity. Given the relative amounts of the proteins present in the FLAG eluate, it was necessary to remove the ~100 kDa purification by-product. Since the sample was stable in 100mM NaCl buffer (no visual precipitation occurred), it was applied to an ion exchange resin. Elution with an increasing ionic strength resulted in the separation of myosin 9a from the nonspecific by-product. The same purification protocol was successfully employed for the purification of GFP-9a-Head and the Minimal Motor Domain constructs. Therefore, a two-step purification procedure involving the FLAG-tag affinity chromatography followed by ion exchange was established as a general method for obtaining homogenous human myosin 9a preps. The established protocol resulted in ~0.6mg pure myosin 9a fractions from 1 x 10^9 cells. The yields obtained were enough to investigate the mechanical, actin-binding and enzymatic properties of the human myosin 9a motor.

Human myosin 9a constructs containing the full head domain hydrolyzed ATP but the basal ATPase rate was not stimulated by actin (discussed in the following section). I considered the possibility that the N-terminal extension of human myosin 9a might affect its intrinsic ATPase properties. In order to investigate it, constructs containing the minimal motor domain (9aMMD and 9aMMD-S1) were developed. Given that the expression procedure developed for GFP-9a-S1 was successful, I no longer needed a fluorescent marker on the minimal motor domain constructs. Furthermore, an expression of GFP alone might happen with fluorescently tagged proteins, unnecessarily engaging the host translational machinery in translation of an off-target protein. Nonetheless, the yields of the minimal motor domain constructs were comparable to those containing the full head region of myosin 9a.

Since there was no significant difference between the ATPase properties of the full head and the minimal motor domain constructs, most of the following experiments focused on the minimal motor domain proteins.

There are 7 putative light chain-binding sites in the S1 region of human myosin 9a – one in the loop 2 insert and 6 in the neck domain. All of them belong to the family of IQ motifs, which are most often occupied by calmodulin light chains (Atcheson et al., 2011). In order to establish if all putative CaM-binding sites in 9a-S1 bind CaM, I quantified the number of CaM molecules bound to 9aMMD and 9aMMD-S1. 9aMMD bound a single CaM light chain, whereas 9aMMD-S1 bound 6. Therefore one IQ motif in 9a-S1 is expected to be unoccupied by CaM. It is possible that one of the IQ motifs in the neck region does not bind CaM. This could be caused by: i) the transient nature of the interaction between CaM and an unoccupied IQ motif in the neck, ii) a complete lack of binding of CaM to an IQ motifs, iii) a requirement for a different light chain. It has been shown before that *C.elegans* myosin 9, which contains 5 putative CaM-binding sites, binds only 4 CaM molecules. One of the IQ motifs in the neck region had a conserved glycine in a consensus sequence IQXXXRGXXXR substituted for lysine (Liao et al., 2010). Substitution at this position could hinder binding of CaM in a compact conformation, leading to a complete loss of CaM binding (Terrak et al., 2005). Indeed, the 5^{th} IQ motif in the neck domain of

human myosin 9a also has glycine substituted for lysine. Therefore it is possible that this particular IQ motif is unoccupied by CaM in human myosin 9a S1.

Proteins were used fresh within two days after the purification and thus the stability of the preps within that time period was established for the minimal motor domain constructs. Assuming that protein degradation within 48h could lead to loss of the enzymatic and mechanical activity, Dynamic Light Scattering was used to assess time-dependent changes in the molecular composition of the samples. In principle, the system measures the diameter of the protein species present in the sample, assuming that the diameter of each molecule corresponds to a minimal sphere that could be drawn around the molecule. Diameters measured for 9aMMD and 9aMMD-S1 were ~8 and 11nm, respectively. 8nm diameter for 9aMMD is in good agreement with what is expected for a single globular myosin head (Morel et al., 1992). If one assumes the the neck domain of a myosin forms a rigid α-helical rod extending from the head domain, the measured diameter of 9aMMD-S1 seems a bit small as compared to 9aMMD. It was suggested previously that each CaM-occupied IQ motif in the neck region of an unconventional myosin has ~3.6nm in length (Tominaga et al., 2012). Assuming that only 5 IQ motifs in the neck region of 9aMMD-S1 are occupied by CaM, this would result in ~18nm long neck. If the neck of 9aMMD-S1 is rigid and extended, the diameter measured by DLS should be much higher than 11nm. It is possible, however, that the neck of 9aMMD-S1 is wrapped around the head domain. Such structural orientation of the neck domain of 9aMMD-S1 is in great agreement with the fact that there was no electron density corresponding to an extended α-helix in the electron micrographs of 9aMMD-S1. Why the neck domain remained wrapped around the head domain in 9aMMD-S1 is not known, but it is possible that the neck domain was not saturated with CaM light chain molecules, as suggested above. This could result in the loss of the rigidity of the neck region of the myosin (Lin et al., 2005; East and Mulvihill, 2011). IQ motifs are hydrophobic in nature and if unoccupied by a light chain could form interactions with other areas of the protein.

Initial attemps at expressing the full length human myosin 9a protein proved fruitless. Despite the successful bacmid and baculovirus generation, there was no protein present in whole cell lysates, as assessed by SDS-PAGE and a western blot. It is possible

that the expression of that protein is too challenging for the host insect cells. It could be tackled by varying the amount of the baculovirus used for cell infection or by codon-optimization of the template DNA.

6.2. Oligomerization state of human myosin 9a

Based on the sequence analysis of full length human myosin 9a, there are two putative coiled-coil regions in its tail domain. This is in great contrast to human myosin 9b and its orthologs, which do not contain any putative coiled-coil regions. It was proposed before that myosin 9 functions as a single-headed processive motor on actin (Inoue et al., 2002; Nishikawa et al., 2006; Liao et al., 2010). The presence of putative coiled-coils in the tail domain of human myosin 9a was suprising, and could suggest that this motor forms dimers under appropriate conditions in the cellular environment.

The tail fragments encompassing the putative coiled-coil regions of human myosin 9a were expressed in a bacterial host and purified to homogeneity by means of the His-tag affinity chromatography. The propensity to dimerize was tested under varying ionic strength conditions by a combination of gel filtration and sucrose density gradient centrifugation. Higher ionic strength can lead to higher helicity of isolated protein fragments and therefore increase the propensity to dimerize (Mateja et al., 2006). Indeed, the tail fragment encompassing the first putative coiled coil region of human myosin 9a dimerized at higher ionic strength, as evident in two times higher native molecular weight than at lower ionic strength (Figure 3.23).

The Paircoil2 analysis of protein sequences automatically assigns individual residues within a putative coiled-coil sequence to their positions within the heptad repeat (McDonnell et al., 2006). Residues at positions ‘a’ and ‘d’ of the heptad repeat are predicted to be apolar and in a native molecule face the hydrophobic core of the coiled-coil (Burkhard et al., 2001). The sequence of the putative coiled coil of myosin 9a with the assignment to the position within the heptad repeat is shown in Figure 3.20. Closer examination of the primary sequence of that putative coiled-coil reveals the majority of the amino acids within it are polar and charged, with only four hydrophobic residues present at

the strategic ‘a’ and ‘d’ positions out of the total of 9 assigned strategic hydrophobic positions. The remaining 5 ‘a’ and ‘d’ positions are occupied by charged or polar amino acids, such as K, E, R (charged), Q and T (polar). The occupancy of ‘a’ and ‘d’ positions by hydrophobic residues is the main factor contributing to the stability of coiled-coil (Wagschal et al., 1999; Tripet et al., 2000), suggesting that in a native protein no coiled-coils would be formed by that sequence. On the other hand, the majority of ‘e’ and ‘g’ residues within the myosin 9a putative coiled-coil are charged, able to form interchain salt bridges and electrostatic interactions that could increase the stability of the coiled-coil. Similarly, mainly charged and polar residues occupy the ‘b’, ‘c’, and ‘f’ positions in the myosin 9a sequence. Residues at those positions are surface-exposed in native coiled-coils (Burkhard et al., 2001). Based on the data presented in this work, the helicity of the putative myosin 9a coiled-coil sequence, and therefore the propensity to form a coiled-coil, is affected by the buffer composition. A potential mechanism regulating the helicity of that region in a native molecule could also contribute to the stability of the coiled-coil.

Many myosin motors contain putative coiled-coil sequences but not all of them are involved in the dimerization of heavy chains. For example, a proximal (N-terminal) part of the myosin 10 tail was predicted to form a coiled-coil based on the primary sequence. Yet, closer investigation revealed that this region forms a single α-helix that served to extend the step size of the myosin (Knight et al., 2005). On the other hand, the putative coiled-coil sequence of myosin 6 is composed of ~150aa, yet the protein does not dimerize on its own and requires binding partners to regulate its dimerization (Park et al., 2006; Phichith et al., 2009). In comparison, both myosin 2 and myosin 5 form stable dimers (Syamaladevi et al., 2012).

In order to investigate the propensity of the native human myosin 9a to dimerize, longer myosin 9a fragments, containing the putative coiled-coil region need to be expressed and purified. It would be interesting to investigate the effect of dimer formation on the mechanochemical activity and the cellular function of human myosin 9a.

6.3. Steady-state ATPase activity of human myosin 9a

The reported maximum ATPase rates of myosin 2 S1 can vary by an order of 10, from 7.8 s^{-1} (Webb and Corrie, 2001) to 29 s^{-1} (Trentham et al., 1976). Such differences might arise from different buffer agents used, different temperature at which experiments were performed or the type of muscle used for the preparation of muscle myosin S1. Nevertheless, the ATPase rate of muscle myosin S1 was stimulated ~100 times (from 0.06 to 7.5 s^{-1}) with half maximal activation at 15μM F-actin, which is in good agreement with reported values. Thus, the buffer composition and actin preparation are compatible with an intrinsic ATPase activity of a myosin.

The basal ATPase rates of myosin 9 isoforms differ significantly between ~0.1-2.5 s^{-1} (Liao et al., 2010; Struchholz et al., 2008). Similarly, some authors report actin-activated ATPase activities of myosin 9 (Nalavadi et al., 2005), whereas others show that the enzymatic activity of myosin 9 is very poorly (~2 times) activated by actin (Kambara and Ikebe, 2005; Struchholz et al., 2008; Liao et al., 2010).

Human myosin 9a truncations, involving the full head or the minimal motor, either with or without the neck domain, all hydrolyzed ATP in the absence of actin at similar rates 0.12-0.18 s^{-1}. Such relatively high basal rate of ATP hydrolysis is unique among the myosin superfamily members. However, the basal ATPase rates of human myosin 9a truncations are in good agreement with the values reported for full length rat myosin 9b with and without the N-terminal extension (Nalavadi et al., 2005). This suggests that neither the tail nor the N-terminal extension participate in the regulation of the basal ATPase activity of myosin 9.

Liao et al., reported that in the absence of Ca^{2+}, the catalytic activity of the head domain of *C.elegans* myosin 9 was stimulated ~5 times by actin, whereas the actin activation of the head-neck construct was negligible (Liao et al., 2010). This would suggest that the neck domain negatively regulates the ATPase activity of myosin 9. However, this is in great contrast to the previously established lack of the ATPase regulation by the neck region (Kurzawa et al., 1997; Woodward et al., 1995; Kuhlman and Bagshaw, 1998; Waller et al., 1995) and to my results on human myosin 9a. It is possible that the neck domain of

the construct used by Liao et al. folds back onto the head domain, as observed in EM images of human myosin 9a S1. The conformation of the molecule in such state could hinder binding of myosin to actin, which would explain the discrepancy between the observed actin-activated ATPase activity of two *C. elegans* myosin 9 constructs. Nevertheless, the activity of human myosin 9a truncations with or without the neck domain was stimulated by actin, which suggests that the neck of human myosin 9a does not regulate the actin-activated ATPase activity of human myosin 9a, in agreement with previously reported data (Kurzawa et al., 1997; Woodward et al., 1995; Kuhlman and Bagshaw, 1998; Waller et al., 1995).

Actin did not stimulate the basal ATPase rate of human myosin 9a in the absence of Ca^{2+}, in great contrast to full length rat myosin 9b which was stimulated 10-20 times (Nalavadi et al., 2005). This might suggest that the tail region participates in the regulation of the actin-activated ATPase activity of myosin 9. It is worth mentioning that Nalavadi et al. performed their experiments at 37^0C (as opposed to 22^0C in this study) in MOPS-HEPES buffer and the extent of actin activation was dependent on the concentration of MOPS and HEPES in their buffers. On the other hand, the head domain of *C. elegans* myosin 9 was stimulated ~5 times in the absence of Ca^{2+} (Liao et al., 2010), suggesting that the motor domain of myosin 9 is enough for an actin-activation of the basal ATPase rate.

Neither the basal nor the actin-activated ATPase rate of human myosin 9a were dependent on ionic strength of the buffer, presence of exogenous calmodulin or phalloidin-stabilization of F-actin. This suggests that the lack of the increase in the maximal ATPase rate as compared to the basal rate lies within the sequence or structural organization of human myosin 9a.

The lack of actin-activation of the basal ATPase rate of human myosin 9a was suprising, especially since the protein clearly was enzymatically active. Amino acid substitutions in conserved regions of the active site elements could contribute to the lack of actin-activation of the ATPase rate of human myosin 9a. Both switch 1 (consensus sequence: NXNSSRFGK) and switch 2 (consensus sequence: DIXGFE) are conserved in human myosin 9a (switch 1 sequence: NNNSSRFGK, switch 2 sequence: DIFGFE). The P-loop (conserved sequence: GESGAGKT) is involved in the coordination of ATP in the

active site and participates in the cleavage of γ-phosphate. The conserved A is substituted for S in human myosin 9a as well as rat myosin 9b and *C. elegans* myosin 9. However, considering structural similarities of those two amino acids, it seems unlikely that this amino acid substitution could be responsible for the lack of actin-activation of human myosin 9a.

Other structural elements within the myosin molecule have also been suggested to participate in the actin activation of the ATPase rate of myosins. For example, a TEDS site within the CM loop contains one of the indicated amino acids at the position corresponding to D403 in *D. discoideum* myosin 2 (Kollmar, 2002). The enzymatic activity of myosin motors with T or S at this position is subject to regulation by phosphorylation, whereas E or D are present in constitutively active myosin motors. A position corresponding to *D. discoideum* D403 is occupied by E480 in human myosin 9a sequence, suggesting that the enzymatic activity of those myosins is not regulated by phosphorylation at this site. Right upstream of the CM loop is conserved R397 (in *D. discoideum* sequence) that is essential for actin-activation of the ATPase (Sasaki et al., 1999). Positively charged K474 in human myosin 9a occupies that position. Finally, a recently characterized activation loop (Várkuti et al., 2012) contains a conserved positively charged residue at position corresponding to R520 in *D. dictiostelium* sequence. That position is occupied by K601 in human myosin 9a. Taken together, the analysis of the primary sequence of human myosin 9a predicts it is a constitutively active, actin-activated molecular motor, and does not suggest any reason for the lack of actin activation.

The mechanism of the activation of the ATPase rate of myosin by actin involves acceleration of the hydrolysis product release rate upon strong binding to actin. This ensures that force production occurs in an actin-bound state of myosin and limits futile kinetic pathways (Holmes et al., 2003). The rate of the ATPase rate observed in the NADH-linked assay is directly associated with the rate of ADP release by myosin. The lack of increase in the ATPase rate as observed in the assay suggests there is no increase in the rate of ADP release by human myosin 9a as compared to its basal rate. This suggests that human myosin 9a might not bind actin in the presence of ATP or that it is unable to undergo a transition from a weakly-bound to a strongly-bound state. Steady-state actin

cosedimentation assays clearly showed that human myosin 9a binds actin in the presence of nucleotides, therefore excluding the former possibility. However, it cannot be excluded that the latter mechanism contributes to the lack of actin activation of the ATPase rate of human myosin 9a in the absence of Ca^{2+}. Fluorescence anisotropy experiments with pyrene-actin would need to be performed to investigate strong actin binding of myosin 9a in the presence of the nucleotide.

Finally, the loop 2 of myosin 9 is greatly extended as compared to other myosin superfamily members, and was suggested to bind calmodulin (Liao et al., 2010). The N-terminal part of loop 2 of human myosin 9a also contains a CaM-binding site. The head of human myosin 9a copurifies with calmodulin, and based on sequence similarities with other myosin 9 members this specific IQ motif in loop 2 is expected to be the CaM-binding site in the head. Loop 2 is the primary actin interaction site in myosin and participates both in weak and strong interactions (Lorenz and Holmes, 2010; Behrmann et al., 2012). It is plausible that the head-bound CaM regulates human myosin 9a interactions with actin in a Ca^{2+}-dependent manner. In line with that, supplementing ATPase reactions with Ca^{2+} led to nearly 4-fold activation of the basal ATPase rate of the motor domain by actin. The regulation of the actin interaction could occur by one of the two mechanisms: i) Ca^{2+}-induced CaM dissociation from the head or ii) Ca^{2+}-induced conformational change of CaM that would stabilize a specific loop 2 conformation, compatible with the acceleration of the ADP release rate. It was shown that as high as 1mM Ca^{2+} does not lead to the dissociation of CaM from the motor domain, thus leaving only the 2nd option as a valid mechanism of regulation. Ca^{2+} did not affect the steady-state binding of the myosin 9a motor to actin in the presence of ATP. Fluorescence anisotropy experiments would need to be performed in order to investigate the effect of Ca^{2+} on strong actin binding by human myosin 9a. It would also be interesting to analyse the interactions between CaM and the loop 2 insert. Ca^{2+} binding to CaM might regulate the affinity of CaM binding to its target site. This in turn could affect the helicity of the target site and result in conformational rearrangements of the neighbouring region (Bähler and Rhoads, 2002). A specific conformation of loop 2 has been proposed before as a contributing factor to strong actin binding by myosin (Lorenz and Holmes, 2010).

The Ca^{2+}-mediated actin-activation of the motor domain of human myosin 9a is in great contrast to Ca^{2+}-induced inhibition of actin activation of the *C. elegans* myosin 9 motor (Liao et al., 2010). The CaM-binding site in the loop 2 insert is conserved within myosin class 9 and belongs to the family of 1-8-14 CaM-binding motifs, characterized by the presence of hydrophobic residues at positions 1, 8 and 14 of the motif. Both *C. elegans* myosin 9 and human myosin 9a contain W, F and F and corresponding positions. Therefore, sequence differences do not underlie the observed differences in the effect of Ca^{2+} on the actin-activated ATPase activity of those myosins. It is plausible that specific interaction mechanisms between CaM and the loop 2 insert of those two myosins constribute to observed differences in ATPase activities.

6.4. Human myosin 9a interactions with actin

It was suggested before that the myosin 9 class-specific insert in loop 2 acts as an additional actin-binding site, enabling crosslinking of actin filaments by myosin 9 (Reinhard et al., 1995; Post et al., 2002; Inoue et al., 2002; Struchholz et al., 2009). The isolated loop 2 of rat myosin 9b was shown to bind actin with high affinity and was proposed to remain bound to actin even in the presence of ATP (Nalavadi et al., 2005; Struchholz et al., 2009).

The ability of human myosin 9a to cross-link F-actin was tested indirectly by low-speed actin sedimentation assays and directly by electron microscopy. Actin was mixed with an increasing amount of myosin and subjected to low-speed centrifugation. Under these conditions, individual actin filaments remain in the solution. Increasing amount of myosin caused sedimentation of actin filaments, suggesting they are being crosslinked by myosin. The native molecular weight of bundled filaments is sufficient to drive their sedimentation. Negatively stained images of the minimal motor domain of human myosin 9a with phalloidin-stabilized F-actin confirmed that myosin 9a crosslinks actin filaments. Upon incubation of 9aMMD with F-actin, two or more filaments were crosslinked by regularly interspaced molecules. Actin filaments in the bundles appeared stiffer and more rigid than individual actin filaments. The molecules dissociated in the presence of ATP, leaving undecorated actin filaments. That confirms that catalytically active motor heads

caused actin cross-linking. Actin crosslinking by myosin 9a also directly demonstrates that myosin isoform is able to interact with actin, and that actin binding by myosin 9a is ATP-dependent.

Actin crosslinking by myosin was previously shown for *Acanthamoeba* myosin 1 (Fujisaki et al., 1985), brush border myosin 1 (Coluccio and Bretscher, 1987), liver myosin 1 isoforms (Coluccio and Conaty, 1993; Stafford et al., 2005) and was accounted for by the presence of an additional actin-binding site in the tail of those monomeric myosins (Hammer et al., 1991). 9aMMD is also monomeric in solution, as confirmed by negatively stained EM images and native molecular weight measurements performed by a combination of gel filtration and sucrose density gradients. That construct was enough to crosslink F-actin. Together with the fact that 9aMMD exists as a monomer in solution, it indicates that the second actin-binding site of human myosin 9a is localized within 149-1019aa of the protein. Based on previous reports, the loop 2 insert is the predicted second actin-binding site of human myosin 9a; nevertheless, studies with an isolated human myosin 9a loop 2 and with myosin 9a mutants lacking the insert would need to be performed to unequovically confirm the role of the insert in cross-linking actin filaments.

Crosslinking of actin filaments increases stiffness of organized actin structures and is responsible for tension generation in cells. Spatiotemporal regulation of such structural rearrangements is necessary for cell migration, division and morphology (Esue et al., 2009; Stafford et al., 2005). In line with that, depletion of myosin 9a caused defects in the stabilization of protrusive actin structures essential for maintenance of cell-cell junctions, ultimately hindering collective cell migration in human bronchial epithelium (16HBE) cells (Omelchenko and Hall, 2012).

The binding affinity of myosin 9a to actin was measured in actin cosedimentation assays. In nucleotide-depleted conditions that enable formation of rigor complexes of actin and myosin, all myosin bound to actin with high affinity (K_d = 425nM). Full depletion of a nucleotide was achieved by addition of EDTA that sequesters Mg^{2+}, and apyrase that cleaves nucleotides. In the presence of ADP and ATP, the amount of myosin that bound to actin decreased to ~70 and ~60%, respectively. The binding affinity in the presence of ADP was slightly smaller than in rigor, wherease the presence of ATP caused ~2-fold decrease in

the affinity as compared to rigor conditions. A fraction of myosin 9a pelleted on its own in the presence of a nucleotide, raising a possibility that a decrease in the maximum amount of myosin bound to actin under those conditions might result from myosin denaturation or aggregation. However, when unbound myosin fraction was remixed with actin, part of it associated with filaments. Therefore, human myosin 9a exists in two subpopulations – one compatible and one incompatible with binding actin. These two subpopulations exist in dynamic equilibrium and interconvert on a timescale of the experiment. The fraction of human myosin 9a that binds to actin in a weak binding state exhibits a relatively high binding affinity (K_d = 810nM in the presence of ATP). The extended loop 2, which is positively charged, could be responsible for tethering myosin to actin in the presence of ATP. Similar behavior was previously described for other myosin 9 isoforms (Nalavadi et al., 2005; Struchholz et al., 2009).

The high affinity actin binding of human myosin 9a in a weakly bound state clearly suggests that the lack of an actin-activated ATPase activity does not result from the lack of myosin binding to actin in the presence of nucleotides, as discussed above. This further supports the idea that the only possibility why myosin 9a is not activated by actin is abnormal 50kDa cleft dynamics. The opening and closing of the cleft, related to the transition between strongly and weakly bound states, could be affected by a specific spatial arrangement of loop 2, a nucleotide present in the active site and/or strain.

Presence of Ca^{2+} resulted in actin activation of the ATPase of myosin 9a, therefore suggesting normal cleft dynamics are Ca^{2+}-dependent. As proposed before, such mechanism could involve binding of Ca^{2+} to loop 2-bound CaM, ultimately causing it to adopt a specific spatial arrangement, compatible with closing of the cleft and formation of a strongly bound myosin state. Addition of Ca^{2+} to cosedimentation assays did not influence the affinity of binding in the presence of ATP under steady-state conditions. The exact mechanism of the transition between weakly and strongly bound actin states in the presence of nucleotides remains to be investigated.

6.5. Mechanical properties of human myosin 9a

Based on sequence analysis of human myosin 9a and previous reports regarding the mechanical activity of other myosin 9 isoforms (Post et al., 2002; Liao et al., 2010; Inoue et al., 2002), human myosin 9a was expected to exhibit mechanical activity and translocate fluorescent actin filaments in the *in vitro* motility assay. Assay conditions used in this work were compatible with robust translocation of actin filaments by rabbit skeletal muscle HMM. The velocities obtained by me were comparable to reported values. Therefore, the assay conditions should support motility of myosin 9a, provided it is a mechanically active motor.

When immobilized nonspecifically on a nitrocellulose-covered coverslip, all myosin 9a constructs released and reattached to actin filaments. Therefore, myosin 9a is able to undergo ATPase cycles when deposited on the flow chamber surface. However, none of the constructs used translocated actin filaments. This could be due to intrinsic inability of myosin 9a to move on actin; alternatively, the conformation of myosin on the nitrocellulose surface inhibits mechanical activity of myosin 9a. In order to tackle the problem of the surface conformation of myosin that is incompatible with motility, I designed, cloned, expressed and purified minimal motor domain constructs with or without the neck region, fused to a C-terminal Avi-tag for a site-specific biotinylation of the protein. Expression and purification protocols described previously, combined with incubation of cell slurry with biotin and BirA ligase in the presence of ATP, were successfully applied to obtaining biotinylated fractions of 9aMMD and 9aMMD-S1. Protein biotinylation was confirmed with a western blot against biotin and proteins were immobilized via a biotin-avidin linkage on the surface of the flow chamber. This ensures specific conformation of myosin on the surface, with its motor domain facing the flow chamber, facilitating interactions of myosin with actin and progression through the mechanochemical cycle. The site-specific immobilization of human myosin 9a constructs on the surface resulted in robust translocation of actin filaments. Therefore, human myosin 9a is a mechanochemically active motor and could move along actin filaments in cells.

Previous reports suggest that adding methylcellulose to motility assays is necessary to maintain translocation of actin filaments by myosin 9 isoforms (Liao et al., 2010; Elfrink

et al., 2014). Methylcellulose is a viscosity agent that compensates for the lack of weak actomyosin interactions and serves to keep actin filaments close to the surface of the flow chamber facilitating actin movement by myosin (Bobkov et al., 1996). However, the sliding velocity of 9aMMD in the presence and absence of methylcellulose was nearly identical and no abrupt dissociation of filaments from the surface was observed. This suggests that, in contract to other myosin 9 isoforms, weak actomyosin interactions are not hindered in myosin 9a.

Since addition of Ca^{2+} to ATPase reactions stimulated the actin-activated ATPase activity of 9aMMD and switched on coupling between the actin- and nucleotide-binding sites, it was surprising the motor moved actin in the absence of Ca^{2+}. Furthermore, addition of 100μM Ca^{2+} to the motility buffer did not increase the sliding velocity of 9aMMD. If Ca^{2+} is necessary to restore normal actin cleft dynamics of myosin 9a, as proposed above, Ca^{2+} should influence the ability and/or velocity of actin gliding. The lack of the effect of Ca^{2+} on the motility of 9aMMD could only be explained if the site-specific immobilization of 9aMMD on the coverslip surface positions it in a conformational state that is compatible with normal cleft dynamics, progression through the mechanochemical cycle and translocation of actin filaments, regardless of the presence or absence of Ca^{2+}. Addition of exogenous CaM also did not affect the velocity or the actin-activated ATPase activity of 9aMMD, indicating that after purification the motor maintains its stability and can perform its mechanochemical activities.

9aMMD sliding velocity was ionic strength-dependent, showing peak velocity at 200mM KCl. Above 200mM KCl, the sliding velocity as well as the number of filaments tethered to the surface drastically dropped. Still, a fraction of filaments was observed to move at as high as 500mM KCl. This indicates high affinity actomyosin interactions of human myosin 9a.

The affinity of ATP binding by 9aMMD in the presence of actin was assessed by measuring sliding velocities of 9aMMD at increasing [ATP]. The obtained K_{ATP} value (0.37mM) is well below 2mM used for ATPase experiments, therefore confirming the amount of ATP in those reactions was not limiting and could not be responsible for the observed lack of actin activation in the absence of Ca^{2+}.

Furthermore, 9aMMD moved actin with the speed of ~35nm/s. This is not exceptionally fast when compared to most myosins (for example, rabbit skeletal HMM moved 5.5μm/s in my assays), but it is faster than some other myosins (for example *Leishmania* myosin 21 moved ~16nm/s; Batters et al., 2012). Considering that 9aMMD consists of the motor domain alone and lacks the neck domain, which increases the step size in other myosins, it was surprising it moved with such relatively high velocity. This suggests that the fulcrum point over which the neck domain of myosin 9a would rotate is located closer to the core of the motor, upstream of the last amino acid of 9aMMD construct.

Previously it was proposed that the neck domain of myosin 9 does not act as a lever arm, i.e. that it does not increase the speed of actin movement (Liao et al., 2010). I addressed that issue by investigating motility properties of 9aMMD-S1, site-specifically immobilized on the surface of the flow chamber. The motor robustly translocated actin filaments at higher rates than 9aMMD, clearly showing that the neck domain of human myosin 9a acts as a lever arm. The rate of 9aMMD-S1 movement was nearly 6 times faster than that of 9aMMD (Figure 6.1)

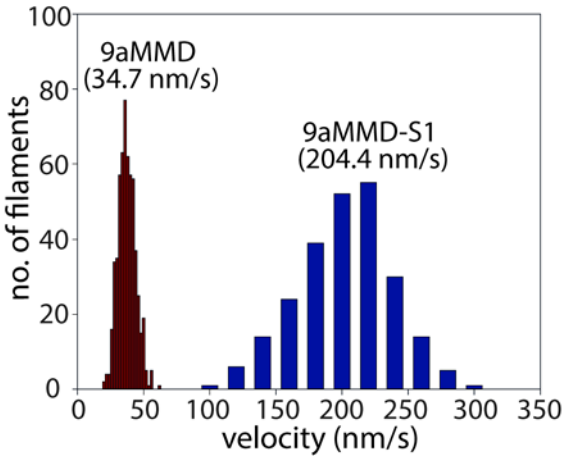

Figure 6.1. A velocity distribution plot of 9aMMD and 9aMMD-S1 at 100mM KCl. Experiments were performed as described in previous chapters. 9aMMD-S1 translocated actin filaments at 204.4nm/s, nearly 6 times faster than 9aMMD (34.7nm/s). Therefore, the neck domain of human myosin 9a acts as a lever arm to increase the step size.

9aMMD-S1 motility was observed only in the presence of exogenous CaM in the motility buffer. This again suggests that at least one IQ motif in the neck domain of human myosin 9a might not be saturated with CaM. This could be caused either by weak interactions of the IQ motif with CaM or by the preference towards binding a different light chain. In the absence of exogenous light chain, the neck domain could not be rigid enough to support motility. Supplementing the motility buffer with subsaturating CaM concentration could support association of the unoccupied IQ motif with CaM, providing enough rigidity of the lever arm to facilitate movement.

Adding as little as 2μM Ca^{2+} to the motility buffer fully inhibited actin translocation by 9aMMD-S1, even in the presence of exogenous CaM. This suggests that Ca^{2+} effectiviely prohibits binding and/or causes dissociation of CaM from the neck of 9aMMD-S1. In order to investigate the effect of Ca^{2+} on the association of CaM light chains with 9aMMD-S1, myosin was bound to actin in the absence and presence of increasing [Ca^{2+}] and subjected to ultracentrifugation. Equal volumes of supernatant and pellet were separated on SDS-PAGE gels. CaM found in the pellet fraction represents myosin-associated light chain molecules, whereas CaM found in the supernatant represents CaM molecules that dissociated from myosin. Surprisingly, even in the absence of Ca^{2+}, a fraction of CaM was found in the supernatant. And, based on visual judgement, no additional CaM dissociated from myosin upon addition of Ca^{2+}. That might suggest that in the absence of Ca^{2+} CaM associated with one or more IQ motifs within the neck region binds with low affinity so that forces acting on the sample during ultracentrifugation are enough to separate CaM from the heavy chain of myosin. Low affinity CaM binding could also contribute to the lack of motility in the absence of exogenous CaM. Alternatively, the integrity and stability of the recombinant protein could be influenced during the purification process, ultimately leading to weakening of the interaction between the light chains and the heavy chain. However, stability measurements performed on 9aMMD-S1 always resulted in a single intensity peak present in the sample, suggesting that 9aMMD-S1 maintains its integrity over time. Therefore, a weak interaction between CaM and IQ motif(s), rather than protein stability, is the most probable cause for the observed dissociation of CaM from

9aMMD-S1 during ultracentrifugation. A possibility that human myosin 9a preferentially binds other light chains cannot be excluded. The exact mechanism of the regulation of motility of human myosin 9a by Ca^{2+} remains to be explored.

Myosin 9 isoforms were previously suggested to move processively along actin filaments despite existing as monomers in solution. Since processive motility of a monomeric molecular motor cannot be explained by a hand-over-hand mechanism proposed for double-headed processive motors, it was proposed that the extended loop 2 of myosin 9 determines processive motility, tethering myosin head to actin as it binds subsequent monomers in the filament during processive motion (Post et al., 2002; Liao et al., 2010; Elfrink et al., 2014; Inoue et al., 2002; Nishikawa et al., 2006). In order to investigate if human myosin 9a acts as a single-headed processive molecular motor, I first examined the native molecular weight of 9aMMD. I used the combination of gel filtration and sucrose density gradients to obtain hydrodynamic properties of 9aMMD. The calculated native molecular weight was in great agreement with the molecular weight calculated from the amino acid sequence of single 9aMMD heavy chain with one bound CaM. Therefore, 9aMMD exists as a monomer in solution. I addressed its processivity by measuring the sliding velocity of actin filaments over a range of myosin surface densities. 9aMMD translocated actin flaments with no significant changes in the velocity over a wide range of surface densities. At lower densities, the probability of more than one molecule interacting with the filament is low. Therefore, the data suggests that human myosin 9a functions as a single-headed molecular motor. The mechanism of a processive motility of a monomeric motor remains to be investigated.

6.6. Final conclusions

That work presents the first successful approach towards expression and purification of recombinant active human myosin 9a fragments. Proteins were obtained in sufficient amounts to perform basic biochemical characterization of myosin function.

Expressed protein constructs exhibited ATPase activity and mechanical activity. Therefore, the properties of human myosin 9a are typical of those of other myosin

superfamily members.

This work provides a solid basis for further investigation of myosin 9a function and enables addressing the role of the tail domain, the N-terminal extension and the loop 2 insert in mechanochemical properties of that myosin superfamily member.

References

Abouhamed, M., Grobe, K., San, I. V., Thelen, S., Honnert, U., Balda, M. S., Matter, K., and Bahler, M. (2009) Myosin IXa regulates epithelial differentiation and its deficiency results in hydrocephalus, *Mol Biol Cell 20*, 5074-5085.

Albanesi, J. P., Coue, M., Fujisaki, H., and Korn, E. D. (1985) Effect of actin filament length and filament number concentration on the actin-activated ATPase activity of Acanthamoeba myosin I, *J Biol Chem 260*, 13276-13280.

Anson, M., Geeves, M. A., Kurzawa, S. E., and Manstein, D. J. (1996) Myosin motors with artificial lever arms, *EMBO J 15*, 6069-6074.

Atcheson, E., Hamilton, E., Pathmanathan, S., Greer, B., Harriott, P., and Timson, D. J. (2011) IQ-motif selectivity in human IQGAP2 and IQGAP3: binding of calmodulin and myosin essential light chain, *Biosci Rep 31*, 371-379.

Bagshaw, C. R. (1997) Muscle contraction. Myosin trapped but not tamed, *Nature 390*, 345-346.

Bagshaw, C. R., and Trentham, D. R. (1974) The characterization of myosin-product complexes and of product-release steps during the magnesium ion-dependent adenosine triphosphatase reaction, *Biochem J 141*, 331-349.

Bahler, M. (2000) Are class III and class IX myosins motorized signalling molecules?, *Biochim Biophys Acta 1496*, 52-59.

Bahler, M., and Rhoads, A. (2002) Calmodulin signaling via the IQ motif, *FEBS Lett 513*, 107-113.

Batters, C., Veigel, C., Homsher, E., and Sellers, J. R. (2014) To understand muscle you must take it apart, *Front Physiol 5*, 90.

Batters, C., Woodall, K. A., Toseland, C. P., Hundschell, C., and Veigel, C. (2012) Cloning, expression, and characterization of a novel molecular motor, Leishmania myosin-XXI, *J Biol Chem 287*, 27556-27566.

Bayley, P. M., Findlay, W. A., and Martin, S. R. (1996) Target recognition by calmodulin: dissecting the kinetics and affinity of interaction using short peptide sequences, *Protein Sci 5*, 1215-1228.

Behrmann, E., Muller, M., Penczek, P. A., Mannherz, H. G., Manstein, D. J., and Raunser, S. (2012) Structure of the rigor actin-tropomyosin-myosin complex, *Cell 150*, 327-338.

Bement, W. M., Hasson, T., Wirth, J. A., Cheney, R. E., and Mooseker, M. S. (1994) Identification and overlapping expression of multiple unconventional myosin genes in vertebrate cell types, *Proc Natl Acad Sci U S A 91*, 11767.

Berg, J. S., Powell, B. C., and Cheney, R. E. (2001) A millennial myosin census, *Mol Biol Cell 12*, 780-794.

Bobkov, A. A., Bobkova, E. A., Lin, S. H., and Reisler, E. (1996) The role of surface loops (residues 204-216 and 627-646) in the motor function of the myosin head, *Proc Natl Acad Sci U S A 93*, 2285-2289.

Burkhard, P., Stetefeld, J., and Strelkov, S. V. (2001) Coiled coils: a highly versatile protein folding motif, *Trends Cell Biol 11*, 82-88.

Capitanio, M., Canepari, M., Cacciafesta, P., Lombardi, V., Cicchi, R., Maffei, M., Pavone, F. S., and Bottinelli, R. (2006) Two independent mechanical events in the interaction cycle of skeletal muscle myosin with actin, *Proc Natl Acad Sci U S A 103*, 87-92.

Cheney, R. E., O'Shea, M. K., Heuser, J. E., Coelho, M. V., Wolenski, J. S., Espreafico, E. M., Forscher, P., Larson, R. E., and Mooseker, M. S. (1993) Brain myosin-V is a two-headed unconventional myosin with motor activity, *Cell 75*, 13-23.

Chieregatti, E., Gartner, A., Stoffler, H. E., and Bahler, M. (1998) Myr 7 is a novel myosin IX-RhoGAP expressed in rat brain, *J Cell Sci 111 (Pt 24)*, 3597-3608.

Coluccio, L. M., and Bretscher, A. (1987) Calcium-regulated cooperative binding of the microvillar 110K-calmodulin complex to F-actin: formation of decorated filaments, *J Cell Biol 105*, 325-333.

Coluccio, L. M., and Conaty, C. (1993) Myosin-I in mammalian liver, *Cell Motil Cytoskeleton 24*, 189-199.

Conibear, P. B., Bagshaw, C. R., Fajer, P. G., Kovacs, M., and Malnasi-Csizmadia, A. (2003) Myosin cleft movement and its coupling to actomyosin dissociation, *Nat Struct Biol 10*, 831-835.

Coureux, P. D., Sweeney, H. L., and Houdusse, A. (2004) Three myosin V structures delineate essential features of chemo-mechanical transduction, *EMBO J 23*, 4527-4537.

Coureux, P. D., Wells, A. L., Menetrey, J., Yengo, C. M., Morris, C. A., Sweeney, H. L., and Houdusse, A. (2003) A structural state of the myosin V motor without bound nucleotide, *Nature 425*, 419-423.

De La Cruz, E. M., and Ostap, E. M. (2004) Relating biochemistry and function in the myosin superfamily, *Curr Opin Cell Biol 16*, 61-67.

De La Cruz, E. M., and Ostap, E. M. (2009) Kinetic and equilibrium analysis of the myosin ATPase, *Methods Enzymol 455*, 157-192.

De La Cruz, E. M., Ostap, E. M., and Sweeney, H. L. (2001) Kinetic mechanism and regulation of myosin VI, *J Biol Chem 276*, 32373-32381.

De La Cruz, E. M., Wells, A. L., Rosenfeld, S. S., Ostap, E. M., and Sweeney, H. L. (1999) The kinetic mechanism of myosin V, *Proc Natl Acad Sci U S A 96*, 13726-13731.

Diensthuber, R. P., Muller, M., Heissler, S. M., Taft, M. H., Chizov, I., Manstein, D. J. (2011) Phalloidin perturbs the interaction of human non-muscle myosin isoforms 2A and 2C1 with F-actin, *FEBS Lett 585*, 767-771.

Dominguez, R., and Holmes, K. C. (2011) Actin structure and function, *Annu Rev Biophys 40*, 169-186.

East, D. A., and Mulvihill, D. P. (2011) Regulation and function of the fission yeast myosins, *J Cell Sci 124*, 1383-1390.

Egelman, E. H. (2010) Reconstruction of helical filaments and tubes, *Methods Enzymol 482*, 167-183.

Elfrink, K., Liao, W., Pieper, U., Oeding, S. J., and Bahler, M. (2014) The loop2 insertion of type IX myosin acts as an electrostatic actin tether that permits processive movement, *PLoS One 9*, e84874.

Esue, O., Tseng, Y., and Wirtz, D. (2009) Alpha-actinin and filamin cooperatively enhance the stiffness of actin filament networks, *PLoS One 4*, e4411.

Finer, J. T., Simmons, R. M., and Spudich, J. A. (1994) Single myosin molecule mechanics: piconewton forces and nanometre steps, *Nature 368*, 113-119.

Foth, B. J., Goedecke, M. C., and Soldati, D. (2006) New insights into myosin evolution and classification, *Proc Natl Acad Sci U S A 103*, 3681-3686.

Frankel, S., Sohn, R., and Leinwand, L. (1991) The use of sarkosyl in generating soluble protein after bacterial expression, *Proc Natl Acad Sci U S A 88*, 1192-1196.

Fujii, T., Iwane, A. H., Yanagida, T., and Namba, K. (2010) Direct visualization of secondary structures of F-actin by electron cryomicroscopy, *Nature 467*, 724-728.

Fujisaki, H., Albanesi, J. P., and Korn, E. D. (1985) Experimental evidence for the contractile activities of Acanthamoeba myosins IA and IB, *J Biol Chem 260*, 11183-

11189.

Fujita, H., Sugiura, S., Momomura, S., Omata, M., Sugi, H., and Sutoh, K. (1997) Characterization of mutant myosins of Dictyostelium discoideum equivalent to human familial hypertrophic cardiomyopathy mutants. Molecular force level of mutant myosins may have a prognostic implication, *J Clin Invest 99*, 1010-1015.

Galkin, V. E., Orlova, A., Schroder, G. F., and Egelman, E. H. (2010) Structural polymorphism in F-actin, *Nat Struct Mol Biol 17*, 1318-1323.

Geeves, M. A., Fedorov, R., and Manstein, D. J. (2005) Molecular mechanism of actomyosin-based motility, *Cell Mol Life Sci 62*, 1462-1477.

Geeves, M. A., Goody, R. S., and Gutfreund, H. (1984) Kinetics of acto-S1 interaction as a guide to a model for the crossbridge cycle, *J Muscle Res Cell Motil 5*, 351-361.

Geeves, M. A., and Holmes, K. C. (2005) The molecular mechanism of muscle contraction, *Adv Protein Chem 71*, 161-193.

Ghaemmaghami, S., Huh, W. K., Bower, K., Howson, R. W., Belle, A., Dephoure, N., O'Shea, E. K., and Weissman, J. S. (2003) Global analysis of protein expression in yeast, *Nature 425*, 737-741.

Glotzer, M. (2005) The molecular requirements for cytokinesis, *Science 307*, 1735-1739.

Gollub, J., Cremo, C. R., and Cooke, R. (1996) ADP release produces a rotation of the neck region of smooth myosin but not skeletal myosin, *Nat Struct Biol 3*, 796-802.

Gyimesi, M., Tsaturyan, A. K., Kellermayer, M. S., and Malnasi-Csizmadia, A. (2008) Kinetic characterization of the function of myosin loop 4 in the actin-myosin interaction, *Biochemistry 47*, 283-291.

Hall, A. (1998) Rho GTPases and the actin cytoskeleton, *Science 279*, 509-514.

Hammer, J. A., 3rd, and Sellers, J. R. (2012) Walking to work: roles for class V myosins as cargo transporters, *Nat Rev Mol Cell Biol 13*, 13-26.

Handa, Y., Durkin, C. H., Dodding, M. P., and Way, M. (2013) Vaccinia virus F11 promotes viral spread by acting as a PDZ-containing scaffolding protein to bind myosin-9A and inhibit RhoA signaling, *Cell Host Microbe 14*, 51-62.

Harada, Y., Noguchi, A., Kishino, A., and Yanagida, T. (1987) Sliding movement of single actin filaments on one-headed myosin filaments, *Nature 326*, 805-808.

Higuchi, H., and Endow, S. A. (2002) Directionality and processivity of molecular motors, *Curr Opin Cell Biol 14*, 50-57.

Holmes, K. C. (1997) The swinging lever-arm hypothesis of muscle contraction, *Curr Biol 7*, R112-118.

Holmes, K. C., Angert, I., Kull, F. J., Jahn, W., and Schroder, R. R. (2003) Electron cryo-microscopy shows how strong binding of myosin to actin releases nucleotide, *Nature 425*, 423-427.

Holmes, K. C., Schroder, R. R., Sweeney, H. L., and Houdusse, A. (2004) The structure of the rigor complex and its implications for the power stroke, *Philos Trans R Soc Lond B Biol Sci 359*, 1819-1828.

Homma, K., Saito, J., Ikebe, R., and Ikebe, M. (2000) Ca(2+)-dependent regulation of the motor activity of myosin V, *J Biol Chem 275*, 34766-34771.

Homsher, E., Nili, M., Chen, I. Y., and Tobacman, L. S. (2003) Regulatory proteins alter nucleotide binding to acto-myosin of sliding filaments in motility assays, *Biophys J 85*, 1046-1052.

Hotulainen, P., and Lappalainen, P. (2006) Stress fibers are generated by two distinct actin assembly mechanisms in motile cells, *J Cell Biol 173*, 383-394.

Howard, J. (1997) Molecular motors: structural adaptations to cellular functions, *Nature 389*, 561-567.

Howard, J., Hudspeth, A. J., and Vale, R. D. (1989) Movement of microtubules by single kinesin molecules, *Nature 342*, 154-158.

Huxley, A. F. (1957) Muscle structure and theories of contraction, *Prog Biophys Biophys Chem 7*, 255-318.

Huxley, A. F., and Simmons, R. M. (1971) Proposed mechanism of force generation in striated muscle, *Nature 233*, 533-538.

Huxley, H. E. (1957) The double array of filaments in cross-striated muscle, *J Biophys Biochem Cytol 3*, 631-648.

Inoue, A., Saito, J., Ikebe, R., and Ikebe, M. (2002) Myosin IXb is a single-headed minus-end-directed processive motor, *Nat Cell Biol 4*, 302-306.

Irving, M., St Claire Allen, T., Sabido-David, C., Craik, J. S., Brandmeier, B., Kendrick-Jones, J., Corrie, J. E., Trentham, D. R., and Goldman, Y. E. (1995) Tilting of the light-chain region of myosin during step length changes and active force generation in skeletal muscle, *Nature 375*, 688-691.

Joel, P. B., Trybus, K. M., and Sweeney, H. L. (2001) Two conserved lysines at the 50/20-kDa junction of myosin are necessary for triggering actin activation, *J Biol Chem 276*, 2998-3003.

Jontes, J. D., Milligan, R. A., Pollard, T. D., and Ostap, E. M. (1997) Kinetic characterization of brush border myosin-I ATPase, *Proc Natl Acad Sci U S A 94*, 14332-14337.

Jontes, J. D., Wilson-Kubalek, E. M., and Milligan, R. A. (1995) A 32 degree tail swing in brush border myosin I on ADP release, *Nature 378*, 751-753.

Kabsch, W., Mannherz, H. G., Suck, D., Pai, E. F., and Holmes, K. C. (1990) Atomic structure of the actin:DNase I complex, *Nature 347*, 37-44.

Kalhammer, G., Bahler, M., Schmitz, F., Jockel, J., and Block, C. (1997) Ras-binding domains: predicting function versus folding, *FEBS Lett 414*, 599-602.

Kambara, T., and Ikebe, M. (2006) A unique ATP hydrolysis mechanism of single-headed processive myosin, myosin IX, *J Biol Chem 281*, 4949-4957.

Knight, P. J., Thirumurugan, K., Xu, Y., Wang, F., Kalverda, A. P., Stafford, W. F., 3rd, Sellers, J. R., and Peckham, M. (2005) The predicted coiled-coil domain of myosin 10 forms a novel elongated domain that lengthens the head, *J Biol Chem 280*, 34702-34708.

Kohler, D., Struchholz, S., and Bahler, M. (2005) The two IQ-motifs and Ca2+/calmodulin regulate the rat myosin 1d ATPase activity, *FEBS J 272*, 2189-2197.

Kojima, S., Konishi, K., Katoh, K., Fujiwara, K., Martinez, H. M., Morales, M. F., and Onishi, H. (2001) Functional roles of ionic and hydrophobic surface loops in smooth muscle myosin: their interactions with actin, *Biochemistry 40*, 657-664.

Kollmar, M., Durrwang, U., Kliche, W., Manstein, D. J., and Kull, F. J. (2002) Crystal structure of the motor domain of a class-I myosin, *EMBO J 21*, 2517-2525.

Krementsov, D. N. Krementsova, E. B., and Trybus, K. M. (2004) Myosin V: regulation by calcium, calmodulin, and the tail domain, *J Cell Biol 164*, 877-886.

Kron, S. J., and Spudich, J. A. (1986) Fluorescent actin filaments move on myosin fixed to a glass surface, *Proc Natl Acad Sci U S A 83*, 6272-6276.

Kuhlman, P. A., and Bagshaw, C. R. (1998) ATPase kinetics of the Dictyostelium discoideum myosin II motor domain, *J Muscle Res Cell Motil 19*, 491-504.

Kurzawa, S. E., Manstein, D. J., and Geeves, M. A. (1997) Dictyostelium discoideum myosin II: characterization of functional myosin motor fragments, *Biochemistry 36*, 317-323.

Li, Y. and Sousa, R. (2012) Expression and purification of E. coli BirA biotin ligase for in vitro biotinylation, *Protein Expr Purif 82*: 162-167.

Liao, W., Elfrink, K., and Bahler, M. (2010) Head of myosin IX binds calmodulin and moves processively toward the plus-end of actin filaments, *J Biol Chem 285*, 24933-24942.

Lichty, J. J., Malecki, J. L., Agnew, H. D., Michelson-Horowitz, D. J., and Tan, S. (2005) Comparison of affinity tags for protein purification, *Protein Expr Purif 41*, 98-105.

Lin, T., Tang, N., and Ostap, E. M. (2005) Biochemical and motile properties of Myo1b splice isoforms, *J Biol Chem 280*, 41562-41567.

Lister, I., Schmitz, S., Walker, M., Trinick, J., Buss, F., Veigel, C., and Kendrick-Jones, J. (2004) A monomeric myosin VI with a large working stroke, *EMBO J 23*, 1729-1738.

Lorenz, M., and Holmes, K. C. (2010) The actin-myosin interface, *Proc Natl Acad Sci U S A 107*, 12529-12534.

Lu, H., Krementsova, E. B. and Trybus, K. M. (2006) Regulation of myosin V processivity by calcium at the single molecule level, *J Biol Chem 281*, 31987-31994.

Lymn, R. W., and Taylor, E. W. (1971) Mechanism of adenosine triphosphate hydrolysis by actomyosin, *Biochemistry 10*, 4617-4624.

Mallik, R., and Gross, S. P. (2004) Molecular motors: strategies to get along, *Curr Biol 14*, R971-982.

Manceva, S., Lin, T., Pham, H., Lewis, J. H., Goldman, Y. E., and Ostap, E. M. (2007) Calcium regulation of calmodulin binding to and dissociation from the myo1c regulatory domain, *Biochemistry 46*, 11718-11726.

Mashanov, G. I., and Molloy, J. E. (2007) Automatic detection of single fluorophores in live cells, *Biophys J 92*, 2199-2211.

Mateja, A., Cierpicki, T., Paduch, M., Derewenda, Z. S., and Otlewski, J. (2006) The dimerization mechanism of LIS1 and its implication for proteins containing the LisH motif, *J Mol Biol 357*, 621-631.

McDonnell, A. V., Jiang, T., Keating, A. E., and Berger, B. (2006) Paircoil2: improved prediction of coiled coils from sequence, *Bioinformatics 22*, 356-358.

McMichael, B. K., Scherer, K. F., Franklin, N. C., and Lee, B. S. (2014) The RhoGAP activity of myosin IXB is critical for osteoclast podosome patterning, motility, and resorptive capacity, *PLoS One 9*, e87402.

Mehta, A. D., Rock, R. S., Rief, M., Spudich, J. A., Mooseker, M. S., and Cheney, R. E. (1999) Myosin-V is a processive actin-based motor, *Nature 400*, 590-593.

Millar, N. C., and Geeves, M. A. (1983) The limiting rate of the ATP-mediated dissociation of actin from rabbit skeletal muscle myosin subfragment 1, *FEBS Lett 160*, 141-148.

Molloy, J. E., Burns, J. E., Kendrick-Jones, J., Tregear, R. T., and White, D. C. (1995) Movement and force produced by a single myosin head, *Nature 378*, 209-212.

Molloy, J. E., Burns, J. E., Sparrow, J. C., Tregear, R. T., Kendrick-Jones, J., and White, D. C. (1995) Single-molecule mechanics of heavy meromyosin and S1 interacting with rabbit or Drosophila actins using optical tweezers, *Biophys J 68*, 298S-303S; 303S-305S.

Moore, J. R., Krementsova, E. B., Trybus, K. M., and Warshaw, D. M. (2001) Myosin V exhibits a high duty cycle and large unitary displacement, *J Cell Biol 155*, 625-635.

Moore, P. B., Huxley, H. E., and DeRosier, D. J. (1970) Three-dimensional reconstruction of F-actin, thin filaments and decorated thin filaments, *J Mol Biol 50*, 279-295.

Mooseker, M. S., and Cheney, R. E. (1995) Unconventional myosins, *Annu Rev Cell Dev Biol 11*, 633-675.

Moran, U., Phillips, R., and Milo, R. (2010) SnapShot: key numbers in biology, *Cell 141*, 1262-1262 e1261.

Morel, J. E., Bachouchi-Salhi, N., and Merah, Z. (1992) Shape and length of myosin heads, *J Theor Biol 156*, 73-90.

Muller, R. T., Honnert, U., Reinhard, J., and Bahler, M. (1997) The rat myosin myr 5 is a GTPase-activating protein for Rho in vivo: essential role of arginine 1695, *Mol Biol Cell 8*, 2039-2053.

Murphy, C. T., and Spudich, J. A. (2000) Variable surface loops and myosin activity: accessories to a motor, *J Muscle Res Cell Motil 21*, 139-151.

Nalavadi, V., Nyitrai, M., Bertolini, C., Adamek, N., Geeves, M. A., and Bahler, M. (2005) Kinetic mechanism of myosin IXB and the contributions of two class IX-specific

regions, *J Biol Chem 280*, 38957-38968.

Narumiya, S. (1996) The small GTPase Rho: cellular functions and signal transduction, *J Biochem 120*, 215-228.

Nascimento, A. A., Cheney, R. E., Tauhata, S. B., Larson, R. E., and Mooseker, M. S. (1996) Enzymatic characterization and functional domain mapping of brain myosin-V, *J Biol Chem 271*, 17561-17569.

Nishikawa, M., Nishikawa, S., Inoue, A., Iwane, A. H., Yanagida, T., and Ikebe, M. (2006) A unique mechanism for the processive movement of single-headed myosin-IX, *Biochem Biophys Res Commun 343*, 1159-1164.

Oda, T., Iwasa, M., Aihara, T., Maeda, Y., and Narita, A. (2009) The nature of the globular- to fibrous-actin transition, *Nature 457*, 441-445.

Odronitz, F., and Kollmar, M. (2007) Drawing the tree of eukaryotic life based on the analysis of 2,269 manually annotated myosins from 328 species, *Genome Biol 8*, R196.

Omelchenko, T. (2012) Regulation of collective cell migration by RhoGAP myosin IXA, *Small GTPases 3*, 213-218.

Omelchenko, T., and Hall, A. (2012) Myosin-IXA regulates collective epithelial cell migration by targeting RhoGAP activity to cell-cell junctions, *Curr Biol 22*, 278-288.

Onishi, H., Mikhailenko, S. V., and Morales, M. F. (2006) Toward understanding actin activation of myosin ATPase: the role of myosin surface loops, *Proc Natl Acad Sci U S A 103*, 6136-6141.

Park, H., Ramamurthy, B., Travaglia, M., Safer, D., Chen, L. Q., Franzini-Armstrong, C., Selvin, P. R., and Sweeney, H. L. (2006) Full-length myosin VI dimerizes and moves processively along actin filaments upon monomer clustering, *Mol Cell 21*, 331-336.

Pettersen, E. F., Goddard, T. D., Huang, C. C., Couch, G. S., Greenblatt, D. M., Meng, E. C., and Ferrin, T. E. (2004) UCSF Chimera--a visualization system for exploratory research and analysis, *J Comput Chem 25*, 1605-1612.

Phichith, D., Travaglia, M., Yang, Z., Liu, X., Zong, A. B., Safer, D., and Sweeney, H. L. (2009) Cargo binding induces dimerization of myosin VI, *Proc Natl Acad Sci U S A 106*, 17320-17324.

Pollard, T. D., and Korn, E. D. (1973a) Acanthamoeba myosin. I. Isolation from Acanthamoeba castellanii of an enzyme similar to muscle myosin, *J Biol Chem 248*, 4682-4690.

Pollard, T. D., and Korn, E. D. (1973a) Acanthamoeba myosin. II. Interaction with actin and with a new cofactor protein required for actin activation of Mg 2+ adenosine triphosphatase activity, *J Biol Chem 248*, 4691-4697.

Pollard, T. D., Stafford, W. F., and Porter, M. E. (1978) Characterization of a second myosin from Acanthamoeba castellanii, *J Biol Chem 253*, 4798-4808.

Post, P. L., Bokoch, G. M., and Mooseker, M. S. (1998) Human myosin-IXb is a mechanochemically active motor and a GAP for rho, *J Cell Sci 111 (Pt 7)*, 941-950.

Post, P. L., Tyska, M. J., O'Connell, C. B., Johung, K., Hayward, A., and Mooseker, M. S. (2002) Myosin-IXb is a single-headed and processive motor, *J Biol Chem 277*, 11679-11683.

Purcell, T. J., Morris, C., Spudich, J. A., and Sweeney, H. L. (2002) Role of the lever arm in the processive stepping of myosin V, *Proc Natl Acad Sci U S A 99*, 14159-14164.

Rayment, I., Rypniewski, W. R., Schmidt-Base, K., Smith, R., Tomchick, D. R., Benning, M. M., Winkelmann, D. A., Wesenberg, G., and Holden, H. M. (1993a) Three-dimensional structure of myosin subfragment-1: a molecular motor, *Science 261*, 50-58.

Rayment, I., Holden, H. M., Whittaker, M., Yohn, C. B., Lorenz, M., Holmes, K. C., and Milligan, R. A. (1993b) Structure of the actin-myosin complex and its implications for muscle contraction, *Science 261*, 58-65.

Reck-Peterson, S. L., Provance, D. W., Jr., Mooseker, M. S., and Mercer, J. A. (2000) Class V myosins, *Biochim Biophys Acta 1496*, 36-51.

Reinhard, J., Scheel, A. A., Diekmann, D., Hall, A., Ruppert, C., and Bahler, M. (1995) A novel type of myosin implicated in signalling by rho family GTPases, *EMBO J 14*, 697-704.

Ricca, B. L., and Rock, R. S. (2010) The stepping pattern of myosin X is adapted for processive motility on bundled actin, *Biophys J 99*, 1818-1826.

Ridley, A. J. (1996) Rho: theme and variations, *Curr Biol 6*, 1256-1264.

Rief, M., Rock, R. S., Mehta, A. D., Mooseker, M. S., Cheney, R. E., and Spudich, J. A. (2000) Myosin-V stepping kinetics: a molecular model for processivity, *Proc Natl Acad Sci U S A 97*, 9482-9486.

Rock, R. S., Rice, S. E., Wells, A. L., Purcell, T. J., Spudich, J. A., and Sweeney, H. L. (2001) Myosin VI is a processive motor with a large step size, *Proc Natl Acad Sci U S A 98*, 13655-13659.

Rock, R. S., Rief, M., Mehta, A. D. and Spudich, J. A. (2000) In vitro assays of processive myosin motors, *Methods 22*: 378-381.

Ross, J. L., Ali, M. Y., and Warshaw, D. M. (2008) Cargo transport: molecular motors navigate a complex cytoskeleton, *Curr Opin Cell Biol 20*, 41-47.

Ruff, C., Furch, M., Brenner, B., Manstein, D. J., and Meyhofer, E. (2001) Single-molecule tracking of myosins with genetically engineered amplifier domains, *Nat Struct Biol 8*, 226-229.

Sasaki, N., Asukagawa, H., Yasuda, R., Hiratsuka, T., and Sutoh, K. (1999) Deletion of the myopathy loop of Dictyostelium myosin II and its impact on motor functions, *J Biol Chem 274*, 37840-37844.

Sasaki, N., and Sutoh, K. (1998) Structure-mutation analysis of the ATPase site of Dictyostelium discoideum myosin II, *Adv Biophys 35*, 1-24.

Sellers, J. R. (2000) Myosins: a diverse superfamily, *Biochim Biophys Acta 1496*, 3-22.

Sellers, J. R. (2001) In vitro motility assay to study translocation of actin by myosin, Cuur *Protoc Cell Biol*, Chapter 13, Unit 13.2.

Sheetz, M. P., Chasan, R., and Spudich, J. A. (1984) ATP-dependent movement of myosin in vitro: characterization of a quantitative assay, *J Cell Biol 99*, 1867-1871.

Sheetz, M. P., and Spudich, J. A. (1983) Movement of myosin-coated fluorescent beads on actin cables in vitro, *Nature 303*, 31-35.

Shiba, K., Niidome, T., Katoh, E., Xiang, H., Han, L., Mori, T., and Katayama, Y. (2010) Polydispersity as a parameter for indicating the thermal stability of proteins by dynamic light scattering, *Anal Sci 26*, 659-663.

Smith, C. A., and Rayment, I. (1996a) Active site comparisons highlight structural similarities between myosin and other P-loop proteins, *Biophys J 70*, 1590-1602.

Smith, C. A., and Rayment, I. (1996b) X-ray structure of the magnesium(II).ADP.vanadate complex of the Dictyostelium discoideum myosin motor domain to 1.9 A resolution, *Biochemistry 35*, 5404-5417.

Spudich, J. A. and Watt, S. (1971) The regulation of rabbit skeletal muscle contraction. Biochemical studies of the interaction of the tropomyosin-troponin complex with

actin and the proteolytic fragments of myosin, *J Biol Chem 246*: 4866-4871.

Stafford, W. F., Walker, M. L., Trinick, J. A., and Coluccio, L. M. (2005) Mammalian class I myosin, Myo1b, is monomeric and cross-links actin filaments as determined by hydrodynamic studies and electron microscopy, *Biophys J 88*, 384-391.

Struchholz, S., Elfrink, K., Pieper, U., Kalhammer, G., Honnert, U., Grutzner, A., Linke, W. A., Liao, W., and Bahler, M. (2009) Functional role of the extended loop 2 in the myosin 9b head for binding F-actin, *J Biol Chem 284*, 3663-3671.

Svoboda, K., Schmidt, C. F., Schnapp, B. J., and Block, S. M. (1993) Direct observation of kinesin stepping by optical trapping interferometry, *Nature 365*, 721-727.

Sweeney, H. L., and Houdusse, A. (2010) Structural and functional insights into the Myosin motor mechanism, *Annu Rev Biophys 39*, 539-557.

Sweeney, H. L., Straceski, A. J., Leinwand, L. A., Tikunov, B. A., and Faust, L. (1994) Heterologous expression of a cardiomyopathic myosin that is defective in its actin interaction, *J Biol Chem 269*, 1603-1605.

Syamaladevi, D. P., Spudich, J. A., and Sowdhamini, R. (2012) Structural and functional insights on the Myosin superfamily, *Bioinform Biol Insights 6*, 11-21.

Szent-Gyorgyi, A. G. (2004) The early history of the biochemistry of muscle contraction, *J Gen Physiol 123*, 631-641.

Takagi, Y., Farrow, R. E., Billington, N., Nagy, A., Batters, C., Yang, Y., Sellers, J. R., and Molloy, J. E. (2014) Myosin-10 produces its power-stroke in two phases and moves processively along a single actin filament under low load, *Proc Natl Acad Sci U S A 111*, E1833-1842.

Tauhata, S. B., dos Santos, D. V., Taylor, E. W., Mooseker, M. S., and Larson, R. E. (2001) High affinity binding of brain myosin-Va to F-actin induced by calcium in the presence of ATP, *J Biol Chem 276*, 39812-39818.

Terrak, M., Rebowski, G., Lu, R. C., Grabarek, Z., and Dominguez, R. (2005) Structure of the light chain-binding domain of myosin V, *Proc Natl Acad Sci U S A 102*, 12718-12723.

Thompson, R. F., and Langford, G. M. (2002) Myosin superfamily evolutionary history, *Anat Rec 268*, 276-289.

Tominaga, M., Kojima, H., Yokota, E., Nakamori, R., Anson, M., Shimmen, T., and Oiwa, K. (2012) Calcium-induced mechanical change in the neck domain alters the activity of plant myosin XI, *J Biol Chem 287*, 30711-30718.

Toprak, E., Yildiz, A., Hoffman, M. T., Rosenfeld, S. S., and Selvin, P. R. (2009) Why kinesin is so processive, *Proc Natl Acad Sci U S A 106*, 12717-12722.

Trentham, D. R., Eccleston, J. F., and Bagshaw, C. R. (1976) Kinetic analysis of ATPase mechanisms, *Q Rev Biophys 9*, 217-281.

Trinick, J., Cooper, J., Seymour, J., and Egelman, E. H. (1986) Cryo-electron microscopy and three-dimensional reconstruction of actin filaments, *J Microsc 141*, 349-360.

Tripet, B., Wagschal, K., Lavigne, P., Mant, C. T., and Hodges, R. S. (2000) Effects of side-chain characteristics on stability and oligomerization state of a de novo-designed model coiled-coil: 20 amino acid substitutions in position "d", *J Mol Biol 300*, 377-402.

Trivedi, D. V., David, C., Jacobs, D. J., and Yengo, C. M. (2012) Switch II mutants reveal coupling between the nucleotide- and actin-binding regions in myosin V, *Biophys J 102*, 2545-2555.

Trybus, K. M., Gushchin, M. L., Lui, H., Hazelwood, L., Krementsova, E. B., Volkmann, N. and Hanein, D. (2007) Effect of calcium on calmodulin bound to the IQ motifs of myosin V, *J Biol Chem 32*, 23316-23325.

Uyeda, T. Q., Abramson, P. D., and Spudich, J. A. (1996) The neck region of the myosin motor domain acts as a lever arm to generate movement, *Proc Natl Acad Sci U S A 93*, 4459-4464.

Uyeda, T. Q., Warrick, H. M., Kron, S. J., and Spudich, J. A. (1991) Quantized velocities at low myosin densities in an in vitro motility assay, *Nature 352*, 307-311.

Vale, R. D. (1999) Millennial musings on molecular motors, *Trends Cell Biol 9*, M38-42.

Vale, R. D. (2003) Myosin V motor proteins: marching stepwise towards a mechanism, *J Cell Biol 163*, 445-450.

van den Boom, F., Dussmann, H., Uhlenbrock, K., Abouhamed, M., and Bahler, M. (2007) The Myosin IXb motor activity targets the myosin IXb RhoGAP domain as cargo to sites of actin polymerization, *Mol Biol Cell 18*, 1507-1518.

Varkuti, B. H., Yang, Z., Kintses, B., Erdelyi, P., Bardos-Nagy, I., Kovacs, A. L., Hari, P., Kellermayer, M., Vellai, T., and Malnasi-Csizmadia, A. (2012) A novel actin binding site of myosin required for effective muscle contraction, *Nat Struct Mol Biol 19*, 299-306.

Veigel, C., Coluccio, L. M., Jontes, J. D., Sparrow, J. C., Milligan, R. A., and Molloy, J. E. (1999) The motor protein myosin-I produces its working stroke in two steps, *Nature*

398, 530-533.

Veigel, C., Molloy, J. E., Schmitz, S., and Kendrick-Jones, J. (2003) Load-dependent kinetics of force production by smooth muscle myosin measured with optical tweezers, *Nat Cell Biol 5*, 980-986.

Veigel, C., and Schmidt, C. F. (2011) Moving into the cell: single-molecule studies of molecular motors in complex environments, *Nat Rev Mol Cell Biol 12*, 163-176.

Veigel, C., Schmitz, S., Wang, F., and Sellers, J. R. (2005) Load-dependent kinetics of myosin-V can explain its high processivity, *Nat Cell Biol 7*, 861-869.

Veigel, C., Wang, F., Bartoo, M. L., Sellers, J. R., and Molloy, J. E. (2002) The gated gait of the processive molecular motor, myosin V, *Nat Cell Biol 4*, 59-65.

Volkmann, N., Hanein, D., Ouyang, G., Trybus, K. M., DeRosier, D. J., and Lowey, S. (2000) Evidence for cleft closure in actomyosin upon ADP release, *Nat Struct Biol 7*, 1147-1155.

Volkmann, N., Ouyang, G., Trybus, K. M., DeRosier, D. J., Lowey, S., and Hanein, D. (2003) Myosin isoforms show unique conformations in the actin-bound state, *Proc Natl Acad Sci U S A 100*, 3227-3232.

Wagschal, K., Tripet, B., and Hodges, R. S. (1999) De novo design of a model peptide sequence to examine the effects of single amino acid substitutions in the hydrophobic core on both stability and oligomerization state of coiled-coils, *J Mol Biol 285*, 785-803.

Walker, M. L., Burgess, S. A., Sellers, J. R., Wang, F., Hammer, J. A., 3rd, Trinick, J., and Knight, P. J. (2000) Two-headed binding of a processive myosin to F-actin, *Nature 405*, 804-807.

Waller, G. S., Ouyang, G., Swafford, J., Vibert, P., and Lowey, S. (1995) A minimal motor domain from chicken skeletal muscle myosin, *J Biol Chem 270*, 15348-15352.

Wang, F., Chen, L., Arcucci, O., Harvey, E. V., Bowers, B., Xu, Y., Hammer, J. A., 3rd, and Sellers, J. R. (2000) Effect of ADP and ionic strength on the kinetic and motile properties of recombinant mouse myosin V, *J Biol Chem 275*, 4329-4335.

Wang, F., Thirumurugan, K., Stafford, W. F., Hammer, J. A. 3rd, Knight, P. J. and Sellers, J. R. (2004) Regulated conformation of myosin V, *J Biol Chem 279*, 2333-2336.

Warshaw, D. M., Guilford, W. H., Freyzon, Y., Krementsova, E., Palmiter, K. A., Tyska, M. J., Baker, J. E., and Trybus, K. M. (2000) The light chain binding domain of expressed smooth muscle heavy meromyosin acts as a mechanical lever, *J Biol*

Chem 275, 37167-37172.

Watanabe, S., Watanabe, T. M., Sato, O., Awata, J., Homma, K., Umeki, N., Higuchi, H., Ikebe, R., and Ikebe, M. (2008) Human myosin Vc is a low duty ratio nonprocessive motor, *J Biol Chem 283*, 10581-10592.

Webb, M. R., and Corrie, J. E. (2001) Fluorescent coumarin-labeled nucleotides to measure ADP release from actomyosin, *Biophys J 81*, 1562-1569.

Whittaker, M., Wilson-Kubalek, E. M., Smith, J. E., Faust, L., Milligan, R. A., and Sweeney, H. L. (1995) A 35-A movement of smooth muscle myosin on ADP release, *Nature 378*, 748-751.

Woldringh, C. L., Huls, P. G., and Vischer, N. O. (1993) Volume growth of daughter and parent cells during the cell cycle of Saccharomyces cerevisiae a/alpha as determined by image cytometry, *J Bacteriol 175*, 3174-3181.

Wolenski, J. S. (1995) Regulation of calmodulin-binding myosins, *Trends Cell Biol 5*, 310-316.

Woodward, S. K., Geeves, M. A., and Manstein, D. J. (1995) Kinetic characterization of the catalytic domain of Dictyostelium discoideum myosin, *Biochemistry 34*, 16056-16064.

Xie, X., Harrison, D. H., Schlichting, I., Sweet, R. M., Kalabokis, V. N., Szent-Gyorgyi, A. G., and Cohen, C. (1994) Structure of the regulatory domain of scallop myosin at 2.8 A resolution, *Nature 368*, 306-312.

Xu, Y., Pektor, S., Balkow, S., Hemkemeyer, S. A., Liu, Z., Grobe, K., Hanley, P. J., Shen, L., Bros, M., Schmidt, T., Bahler, M., and Grabbe, S. (2014) Dendritic cell motility and T cell activation requires regulation of Rho-cofilin signaling by the Rho-GTPase activating protein myosin IXb, *J Immunol 192*, 3559-3568.

Yildiz, A., Forkey, J. N., McKinney, S. A., Ha, T., Goldman, Y. E., and Selvin, P. R. (2003) Myosin V walks hand-over-hand: single fluorophore imaging with 1.5-nm localization, *Science 300*, 2061-2065.

Yildiz, A., Park, H., Safer, D., Yang, Z., Chen, L. Q., Selvin, P. R., and Sweeney, H. L. (2004) Myosin VI steps via a hand-over-hand mechanism with its lever arm undergoing fluctuations when attached to actin, *J Biol Chem 279*, 37223-37226.

Yildiz, A., and Selvin, P. R. (2005) Fluorescence imaging with one nanometer accuracy: application to molecular motors, *Acc Chem Res 38*, 574-582.

Yount, R. G., Lawson, D., and Rayment, I. (1995) Is myosin a "back door" enzyme?, *Biophys J 68*, 44S-47S; discussion 47S-49S.

Zhu, T., Sata, M., and Ikebe, M. (1996) Functional expression of mammalian myosin I beta: analysis of its motor activity, *Biochemistry 35*, 513-522.

Acknowledgements

First and foremost, I would like to thank my parents and family for their support. This thesis would not be completed if it wasn't for them.

The majority of this thesis was performed in the laboratory of Prof. Claudia Veigel at the Department of Cellular Physiology, Medical Faculty, LMU. Part of the thesis was performed in the laboratory of Dr. James R. Sellers (Laboratory of Molecular Physiology) at NHLBI, NIH, USA.

I would like to acknowledge Dr. Christopher Batters from LMU and Dr. Sarah Heissler from NIH for their advice and feedback.

Electron microscopy data was collected by Dr. Neil Billington from the Laboratory of Molecular Physiology, NIH, and Dario Saczko-Brack from Prof. Veigel's group.

I am thankful for the technical help of Roswitha Maul, Susanne Schickle, Sascha Blumentritt and Irene Schneider.

I am grateful to friends I made during my stay in Munich (Justin, Rounak, Ewelina and Bożena) for fun times.

Finally, I would like to thank my current lab team for their support and motivation.

Eidesstattliche Erklärung

Ewa Warchoł

Ich erkläre hiermit an Eides statt,

dass ich die vorliegende Dissertation mit dem Thema:

Expression, purification and characterization of human myosin 9a

selbständig verfasst, mich außer der angegebenen keiner weiteren Hifsmittel bedient und alle Erkenntnisse, die aus dem Schrifttum ganz oder annährend übernommen sind, als solche kenntlich gemacht und nach ihrer Herkunft unter Bezeichnung der Fundstelle einzeln nachgewiesen habe.

Ich erkläre des Weiteren, dass die hier vorgelegte Dissertation nicht in gleicher oder in ähnlicher Form bei einer anderen Stelle zur Erlangung eines akademischen Grades eingereicht wurde.

……
Ort

……
Datum

……
Unterschrift